frontiers | Research Topics

Advances in surgical approaches for the treatment of glioma

Edited by
Ying Mao, Mitchel Berger, Yan Qu, Hongmin Bai, Danny TM Chan, Songbai Xu and Zhifeng Shi

Published in
Frontiers in Oncology
Frontiers in Neurology

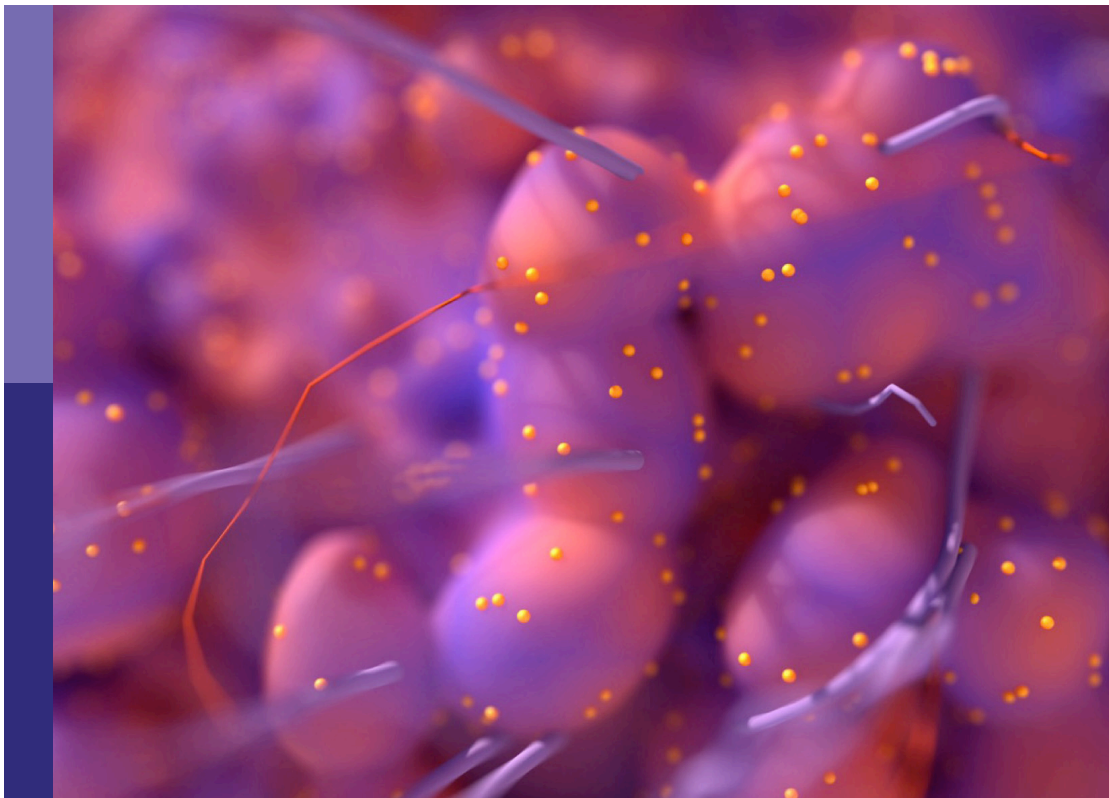

ISSN 1664-8714
ISBN 978-2-8325-3082-5
DOI 10.3389/978-2-8325-3082-5

About Frontiers

Frontiers is more than just an open access publisher of scholarly articles: it is a pioneering approach to the world of academia, radically improving the way scholarly research is managed. The grand vision of Frontiers is a world where all people have an equal opportunity to seek, share and generate knowledge. Frontiers provides immediate and permanent online open access to all its publications, but this alone is not enough to realize our grand goals.

Frontiers journal series

The Frontiers journal series is a multi-tier and interdisciplinary set of open-access, online journals, promising a paradigm shift from the current review, selection and dissemination processes in academic publishing. All Frontiers journals are driven by researchers for researchers; therefore, they constitute a service to the scholarly community. At the same time, the *Frontiers journal series* operates on a revolutionary invention, the tiered publishing system, initially addressing specific communities of scholars, and gradually climbing up to broader public understanding, thus serving the interests of the lay society, too.

Dedication to quality

Each Frontiers article is a landmark of the highest quality, thanks to genuinely collaborative interactions between authors and review editors, who include some of the world's best academicians. Research must be certified by peers before entering a stream of knowledge that may eventually reach the public - and shape society; therefore, Frontiers only applies the most rigorous and unbiased reviews. Frontiers revolutionizes research publishing by freely delivering the most outstanding research, evaluated with no bias from both the academic and social point of view. By applying the most advanced information technologies, Frontiers is catapulting scholarly publishing into a new generation.

What are Frontiers Research Topics?

Frontiers Research Topics are very popular trademarks of the *Frontiers journals series*: they are collections of at least ten articles, all centered on a particular subject. With their unique mix of varied contributions from Original Research to Review Articles, Frontiers Research Topics unify the most influential researchers, the latest key findings and historical advances in a hot research area.

Find out more on how to host your own Frontiers Research Topic or contribute to one as an author by contacting the Frontiers editorial office: frontiersin.org/about/contact

Advances in surgical approaches for the treatment of glioma

Topic editors

Ying Mao — Fudan University, China
Mitchel Berger — University of California, San Francisco, United States
Yan Qu — Air Force Military Medical University, China
Hongmin Bai — Neurosurgical Department of General Hospital of Southern Theatre Command, China
Danny TM Chan — The Chinese University of Hong Kong, China
Songbai Xu — First Affiliated Hospital of Jilin University, China
Zhifeng Shi — Fudan University, China

Citation

Mao, Y., Berger, M., Qu, Y., Bai, H., Chan, D. T., Xu, S., Shi, Z., eds. (2023). *Advances in surgical approaches for the treatment of glioma.* Lausanne: Frontiers Media SA. doi: 10.3389/978-2-8325-3082-5

Table of contents

05 Editorial: Advances in surgical approaches for the treatment of glioma
Hongmin Bai and Che Jiang

08 Raman spectroscopy: A prospective intraoperative visualization technique for gliomas
Yi Zhang, Hongquan Yu, Yunqian Li, Haiyang Xu, Liu Yang, Peilin Shan, Yuejiao Du, Xiaokai Yan and Xuan Chen

21 Clinical feasibility of miniaturized Lissajous scanning confocal laser endomicroscopy for indocyanine green-enhanced brain tumor diagnosis
Duk Hyun Hong, Jang Hun Kim, Jae-Kyung Won, Hyungsin Kim, Chayeon Kim, Kyung-Jae Park, Kyungmin Hwang, Ki-Hun Jeong and Shin-Hyuk Kang

36 Predictive model of language deficit after removing glioma involving language areas under general anesthesia
Meng Cui, Qingbao Guo, Yihong Chi, Meng Zhang, Hui Yang, Xin Gao, Hewen Chen, Yukun Liu and Xiaodong Ma

47 Advances in the intraoperative delineation of malignant glioma margin
Shan Jiang, Huihui Chai and Qisheng Tang

54 Preoperative individual-target transcranial magnetic stimulation demonstrates an effect comparable to intraoperative direct electrical stimulation in language-eloquent glioma mapping and improves postsurgical outcome: A retrospective fiber-tracking and electromagnetic simulation study
Sanzhong Li, Yunfeng Mu, Yang Rao, Chuanzhu Sun, Xiang Li, Huan Liu, Xun Yu, Xiao Yan, Yunxia Ding, Yangtao Wang and Zhou Fei

63 Maximal safe resection of diffuse lower grade gliomas primarily within central lobe using cortical/subcortical direct electrical stimulation under awake craniotomy
Shujing Yao, Ruixin Yang, Chenggang Du, Che Jiang, Yang Wang, Chongqi Peng and Hongmin Bai

74 The clinical and neurocognitive functional changes with awake brain mapping for gliomas invading eloquent areas: Institutional experience and the utility of The Montreal Cognitive Assessment
Yuan Wang, Shaochun Guo, Na Wang, Jinghui Liu, Fan Chen, Yulong Zhai, Yue Wang, Yang Jiao, Wenjian Zhao, Chao Fan, Yanrong Xue, GuoDong Gao, Peigang Ji and Liang Wang

85 A review on surgical treatment options in gliomas
Zhongxi Yang, Chen Zhao, Shan Zong, Jianmin Piao, Yuhao Zhao and Xuan Chen

92 Automatic bundle-specific white matter fiber tracking tool using diffusion tensor imaging data: A pilot trial in the application of language-related glioma resection
Yifan Yuan, Tianming Qiu, Shin Tai Chong, Sanford Pin-Chuan Hsu, Ying-Hua Chu, Yi-Cheng Hsu, Geng Xu, Yu-Ting Ko, Kuan-Tsen Kuo, Zixiao Yang, Wei Zhu, Ching-Po Lin and Jianping Song

101 Minimally invasive treatment for glioblastoma through endoscopic surgery including tumor embolization when necessary: a technical note
Tomohiro Sakata, Motoki Tanikawa, Hiroshi Yamada, Ryota Fujinami, Yusuke Nishikawa, Shigeki Yamada and Mitsuhito Mase

109 Bibliometric research on the developments of artificial intelligence in radiomics toward nervous system diseases
Jiangli Cui, Xingyu Miao, Xiaoyu Yanghao and Xuqiu Qin

frontiers | Frontiers in Oncology

TYPE Editorial
PUBLISHED 11 July 2023
DOI 10.3389/fonc.2023.1236341

OPEN ACCESS

EDITED AND REVIEWED BY
David D. Eisenstat,
Royal Children's Hospital, Australia

*CORRESPONDENCE
Hongmin Bai
baihmfmmu@vip.163.com

†These authors have contributed equally to this work and share first authorship

RECEIVED 07 June 2023
ACCEPTED 03 July 2023
PUBLISHED 11 July 2023

CITATION
Bai H and Jiang C (2023) Editorial: Advances in surgical approaches for the treatment of glioma.
Front. Oncol. 13:1236341.
doi: 10.3389/fonc.2023.1236341

Editorial: Advances in surgical approaches for the treatment of glioma

Hongmin Bai*† and Che Jiang†

Department of Neurosurgery, General Hospital of Southern Theater Command, Guangzhou, Guangdong, China

KEYWORDS

surgery, glioma, direct electrical stimulation (DES), IMRI, histological examination

Editorial on the Research Topic
Advances in surgical approaches for the treatment of glioma

Presently, maximal-safe resection is still the primary pursuit for surgically treating glioma. Accordingly, there are a variety of novel techniques being developed. Therefore, this Research Topic aimed to summarize advances in glioma surgery along with emerging auxiliary techniques.

On the whole, there are four aspects to consider: balancing between the extent of resection and preserving neurological function, shortening intraoperative examination time while improving the accuracy of detection, minimizing surgical incision while achieving total resection, and utilizing *in vivo* histological testing just before completion of resection while guaranteeing patient safety.

1 Clinical studies

Intraoperative direct electrical stimulation (DES) can directly identify neural networks crucial for brain function and remains the gold standard for eloquent cortex localization (1, 2). Although there remains some debate (3, 4), awake brain mapping plus DES is generally associated with more extensive resection, better overall survival, and fewer severe persistent neurological deficits compared with resection under general anesthesia (5–8). Wang et al. presented their experience in awake craniotomy with intraoperative DES mapping for gliomas invading eloquent areas. With a similar surgical strategy, Yao et al. reviewed their single-center experience of treating diffuse lower grade glioma (DLGG) in the central lobe (including precentral and postcentral gyri and paracentral lobule). Both studies reported favorable results. Moreover, Wang et al. established a high sensitivity of the Montreal Cognitive Assessment (MoCA), a relatively brief screening tool for assessment of this population's cognitive impairment.

Compared with awake surgery, surgery under general anesthesia is less time-consuming, with lower intraoperative risk (9, 10). Cui et al. reported their experience of removing glioma under general anesthesia assisted by intraoperative multimodal techniques (combined use of neuronavigation, iMRI, with/without DES/neuromonitoring). The large sample size (nearly 500 patients) was the strength of this study. The researchers confirmed that the application of

multimodal techniques improved the extent of resection (EOR) and rate of gross total resection (GTR) while associated with a lower incidence of permanent language deficits (PLD). They also found clinical factors for predicting language deficit. It is worth noting that the researchers achieved a higher rate of GTR (72.7%) than all previous studies of awake craniotomy, with only a slightly higher incidence of PLD (13.4%). The established predictive model may provide surgeons and patients a reference in choosing an appropriate surgical strategy (e.g., awake craniotomy with DES for patients with the highest risk of language deficit, while multimodal techniques under general anesthesia for those with moderate risk). However, the model should be validated with more studies.

Transcranial magnetic stimulation (TMS) can generate a magnetic field, inducing transient electric fields within the targeted brain cortex. High/low frequency stimulation excites/inhibits neuron activity (11). As another way to directly test the crucial neurocircuits of brain function besides DES, navigated TMS (nTMS) has a similar effect in predicting the location of eloquent areas (12–15). Li et al. verified the reliability of individual-target TMS in preoperative mapping. They showed that compared to intraoperative DES in awake surgery, the combination of nTMS can lead to an improvement in language performance as well as in brain-structure preservation. Precise localization by preoperative methods may help reduce the time required for awake surgery.

It has been reported that subtle neuropsychological disturbances are more frequent than traditional thoughts after glioma surgery (16–18). Therefore, some scholars even proposed performing awake surgery in all LGG patients regardless of tumor location and monitoring more subtle cognitive and behavioral functions intra-operatively (19). As studies showed mental disorders such as depression (20–22) and post-traumatic stress disorder (23, 24) were associated with shorter survival periods of LGG patients, the underlying neurocircuitry of emotion may also be considered.

Less traumatic procedures could reduce patients' pain, improve cosmetic appearance, mitigate neurophysiological reflex response, and reduce the risk of infection (25, 26). Some previous studies have utilized an endoscope to resect deep-seated glioblastoma (27, 28). Sakata et al. further expanded its use in resecting superficial glioblastomas. In their six-case series, all achieved gross total/near total resection. The author emphasized the importance of prior endovascular tumor embolization. Huge intraoperative blood loss (>1000 ml) only occurred in one case, for whom the preceding embolization could not be performed due to the non-localization of a proper feeder artery.

2 Imaging studies

Jiang et al. reviewed four main intraoperative systems for delineating malignant tumors: intraoperative MRI (iMRI), fluorescence, Raman histology, and mass spectrometry. iMRI overcomes brain drift defects and has been shown to increase the complete resection rate (29, 30). Besides, functional MRI (fMRI), diffusion tensor imaging (DTI), and MR spectroscopy (MRS) can be applied with patients asleep for the whole surgical procedure, giving a panoramic view of the functional brain cortex, fiber tracts, and metabolic change levels. To solve the problem that the DTI reconstruction process relies on the experience of operators and is time-consuming, Yuan et al. developed an in-house software, "DiffusionGo." It can reconstruct DTI automatically and quickly. The researchers demonstrated its efficacy in language function preservation for three patients who underwent surgical resection of gliomas. DiffusionGo is especially suitable for intraoperative use, and its adaptation to iMRI may be a future research direction. Although clinical implementation should be further established with a larger sample size, this software has presented promising value.

Yang et al. also mentioned in their review of surgical treatment options in gliomas, the augmented reality (AR) neuronavigation system, which integrates MR/CT images into the surgical field and presents three-dimensional virtual tissues to guide resection (31–33).

Cui et al. did bibliometric research on artificial intelligence developments in nervous system diseases. They found "glioma" to be the leading research hotspot, and "machine learning," "brain metastasis," and "gene mutations" were at the research frontier. This result indicated a promising prospect for radiomics biomarkers and multi-omics studies.

3 Histological studies

Hong et al. developed a new confocal laser endomicroscopy with a "Lissajous scanning pattern." In *in vitro* and ex vivo experiments, they demonstrated its feasibility for indocyanine green (ICG) fluorescence-guided brain tumor diagnosis. Through direct tumor cell visualization, confocal laser endomicroscopy (CLE) can reveal tumor cell invasion in the adjacent normal brain and display the tumor-brain interface. Zhang et al. reviewed the latest research on Raman spectroscopy (RS) in glioma. RS is a label-free imaging method that uses intrinsic biochemical markers to identify tumors (34, 35) and has the advantages of being non-destructive, rapid and accurate. Presently, the above two techniques for histological tests are used for resected human tissue. Both methods can be equipped with miniaturized hand-held probes, so they can potentially test *in vivo* tumor tissue, offering guidance on the range of resection. However, their respective safety and accuracy should be further evaluated.

In summary, the 11 studies included in this Research Topic included advances in surgical approaches from various aspects, and future progress in this realm can be anticipated.

Author contributions

HB and CJ wrote the manuscript. HB revised the manuscript. All authors contributed to the article and approved the submitted version.

Conflict of interest

The authors declare that the research was conducted in the absence of any commercial or financial relationships that could be construed as a potential conflict of interest.

Publisher's note

References

1. Duffau H. Stimulation mapping of white matter tracts to study brain functional connectivity. *Nat Rev Neurol* (2015) 11:255–65. doi: 10.1038/nrneurol.2015.51

2. Gogos AJ, Young JS, Morshed RA, Hervey-Jumper SL, Berger MS. Awake glioma surgery: technical evolution and nuances. *J Neurooncol* (2020) 147:515–24. doi: 10.1007/s11060-020-03482-z

3. Fukui A, Muragaki Y, Saito T, Nitta M, Tsuzuki S, Asano H, et al. Impact of awake mapping on overall survival and extent of resection in patients with adult diffuse gliomas within or near eloquent areas: a retrospective propensity score-matched analysis of awake craniotomy vs. general anesthesia. *Acta Neurochir (Wien)* (2022) 164:395–404. doi: 10.1007/s00701-021-04999-6

4. Pichierri A, Bradley M, Iyer V. Intraoperative magnetic resonance imaging-guided glioma resections in awake or asleep settings and feasibility in the context of a public health system. *World Neurosurg X* (2019) 3:100022. doi: 10.1016/j.wnsx.2019.100022

5. Gerritsen JKW, Arends L, Klimek M, Dirven CMF, Vincent AJE. Impact of intraoperative stimulation mapping on high-grade glioma surgery outcome: a metaanalysis. *Acta Neurochir (Wien)* (2019) 161:99–107. doi: 10.1007/s00701-018-3732-4

6. Lima GLO, Dezamis E, Corns R, Rigaux-Viode O, Moritz-Gasser S, Roux A, et al. Surgical resection of incidental diffuse gliomas involving eloquent brain areas. rationale, functional, epileptological and oncological outcomes. *Neurochirurgie* (2017) 63:250–8. doi: 10.1016/j.neuchi.2016.08.007

7. Staub-Bartelt F, Radtke O, Hänggi D, Sabel M, Rapp M. Impact of anticipated awake surgery on psychooncological distress in brain tumor patients. *Front Oncol* (2022) 11:795247/PDF. doi: 10.3389/FONC.2021.795247/PDF

8. Duffau H. Awake mapping with transopercular approach in right insularcentered low-grade gliomas improves neurological outcomes and return to work. *Neurosurgery* (2022) 91:182–90. doi: 10.1227/neu.0000000000001966

9. Gravesteijn BY, Keizer ME, Vincent A, Schouten JW, Stolker RJ, Klimek M. Awake craniotomy versus craniotomy under general anesthesia for the surgical treatment of insular glioma: choices and outcomes. *Neurol Res* (2018) 40(2):87–96. doi: 10.1080/01616412.2017.1402147

10. Chowdhury T, Gray K, Sharma M, Mau C, McNutt S, Ryan C, et al. Brain cancer progression: a retrospective multicenter comparison of awake craniotomy versus general anesthesia in high-grade glioma resection. *J Neurosurg Anesthesiol* (2022) 34:392–400. doi: 10.1097/ANA.0000000000000778

11. Siebner H, Rothwell J. Transcranial magnetic stimulation: new insights into representational cortical plasticity. *Exp Brain Res* (2003) 148:1–16. doi: 10.1007/s00221-002-1234-2

12. Takakura T, Muragaki Y, Tamura M, Maruyama T, Nitta M, Niki C, et al. Navigated transcranial magnetic stimulation for glioma removal: prognostic value in motor function recovery from postsurgical neurological deficits. *J Neurosurg* (2017) 127:877–91. doi: 10.3171/2016.8.JNS16442

13. Frey D, Schilt S, Strack V, Zdunczyk A, Rösler J, Nraula B, et al. Navigated transcranial magnetic stimulation improves the treatment outcome in patients with brain tumors in motor eloquent locations. *Neuro Oncol* (2014) 16:1365–72. doi: 10.1093/neuonc/nou110

14. Aonuma S, Gomez-Tames J, Laakso I, Hirata A, Takakura T, Tamura M, et al. A high-resolution computational localization method for transcranial magnetic stimulation mapping. *NeuroImage* (2018) 172:85–93. doi: 10.1016/j.neuroimage.2018.01.039

15. Raffa G, Quattropani MC, Germanò A. When imaging meets neurophysiology: the value of navigated transcranial magnetic stimulation for preoperative neurophysiological mapping prior to brain tumor surgery. *Neurosurgical Focus* (2019) 47:E10. doi: 10.3171/2019.9.FOCUS19640

16. Mandonnet E, De Witt Hamer P, Poisson I, Whittle I, Bernat AL, Bresson D, et al. Initial experience using awake surgery for glioma: oncological, functional, and employment outcomes in a consecutive series of 25 cases. *Neurosurgery* (2015) 76:382–9. doi: 10.1227/NEU.0000000000000644

17. Moritz-Gasser S, Herbet G, Maldonado IL, Duffau H. Lexical access speed is significantly correlated with the return to professional activities after awake surgery for low-grade gliomas. *J Neuro-Oncol* (2012) 107:633–41. doi: 10.1007/s11060-011-0789-9

18. Racine CA, Li J, Molinaro AM, Butowski N, Berger MS. Neurocognitive function in newly diagnosed low-grade glioma patients undergoing surgical resection with awake mapping techniques. *Neurosurgery* (2015) 77:371–9. doi: 10.1227/NEU.0000000000000779

19. Duffau H. Is non-awake surgery for supratentorial adult low-grade glioma treatment still feasible? *Neurosurg Rev* (2018) 41:133–9. doi: 10.1007/s10143-017-0918-9

20. Mainio A, Hakko H, Timonen M, Niemela A, Koivukangas J, Rasanen P. Depression in relation to survival among neurosurgical patients with a primary brain tumor: a 5-year follow-up study. *Neurosurgery* (2005) 56:1234–41. doi: 10.1227/01.neu.0000159648.44507.7f

21. Litofsky NS, Farace E, Anderson FJr, Meyers CA, Huang W, Laws ERJr. Depression in patients with high-grade glioma: results of the glioma outcomes project. *Neurosurgery* (2004) 54:358–66. doi: 10.1227/01.neu.0000103450.94724.a2

22. Gathinji M, McGirt MJ, Attenello FJ, Chaichana KL, Than K, Olivi A, et al. Association of preoperative depression and survival after resection of malignant brain astrocytoma. *Surg Neurol* (2009) 71:299–303. doi: 10.1016/j.surneu.2008.07.016

23. Jiang C, Wang J. Post-traumatic stress disorders in patients with low-grade glioma and its association with survival. *J Neurooncol* (2019) 142:385–92. doi: 10.1007/s11060-019-03112-3

24. Chen Z, Wang G, Jiang C. Post-traumatic stress symptoms (PTSS) in patients with cushing's disease before and after surgery: a prospective study. *J Clin Neurosci* (2019) 66:1–6. doi: 10.1016/j.jocn.2019.05.059

25. Jensen KK, Henriksen NA, Jorgensen LN. Endoscopic component separation for ventral hernia causes fewer wound complications compared to open components separation: a systematic review and meta-analysis. *Surg Endosc* (2014) 28:3046–52. doi: 10.1007/s00464-014-3599-2

26. Shabanzadeh DM, Sorensen LT. Laparoscopic surgery compared with open surgery decreases surgical site infection in obese patients: a systematic review and meta-analysis. *Ann Surg* (2012) 256:934–45. doi: 10.1097/SLA.0b013e318269a46b

27. Ogura K, Tachibana E, Aoshima C, Sumitomo M. New microsurgical technique for intraparenchymal lesions of the brain: transcylinder approach. *Acta Neurochir* (2006) 148:779–85. doi: 10.1007/s00701-006-0768-7

28. Kassam AB, Engh JA, Mintz AH, Prevedello DM. Completely endoscopic resection of intraparenchymal brain tumors. *J Neurosurg* (2009) 110:116–23. doi: 10.3171/2008.7.JNS08226

29. Senft C, Bink A, Franz K, Vatter H, Gasser T, Seifert V. Intraoperative mri guidance and extent of resection in glioma surgery: a randomised, controlled trial. *Lancet Oncol* (2011) 12:997–1003. doi: 10.1016/S1470-2045(11)70196-6

30. Qiu TM, Yao CJ, Wu JS, Pan ZG, Zhuang DX, Xu G, et al. Clinical experience of 3T intraoperative magnetic resonance imaging integrated neurosurgical suite in shanghai huashan hospital. *Chin Med J (Engl)* (2012) 125:4328–33.

31. Contreras López WO, Navarro PA, Crispin S. Intraoperative clinical application of augmented reality in neurosurgery: a systematic review. *Clin Neurol Neurosurg* (2019) 177:6–11. doi: 10.1016/j.clineuro.2018.11.018

32. Deng W, Li F, Song Z. Easy-to-use augmented reality neuronavigation using wireless tablet PC. *Stereotact Funct Neurosurg* (2014) 92:17–24. doi: 10.1159/000354816

33. Mahvash M, Tabrizi LB. A novel augmented reality system of image projection for image-guided neurosurgery. *Acta Neurochir* (2013) 155:943–7. doi: 10.1007/s00701-013-1668-2

34. Hansen RW, Pedersen CB, Halle B, Korshoej AR, Schulz MK, Kristensen BW, et al. Comparison of 5-aminolevulinic acid and sodium fluorescein for intraoperative tumor visualization in patients with high-grade gliomas: a single-center retrospective study. *J Neurosurg* (2019) 133:1324–31. doi: 10.3171/2019.6.JNS191531

35. Di L, Eichberg DG, Huang K, Shah AH, Jamshidi AM, Luther EM, et al. Stimulated raman histology for rapid intraoperative diagnosis of gliomas. *World Neurosurg* (2021) 150:e135–43. doi: 10.1016/j.wneu.2021.02.122

frontiers | Frontiers in Oncology

TYPE Review
PUBLISHED 05 January 2023
DOI 10.3389/fonc.2022.1086643

OPEN ACCESS

EDITED BY
Zhifeng Shi,
Fudan University, China

REVIEWED BY
Mitchel Berger,
University of California, San Francisco, United States
Xiaolei Chen,
People's Liberation Army General Hospital, China

*CORRESPONDENCE
Xuan Chen
chen_xuan@jlu.edu.cn

†These authors have contributed equally to this work

SPECIALTY SECTION
This article was submitted to Neuro-Oncology and Neurosurgical Oncology, a section of the journal Frontiers in Oncology

RECEIVED 01 November 2022
ACCEPTED 05 December 2022
PUBLISHED 05 January 2023

CITATION
Zhang Y, Yu H, Li Y, Xu H, Yang L, Shan P, Du Y, Yan X and Chen X (2023) Raman spectroscopy: A prospective intraoperative visualization technique for gliomas.
Front. Oncol. 12:1086643.
doi: 10.3389/fonc.2022.1086643

Raman spectroscopy: A prospective intraoperative visualization technique for gliomas

Yi Zhang†, Hongquan Yu†, Yunqian Li, Haiyang Xu, Liu Yang, Peilin Shan, Yuejiao Du, Xiaokai Yan and Xuan Chen*

Department of Neurosurgery, The First Hospital of Jilin University, Changchun, Jilin, China

The infiltrative growth and malignant biological behavior of glioma make it one of the most challenging malignant tumors in the brain, and how to maximize the extent of resection (EOR) while minimizing the impact on normal brain tissue is the pursuit of neurosurgeons. The current intraoperative visualization assistance techniques applied in clinical practice suffer from low specificity, slow detection speed and low accuracy, while Raman spectroscopy (RS) is a novel spectroscopy technique gradually developed and applied to clinical practice in recent years, which has the advantages of being non-destructive, rapid and accurate at the same time, allowing excellent intraoperative identification of gliomas. In the present work, the latest research on Raman spectroscopy in glioma is summarized to explore the prospect of Raman spectroscopy in glioma surgery.

KEYWORDS

Raman spectroscopy, glioma, intraoperative, SERS, SRH, EOR

1 Introduction

Glioma is one of the most common malignant brain tumors with a high mortality rate and a low chance of cure. Currently, the treatments for gliomas consist of surgery (usually the most optimal treatment), chemotherapy (mostly alkylating agents such as temozolomide), radiation therapy, and tumor treating fields (TTFields) which is a more promising treatment modality. Over the past 20 years, neurosurgeons have constantly pursued the safety of maximizing the extent of resection (EOR) for the surgical treatment of gliomas, which has a critical impact on patient prognosis which refers to overall survival and progression-free survival etc. A growing number of studies have demonstrated the association between EOR and patient prognosis, which present that maximized EOR achieves a dramatic improvement

in patient survival compared to partial resection (1–5). The infiltrative growth of glioma leads to unclear tumor boundaries and the complex relationship between tumor growth locations and important functional areas in the brain, are the most major factors affecting EOR in actual surgery for glioma, and improving the capability to recognize tumor boundaries is a relatively more plausible option. Current auxiliary methods for identifying tumor boundaries involve intraoperative fluorescence-guided microsurgery, intraoperative MRI (iMRI), intraoperative ultrasound (IOUS), intraoperative neuronavigation, and intraoperative frozen section, but there is a lack of a method that can simultaneously perform with high accuracy, rapidity, and non-invasiveness.

Raman spectroscopy (RS) is a technique that has been increasingly used in tumor detection over the past 20 years. Inelastic scattering occurs following the interaction of incident light with a material, where a small fraction of photons absorb or lose energy and change wavelength, and this process of a change in wavelength is called the Raman effect (6). Such a feature allows Raman spectroscopy to identify the chemical composition patterns of the corresponding samples. Several studies have used Raman spectroscopy in animals (7–9) and human samples (10–12) for chemical composition patterns to distinguish tumor from normal brain tissue, with excellent performance results similar to the accuracy of pathology. Moreover, the Rapidity and non-invasive properties of Raman spectroscopy also enable its potential as an intraoperative inspection method to improve the EOR of glioma surgery, so as to improve surgical outcomes and promote patient prognosis (13–15). Numerous studies have reported the applicability of Raman spectroscopy in the diagnosis of several tumors, which include colorectal cancer (16), breast cancer (17), nasopharyngeal carcinoma (18), skin cancer (19, 20), gastric cancer (21), and prostate cancer (22), etc. These studies show the prospect of Raman spectroscopy as a novel surgical adjunct to assist in the diagnosis of tumors, and the prominence of Raman spectroscopy in the diagnosis of these tumors and its specific properties - non-invasive, rapid, and accurate - makes it potentially capable of supporting neurosurgeons in the rapid identification of glioma boundaries during surgery (8, 23, 24).

The present work focuses on the advantages of Raman spectroscopy and its current applications in the diagnosis and treatment of glioma, to summarize and analyze the auxiliary role offered by Raman spectroscopy in glioma surgery. In conjunction with the recent research progress, it is expected that Raman spectroscopy might be able to provide a new perspective for neurosurgeons, that is, there is a technique that allows a surgeon to conveniently, rapidly and accurately capture the properties of tissues within the surgical field, which means that Raman spectroscopy is able to provide the power to rapidly identify tumor tissues intraoperatively so that patients can have better benefit from surgery. Meanwhile, we also integrate the latest research about Raman spectroscopy in glioma application and prospect the future development in glioma surgery.

2 Application of Raman spectroscopy in tumor

Raman spectroscopy, a spectroscopic technique consisting of a frequency-changing inelastic scattering caused by a change in the vibrational or rotational energy levels of molecules when a fixed monochromatic light is incident on a medium, was discovered by Indian physicist C. V. Raman in 1928, compared another one is constant frequency Rayleigh scattering caused by elastic collisions (6, 25). Raman spectroscopy was first used by Tashibu in 1990 to analyze the water content in normal and edematous brain tissue of rats by measuring the CH and OH groups (26). Subsequent studies have gradually overcome the low signal-to-noise ratio and low sensitivity of the earlier technique in recent years with the development of optical and data processing techniques, and studies using the technique to identify tumor cells on postoperative Formalin-fixed paraffin-embedded (FFPE) pathology sections have gradually emerged (15, 27). Latest studies have also utilized intraoperative frozen pathology sections (14), intraoperative fresh tissue blocks (28), and *in situ* tissue in the operative area (11, 29) for the identification and diagnosis of gliomas, while data processing techniques such as machine learning and deep learning have also been used to enhance the accuracy of Raman techniques (30–32).

Since the composition of nucleic acids, proteins and lipids in tumor cells are dramatically different from normal brain cells, while Raman spectroscopy is able to identify the chemical composition of a sample by measuring the Raman shift caused by the difference between the frequency of the scattered light and incident light in the Raman effect (33), as Ji reported that glioma and normal brain tissues have significantly different spectral peaks at 1080 cm-1 (nucleic acid), 2845 cm-1 (lipid) and 2930 cm-1 (protein) positions (34). Instead, the differences just depend on their chemical group, independent of the excitation wavelength, while the intensity of Raman peaks is related to the excitation light wavelength, power and concentration of the measured substance (35), so the Raman spectroscopy have the possibility to evaluate tumors and normal tissues according to the differences (Figure 1) (12). Currently, the major diagnostic methods for glioma in clinical practice include imaging and pathology, and imaging primarily covers CT, MRI and PET. CT serves merely as a way to screen for tumors, whereas MRI is a more reliable way to assess the properties of tumors. MRI is based on the nuclear magnetic resonance (NMR), according to the different attenuation of the energy released in different structural environments within the material, the position and type of atomic nuclei of the object can be learned through the

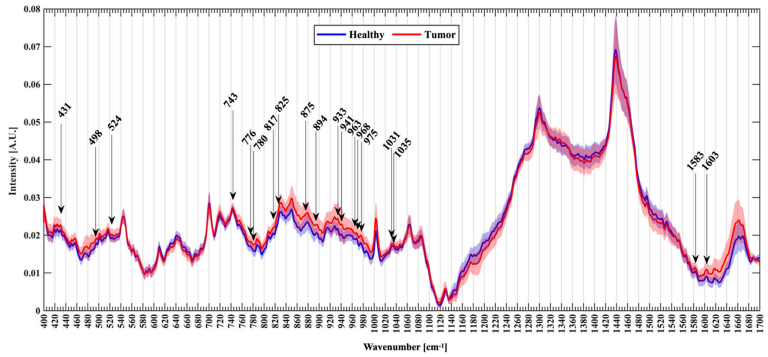

FIGURE 1
An example of Raman spectroscopy shows normalized mean spectra with standard deviation between healthy (blue) and tumor patients (red). Arrows mark the new Raman peaks about glioma identified by the researcher (28).

detection of the emitted electromagnetic waves by the applied gradient magnetic field, and the internal structure of the object can be visualized accordingly (36), nevertheless, MRI is an indirect method to determine the morphology and properties of tumors, without a satisfactory sensitivity and specificity. PET, a new imaging method that has developed rapidly in recent years, labels the tumor-specific metabolic substances with radioisotopes to judge the properties and morphology of tumors *via* the metabolic characteristics of intracranial occurrences by using the metabolic characteristics of tumors. The current gold standard pathology for tumor diagnosis consists of formalin fixation of intraoperatively resected tissues, paraffin embedding and staining of sections, followed by microscopic view of cellular staining, morphology, size, arrangement pattern and other cytological features to make a diagnosis, which relies on the subjective judgment of experienced senior pathologists. Consequently, the complexity of the process and the requirement for experienced pathologists contributes to a time-consuming approach to pathology diagnosis; additionally, biomarkers are typically detected in other tumors, which are not as widely available in gliomas due to factors like the blood-brain barrier. The high sensitivity of Raman spectroscopy to the detected substances provides accurate results, and the detection time of only tens of seconds greatly boosts the efficiency of detection.

Despite the high sensitivity and accuracy of Raman spectroscopy, the Raman signal received by the device is remarkably weak since only one ten-millionth of the photons will produce the Raman effect. Meanwhile, a lot of factors in the environment will influence the final acquisition result, thus various Raman signal enhancement methods have been developed, such as Resonance Raman spectroscopy (RRS), surface-enhanced Raman spectroscopy (SERS), tip-enhanced Raman spectroscopy (TERS) and stimulated Raman spectroscopy (SRS) etc. (35) One of the most sensitive detection modalities is SERS, which can enhance the Raman signal by 10^6 - 10^14 times and increase the detection level to single molecules, except that a metal surface or metal nanoparticle surface is required (37, 38). Other Raman imaging techniques useful for intraoperative glioma surgery are coherent anti-Stokes Raman scattering (CARS) microscopy and stimulated Raman histology (SRH). CARS and SRS are coherent Raman imaging that coherently affects the Raman effect of a specific chemical bond by emitting a second light source to increase the signal intensity. SRH is the only Raman spectroscopy method approved by the FDA for now, which uses SRS to generate virtual imaging of fresh tissue whose imaging quality approximates H&E section images (39). Raman shift is the part of the Raman effect that varies in frequency, and whose common range is 400-3500 cm-1. The results of Raman spectroscopy can be divided into the Raman fingerprint region (FP, 400-1800 cm-1), the high wavenumber region (HW, 2,800-3,200 cm-1), and the intermediate region according to wavenumber. In most studies, simultaneous acquisition of the FP and HW regions has shown a higher value, which means the Raman results should be analyzed focusing on the 400-1800 and 2800-3200 cm-1 (40, 41), and should increase the integration time as much as possible instead of increasing the laser power (42).

Raman spectroscopy plays a role in the detection of many cancers, and some studies have exploited the high sensitivity of Raman spectroscopy to chemical components to detect colorectal cancer through liquid biopsies and endoscopy with direct access to the lesion (16). As in gastric cancer, which is similar to colorectal cancer, studies have applied Raman spectroscopy to diagnose gastric cancer through tissue removed during surgery or endoscopic biopsy, besides being able to analyze patients with gastric cancer *in situ* in real time using fiber optic probes (21, 35). Raman spectroscopy in breast cancer is dominantly performed from breast samples, including

handheld Raman probes for tissue classification and assessment of surgical margins (17). Since skin cancer lesions usually lie on the surface of the body and facilitate Raman spectroscopy, several studies examined skin cancer biopsy specimens for Raman detection to improve the time and convenience needed to confirm the properties of the excised tissue intraoperatively, as well as the strict requirement to expand the extent of excised tumor for reasons similar to the aesthetic needs arising from the excision of facial tumors, where Raman spectroscopy is used to confirm the properties of the edge of the surgical resection area as much as possible intraoperatively (19, 20). The successful application of Raman spectroscopy in tumors mentioned above and others for instance nasopharyngeal carcinoma (18) and prostate cancer (22) reveals that Raman spectroscopy accepted a wide range of biological samples thanks to its highly sensitive features than the other detection means. The applications of Raman spectroscopy in the diagnosis and treatment of glioma include tumor tissue (43), in which typically tumor cells have higher protein and less lipid, and the fingerprint profile of chemicals that are different for tumor and normal tissues can be targeted to distinguish the properties of a given tissue. Brain-tumor margin tissue can be depicted by SRH, CARS and other methods as a virtual image, and then delineate the tumor margin at the cellular level by pre-trained predictive models (44). As a result of the presence of altered microenvironment around the tumor, Raman can also indirectly identify tumors based on the changes in the chemical composition of the body fluids, e.g., the pH value is generally lower in the microenvironment around the tumor (29, 45). The blood of tumor patients commonly exhibits elements from tumors like exosomes, and Raman provides an indirect indication of the presence of tumors by working with it (46). *In-situ* tissue in the operative area (11), which is one of the most prospective developments in surgery, Raman directly measures the molecular composition signatures of the *in-situ* tissue in the operative area by fiber optic probe, then offer an answer for tumor or not through pre-trained prediction algorithms, providing the operator with a decision aid on whether or not the tissue of the operative area should be extended for resection during the surgery.

3 Raman spectroscopy for glioma resection

The most common adjuncts applied in glioma surgery today range from intraoperative fluorescence-guided microsurgery, intraoperative MRI (iMRI), intraoperative ultrasound (IOUS), intraoperative neuronavigation, and intraoperative frozen section. Intraoperative MRI is a technique that has been developed over the past 20 years to evaluate the EOR during surgery by using the MRI machine installed in the operating room after eliminating factors that may affect the MRI machine in the operating room (47), but it must be designed before the construction of the operating room in order to install perfectly the intraoperative MRI, besides, the time and environmental requirements of the examination have limited the popularity of this technique. More rapid depiction of Raman spectroscopy in the operative area versus intraoperative MRI allows results to be reported within tens of seconds, and Raman detection equipment has better mobility than MRI equipment, requiring less environmental requirements for use without special operating room planning before. Intraoperative ultrasound is considered a simple and inexpensive surgical adjunct, as it is a cheaper device than MRI and the probe can be deployed intraoperatively, and the detection time is instant, but limitations of the ultrasound technology itself mean that its sensitivity for residual tumor identification is poor and dependent on an experienced surgeon. With relatively inexpensive detection equipment and slightly slower detection speed than ultrasound, Raman spectroscopy has superior sensitivity and specificity for tumor tissue identification. Intraoperative neuronavigation is usually performed by preoperative high-resolution MRI, and the patient's head is fixed relative to the navigation markers in preoperative preparation, and then the exact position of the probe in the patient's head is displayed on the screen in real-time by locating the probe position intraoperatively after position information is registered. Intraoperative navigation offers high accuracy and timely feedback on the location of the probe, but the cerebrospinal fluid released during brain surgery will result in the relative position of the brain tissue to the registration point changes or drifts, which leads to the position indicated by the intraoperative navigation no longer be accurate and thus the relationship between the location of the probe and the tumor can no longer be determined. Raman spectroscopy does not be affected by the intraoperative drift problem as the samples located *in situ* tissues or removed from the tissues of operative area intraoperatively. Intraoperative fluorescence-guided microsurgery aims to indicate the location of the tumor intraoperatively by injecting fluorescent contrast agents such as 5-aminolevulinic acid (5-ALA) or fluorescein sodium into the patient intraoperatively or preoperatively, taking advantage of the fact that glioma would disrupt the blood-brain barrier and therefore induces the fluorescent agent to be trapped and accumulated in the tumor. In contrast, Raman spectroscopy is a label-free method that does not require the addition of drugs to label the tumor. Although the intraoperative frozen section is an intraoperative adjunct providing the pathology of the excised tissues to the surgeon, due to the high water content of the brain tissue and the softness of the tissue, the Intraoperative frozen section for gliomas is frequently confused by the morphology of the tissues, which prevents the pathologist from reaching a more valid conclusion. With Raman spectroscopy, it is possible to achieve intraoperative results in just a few tens of seconds, while keeping the accuracy close to that of postoperative FFPE pathology (11, 48–50). In summary, Raman spectroscopy as an

intraoperative technique has the great advantages of being more rapid, label-free, accurate, and non-invasive than current intraoperative diagnostic methods.

3.1 Raman spectroscopy for intraoperative fresh tissue determination of glioma

One of the most common and direct applications of Raman spectroscopy is to examine the intraoperatively obtained tissue directly, and the results derived in this way represent the actual intraoperative situation of the tissue more directly and better than FFPE samples. A prospective study in 2022 carried out direct Raman imaging on 29 freshly collected ex vivo brain tissue samples, each of which was split into 2-4 mm and examined for pathology, and finally, the results were trained by machine learning algorithms as a predictive model that could classify tumors from normal tissue with an accuracy of 89.8%, sensitivity of 84.9%, and specificity of 92.3%, as well as LGG and normal tissue with an accuracy of 86.2%, sensitivity of 91.3%, and specificity of 81.2% (Figure 2) (30). By analyzing a total of 3450 spectral results from 63 fresh glioma samples, Riva et al. identified 19 Raman shifts specific to glioma, whereby the predictions could reach 82% precision (28). A study has proposed that the effect of Raman spectroscopy is superior to the value derived from 5-ALA, while Livermore's team created a model by samples from actual patients following a PCA-LDA machine learning approach and compared the predictive effect of 23 samples taken from 8 patients during surgery with 5-ALA, where each sample was confirmed under the microscope to confirm 5-ALA, showing that Raman spectroscopy (1.00 sensitivity, 1.00 specificity, and 1.00 accuracy) was significantly better than 5-ALA (0.07 sensitivity, 1.00 specificity, and 0.24 accuracy ($p = 0.0009$)) for prediction of glioma (27).

From the above study, it is clear that the power of Raman spectroscopy to differentiate glioma from normal brain tissue is robust when augmented by simple machine learning algorithms compared to current intraoperative adjuncts like intraoperative fluorescence-guided microsurgery. According to the high precision identification of glioma by Raman spectroscopy, surgeons can obtain the properties of the intraoperative

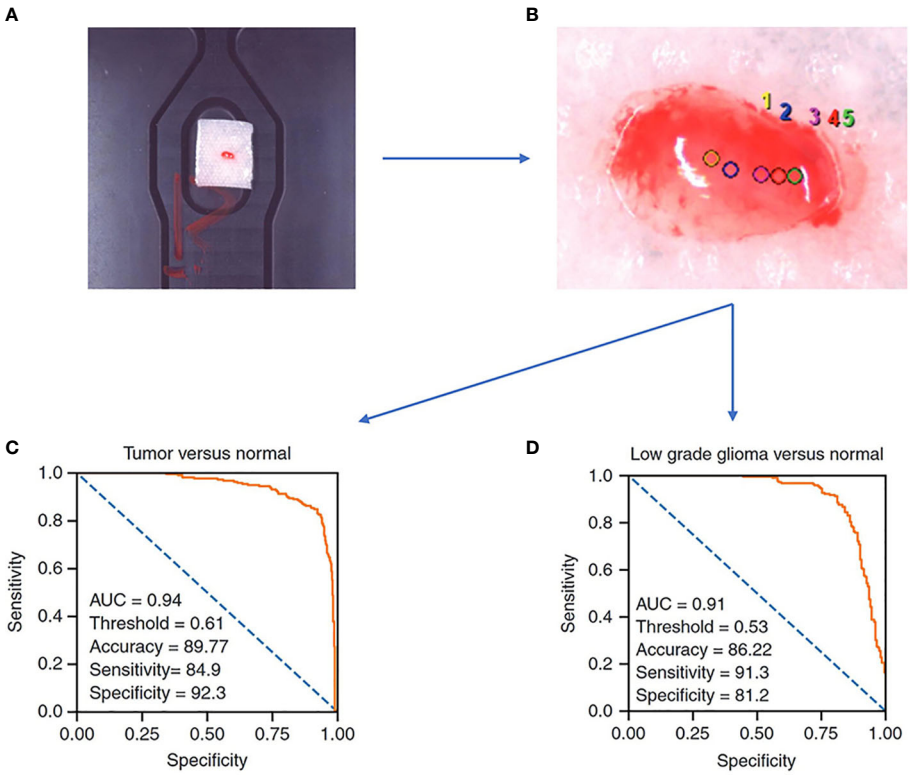

FIGURE 2
A Raman spectroscopy study examines freshly collected ex vivo brain tissue and achieves good results with a predictive model constructed by machine learning algorithms. **(A)** samples of size 2-4 mm in length, width, and height are needed. **(B)** Selection of sites for Raman spectroscopy. **(C)** ROC curve of a trained logistic regression model to identify tumor and normal brain tissue. **(D)** ROC curve of a trained logistic regression model to identify low grade glioma and normal brain tissue (30).

excised tissue by subjecting it to rapid inspection to determine whether the tissue at the current point of interest in the operative area is tumor or normal tissue for further surgical decisions. Raman spectroscopy of intraoperatively extracted tissues requires minimal operator effort, has little impact on the present surgical procedure. Simultaneously, RS is a more preferable way of detection with fresh tissue retaining the most original information. But correspondingly, the Raman detection which is usually to predict the type of tissue extracted by pre-training the model yields limited results and lacks more information to make judgments such as virtual staining.

3.2 Stimulated Raman histology for rapid intraoperative diagnosis of gliomas

Typically, the Raman effect is so weak that the detection equipment is often subject to various external disturbances. Coherent Raman spectroscopy was born as an attempt to enhance the Raman effect, which affects the Raman effect of a specific chemical bond by a second incident beam of light coherently, increasing the signal intensity. SRH builds on the technology of Raman spectroscopy to generate virtual tissue imaging of slices so that the results of Raman spectroscopy are no longer limited to just being a classifier, instead, providing more information such as the cellular morphology, arrangement, and structure of the tissue. Hollon's team demonstrated in a large sample multicenter, prospective clinical trial (n = 278) that the diagnostic accuracy of SRH-based images is consistent with that of pathologists for conventional histological images (overall accuracy, 94.6% vs. 93.9%) (51). After training on 2.5 million SRH images using convolutional neural networks (CNN), a neural network structure widely used in image recognition and inspection, the team applied the model in the operating room to predict brain tumors, and the model could distinguish not only tumor tissue with high accuracy but even the main histopathological classification of brain tumors, in addition to identifying tumor infiltrates from SRH images. In a later study, Hollon's team enhanced the SRH technique with fiber optic laser imaging in 35 patients with recurrent glioma, after which the resulting SRH images were trained using a CNN, and finally, the trained model was applied to a retrospective cohort to score a diagnostic accuracy of 95.8% (Figure 3) (52). This demonstrates how more advanced algorithms combined with more advanced Raman imaging techniques can play a significant role in the diagnosis of gliomas, not only by achieving intraoperative accuracy similar to that of conventional pathological diagnosis but also by producing results in an order of magnitude faster than intraoperative frozen section, making it more promising as a novel method that can join or even replace existing intraoperative assist techniques. Another study conducted a blinded, prospective cohort study in 21 patients with central nervous system (CNS) tumors, investigating the differences in accuracy and diagnostic time between conventional pathology and Raman spectroscopy, found no significant differences in diagnostic accuracy between the methods (P = 1.00) and a significantly shorter mean time to diagnosis (TTD) for SRH-based diagnosis than frozen sections (43 min versus 9.7 min, P < 0.0001) (12). This study illustrates that Raman spectroscopy reduces the time required for diagnosis significantly while maintaining a high level of accuracy, and has great advantages in neurosurgery, by comparing the SRH-based diagnostic method with the traditional gold standard diagnostic method of frozen sections and FFPE sections.

The breakthrough of SRH in glioma surgery is far more exciting, as it broadens the use of Raman spectroscopy, enabling RS not only to distinguish tumor tissue from normal tissue but also to present Raman-detected results in the form of images, not only to overcome some of the shortcomings encountered in the intraoperative frozen section but also more fully exploit the characteristics of Raman spectroscopy for the detection of samples with high sensitivity, which enables pathologists to open the third eye in the existing diagnostic process of the intraoperative frozen section, thus improving the diagnostic ability and further promoting the EOR of glioma surgery. This approach provides the surgeon with more accurate and detailed visualization of the tumor boundary than the Section 3.1 approach. However, SRH still requires further processing of the sample and cannot immediately image the tissue removed intraoperatively, so its usefulness remains to be explored.

3.3 More convenient handheld Raman spectroscopy

Because of the optical path design and other reasons in Raman spectroscopy equipment, most detection devices are designed to be larger, and the detection method also usually requires a series of steps that the samples need to be placed on the detection table. Although such complex operation logic ensures that it will not affect the patient itself, it still requires removing the tissue from the surgery and trimming it to the right size before putting it into the device for detection, which invariably prolongs the detection time and may lead to the risk of removing more normal tissues caused by edge uncertainty. These issues in the research process will probably not pose a serious impact, but if Raman technology is expected to become clinical tool, it must possess features that can be easily operated by neurosurgeons. Based on the optical properties of Raman spectroscopy, some works have been done to solve the above problems of complex operation logic by designing fiber optic probes, and some practical applications have been made. Evaluation of the feasibility and accuracy of handheld Raman spectroscopy devices as an intraoperative neuronavigation adjunct was performed on a dog model (9). Eleven tumor

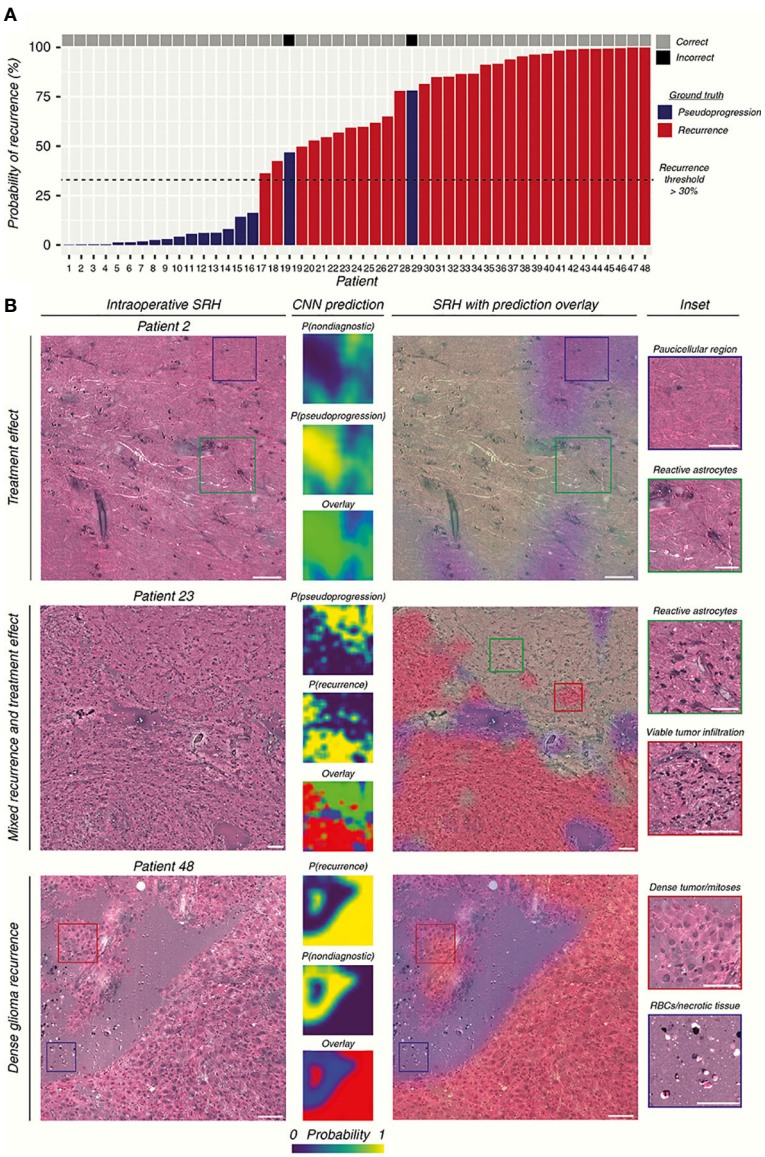

FIGURE 3
The researchers used CNN to construct the prediction model by SRH images. **(A)** The prediction results of the SRH-based prediction model are demonstrated. **(B)** SRH images and CNN probability heatmaps. The model was able to correctly identify pseudoprogression, tumor recurrence, and infiltrative glioma. Scale bars = 50 μm (52).

resection and intraoperative handheld Raman devices were examined on 11 dog models, and Raman signals were collected using the handheld devices in direct contact with the intraoperative tissue, and pathology was determined for the sample sites, finally, the results showed that the handheld device had a sensitivity of 85.7% and specificity of 90% with a positive predictive value of 92.3% and negative predictive value of 81.6% compared to pathology. These efforts validate the feasibility of using handheld devices in neurosurgery by providing rapid intraoperative results for the operator's reference with comparable accuracy to gold standard pathology. Apart from that, it would be a great help for surgery if the tumor border location could be provided to the operator intraoperatively through a handheld device. A handheld macro Raman imaging system was reported to be designed for detecting tissue edge features, and the team concluded that it is necessary to work on a detection system with a larger field of view for tumor margin detection in hand (23). In this project, they conducted experiments on the fat and muscle tissues of pigs and trained the classifier with the obtained

data using machine learning methods, which resulted in an *in vitro* validation result of 99% accuracy and plotting the boundary probabilities by the phenomenon that the classifier is found to decrease the prediction rate at the junction of fat and muscle tissues. What's more interesting is that a study found that tumor infiltration was still detected 3.7-2.4 cm outside the MRI-determined tumor border with 92% accuracy, 92% sensitivity, and 93% specificity (53), using a fiber-optic probe in direct contact with the brain at the edge of the resection cavity in surgery with a handheld Raman imaging system during a total acquisition time of 0.2 seconds per measurement (Figure 4). The results were evaluated by H&E section pathology, and the effect of the handheld RS device was undoubted to improve the surgical outcome and prolong patient survival.

Compared to the Raman spectroscopy method described in Section 3.1, there is no visible difference in the accuracy of the handheld Raman spectroscopy method, but the handheld Raman spectroscopy device significantly improves the convenience for surgeons to use during surgery. These portable handheld Raman spectroscopy systems address the complexities of previous studies that require sample isolation and avoid patient harm. These portable handheld Raman spectroscopy systems address the complexities of previous studies that require sample isolation and avoid patient harm. Combined with the relatively small size of the device, fast acquisition time, and high accuracy, RS is a convenient way for neurosurgeons to detect tissue properties in the operative area, identify tumor cell margins and infiltrations, provide guidance for surgical procedures, and improve EOR compared to other intraoperative detection methods, and has great potential to serve as a new method to supplement or even replace existing intraoperative tumor margin detection methods. Unfortunately, the interaction between the incident laser and brain tissue needs to be taken into account when handheld Raman devices are used intraoperatively to assist the operator in analyzing the properties of the resected sample. Generally, Raman spectroscopy is considered to be harmless to humans, but the potential long-term damage to brain tissue from repeated applications over a long period of time is not known, so the safety and necessity of RS before widespread use in the clinic needs to be further explored (17).

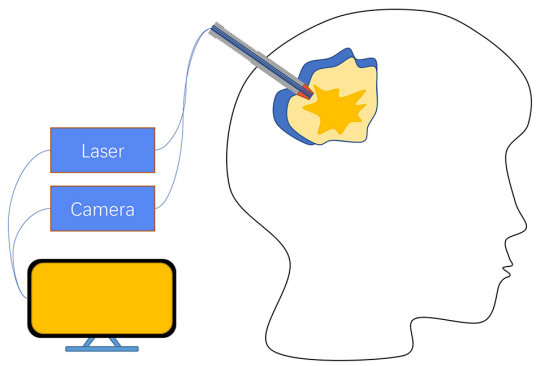

FIGURE 4
A hand-held fiber optic probe consists of a laser emitter connected to a spectral detector, with data acquisition ultimately controlled by a PC. The illumination and detection light paths are spatially coincident. When the probe performs measurements, it is in direct contact with the brain at the resection edge (53).

3.4 Unprecedented rapid intraoperative molecular detection

Based on the 2016 WHO classification system of the CNS, glioma could be classified as followed: lower grade glioma (LGG) with isocitrate dehydrogenase (IDH) mutation with or without 1p/19q-codel, LGG with IDH-wildtype subtype, glioblastoma multiforme (GBM) with IDH mutation or not (54). IDH and other molecular biomarkers have become a critical part of the glioma diagnosis and treatment process. As Raman spectroscopy is excellent in discriminating substances, a few works have been conducted on the ability of Raman spectroscopy to distinguish IDH subtypes in glioma biopsies with 2073 Raman spectroscopic results taken from 38 samples, using the eXtreme Gradient Boosted trees (XGB) and Support Vector Machine with Radial Basis Function kernel (RBF-SVM) to perform the classification task and found 52 different Raman shifts between IDH-mut and IDH-wt groupings, which shifts representing lipids, collagen, DNA and cholesterol/phospholipids, with a final accuracy of 87% (14). Further studies have predicted glioma IDH subtypes by a simple PCA-LDA method on fresh tissue samples from 62 patients, achieving 91% sensitivity and 95% specificity (Figure 5) (55). Moreover, subtype differentiation by differences in protein profiles (498, 826, 1003, 1174, and 1337 cm-1 were selected) between different molecular subtypes of glioma (n = 36) was also studied with a likewise high accuracy rate of 89% (43).

Given the high sensitivity of Raman spectroscopy for the detection of samples, Raman spectroscopy is playing an increasing role in the diagnosis and treatment of glioma in the future as molecular biology becomes a growing involvement in glioma. The ability of Raman spectroscopy to rapidly assess the molecular biology of glioma samples during surgery provides the operator with a three-dimensional understanding of the possible grading and staging of glioma, and then adjusts the EOR according to the degree of malignancy to achieve a better treatment prognosis. The application of Raman spectroscopy in glioma surgery is a unique approach to intraoperative adjuncts commonly used in clinical practice, as it can provide the operator with long postoperative molecular typing detection in near real-time, which is a novel approach for gliomas whose malignancy cannot be easily identified intraoperatively.

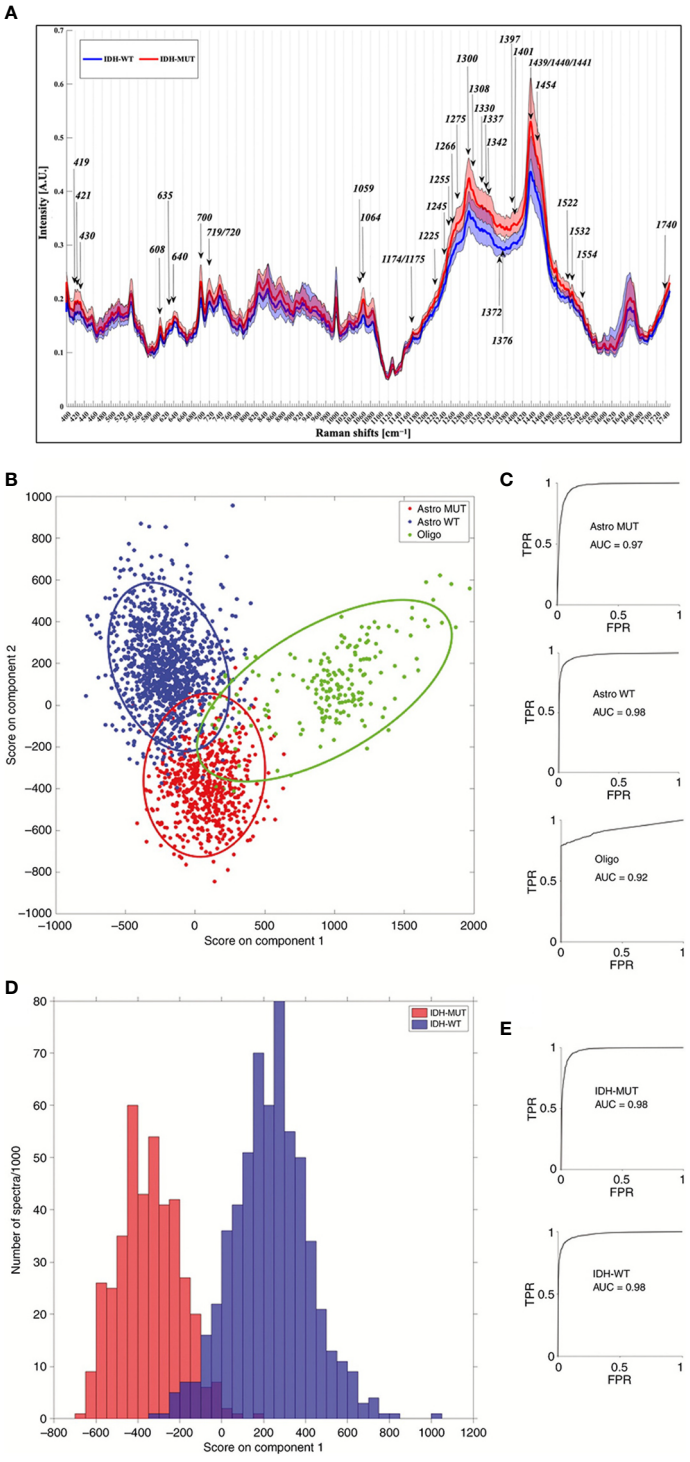

FIGURE 5
(A) Results of one study for IDH-WT and IDH-MUT, with arrows representing the most discriminant peaks with a known biological assignment. **(B–E)** are the 3-group model and 2-group model, respectively, of another study for molecular typing of gliomas based on Raman spectroscopy results. (TPR = true positive rate; FPR = false positive rate; Astro MUT = Astroglial tumor isocitrate dehydrogenase IDH-mutant; Astro WT = Astroglial tumor, IDH-wild-type; Oligo = Oligodendroglioma) (14, 55).

4 The development direction of Raman spectroscopy

Raman spectroscopy can be safely used in clinical practice owing to the fast, accurate, non-invasive, and label-free features that enable it to be performed without more interaction with the patient's body. Yet, the Raman effect is very weak considering that the photons producing the Raman effect are merely one ten-millionth of the incident light, and the weak interference in the environment will affect the final imaging results. Coherent Raman techniques such as SRS and CARS can significantly increase the Raman signal intensity, but a more sensitive SERS technique can amplify the Raman effect by $10^{6\text{-}10}14$ times through a metal surface, even to the resolution of single molecules (56). Besides, the huge amount of data generated per second by the high resolution of Raman spectroscopy render more advanced data processing techniques necessary. Nowadays, concerning the results of Raman detection, except for the traditional statistical methods such as principal component analysis (PCA), partial least squares (PLS), linear discriminant analysis (LDA), etc. to find the differences between glioma and normal brain tissue (27, 31, 51, 55), machine learning algorithms such as k-nearest neighbors (KNN), support vector machine (SVM), random forest (RF) and eXtreme Gradient Boosting (XGB) are quite often adopted to perform classification and prediction (14, 57–59). With the hot trend of neural network algorithms over the past few years, a growing number of deep learning algorithms have been trained to predict Raman detection results, commonly available methods include convolutional neural networks (CNN), artificial neural networks (ANN), etc. (32, 52) While hot new frameworks such as long short-term memory (LSTM) and Transformer (60, 61) also have application potential in targeting Raman detection results, the new algorithms can be expected to give us more surprises in predicting.

4.1 Ultra-high sensitivity Raman spectroscopy method brings new visions

SERS was developed to enhance the Raman scattering of molecules from nanostructured materials, allowing the detection of very low levels of material, even individual molecules, through a proton-mediated enhancement effect (56), and the extremely high sensitivity making SERS important for the intraoperative detection of gliomas. A SERS probe with a detection limit of 5 pM in an aqueous solution was reported to be developed to delineate tumor invasion margins by a time-distance function on a mouse glioma xenograft model using extravasation in the tumor vasculature of the probe, and resection experiments were performed with the aid of handheld Raman scanning equipment (8). The experimental procedure resembled intraoperative fluorescence-guided surgery, which ultimately improved the overall survival rate of the rat model compared to normal resection and possessed a detection accuracy of pM precision than fluorescent methods such as 5-ALA. The Warburg effect refers to the tendency of tumors to metabolize anaerobically, which is reflected in the large amount of lactic acid produced by tumors during the metabolic process (62). The SERS technique has been used to define tumor boundaries by preparing a SERS substrate 4-mercaptopyridine (4-MPY) to detect changes in pH around the target based on the Warburg effect, which introduces gliomas produce large amounts of lactic acid that cause their microenvironmental pH to drop and appear acidic, and 4-MPY is a type of silver nanoparticle with different SERS peak characteristics at different pH values (29). In follow-up work, the team did the same thing using U87 cells grown in mice. Building on the same characterization of the tumor microenvironment as acidic, a study was conducted in animal experiments to develop a SERS-based surgical navigation system to identify tumor boundaries, which was detected by transferring metabolites from tumor resection margins to a PH-sensitive SERS chip (45). According to the research, the overall survival of animal models operated under this surgical navigation system was dramatically increased, but unfortunately, exogenous probes were not used in the study due to approval issues by the drug supervision authority (45).

The ultra-sensitivity of SERS permits the detection of gliomas from a wider range of angles, such as more accurate biomarker results for intraoperative samples of gliomas. Whereas the need to prepare nano-metals limits its use in humans, we can still access patient samples from other angles, such as blood (63) to evaluate the postoperative outcome of glioma patients, as well as the routine screening of normal people. Because of the SERS technology advances and the indications for nanometals in humans continue to expand over time, it is expected that SERS will accomplish greater improvements in intraoperative glioma guidance.

4.2 Raman spectroscopy desires a better data processing method

Whether using Raman spectroscopy as a method of glioma identification or intraoperative generation of virtual tissue images, or as an intraoperative aid to the operator, one needs to face the large amount of data generated by Raman spectroscopy, and how to use these Raman data to get better-expected results is a part that needs attention. Generally speaking, Raman spectroscopy results are obtained in two forms, one is the result of molecular composition information

represented by Raman shift raw data, and the other is the result of virtual images generated by SRH, CARS, etc. In recent studies, the most popular way of analyzing the data collected by Raman spectroscopy in glioma continues to be the dimensionality reduction approach with PCA, PLS, and LDA (27, 31, 51, 55). Taking the data collected by Raman spectroscopy and extracting the main differences by which tumors and normal cells can be distinguished, these studies often achieve excellent accurateness thanks to the inherent high sensitivity of Raman spectroscopy. In order to further improve the accuracy of Raman spectroscopy and make the new technology more acceptable to clinicians, a number of studies set out to process the data from Raman spectroscopy using popular machine learning methods, and some currently growing neural network algorithms have been added to the processing of Raman spectroscopy results. Some scholars reduced the dimensionality of the data by PLS and PCA, after which the principal components were selected using four methods, Relief-F, Pearson correlation coefficient (PCC), F-score (FS) and term variance (TV), and finally, back propagation neural network (BP), linear discriminant analysis (LDA) and support vector machine (SVM) classification models were established (58); Sciortino et al. used eXtreme Gradient Boosted trees (XGB) and a support vector machine with Radial Basis Function kernel (RBF-SVM) to evaluate classification performance (14, 59), with a LOO approach to achieve a balanced trade-off between performance and robustness; Stables employed three methods, SVM, KNN and LDA, to classify glioma samples (57); Another scholar has focused on feature engineering to develop a new representation specifically for brain diagnosis while retaining as much information as possible to improve prediction accuracy (31); Jermyn argues that ANNs can overcome the aspect of spectral artifacts generated by lights in operating rooms using nonparametric and adaptive models, reducing the changes required in neurosurgical workflows for Raman spectroscopy detection thereby simplifying the barriers to intraoperative use of Raman spectroscopy (32); CNNs, which excelled in the image field, were also trained to recognize SRH images to detect recurrent gliomas (52); and deep learning models based on simulated annealing algorithms were also applied to deal with the Raman spectroscopy detection results of gliomas (64).

All these efforts have revealed enormous value in the study of Raman spectroscopy of glioma, effectively boosting the predictive ability of Raman spectroscopy for glioma, creating a new direction for future efforts to improve the application of Raman spectroscopy, and enhancing the value of Raman spectroscopy applications. However, it is undesirable to create excessive reliance on algorithms and attempt to take care of all the problems of inaccurate results arising from external factors such as sampling, environment, and improper usage through algorithms. A proper approach should be to ensure the accuracy and standardization of each step in the data acquisition process as much as possible, minimize the interference brought by the outside world, and finally improve the robustness by multiple sampling or upgrading the algorithm. Thanks to the rapid development of deep learning in recent years, more algorithms can be applied to the processing of Raman spectroscopy in the future, such as Transformer and LSTM, both of which do not seem to have been applied to the data processing of Raman spectroscopy in glioma (60, 61), the potential of the algorithm in improving the accuracy of Raman spectroscopy detection is still wide.

5 Conclusion and future perspectives

Today, various clinical techniques are available to assist in the EOR of glioma surgery, but they are limited in terms of invasiveness, speed of detection, and accuracy, which slow down the improvement in the EOR of glioma surgery. Raman spectroscopy, however, has excellent characteristics that make it possible to identify tumor margins in glioma surgery while being non-invasive, fast, and accurate. Raman spectroscopy not only compensates for the shortcomings of current intraoperative adjuncts but also enables the detection and understanding of glioma at the molecular level, while the research of fiber optic probes also gives Raman spectroscopy a broader scope of application. But some problems still exist in the application of Raman spectroscopy in glioma, firstly, the sample acquisition, most of the Raman detection devices need to transfer the intraoperative tissues to the detection devices for detection, and SRH technology needs to detect and image the slices. Secondly, Raman spectroscopy results cover a large amount of raw data, and it is still a proposition worth exploring how to extract the key from the huge amount of data and how to enhance the data processing algorithm to improve the accuracy. Additionally, the Raman effect requires a certain power of incident light as the excitation, and SERS and other Raman techniques demand the assistance of nanomaterials, all of which need to be in contact with the patient's brain tissue, and the potential safety hazards brought by these operations should be strictly evaluated to avoid secondary injuries to patients. Precisely speaking, Raman spectroscopy has a most attractive prospect in glioma surgery, and there is a steady stream of research on the application of Raman spectroscopy in glioma, suggesting that Raman spectroscopy will one day become the most commonly used intraoperative adjunct technique in clinical practice.

Author contributions

YZ and HY contributed equally to write the original manuscript and should be considered co-first authors. YL and HX provided suggestions for revisions. LY, PS, YD and XY provided pictures and critical revisions. XC reviewed and edited the manuscript. All authors contributed to the article and approved the submitted version.

Funding

Project of Jilin Provincial Department of Education, JJKH20211155KJ.

Conflict of interest

The authors declare that the research was conducted in the absence of any commercial or financial relationships that could be construed as a potential conflict of interest.

Publisher's note

All claims expressed in this article are solely those of the authors and do not necessarily represent those of their affiliated organizations, or those of the publisher, the editors and the reviewers. Any product that may be evaluated in this article, or claim that may be made by its manufacturer, is not guaranteed or endorsed by the publisher.

References

1. Bloch O, Han SJ, Cha S, Sun MZ, Aghi MK, McDermott MW, et al. Impact of extent of resection for recurrent glioblastoma on overall survival: clinical article. *J Neurosurg* (2012) 117(6):1032–8. doi: 10.3171/2012.9.JNS12504

2. Coburger J, Merkel A, Scherer M, Schwartz F, Gessler F, Roder C, et al. Low-grade glioma surgery in intraoperative magnetic resonance imaging: Results of a multicenter retrospective assessment of the German study group for intraoperative magnetic resonance imaging. *Neurosurgery* (2016) 78(6):775–86. doi: 10.1227/NEU.0000000000001081

3. Fukui A, Muragaki Y, Saito T, Maruyama T, Nitta M, Ikuta S, et al. Volumetric analysis using low-field intraoperative magnetic resonance imaging for 168 newly diagnosed supratentorial glioblastomas: Effects of extent of resection and residual tumor volume on survival and recurrence. *World Neurosurg* (2017) 98:73–80. doi: 10.1016/j.wneu.2016.10.109

4. Lacroix M, Abi-Said D, Fourney DR, Gokaslan ZL, Shi W, DeMonte F, et al. A multivariate analysis of 416 patients with glioblastoma multiforme: prognosis, extent of resection, and survival. *J Neurosurg* (2001) 95(2):190–8. doi: 10.3171/jns.2001.95.2.0190

5. McGirt MJ, Chaichana KL, Gathinji M, Attenello FJ, Than K, Olivi A, et al. Independent association of extent of resection with survival in patients with malignant brain astrocytoma. *J Neurosurg* (2009) 110(1):156–62. doi: 10.3171/2008.4.17536

6. Raman CV, Krishnan KS. A new type of secondary radiation. *Nature* (1928) 121(3048):501–2. doi: 10.1038/121501c0

7. Soltani S, Guang Z, Zhang Z, Olson J, Robles F. Label-free detection of brain tumors in a 9L gliosarcoma rat model using stimulated raman scattering-spectroscopic optical coherence tomography. *J BioMed Opt* (2021) 26(7):076004. doi: 10.1117/1.JBO.26.7.076004

8. Han L, Duan W, Li X, Wang C, Jin Z, Zhai Y, et al. Surface-enhanced resonance raman scattering-guided brain tumor surgery showing prognostic benefit in rat models. *ACS Appl Mater Interfaces* (2019) 11(17):15241–50. doi: 10.1021/acsami.9b00227

9. Doran CE, Frank CB, McGrath S, Packer RA. Use of handheld raman spectroscopy for intraoperative differentiation of normal brain tissue from intracranial neoplasms in dogs. *Front Vet Sci* (2021) 8:819200. doi: 10.3389/fvets.2021.819200

10. Di L, Eichberg DG, Park YJ, Shah AH, Jamshidi AM, Luther EM, et al. Rapid intraoperative diagnosis of meningiomas using stimulated raman histology. *World Neurosurg* (2021) 150:e108–16. doi: 10.1016/j.wneu.2021.02.097

11. Hollon T, Stummer W, Orringer D, Suero Molina E. Surgical adjuncts to increase the extent of resection: Intraoperative MRI, fluorescence, and raman histology. *Neurosurg Clin N Am* (2019) 30(1):65–74. doi: 10.1016/j.nec.2018.08.012

12. Di L, Eichberg DG, Huang K, Shah AH, Jamshidi AM, Luther EM, et al. Stimulated raman histology for rapid intraoperative diagnosis of gliomas. *World Neurosurg* (2021) 150:e135–43. doi: 10.1016/j.wneu.2021.02.122

13. Schipmann S, Schwake M, Suero Molina E, Stummer W. Markers for identifying and targeting glioblastoma cells during surgery. *J Neurol Surg A Cent Eur Neurosurg* (2019) 80(6):475–87. doi: 10.1055/s-0039-1692976

14. Sciortino T, Secoli R, d'Amico E, Moccia S, Conti Nibali M, Gay L, et al. Raman spectroscopy and machine learning for IDH genotyping of unprocessed glioma biopsies. *Cancers (Basel)* (2021) 13(16):4196. doi: 10.3390/cancers13164196

15. Yue Q, Gao X, Yu Y, Li Y, Hua W, Fan K, et al. An EGFRvIII targeted dual-modal gold nanoprobe for imaging-guided brain tumor surgery. *Nanoscale* (2017) 9(23):7930–40. doi: 10.1039/C7NR01077J

16. Noothalapati H, Iwasaki K, Yamamoto T. Non-invasive diagnosis of colorectal cancer by raman spectroscopy: Recent developments in liquid biopsy and endoscopy approaches. *Spectrochim Acta A Mol Biomol Spectrosc* (2021) 258:119818. doi: 10.1016/j.saa.2021.119818

17. Hanna K, Krzoska E, Shaaban AM, Muirhead D, Abu-Eid R, Speirs V. Raman spectroscopy: Current applications in breast cancer diagnosis, challenges and future prospects. *Br J Cancer* (2022) 126(8):1125–39. doi: 10.1038/s41416-021-01659-5

18. Lin K, Zheng W, Lim CM, Huang Z. Real-time *In vivo* diagnosis of nasopharyngeal carcinoma using rapid fiber-optic raman spectroscopy. *Theranostics* (2017) 7(14):3517–26. doi: 10.7150/thno.16359

19. Zhao J, Zeng H, Kalia S, Lui H. Using raman spectroscopy to detect and diagnose skin cancer in vivo. *Dermatol Clin* (2017) 35(4):495–504. doi: 10.1016/j.det.2017.06.010

20. Araújo DC, Veloso AA, de Oliveira Filho RS, Giraud MN, Raniero LJ, Ferreira LM, et al. Finding reduced raman spectroscopy fingerprint of skin samples for melanoma diagnosis through machine learning. *Artif Intell Med* (2021) 120:102161. doi: 10.1016/j.artmed.2021.102161

21. Kawabata T, Mizuno T, Okazaki S, Hiramatsu M, Setoguchi T, Kikuchi H, et al. Optical diagnosis of gastric cancer using near-infrared multichannel raman spectroscopy with a 1064-nm excitation wavelength. *J Gastroenterol* (2008) 43(4):283–90. doi: 10.1007/s00535-008-2160-2

22. Kast RE, Tucker SC, Killian K, Trexler M, Honn KV, Auner GW. Emerging technology: applications of raman spectroscopy for prostate cancer. *Cancer Metastasis Rev* (2014) 33(2–3):673–93. doi: 10.1007/s10555-013-9489-6

23. Daoust F, Nguyen T, Orsini P, Bismuth J, de Denus-Baillargeon MM, Veilleux I, et al. Handheld macroscopic raman spectroscopy imaging instrument for machine-learning-based molecular tissue margins characterization. *J BioMed Opt* (2021) 26(2):022911. doi: 10.1117/1.JBO.26.2.022911

24. Jermyn M, Mok K, Mercier J, Desroches J, Pichette J, Saint-Arnaud K, et al. Intraoperative brain cancer detection with raman spectroscopy in humans. *Sci Transl Med* (2015) 7(274):274ra19. doi: 10.1126/scitranslmed.aaa2384

25. *Raman spectroscopy. in: Wikipedia* (2022). Available at: https://en.wikipedia.org/w/index.php?title=Raman_spectroscopy&oldid=1109195559#Theory.

26. Tashibu K. [Analysis of water content in rat brain using raman spectroscopy]. *No To Shinkei* (1990) 42(10):999–1004.

27. Livermore LJ, Isabelle M, Bell IM, Edgar O, Voets NL, Stacey R, et al. Raman spectroscopy to differentiate between fresh tissue samples of glioma and normal brain: a comparison with 5-ALA-induced fluorescence-guided surgery. *J Neurosurg* (2020) 135(2):469–79. doi: 10.3171/2020.5.JNS20376

28. Riva M, Sciortino T, Secoli R, D'Amico E, Moccia S, Fernandes B, et al. Glioma biopsies classification using raman spectroscopy and machine learning models on fresh tissue samples. *Cancers (Basel)* (2021) 13(5):1073. doi: 10.3390/cancers13051073

29. Yang G, Zhang K, Qu X, Xu W, Xu S. Ratiometric pH-responsive SERS strategy for glioma boundary determination. *Talanta* (2022) 250:123750. doi: 10.1016/j.talanta.2022.123750

30. Jabarkheel R, Ho CS, Rodrigues AJ, Jin MC, Parker JJ, Mensah-Brown K, et al. Rapid intraoperative diagnosis of pediatric brain tumors using raman spectroscopy: A machine learning approach. *Neurooncol Adv* (2022) 4(1): vdac118. doi: 10.1093/noajnl/vdac118

31. Lemoine É, Dallaire F, Yadav R, Agarwal R, Kadoury S, Trudel D, et al. Feature engineering applied to intraoperative *in vivo* raman spectroscopy sheds light on molecular processes in brain cancer: a retrospective study of 65 patients. *Analyst* (2019) 144(22):6517–32. doi: 10.1039/c9an01144g

32. Jermyn M, Desroches J, Mercier J, Tremblay MA, St-Arnaud K, Guiot MC, et al. Neural networks improve brain cancer detection with raman spectroscopy in the presence of operating room light artifacts. *J BioMed Opt* (2016) 21(9):94002. doi: 10.1117/1.JBO.21.9.094002

33. Bergholt MS, Zheng W, Ho KY, Teh M, Yeoh KG, Yan So JB, et al. Fiberoptic confocal raman spectroscopy for real-time *in vivo* diagnosis of dysplasia in barrett's esophagus. *Gastroenterology* (2014) 146(1):27–32. doi: 10.1053/j.gastro.2013.11.002

34. Ji M, Orringer DA, Freudiger CW, Ramkissoon S, Lau D, Golby AJ, et al. Rapid, label-free detection of brain tumors with stimulated raman scattering microscopy. (2014) 5(201):201ra119. doi: 10.1126/scitranslmed.3005954

35. Liu K, Zhao Q, Li B, Zhao X. Raman spectroscopy: A novel technology for gastric cancer diagnosis. *Front Bioeng Biotechnol* (2022) 10:856591. doi: 10.3389/fbioe.2022.856591

36. *Magnetic resonance imaging. in: Wikipedia* (2022). Available at: https://en.wikipedia.org/w/index.php?title=Magnetic_resonance_imaging&oldid=1116005571.

37. Kneipp K, Wang Y, Kneipp H, Perelman LT, Itzkan I, Dasari RR, et al. Single molecule detection using surface-enhanced raman scattering (SERS). *Phys Rev LETTERS* (1997) 78(9):4. doi: 10.1103/PhysRevLett.78.1667

38. Nie S, Emory SR. Probing single molecules and single nanoparticles by surface-enhanced raman scattering. *Science* (1997) 275(5303):1102–6. doi: 10.1126/science.275.5303.1102

39. Hollon T, Orringer DA. Label-free brain tumor imaging using raman-based methods. *J Neurooncol* (2021) 151(3):393–402. doi: 10.1007/s11060-019-03380-z

40. Lin K, Wang J, Zheng W, Ho KY, Teh M, Yeoh KG, et al. Rapid fiber-optic raman spectroscopy for real-time *In vivo* detection of gastric intestinal metaplasia during clinical gastroscopy. *Cancer Prev Res (Phila)* (2016) 9(6):476–83. doi: 10.1158/1940-6207.CAPR-15-0213

41. Zhou X, Dai J, Chen Y, Duan G, Liu Y, Zhang H, et al. Evaluation of the diagnostic potential of ex vivo raman spectroscopy in gastric cancers: fingerprint versus high wavenumber. *J BioMed Opt* (2016) 21(10):105002. doi: 10.1117/1.JBO.21.10.105002

42. Chen H, Li X, Broderick NGR, Xu W. Low-resolution fiber-optic raman spectroscopy for bladder cancer diagnosis: A comparison study of varying laser power, integration time, and classification methods. *J Raman Spectroscopy* (2020) 51(2):323–34. doi: 10.1002/jrs.5783

43. Uckermann O, Yao W, Juratli TA, Galli R, Leipnitz E, Meinhardt M, et al. IDH1 mutation in human glioma induces chemical alterations that are amenable to optical raman spectroscopy. *J Neurooncol* (2018) 139(2):261–8. doi: 10.1007/s11060-018-2883-8

44. Einstein EH, Ablyazova F, Rosenberg A, Harshan M, Wahl S, Har-El G, et al. Stimulated raman histology facilitates accurate diagnosis in neurosurgical patients: a one-to-one noninferiority study. *J Neurooncol* (2022) 159(2):369–75. doi: 10.1007/s11060-022-04071-y

45. Jin Z, Yue Q, Duan W, Sui A, Zhao B, Deng Y, et al. Intelligent SERS navigation system guiding brain tumor surgery by intraoperatively delineating the metabolic acidosis. *Adv Sci (Weinh)* (2022) 9(7):e2104935. doi: 10.1002/advs.202104935

46. Jalali M, Isaac Hosseini I, AbdelFatah T, Montermini L, Wachsmann Hogiu S, Rak J, et al. Plasmonic nanobowtiefluidic device for sensitive detection of glioma extracellular vesicles by raman spectrometry. *Lab Chip* (2021) 21(5):855–66. doi: 10.1039/D0LC00957A

47. Wirtz CR, Bonsanto MM, Knauth M, Tronnier VM, Albert FK, Staubert A, et al. Intraoperative magnetic resonance imaging to update interactive navigation in neurosurgery: Method and preliminary experience. *Comput Aided Surg* (1997) 2 (3–4):172–9. doi: 10.3109/10929089709148110

48. Orillac C, Stummer W, Orringer DA. Fluorescence guidance and intraoperative adjuvants to maximize extent of resection. *Neurosurgery* (2021) 89 (5):727–36. doi: 10.1093/neuros/nyaa475

49. Brahimaj BC, Kochanski RB, Pearce JJ, Guryildirim M, Gerard CS, Kocak M, et al. Structural and functional imaging in glioma management. *Neurosurgery* (2021) 88(2):211–21. doi: 10.1093/neuros/nyaa360

50. Garzon-Muvdi T, Kut C, Li X, Chaichana KL. Intraoperative imaging techniques for glioma surgery. *Future Oncol* (2017) 13(19):1731–45. doi: 10.2217/fon-2017-0092

51. Hollon TC, Pandian B, Adapa AR, Urias E, Save AV, Khalsa SSS, et al. Near real-time intraoperative brain tumor diagnosis using stimulated raman histology and deep neural networks. *Nat Med* (2020) 26(1):52–8. doi: 10.1038/s41591-019-0715-9

52. Hollon TC, Pandian B, Urias E, Save AV, Adapa AR, Srinivasan S, et al. Rapid, label-free detection of diffuse glioma recurrence using intraoperative stimulated raman histology and deep neural networks. *Neuro Oncol* (2021) 23 (1):144–55. doi: 10.1093/neuonc/noaa162

53. Jermyn M, Desroches J, Mercier J, St-Arnaud K, Guiot MC, Leblond F, et al. Raman spectroscopy detects distant invasive brain cancer cells centimeters beyond MRI capability in humans. *BioMed Opt Express BOE* (2016) 7(12):5129–37. doi: 10.1364/BOE.7.005129

54. Louis DN, Perry A, Reifenberger G, von Deimling A, Figarella-Branger D, Cavenee WK, et al. The 2016 world health organization classification of tumors of the central nervous system: a summary. *Acta Neuropathol* (2016) 131(6):803–20. doi: 10.1007/s00401-016-1545-1

55. Livermore LJ, Isabelle M, Bell IM, Scott C, Walsby-Tickle J, Gannon J, et al. Rapid intraoperative molecular genetic classification of gliomas using raman spectroscopy. *Neurooncol Adv* (2019) 1(1):vdz008. doi: 10.1093/noajnl/vdz008

56. Han XX, Rodriguez RS, Haynes CL, Ozaki Y, Zhao B. Surface-enhanced raman spectroscopy. *Nat Rev Methods Primers* (2022) 1(1):1–17. doi: 10.1038/s43586-021-00083-6

57. Stables R, Clemens G, Butler HJ, Ashton KM, Brodbelt A, Dawson TP, et al. Feature driven classification of raman spectra for real-time spectral brain tumour diagnosis using sound. *Analyst* (2016) 142(1):98–109. doi: 10.1039/c6an01583b

58. Ma M, Tian X, Chen F, Ma X, Guo W, Lv X. The application of feature engineering in establishing a rapid and robust model for identifying patients with glioma. *Lasers Med Sci* (2022) 37(2):1007–15. doi: 10.1007/s10103-021-03346-6

59. Desroches J, Jermyn M, Pinto M, Picot F, Tremblay MA, Obaid S, et al. A new method using raman spectroscopy for *in vivo* targeted brain cancer tissue biopsy. *Sci Rep* (2018) 8:1792. doi: 10.1038/s41598-018-20233-3

60. Hochreiter S, Schmidhuber J. Long short-term memory. *Neural Comput* (1997) 9(8):1735–80. doi: 10.1162/neco.1997.9.8.1735

61. Vaswani A, Shazeer N, Parmar N, Uszkoreit J, Jones L, Gomez AN, et al. Attention is all you need. In: *Advances in neural information processing systems*. Curran Associates, Inc (2017) 5998–6008. doi: 10.48550/arXiv.1706.03762

62. Vander Heiden MG, Cantley LC, Thompson CB. Understanding the warburg effect: the metabolic requirements of cell proliferation. *Science* (2009) 324(5930):1029–33. doi: 10.1126/science.1160809

63. Dhinakaran AK, Dharmalingam P, Ganesh S, Venkatakrishnan K, Das S, Tan B. Molecular crosstalk between T cells and tumor uncovers GBM-specific T cell signatures in blood: Noninvasive GBM diagnosis using immunosensors. *ACS Nano* (2022) 16(9):14134–48. doi: 10.1021/acsnano.2c04160

64. Sui A, Deng Y, Wang Y, Yu J. A deep learning model designed for raman spectroscopy with a novel hyperparameter optimization method. *Spectrochim Acta A Mol Biomol Spectrosc* (2022) 280:121560. doi: 10.1016/j.saa.2022.121560

frontiers | Frontiers in Oncology

TYPE Original Research
PUBLISHED 13 January 2023
DOI 10.3389/fonc.2022.994054

OPEN ACCESS

EDITED BY
Songbai Xu,
First Affiliated Hospital of Jilin University, China

REVIEWED BY
Francesco Restelli,
IRCCS Carlo Besta Neurological Institute Foundation, Italy
Yuanli Zhao,
Beijing Tiantan Hospital, Capital Medical University, China

*CORRESPONDENCE
Shin-Hyuk Kang
hermes23@kumc.or.kr

†These authors have contributed equally to this work

SPECIALTY SECTION
This article was submitted to Neuro-Oncology and Neurosurgical Oncology, a section of the journal Frontiers in Oncology

RECEIVED 14 July 2022
ACCEPTED 15 December 2022
PUBLISHED 13 January 2023

CITATION
Hong DH, Kim JH, Won J-K, Kim H, Kim C, Park K-J, Hwang K, Jeong K-H and Kang S-H (2023) Clinical feasibility of miniaturized Lissajous scanning confocal laser endomicroscopy for indocyanine green-enhanced brain tumor diagnosis.
Front. Oncol. 12:994054.
doi: 10.3389/fonc.2022.994054

Clinical feasibility of miniaturized Lissajous scanning confocal laser endomicroscopy for indocyanine green-enhanced brain tumor diagnosis

Duk Hyun Hong[1†], Jang Hun Kim[1†], Jae-Kyung Won[2], Hyungsin Kim[1], Chayeon Kim[3], Kyung-Jae Park[1], Kyungmin Hwang[3], Ki-Hun Jeong[4] and Shin-Hyuk Kang[1*]

[1]Department of Neurosurgery, Korea University Hospital, Korea University College of Medicine, Seoul, Republic of Korea, [2]Department of Pathology, Seoul National University Hospital, Seoul National University College of Medicine, Seoul, Republic of Korea, [3]VPIX Medical Inc., Daejeon, Republic of Korea, [4]Department of Bio and Brain Engineering, KAIST Institute for Health Science and Technology (KIHST), Korea Advanced Institute of Science and Technology (KAIST), Seoul, Republic of Korea

Background: Intraoperative real-time confocal laser endomicroscopy (CLE) is an alternative modality for frozen tissue histology that enables visualization of the cytoarchitecture of living tissues with spatial resolution at the cellular level. We developed a new CLE with a "Lissajous scanning pattern" and conducted a study to identify its feasibility for fluorescence-guided brain tumor diagnosis.

Materials and methods: Conventional hematoxylin and eosin (H&E) histological images were compared with indocyanine green (ICG)-enhanced CLE images in two settings (1): experimental study with in vitro tumor cells and ex vivo glial tumors of mice, and (2) clinical evaluation with surgically resected human brain tumors. First, CLE images were obtained from cultured U87 and GL261 glioma cells. Then, U87 and GL261 tumor cells were implanted into the mouse brain, and H&E staining was compared with CLE images of normal and tumor tissues *ex vivo*. To determine the invasion of the normal brain, two types of patient-derived glioma cells (CSC2 and X01) were used for orthotopic intracranial tumor formation and compared using two methods (CLE vs. H&E staining). Second, in human brain tumors, tissue specimens from 69 patients were prospectively obtained after elective surgical resection and were also compared using two methods, namely, CLE and H&E staining. The comparison was performed by an experienced neuropathologist.

Results: When ICG was incubated *in vitro*, U87 and GL261 cell morphologies were well-defined in the CLE images and depended on dimethyl sulfoxide. *Ex vivo* examination of xenograft glioma tissues revealed dense and heterogeneous glioma cell cores and peritumoral necrosis using both methods. CLE images also detected invasive tumor cell clusters in the normal brain of the patient-derived glioma xenograft model, which

corresponded to H&E staining. In human tissue specimens, CLE images effectively visualized the cytoarchitecture of the normal brain and tumors. In addition, pathognomonic microstructures according to tumor subtype were also clearly observed. Interestingly, in gliomas, the cellularity of the tumor and the density of streak-like patterns were significantly associated with tumor grade in the CLE images. Finally, panoramic view reconstruction was successfully conducted for visualizing a gross tissue morphology.

Conclusion: In conclusion, the newly developed CLE with Lissajous laser scanning can be a helpful intraoperative device for the diagnosis, detection of tumor-free margins, and maximal safe resection of brain tumors.

KEYWORDS

brain neoplasm, confocal microscopy, Lissajous scanning, indocyanine green, real-time diagnosis

1 Introduction

Resection of brain tumors improves patient conditions, including reduced mass effect on the brain, prevention of tumor recurrence, and increased patient survival (1–4). However, total tumor removal is not always possible, and increasing the resection area could result in a permanent neurological deficit because it is not easy to determine the normal brain tissue at the tumor interface during a surgical operation. With technological advances, neuronavigation systems and 5-aminolevulinic acid (5-ALA) fluorescence dyes have improved surgical outcomes in tumor resection (5, 6). However, these tools remain insufficient because of the brain shifts and low fluorescence specificity (7). Therefore, direct histological visualization *via* multiple optical biopsies could be performed for proper intraoperative diagnosis, identification of existing remnant tumors, and increased tumor resection (8).

Thus far, the classical tool for intraoperative brain tumor detection has been to obtain frozen section examination. To identify the histological diagnosis and tumor margins, tissue samples were delivered to a pathologist, who then performed frozen tissue preparation for rapid interpretation. This process has several limitations (9, 10). Usually, it requires up to 20 min or longer per sample for diagnosis, thus increasing the operation time (11), and a longer surgical time can cause postoperative complications in cases of multiple tissue examinations (12). In addition, proper diagnosis cannot be achieved in a small tissue sample. Moreover, mechanical tissue disruption due to tumor removal is a non-diagnostic or misleading problem in frozen tissue diagnosis (13). Examination of normal tissue and tumor interfaces sometimes causes irreversible neurological deficits (14). Therefore, the surgical room still requires a more rapid and efficient method to properly diagnose tumors and improve surgical outcomes in patients with gliomas and other brain tumors. It would be greatly advantageous to develop a minimally invasive, real-time, intraoperative tissue diagnostic method.

Intraoperative confocal laser endomicroscopy (CLE) is a novel technology that enables the visualization of living tissue cytoarchitecture with cellular level spatial resolution (15). It was developed for microscopic miniaturization with a handheld probe and for the slide-free imaging of thin planes within the whole tissue. Therefore, minimized CLE can be used to examine freshly excised tissue from patients after staining with biocompatible dyes, such as fluorescein and indocyanine green (ICG). Previous studies have reported the clinical feasibility of diagnosis in various cancers, including gastrointestinal and lung cancers (16, 17). In the field of brain tumor surgery, CLE has been reported to be suitable for clinical applications (18–20). Recently, we developed a handheld CLE in the near-infrared band that is capable of ICG imaging (21, 22). This product can acquire fast and clear images using an ultracompact laser scanner that implements a Lissajous scanning pattern. We acquired *ex vivo* images of various extracted mouse organs, such as the lungs, kidneys, and bladder, from ICG-injected mice without the usual preparation of samples and showed the distinct structures of each organ. These data can be used to evaluate various brain tumor scenarios.

In this study, we examined cell morphology *in vitro* and tissue microstructures *ex vivo* in two glioma cell lines. In addition, tumor invasion into normal tissue was identified in two patient-derived xenograft models using Lissajous scanning CLE. To further evaluate clinical applications for real-time diagnosis, we used freshly resected specimens of various brain tumors for *ex vivo* direct CLE imaging. Hematoxylin and eosin (H&E)-stained images served as the gold standard in all models and were compared with CLE images.

2 Materials and methods

2.1 Patient enrollment and ethics statement

Patients with tumorous conditions in the brain that required surgical resection from January 2021 to June 2022 were included in the study. They consisted of various types of brain tumors such as meningiomas, astrocytomas, pituitary adenomas, and metastatic tumors. All experiments using human tissues were performed with the approval of the Institutional Review Board of Korea University Anam Hospital in strict accordance with the Code of Ethics of the World Medical Association for experiments (approval number: 2019AN0133). Before elective brain tumor surgery, voluntary informed consent was obtained from the patients and their legal guardians after they were fully informed about the study design and that the experiments were conducted using *ex vivo* methods, which is not be potentially harmful to the patients. Patients were excluded if the resected tissue was inadequate for examination by CLE, such as presence of hemorrhagic changes or a small amount of volume <0.0314cm^3 (suspected volume of one-piece tumor tissue *via* stereotactic navigation biopsy system, StealthStation S8, Medtronic, Minneapolis, MN, USA). The flowchart of the study was presented in Figure 1.

2.2 Cell culture

The GL261 mouse glioma cell line and U87 human glioma cell line were cultured in high-glucose Dulbecco's modified Eagle's medium (DMEM; Welgene, Gyeongsan, Republic of Korea) supplemented with 10% fetal bovine serum (Welgene), 100 U/mL penicillin, and 0.1 mg/mL streptomycin in a monolayer culture at 37°C in a humidified atmosphere containing 5% CO_2. Patient-derived glioma stem-like cells, CSC2 and X01, were cultured in a proliferation medium composed of DMEM/F-12, B-27 supplement (Gibco, Waltham, MA, USA), 10 ng/mL recombinant human bFGF (PeproTech, Cranbury, NJ, USA), 20 ng/mL recombinant human EGF (R&D Systems, Minneapolis, MN, USA), 20 U/mL penicillin, and 20 µg/mL streptomycin at 37°C in a humidified atmosphere containing 5% CO_2.

2.3 Tumor implantation

All procedures were conducted in accordance with the guidelines and protocols approved by the Institutional Animal Care and Use Committee of the Korea University College of Medicine (approval number: KOREA-2020-0079). Five- to six-week-old BALB/c nude and C57BL/6 mice were purchased from Orient Bio (Seongnam, Republic of Korea). For intracranial implantation, animals were anesthetized with ketamine (100

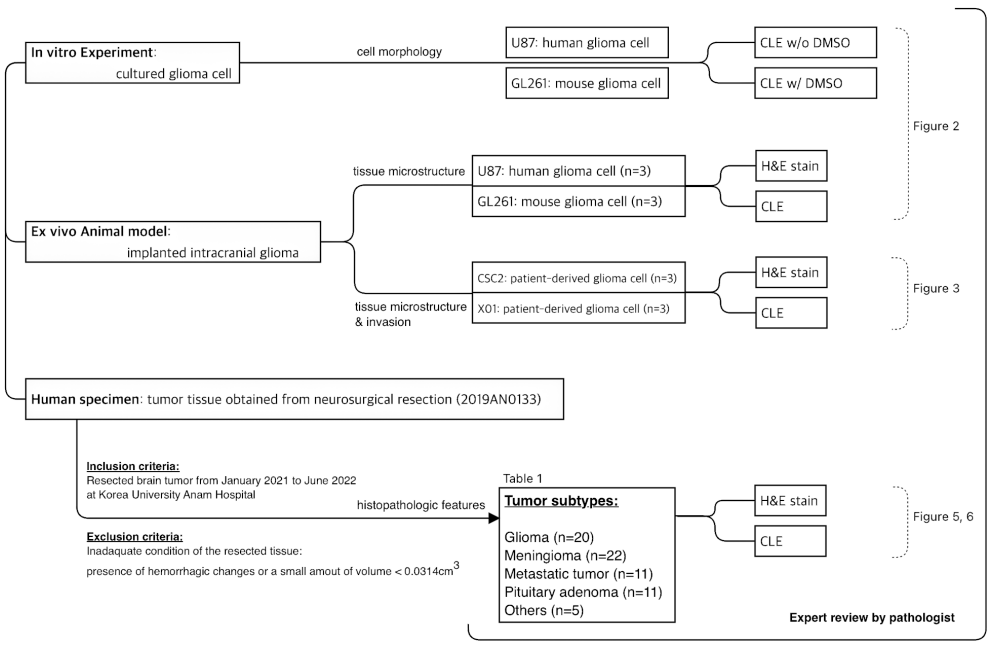

FIGURE 1
The flowchart of the study.

mg/kg) and xylazine (10 mg/kg). A total of 1×10^5 cells in 3 µL of Hanks' balanced salt solution were injected into the brain at a rate of 1 µL/min using a Hamilton syringe controlled by a stereotaxic device (David Kopf Instruments, Tujunga, CA). Coordinates for intracranial inoculation were −0.2 mm anteroposterior, +2.2 mm mediolateral, and −3.5 mm dorsoventral from the bregma.

2.4 Imaging device

A CLE system (cCeLL ex vivo; VPIX Medical, Daejeon, Republic of Korea) was used for histoarchitectural imaging of slide-free whole tissues stained with a fluorescent dye. The cCeLL ex vivo image was based on a 785-nm laser system with a near-infrared filter to detect emissions from 800–860 nm. A microscope head and probe (PixectionTM, VPIX Medical) with an outer diameter of 4 mm directly contacted the patient's tissue and irradiated the tissue with a Lissajous laser-scanning pattern to acquire a tissue image within 100 µm from the surface. The probe scanned patient tissues with 10 frame rates at a field of view (FOV) of 300 µm × 300 µm, corresponding to approximately 660x magnification. The system reconstructed the acquired data as high-quality images of 1024 × 1024 pixels that were saved as images or videos. The probe was also used with a dedicated probe stage for fine movement in the XYZ direction.

2.5 ICG treatment and image acquisition

For image acquisition both *in vitro* and *ex vivo*, ICG (Sigma-Aldrich, St. Louis, MO) fluorescence was used. ICG solvent dissolved in 30% EtOH at a concentration of 0.5 mg/mL was utilized for labelling both cell lines and patient tissue samples. U87MG and GL261 cells were seeded at 5×10^4 cells/well in 12-well plates to 70% confluence on top of sterile glass coverslips. The medium was removed and the cells were washed three times with phosphate-buffered saline (PBS) for 5 min. Cells grown on coverslips were incubated in ICG with or without 10% dimethyl sulfoxide (DMSO) and imaged using CLE.

The mouse brain image acquisition was utilized according to the following methods: intravenous tail injection of ICG before mouse sacrifice or *ex vivo* incubation of the mouse brain into the ICG solution. Intravenously administered mice were injected with 100 µL of ICG solution (0.5 mg/mL) and left for 5 min to allow the full diffusion of ICG. Thereafter, the brains were removed, and a coronal section of the sample was placed at a thickness of 1 cm before CLE was conducted. Similarly, in the ICG incubation group, the tissues were sectioned and placed in a Petri dish for incubation following brain removal. Brain tissue was incubated with 100 µL of ICG solution (0.5 mg/mL) prior to CLE imaging. Excess ICG solution left on the imaging surface of the sample was cleaned with a tissue wiper for optimal image acquisition.

The method used to image the tumor tissues was identical to that used for the mouse brain preparations. Tumor specimen was obtained in the center of the resected tumor and sectioned at a thickness of 1 cm before incubation with 100 µL of ICG solution (0.5 mg/mL) for 5 min. Following incubation, the tissues were cleaned with a tissue wiper to remove excess ICG before imaging with CLE.

2.6 H&E and immunofluorescence staining

After the CLE imaging experiments, tumor tissues corresponding to the imaging site were resected and fixed in 4% formalin. Formalin-fixed and paraffin-embedded sections (4 µm thickness) were prepared for H&E staining. Immunofluorescence (IF) staining was performed on sections fixed in cold methanol for 10 min at -20°C, rinsed in PBS, incubated with primary antibodies, and diluted in PBS containing 1% bovine serum albumin (BSA) and 0.25% Triton X-100 overnight at 4°C. Antibodies against myelin basic protein (MBP, ab40390; Abcam, Cambridge, UK), glial fibrillary acidic protein (z0334; Dako, Glostrup, Denmark), and neurofilament-M (2H3; DSHB, Iowa City, IA) were used. Slides were then incubated with fluorescence-conjugated secondary antibodies and mounted with Vectashield® Hard Set™ mounting medium (Vector Laboratories, Newark, CA) containing 4',6-diamidino-2-phenylindole (DAPI). H&E and immunostained slices were observed using light and fluorescence microscopy (Carl Zeiss, Oberkochen, Germany) and compared with CLE images obtained by an experienced pathologist (JKW).

3 Results

3.1 *In vitro* and *ex vivo* glial tumors of mice

3.1.1 CLE imaging of glial tumor cells and orthotopic tumors

Using the ICG dye on a handheld CLE with special laser scanning called "Lissajous pattern" (cCell, VPIX Medical) (Figure 2A), we first verified the CLE images against U87 and GL261 glioma cell lines in the presence or absence of DMSO. Interestingly, the *in vitro* CLE images showed different patterns depending on the presence of DMSO. In the absence of DMSO, ICG could not penetrate the cells, resulting in a mesh-like shape, in which only the cell membrane was stained. In contrast, in the presence of DMSO, ICG penetrated the cell, and CLE images demonstrated a morphology that is similar to fluorescence immunocytochemical staining, which identifies the nucleus and cell membrane (Figures 2B, C). To reproduce the clinical conditions

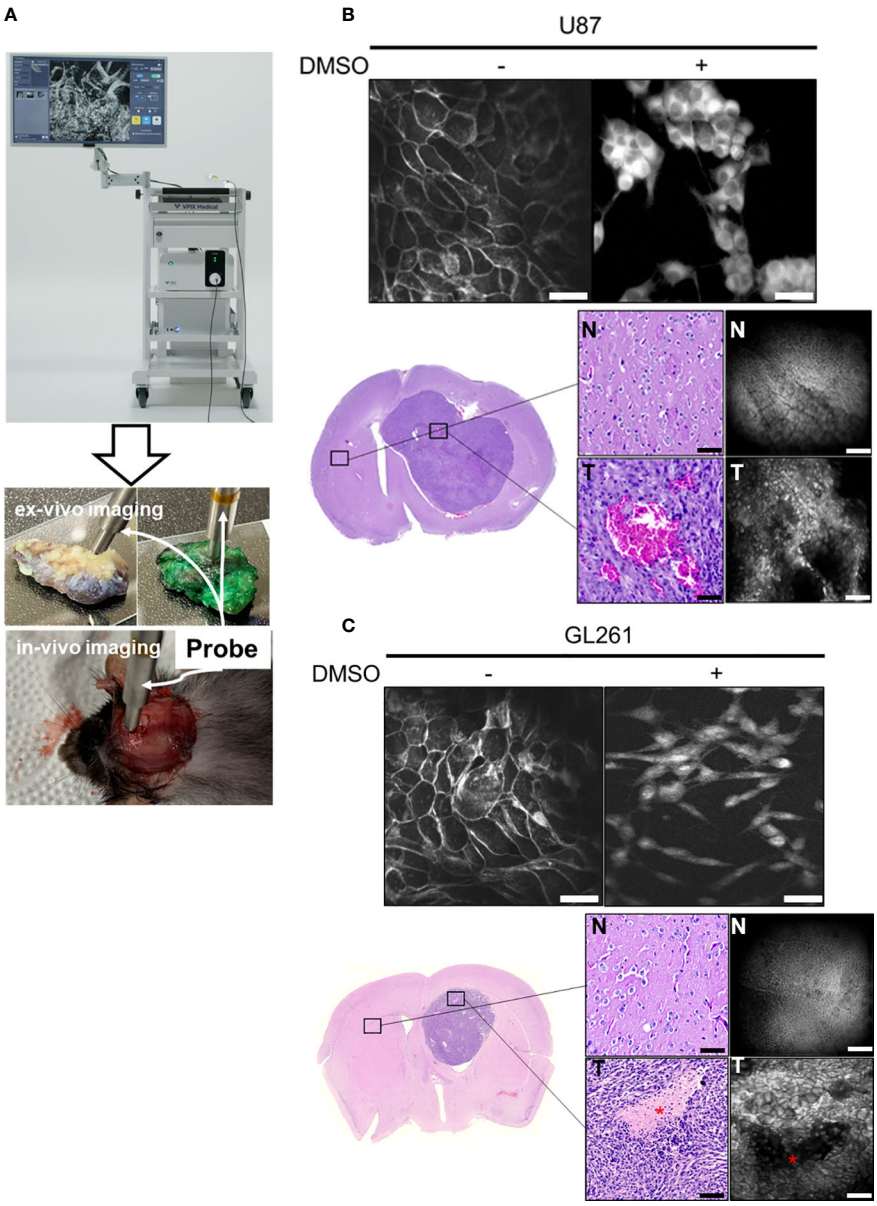

FIGURE 2
CLE systems and photomicrographs of various glioma models **(A)** The Lissajous scanning CLE system consists of an imaging screen, miniaturized probe, and excitation light source. The probe can detect the CLE images of brain tumor tissue both *ex vivo* and *in vivo*. In the current study, only *ex-vivo* imaging was obtained and compared. **(B, C)** Image acquisition of U87 human and GL261 mouse glioma cells was conducted using CLE following incubation with 5 mg/mL indocyanine green (ICG) (upper panel). Cell morphology was examined in the presence/absence of dimethyl sulfoxide (DMSO). In an orthotopic xenograft model, ICG-induced fluorescent imaging and the corresponding H&E stain were obtained at the tumor core and normal brain (lower panel). CLE image shows dense fluorescent neoplastic cells following ICG incubation *ex vivo*. N: normal brain, T: tumor, Asterix: necrosis. Scale bar: 50 μm. H&E = hematoxylin and eosin.

of intraoperative tumor tissue diagnosis, we compared *ex vivo* CLE images with pathological H&E staining using an orthotopic glioma model. U87 human and GL261 mouse glioma cells (1×10^5 cells) were implanted into the brain parenchyma of BALB/c nude mice and C57BL/6 mice, respectively. The mouse brains were removed and cut horizontally, and CLE and H&E staining were performed on the same tissue specimens. The U87 xenograft and GL261 syngeneic gliomas showed variegated and large tumor cells with increased cellularity in the core region, whereas normal brain tissues were found to be relatively homogeneous with sparse cell density (Figures 2B, C). In addition, necrotic areas were observed in both the CLE images and H&E staining (Figure 2C).

3.1.2 Tumor invasion at patient-derived xenograft model

We used an orthotopic mouse model with patient-derived glioma cells to identify tumor invasion adjacent to the normal brain tissue. CSC2 and X01 cells (1×10^5 cells) were implanted into the brain parenchyma of BALB/c nude mice. After 42 days, CLE imaging was performed using the strategy shown in Figure 2B. Surprisingly, at multiple different regions, invasive tumor cells were observed in the dense cell cluster adjacent to normal tissue borders in both CSC2 and X01 orthotopic gliomas (Figures 3A, B and Supplementary Video 1). The tissue morphology and tumor cell infiltration in the CLE images were similar to those observed by histological staining. CLE images demonstrated the same morphological features in CSC2 glioma tissue when ICG was incubated or injected into the tail vein (Supplementary Figure 1).

3.2 Surgically resected human brain tumor tissues

A total of 69 patients were prospectively enrolled in this study, with a mean age of 56.06 years (range: 20–84 years). The detailed tumor subtypes are listed in Table 1.

3.2.1 CLE images and histology in normal brain parenchyma

To identify normal human brain morphology in the CLE images, three normal brain tissues were obtained from regions adjacent to the resected intraparenchymal tumors. ICG (5 mg/mL) incubation was performed after surgical resection, and normal brain specimens were examined *ex vivo* using CLE. To obtain consistent image data, at least 100 images were acquired at multiple locations per tissue sample (Figure 4). In the gray matter, large neuronal cells were identified in the CLE images, similar to those observed with H&E staining (Figure 4A). Compared with the cortical region, glial cells were smaller in size in the subcortical white matter, and a dense streak-like pattern was more frequently observed in the extracellular space, suggesting the presence of myelin fibers (Figure 4B). IF staining of MBP revealed myelination of the brain parenchyma in both the gray and white matter. No autofluorescence was observed in the CLE images when ICG incubation was not performed (data not shown).

3.2.2 Pathognomonic CLE findings according to tumor subtypes

We examined the concordance between CLE images and histological features using H&E staining of patient tumor tissues. As shown in Figure 5 and Supplementary Figures 2–4, various brain tumors have distinct tissue microstructures. The pituitary adenoma showed a salt-and-pepper pattern, in which tumor cells had monomorphic nuclei and granular cytoplasm in histology and CLE images (Figure 5A and Supplementary Video 2). In meningiomas, pathognomonic features of the meningothelial type were observed in both images. Meningiomas, which had unclear cell borders and abundant cytoplasm, demonstrated a sheet or lobular pattern (whorl formation) (Figure 5B, Supplementary Figure 2B and Supplementary Video 3). The CLE and H&E images of the glioblastoma showed overall hypercellularity and atypical features (Figure 5C and Supplementary Figure 3B). Metastatic brain adenocarcinoma also showed a similar pattern in both images, demonstrating atypical cell nests or cord-like structures (Figure 5D and Supplementary Figure 3C). In vestibular schwannoma, low cellularity and a spiral whorl formation were observed in the H&E images, and similar morphological features were also revealed in the CLE images (Figure 5E and Supplementary Figure 2C). Primary central nervous system (CNS) lymphoma had large and atypical basophilic lymphocytes with frequent necrosis in both images (Figure 5F and Supplementary Figure 4A). Histological examination of the choroid plexus papilloma revealed tumor cells containing papillary structures lined by uniform cuboidal or columnar epithelial cells. In CLE images, globular cauliflower-like masses were formed by cuboidal to columnar cells (Figure 5G and Supplementary Figure 4B).

Gliomas originate from glial cells in the brain parenchyma and are classified into different grades based on tumor aggressiveness. To identify whether the tumor grade could be divided into CLE images, we compared the histology with CLE images of normal brain tissues and different gliomas (Figure 6). In the normal brain, glial cells were sparsely distributed on H&E staining, and dense axonal fibers were identified in the IF image of MBP and neurofilaments that exhibited CNS myelination. In addition, dense streak-like axonal patterns were observed in CLE images. In gliomas, tumor cellularity was positively associated with tumor grade on histology and CLE images. In particular, high-grade gliomas had significantly increased cellularity, and the tumor cell distribution was dysmorphic and heterogeneous. Conversely, the amount of MBP and neurofilaments was lower in high-grade gliomas than in low-grade gliomas in IF staining. This pattern also revealed CLE images, in which streak-like patterns were rarely identified in high-grade gliomas.

3.2.3 Panoramic CLE images with 3D depth information

To obtain panoramic cCeLL images of the brain tumor tissue, two consecutive steps were followed: Z-merge and stitching techniques. We reconstructed CLE images using a meningioma tissue sample. First, CLE images cannot always be used to obtain the whole tissue microstructure per image, because the tumor tissue has a 3D structure (Figure 7A, left). To overcome this issue, a series of images of multiple focal planes was captured and merged into one image or Z-merged at each spot with an overlapping area of approximately 30% (Figure 7A, right). In addition, the FOV of the CLE images is

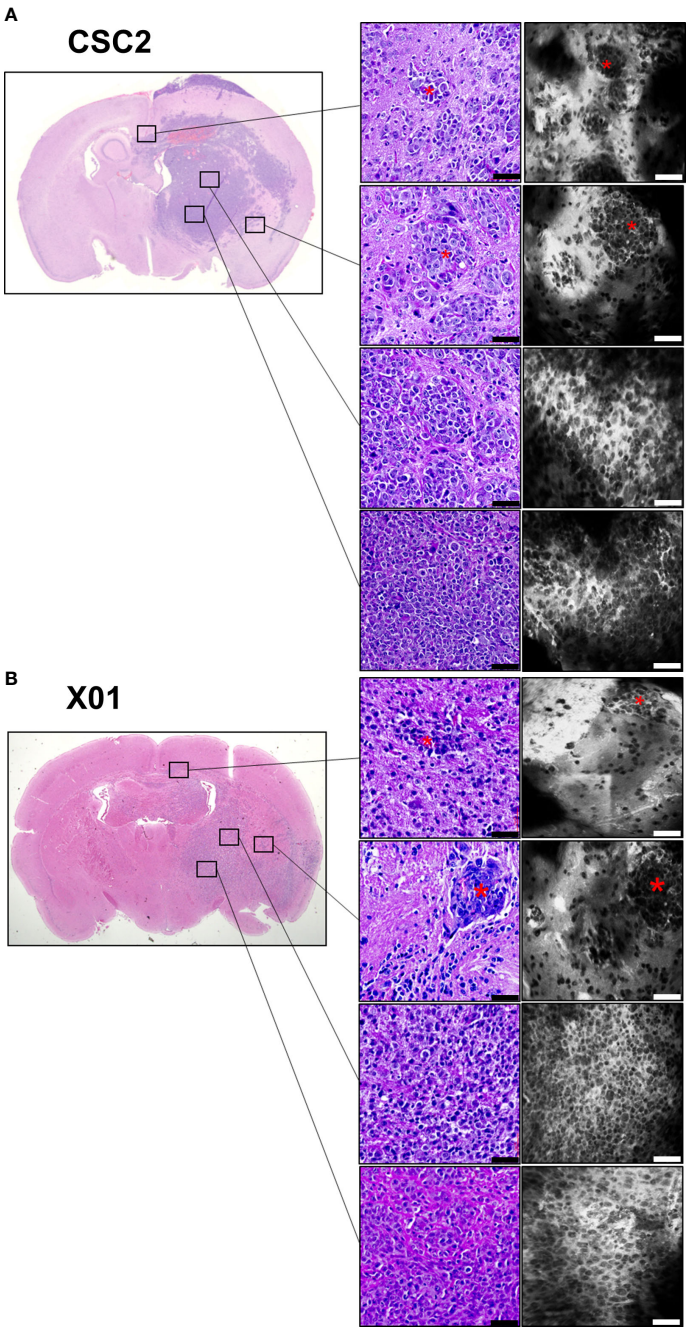

FIGURE 3
Photomicrographs in patient-derived orthotopic xenograft models. CSC2 **(A)** and X01 **(B)** patient-derived glioma stem-like cells (1×10^5) were injected into BALB/c nude mouse brains. Six weeks later, the mouse brain was obtained and incubated with indocyanine green fluorescent dye. CLE images and H&E staining of the same tissues demonstrated two different glioma tissue cores and peripheral tumor margins, respectively. Asterix: Invasive cells. Scale bar: 50 μm. H&E, hematoxylin and eosin.

limited to 300 × 300 μm and does not demonstrate a large tissue area. Therefore, Z-merged images of the tissue were combined or stitched to produce panoramic images with 3D depth information (Figure 7B).

4 Discussion

In this study, we identified the clinical feasibility of real-time brain tumor diagnosis using the Lissajous scanning CLE. Using

TABLE 1 Histopathologic diagnosis of 69 human brain tumor samples.

Diagnosis	Histopathologic subtype	Number of cases
Glioma	WHO Grade 2	4
	WHO Grade 3	5
	WHO Grade 4	11
Meningioma	Meningothelial	10
	Transitional	9
	Psammomatous	1
	Atypical	2
Metastatic tumor	Adenocarcinoma	4
	Squamous cell carcinoma	2
	Melanoma	2
	Others	3
Pituitary adenoma		11
Schwannoma		2
Primary CNS lymphoma	Diffuse large B cell	1
Solitary fibrous tumor		1
Choroid plexus papilloma		1

WHO, World Health Organization; CNS, central nervous system.

an ICG fluorescent dye, various brain tumors showed typical cellular morphologies and distinct tissue microstructures. In addition, CLE clearly identified the normal brain to tumor lesions and revealed tumor cell invasion in the adjacent normal brain. Finally, the Z-merge and stitching techniques overcome the limited FOV acquisition due to tumor tissue irregularity and improve the diagnostic potential.

Handheld CLEs have been successfully developed to detect real-time histologic images in clinical studies (23, 24). In the current study, we used a confocal laser-scanning imaging system based on the Lissajous pattern. It visualizes tissue microstructure using ICG fluorescent dye and obtains high-resolution images of 1024 × 1024 pixels with high frame rates of up to 10 Hz. Unlike other pattern-based micro-laser scanners, Lissajous scanning has a great advantage in that it has a high degree of freedom to adjust the image resolution and frame rate by selecting a driving frequency in a pseudo-resonant frequency range that realizes a satisfactory scanning amplitude (25). This feature allows our system to be used in a mode capable of high-speed imaging when operated with a handheld and high-resolution mode when used with an auto-stage capable of precise movement.

In our study, brain tissue visualization *via* CLE imaging allowed for the distinction of brain tumors based on their unique morphological features (26). The CLE images closely resembled the H&E-stained histological images. It is well known that tumor tissues can disrupt normal extracellular composition (27), increase cellularity (28), and display unique brain tumor phenotypic morphologies, such as the presence of psammoma bodies in meningioma tissues (29). In our CLE and histologic images, there were synchronous typical cell morphologies, such as salt-and-pepper patterns in pituitary adenoma and uniform cuboidal or columnar epithelial cells in choroid plexus papilloma. In addition, other tissue microstructures were also found, including whorl formation in meningiomas, atypical cell nests in metastatic adenocarcinomas, and spiral patterns in schwannomas. Furthermore, some tumor cells, such as pituitary adenoma and choroid plexus papilloma, revealed intracellular morphology, but ICG could not penetrate the cell membrane in U87 glioma cells. It has been suggested that intracellular ICG uptake correlates with endocytosis potential and tight junctions, although the mechanism of intracellular ICG uptake remains unclear (30). The CLE images not only increased the diagnostic potential but also significantly shortened the time to reach a precise diagnosis. For instance, in the current study, the mean operation time to obtain a CLE image was less than one second per frame. Considering that seven *ex vivo* images were acquired before the identification of the first brain tumor diagnostic image, real-time diagnosis could be performed intraoperatively (11).

Maximal surgical resection of glial tumors is critical for patient survival and recurrence rates (31–33). Current methods of tumor detection, including a neuronavigation system and intraoperative

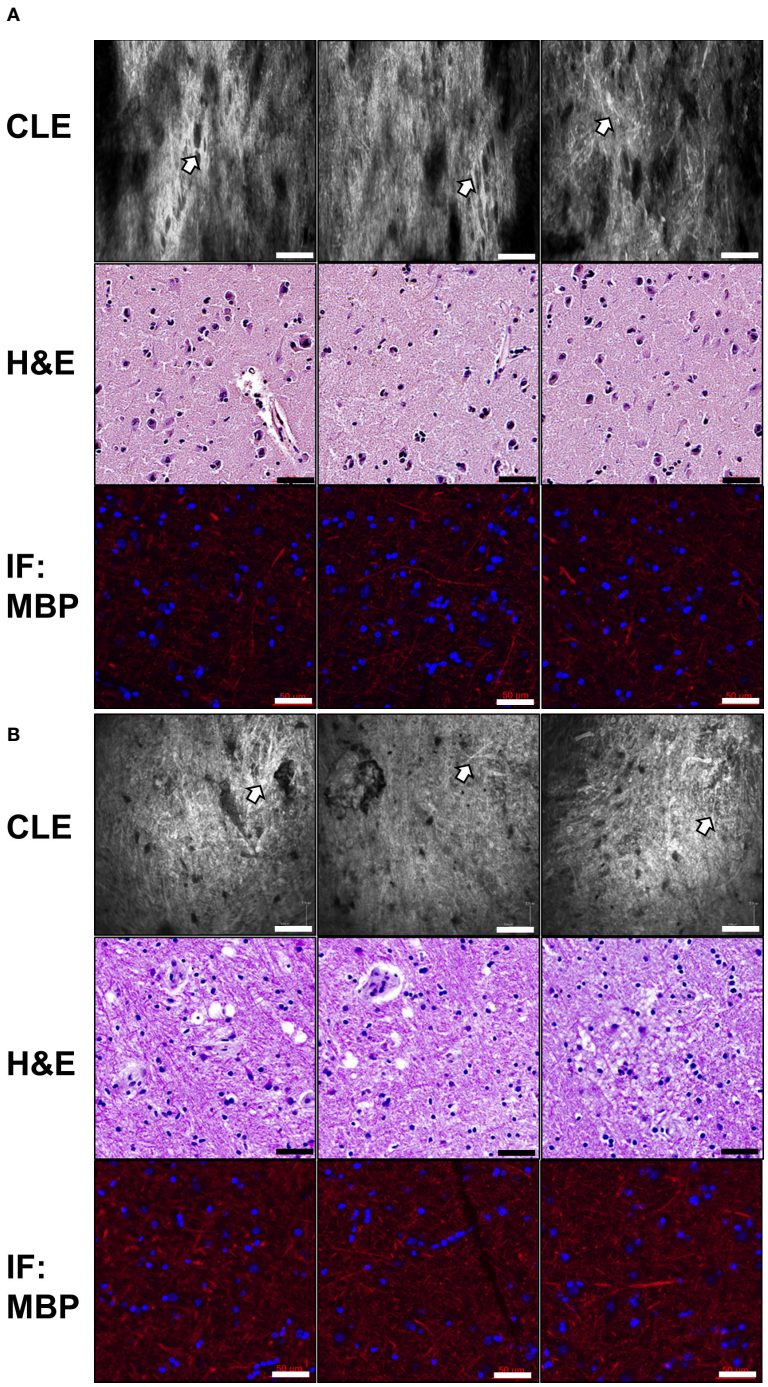

FIGURE 4
Representative images of normal human brain tissues Normal brain tissues were obtained from the cerebral cortex **(A)** and subcortical areas **(B)** during surgical resection. CLE images show a dense streak-like pattern throughout most of the brain mass (white arrows). H&E staining revealed the presence of large neuronal cells **(A)** and glial cells **(B)**. Myelin basic protein (MBP) immunostaining of the same tissue sample revealed dense axonal fibers (red). Scale bar: 50 μm. H&E, hematoxylin and eosin.

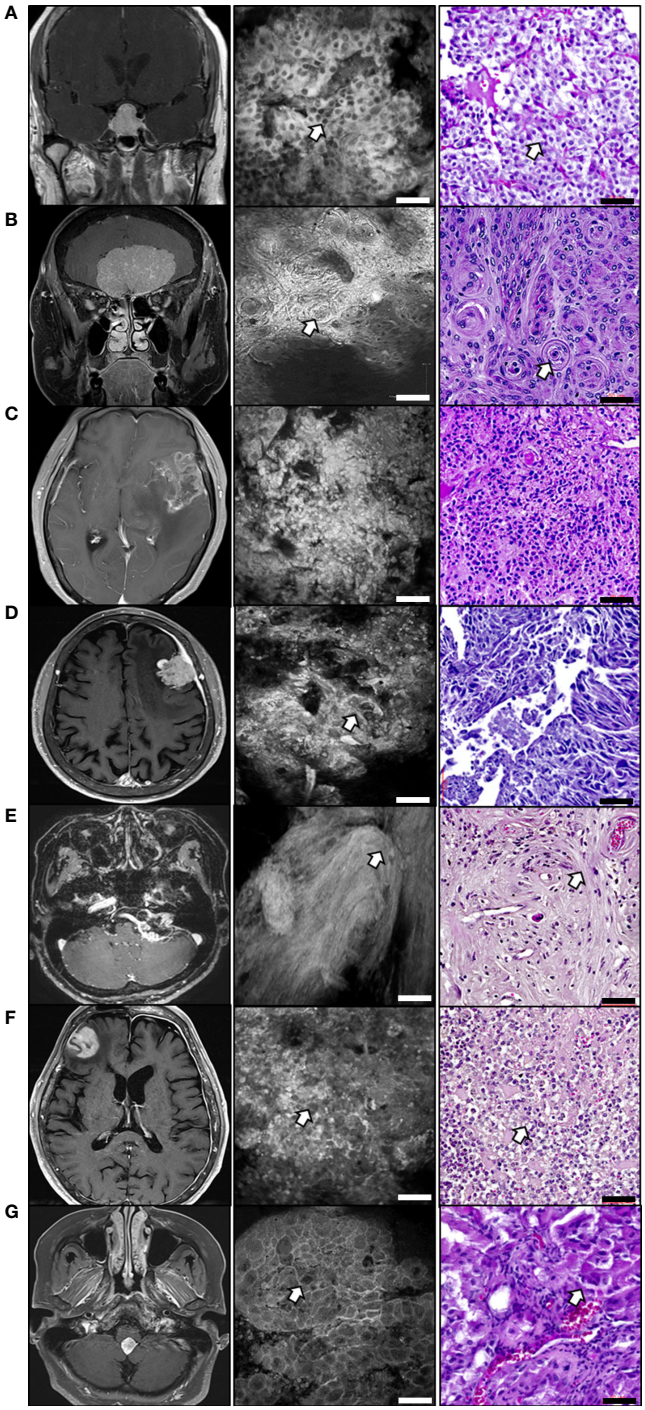

FIGURE 5
Ex vivo CLE images compared to histology in various brain tumor tissues Corresponding representative images of brain tumors consist of T1 enhanced magnetic resonance images (left), CLE images (middle), and H&E staining (right). **(A)** Pituitary adenoma. White arrows indicate the salt-and-pepper patterns. **(B)** Olfactory groove meningioma. White arrows indicate a sheet or lobular architecture that contains a whorl pattern. **(C)** Glioblastoma image showing the overall hypercellularity and atypia. **(D)** Metastatic adenocarcinoma. White arrows indicate atypical cell nests. **(E)** Vestibular schwannoma. White arrows indicate the spiral pattern of whorl formation. **(F)** Primary central nervous system lymphoma. White arrows indicate the large, atypical lymphocytes. **(G)** Choroidal plexus papilloma. White arrows indicate papillary structures lined with uniform cuboidal or columnar epithelial cells. Scale bar: 50 μm. H&E, hematoxylin and eosin.

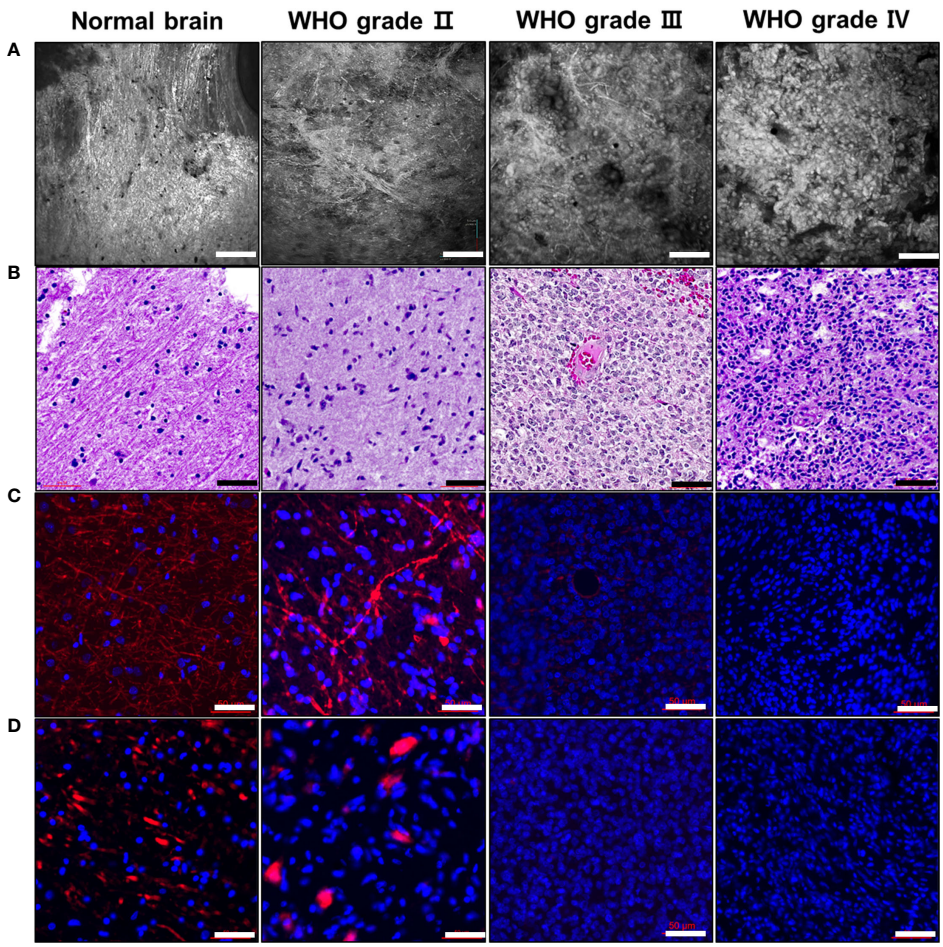

FIGURE 6
Representative photomicrographs of CLE images and glioma histology Compared to normal brain tissue, gliomas are classified as *IDH1*-mutant gliomas (WHO grade II), anaplastic oligodendroglioma (WHO grade III), and glioblastoma (WHO grade IV). **(A)** CLE images of different glioma samples, according to their corresponding WHO grades, were obtained. Each glioma sample displayed a variety of morphological phenotypes, including cellularity and streak-like patterns. **(B)** H&E staining of the same tissue showing distinct histological differences in glioma grade, which was examined to identify cellularity, atypia, mitosis, and angiogenesis. **(C, D)** As a typical marker for axon fibers, myelin basic protein (MBP) and neurofilament stains were examined at the corresponding glioma tissues. Similar to the CLE images, the amount of MBP and neurofilament staining were significantly decreased in high-grade gliomas. Scale bar: 50 μm. H&E, hematoxylin and eosin; WHO, World Health Organization.

visualization *via* 5-ALA, have improved tumor resection (5, 6). However, there are some limitations, including brain shifts and variable fluorescence in the glioma tissues (34). In addition, glioma cell invasion into the normal brain is not determined during intraoperative neuronavigation or macroscopic 5-ALA tumor fluorescence. Recently, fluorescein sodium (FNa) was used as a fluorescent agent for glioma resection during intraoperative glioma visualization. Intravenously injected FNa selectively accumulates in the brain and can pass through an altered blood-brain barrier (BBB). This selectivity provides the ability of FNa to be used as a guide during fluorescein-guided resection of gliomas (35, 36). However, FNa is also not specific and can accumulate in some peritumoral areas, leading to reduced accuracy in terms of tumor identification (37). It has been suggested that direct tumor cell visualization can overcome these issues. CLE is a useful tool for glioma diagnosis in the neurosurgical field. Fluorescent agents, including FNa and ICG, have been used to detect cytoarchitectures of normal and glioma tissues (38, 39). In the current study, we developed an orthotopic intracranial model using patient-derived glioma cells that were histologically identical to human glioma tissue (40). In the CLE images, heterogeneous and hypercellular regions were found at the tumor core and infiltrative glioma cell clusters were observed at the edge of the glioma. These features are identical to those observed in the histological images. In addition, obtaining CLE images and determining whether the ICG fluorescence dye was injected into the vein or incubated with glioma tissue *ex vivo* were not critical issues in our study (Supplementary Figure 1).

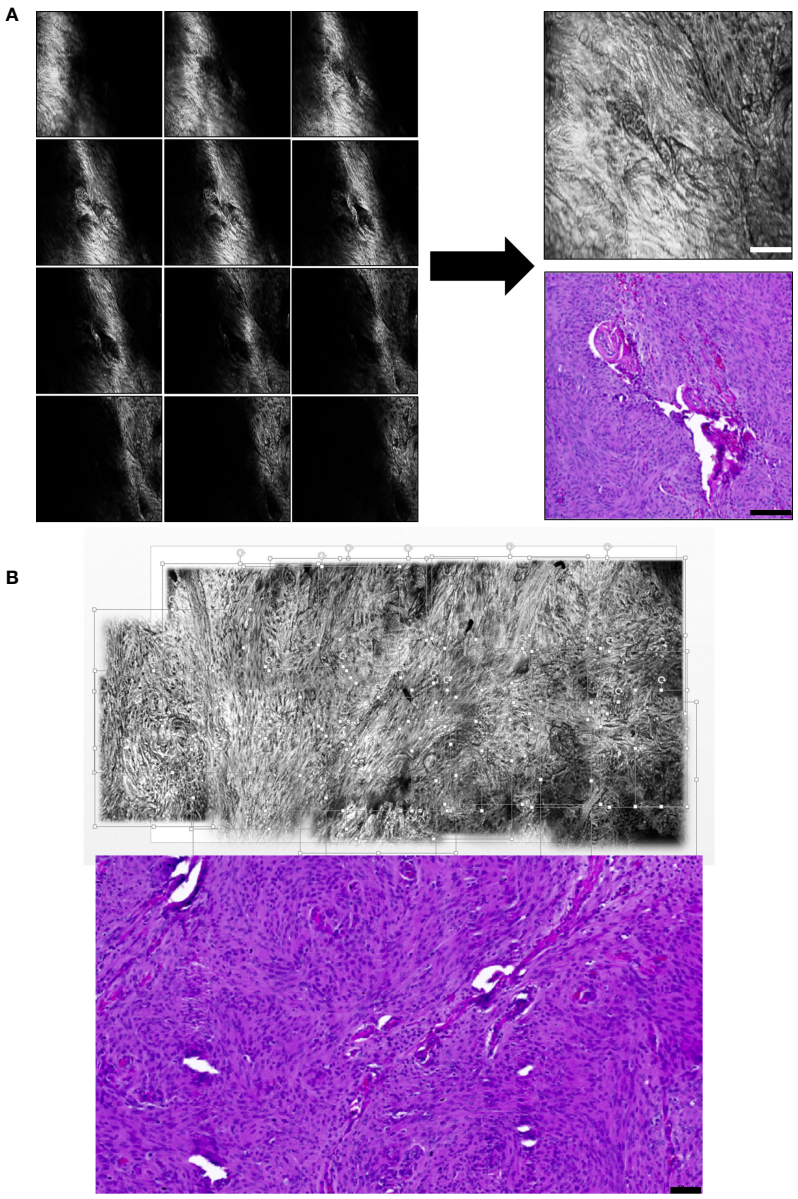

FIGURE 7
Panoramic CLE images with 3D depth information and their comparison with conventional hematoxylin and eosin stain A series of images taken while changing the distance between the probe and the tissue in the Z-axis were merged into one image (i.e., Z-merged). **(A)** The Z-merged CLE image and the histology of the benign meningioma tissue show similar microstructural features. **(B)** Using meningioma tissue, each Z-merged CLE image was combined into a panoramic image to provide a large field of view as much as conventional H&E stain. Scale bar: 50 μm. H&E, hematoxylin and eosin.

In the CLE images, we easily identified the differences between normal brain and glioma tissues. Compared to the normal brain, gliomas revealed hypercellularity and dysmorphic morphological features that were positively associated with tumor grade. Interestingly, CLE imaging of normal brain and low-grade glioma tissues demonstrated a distinct streak-like pattern throughout most of the tissue areas. To determine whether these streak-like patterns represent myelin fibers, MBP and neurofilament staining were performed in one normal brain tissue and three different glioma types: *IDH1*-mutant glioma, anaplastic oligodendroglioma, and glioblastoma. The density of the streak-like pattern in CLE images was strongly correlated with the amount of MBP and neurofilament in the normal brain and gliomas, and there was a reverse correlation between glioma grade and the quantity of these myelin fibers. Therefore, streak-like patterns can be utilized as cues to identify glioma grade in CLE images.

The FOV of a CLE image is limited by the scanning amplitude of the micro-laser scanner. Given that a micro-laser scanner needs

to come into contact with the patient's body, it is difficult to acquire large-area images simultaneously because high voltages and currents are required for this process. Therefore, most commercially available CLEs generally have a narrow FOV of 240 × 240 μm to 600 × 500 μm (41). In addition, CLE images are obtained from black areas outside the focus because the tumor tissue has a 3D structure, and the image signal is blocked because of the high axial resolution. These drawbacks can be overcome with stitching or mosaicing techniques that connect the acquired images *via* the Z-merge function, which moves the probe in the depth direction to acquire tissue images along different Z-axes and merges the images into one image (17). In this study, a panoramic image was obtained by connecting the Z-merged images horizontally and vertically (Figure 7B). It took approximately 10 min to manually connect the 20 images. If a real-time panoramic function based on an automatic stitching algorithm is developed, its clinical usefulness is expected to increase.

On summary, a newly developed CLE device can be equipped in operation settings and easily utilized with miniaturized hand-held probe. It can visualize the cytoarchitecture of the fresh or resected human tissue including brain and other organs. It is potentially safe because it does not contact the tissue and we do not need to resect the tissue for histologic confirmation. Further panoramic view reconstruction and pseudo-coloring effects are now being exploited. After verifying the diagnosis accuracy for brain tumor subtype, we hope it can substitute the frozen tissue histology performed by pathologist outside the operation room.

The current study had several limitations. First, it was designed as an observational study that focused on verifying the feasibility of a new CLE device, so the *ex vivo* brain tumor samples were inhomogenously included as electively scheduled. Second, a glioma cell line only exists in experimental *in vitro* brain tumor settings, and other subtypes of brain tumor were not observed. To overcome these limitations, we are currently conducting a multicenter clinical prospective study to identify the diagnostic accuracy of the device in depth. Third, the current findings were obtained from a single center and multicentered study design is necessary for the device application. Finally, the current study was designed as an observational study and did not include statistical analysis. Again, a future multicenter clinical trial with statistical analysis is needed.

Data availability statement

The original contributions presented in the study are included in the article/Supplementary Material. Further inquiries can be directed to the corresponding author.

Ethics statement

The studies involving human participants were reviewed and approved by Institutional Review Board of Korea University Anam Hospital. The patients/participants provided their written informed consent to participate in this study. The animal study was reviewed and approved by Institutional Animal Care and Use Committee of Korea University College of Medicine. Written informed consent was obtained from the individual(s) for the publication of any potentially identifiable images or data included in this article.

Author contributions

DH and JK designed and performed most of the experiments, analyzed the data, and wrote the manuscript. CK, KH, and K-HJ performed CLE imaging and wrote the manuscript. HK helped design and perform the animal experiments. K-JP helped in writing the manuscript. J-KW provided the pathologist's expertise in comparing the CLE images to the H&E histological images. S-HK helped to design the experiments, co-wrote the manuscript, and provided an overall direction.

Funding

This research was supported by a grant from the Korea Health Technology R&D Project through the Korea Health Industry Development Institute (KHIDI), funded by the Ministry of Health & Welfare, Republic of Korea (grant number: HI22C1302), and by the Korea Medical Device Development Fund grant funded by the Korea government (the Ministry of Science and ICT, the Ministry of Trade, Industry and Energy, the Ministry of Health & Welfare, the Ministry of Food and Drug Safety) (grant number: RS-2022-00197971).

Conflict of interest

KH and CK are employed by VPIX Medical, Inc.

The remaining authors declare that the research was conducted in the absence of any commercial or financial relationships that could be construed as potential conflicts of interest.

Publisher's note

All claims expressed in this article are solely those of the authors and do not necessarily represent those of their affiliated organizations, or those of the publisher, the editors and the

reviewers. Any product that may be evaluated in this article, or claim that may be made by its manufacturer, is not guaranteed or endorsed by the publisher.

Supplementary material

The Supplementary Material for this article can be found online at: https://www.frontiersin.org/articles/10.3389/fonc.2022.994054/full#supplementary-material

SUPPLEMENTARY VIDEO 1

Real-time examination of the implanted patient-derived glioma tissue (CSC2) from BALB/c nude mouse brain. The H&E stained, and CLE scanned images from the same mouse were presented in Figure 3A.

SUPPLEMENTARY VIDEO 2

Real-time examination of the pituitary adenoma tissue from resected human specimen. The H&E stained, and CLE scanned images from the same tissue were presented in Figure 5A and Supplementary Figure 2A.

SUPPLEMENTARY VIDEO 3

Real-time examination of the meningothelial meningioma tissue from resected human specimen. The H&E stained, and CLE scanned images from the same tissue were presented in Figure 5B and Supplementary Figure 3B.

References

1. Suchorska B, Weller M, Tabatabai G, Senft C, Hau P, Sabel MC, et al. Complete resection of contrast-enhancing tumor volume is associated with improved survival in recurrent glioblastoma-results from the director trial. *Neuro-Oncology* (2016) 18:549–56. doi: 10.1093/neuonc/nov326

2. Molitch ME. Diagnosis and treatment of pituitary adenomas: A review. *JAMA* (2017) 317:516–24. doi: 10.1001/jama.2016.19699

3. Rogers L, Barani I, Chamberlain M, Kaley TJ, McDermott M, Raizer J, et al. Meningiomas: Knowledge base, treatment outcomes, and uncertainties. A rano review. *J Neurosurg* (2015) 122:4–23. doi: 10.3171/2014.7.JNS131644

4. Ellingson BM, Abrey LE, Nelson SJ, Kaufmann TJ, Garcia J, Chinot O, et al. Validation of postoperative residual contrast-enhancing tumor volume as an independent prognostic factor for overall survival in newly diagnosed glioblastoma. *Neuro-Oncology* (2018) 20:1240–50. doi: 10.1093/neuonc/noy053

5. Stummer W, Pichlmeier U, Meinel T, Wiestler OD, Zanella F, Reulen HJ, et al. Fluorescence-guided surgery with 5-aminolevulinic acid for resection of malignant glioma: A randomised controlled multicentre phase iii trial. *Lancet Oncol* (2006) 7:392–401. doi: 10.1016/S1470-2045(06)70665-9

6. Orringer DA, Golby A, Jolesz F. Neuronavigation in the surgical management of brain tumors: Current and future trends. *Expert Rev Med Devices* (2012) 9:491–500. doi: 10.1586/erd.12.42

7. Hadjipanayis CG, Widhalm G, Stummer W. What is the surgical benefit of utilizing 5-aminolevulinic acid for fluorescence-guided surgery of malignant gliomas? *Neurosurgery* (2015) 77:663–73. doi: 10.1227/NEU.0000000000000929

8. Richter JCO, Haj-Hosseini N, Hallbeck M, Wårdell K. Combination of hand-held probe and microscopy for fluorescence guided surgery in the brain tumor marginal zone. *Photodiagn Photodyn Ther* (2017) 18:185–92. doi: 10.1016/j.pdpdt.2017.01.188

9. Chand P, Amit S, Gupta R, Agarwal A. Errors, limitations, and pitfalls in the diagnosis of central and peripheral nervous system lesions in intraoperative cytology and frozen sections. *J Cytol* (2016) 33:93–7. doi: 10.4103/0970-9371.182530

10. Plesec TP, Prayson RA. Frozen section discrepancy in the evaluation of central nervous system tumors. *Arch Pathol Lab Med* (2007) 131:1532–40. doi: 10.5858/2007-131-1532-FSDITE

11. Martirosyan NL, Eschbacher JM, Kalani MYS, Turner JD, Belykh E, Spetzler RF, et al. Prospective evaluation of the utility of intraoperative confocal laser endomicroscopy in patients with brain neoplasms using fluorescein sodium: Experience with 74 cases. *Neurosurg Focus* (2016) 40:E11. doi: 10.3171/2016.1.FOCUS15559

12. Cinotti R, Bruder N, Srairi M, Paugam-Burtz C, Beloeil H, Pottecher J, et al. Prediction score for postoperative neurologic complications after brain tumor craniotomy: A multicenter observational study. *Anesthesiology* (2018) 129:1111–20. doi: 10.1097/ALN.0000000000002426

13. Chatterjee S. Artefacts in histopathology. *J Oral Maxillofac Pathol* (2014) 18 (Suppl 1):S111–6. doi: 10.4103/0973-029X.141346

14. Serletis D, Bernstein M. Prospective study of awake craniotomy used routinely and nonselectively for supratentorial tumors. *J Neurosurg* (2007) 107:1–6. doi: 10.3171/JNS-07/07/0001

15. Zehri AH, Ramey W, Georges JF, Mooney MA, Martirosyan NL, Preul MC, et al. Neurosurgical confocal endomicroscopy: A review of contrast agents, confocal systems, and future imaging modalities. *Surg Neurol Int* (2014) 5:60. doi: 10.4103/2152-7806.131638

16. Fuchs FS, Zirlik S, Hildner K, Schubert J, Vieth M, Neurath MF. Confocal laser endomicroscopy for diagnosing lung cancer *in vivo*. *Eur Respir J* (2013) 41:1401–8. doi: 10.1183/09031936.00062512

17. Capuano A, Andreuzzi E, Pivetta E, Doliana R, Favero A, Canzonieri V, et al. The probe based confocal laser endomicroscopy (Pcle) in locally advanced gastric cancer: A powerful technique for real-time analysis of vasculature. *Front Oncol* (2019) 9:513. doi: 10.3389/fonc.2019.00513

18. Belykh E, Ngo B, Farhadi DS, Zhao XC, Mooney MA, White WL, et al. Confocal laser endomicroscopy assessment of pituitary tumor microstructure: A feasibility study. *J Clin Med* (2020) 9:3146. doi: 10.3390/jcm9103146

19. Charalampaki P, Javed M, Daali S, Heiroth HJ, Igressa A, Weber F. Confocal laser endomicroscopy for real-time histomorphological diagnosis: Our clinical experience with 150 brain and spinal tumor cases. *Neurosurgery* (2015) 62(Suppl 1):171–6. doi: 10.1227/NEU.0000000000000805

20. Martirosyan NL, Georges J, Eschbacher JM, Cavalcanti DD, Elhadi AM, Abdelwahab MG, et al. Potential application of a handheld confocal endomicroscope imaging system using a variety of fluorophores in experimental gliomas and normal brain. *Neurosurg Focus* (2014) 36:E16. doi: 10.3171/2013.11.FOCUS13486

21. Hwang K, Seo YH, Kim DY, Ahn J, Lee S, Han KH, et al. Handheld endomicroscope using a fiber-optic harmonograph enables real-time and *in vivo* confocal imaging of living cell morphology and capillary perfusion. *Microsyst Nanoeng: ARTN* (2020) 72:6. doi: 10.1038/s41378-020-00182-6

22. Kim DY, Hwang K, Ahn J, Seo YH, Kim JB, Lee S, et al. Lissajous Scanning two-photon endomicroscope for *in vivo* tissue imaging. *Sci Rep* (2019) 9:3560. doi: 10.1038/s41598-019-38762-w

23. Krishnamurthy S, Sabir S, Ban K, Wu Y, Sheth R, Tam A, et al. Comparison of real-time fluorescence confocal digital microscopy with hematoxylin-eosin-stained sections of core-needle biopsy specimens. *JAMA Netw Open* (2020) 3: e200476. doi: 10.1001/jamanetworkopen.2020.0476

24. Krishnamurthy S, Ban KC, Shaw K, Mills G, Sheth R, Tam A, et al. Confocal fluorescence microscopy platform suitable for rapid evaluation of small fragments of tissue in surgical pathology practice. *Arch Pathol Lab Med* (2019) 143:305–13. doi: 10.5858/arpa.2018-0352-OA

25. Hwang K, Seo YH, Ahn J, Kim P, Jeong KH. Frequency selection rule for high definition and high frame rate lissajous scanning. *Sci Rep* (2017) 7:14075. doi: 10.1038/s41598-017-13634-3

26. Charalampaki P, Nakamura M, Athanasopoulos D, Heimann A. Confocal-assisted multispectral fluorescent microscopy for brain tumor surgery. *Front Oncol* (2019) 9:583. doi: 10.3389/fonc.2019.00583

27. Mohiuddin E, Wakimoto H. Extracellular matrix in glioblastoma: Opportunities for emerging therapeutic approaches. *Am J Cancer Res* (2021) 11:3742–54.

28. Ye ZZ, Srinivasa K, Meyer A, Sun P, Lin J, Viox JD, et al. Diffusion histology imaging differentiates distinct pediatric brain tumor histology. *Sci Rep* (2021) 11:4749. doi: 10.1038/s41598-021-84252-3

29. Das DK. Psammoma body: A product of dystrophic calcification or of a biologically active process that aims at limiting the growth and spread of tumor? *Diagn Cytopathol* (2009) 37:534–41. doi: 10.1002/dc.21081

30. Onda N, Kimura M, Yoshida T, Shibutani M. Preferential tumor cellular uptake and retention of indocyanine green for *in vivo* tumor imaging. *Int J Cancer* (2016) 139:673–82. doi: 10.1002/ijc.30102

31. Marko NF, Weil RJ, Schroeder JL, Lang FF, Suki D, Sawaya RE. Extent of resection of glioblastoma revisited: Personalized survival modeling facilitates more accurate survival prediction and supports a maximum-safe-resection approach to surgery. *J Clin Oncol* (2014) 32:774–82. doi: 10.1200/JCO.2013.51.8886

32. Nanda A, Bir SC, Maiti TK, Konar SK, Missios S, Guthikonda B. Relevance of Simpson grading system and recurrence-free survival after surgery for world health organization grade I meningioma. *J Neurosurg* (2017) 126:201–11. doi: 10.3171/2016.1.JNS151842

33. Jakola AS, Skjulsvik AJ, Myrmel KS, Sjåvik K, Unsgård G, Torp SH, et al. Surgical resection versus watchful waiting in low-grade gliomas. *Ann Oncol* (2017) 28:1942–8. doi: 10.1093/annonc/mdx230

34. Sanai N, Snyder LA, Honea NJ, Coons SW, Eschbacher JM, Smith KA, et al. Intraoperative confocal microscopy in the visualization of 5-aminolevulinic acid fluorescence in low-grade gliomas. *J Neurosurg* (2011) 115:740–8. doi: 10.3171/2011.6.JNS11252

35. Acerbi F, Broggi M, Schebesch KM, Höhne J, Cavallo C, De Laurentis C, et al. Fluorescein-guided surgery for resection of high-grade gliomas: A multicentric prospective phase ii study (Fluoglio). *Clin Cancer Res* (2018) 24:52–61. doi: 10.1158/1078-0432.CCR-17-1184

36. Francaviglia N, Iacopino DG, Costantino G, Villa A, Impallaria P, Meli F, et al. Fluorescein for resection of high-grade gliomas: A safety study control in a single center and review of the literature. *Surg Neurol Int* (2017) 8:145. doi: 10.4103/sni.sni_89_17

37. Katsevman GA, Turner RC, Urhie O, Voelker JL, Bhatia S. Utility of sodium fluorescein for achieving resection targets in glioblastoma: Increased gross- or near-total resections and prolonged survival. *J Neurosurg* (2019) 132:914–20. doi: 10.3171/2018.10.JNS181174

38. Foersch S, Heimann A, Ayyad A, Spoden GA, Florin L, Mpoukouvalas K, et al. Confocal laser endomicroscopy for diagnosis and histomorphologic imaging of brain tumors *in vivo*. *PloS One* (2012) 7:e41760. doi: 10.1371/journal.pone.0041760

39. Martirosyan NL, Cavalcanti DD, Eschbacher JM, Delaney PM, Scheck AC, Abdelwahab MG, et al. Use of *in vivo* near-infrared laser confocal endomicroscopy with indocyanine green to detect the boundary of infiltrative tumor. *J Neurosurg* (2011) 115:1131–8. doi: 10.3171/2011.8.JNS11559

40. Singh SK, Hawkins C, Clarke ID, Squire JA, Bayani J, Hide T, et al. Identification of human brain tumour initiating cells. *Nature* (2004) 432:396–401. doi: 10.1038/nature03128

41. Mooney MA, Zehri AH, Georges JF, Nakaji P. Laser scanning confocal endomicroscopy in the neurosurgical operating room: A review and discussion of future applications. *Neurosurg Focus* (2014) 36:E9. doi: 10.3171/2013.11.FOCUS13484

frontiers | Frontiers in Oncology

TYPE Original Research
PUBLISHED 19 January 2023
DOI 10.3389/fonc.2022.1090170

OPEN ACCESS

EDITED BY
Yan Qu,
Air Force Military Medical University, China

REVIEWED BY
Jun-Feng Lu,
Fudan University, China
Jie Zhang,
Fudan University, China

*CORRESPONDENCE
Meng Cui
mcmeng182@163.com
Xiaodong Ma
xiaodongm@hotmail.com

†These authors have contributed equally to this work

SPECIALTY SECTION
This article was submitted to Neuro-Oncology and Neurosurgical Oncology, a section of the journal Frontiers in Oncology

RECEIVED 05 November 2022
ACCEPTED 19 December 2022
PUBLISHED 19 January 2023

CITATION
Cui M, Guo Q, Chi Y, Zhang M, Yang H, Gao X, Chen H, Liu Y and Ma X (2023) Predictive model of language deficit after removing glioma involving language areas under general anesthesia.
Front. Oncol. 12:1090170.
doi: 10.3389/fonc.2022.1090170

Predictive model of language deficit after removing glioma involving language areas under general anesthesia

Meng Cui [1,2*], Qingbao Guo [2,3†], Yihong Chi [4†], Meng Zhang [5], Hui Yang [2,3], Xin Gao [2,3], Hewen Chen [2,3], Yukun Liu [2,3] and Xiaodong Ma [2,3*]

[1]Department of Emergency, The Sixth Medical Center, Chinese People's Liberation Army General Hospital, Beijing, China, [2]Medical School of Chinese People's Liberation Army, Beijing, China, [3]Department of Neurosurgery, The First Medical Center, Chinese People's Liberation Army General Hospital, Beijing, China, [4]Department of Information Technology, Xian Janssen Pharmaceutical Ltd., Beijing, China, [5]Department of Neurosurgery, The Second Hospital of Southern District of Chinese People's Liberation Army Navy, Sanya, China

Purpose: To establish a predictive model to predict the occurrence of language deficit for patients after surgery of glioma involving language areas (GILAs) under general anesthesia (GA).

Methods: Patients with GILAs were retrospectively collected in our center between January 2009 and December 2020. Clinical variables (age, sex, aphasia quotient [AQ], seizures and KPS), tumor-related variables (recurrent tumor or not, volume, language cortices invaded or not, shortest distance to language areas [SDLA], supplementary motor area or premotor area [SMA/PMA] involved or not and WHO grade) and intraoperative multimodal techniques (used or not) were analyzed by univariate and multivariate analysis to identify their association with temporary or permanent language deficits (TLD/PLD). The predictive model was established according to the identified significant variables. Receiver operating characteristic (ROC) curve was used to assess the accuracy of the predictive model.

Results: Among 530 patients with GILAs, 498 patients and 441 patients were eligible to assess TLD and PLD respectively. The multimodal group had the higher EOR and rate of GTR than conventional group. The incidence of PLD was 13.4% in multimodal group, which was much lower than that (27.6%, P<0.001) in conventional group. Three factors were associated with TLD, including SDLA (OR=0.85, P<0.001), preoperative AQ (OR=1.04, P<0.001) and multimodal techniques used (OR=0.41, P<0.001). Four factors were associated with PLD, including SDLA (OR=0.83, P=0.001), SMA/PMA involved (OR=3.04, P=0.007), preoperative AQ (OR=1.03, P=0.002) and multimodal techniques used (OR=0.35, P<0.001). The optimal shortest distance thresholds in detecting the occurrence of TLD/PLD were 1.5 and 4mm respectively. The optimal AQ thresholds in detecting the occurrence of TLD/PLD were 52 and 61 respectively. The cutoff values of the predictive probability for TLD/PLD were

23.7% and 16.1%. The area under ROC curve of predictive models for TLD and PLD were 0.70 (95%CI: 0.65-0.75) and 0.72 (95%CI: 0.66-0.79) respectively.

Conclusion: The use of multimodal techniques can reduce the risk of postoperative TLD/PLD after removing GILAs under general anesthesia. The established predictive model based on clinical variables can predict the probability of occurrence of TLD and PLD, and it had a moderate predictive accuracy.

KEYWORDS

glioma, language, multimodal techniques, general anesthesia, predictive model

Introduction

Glioma is the most common primary intracranial tumor, with an annual incidence of 4.67-5.73 per 100,000 (1). With the introduction of molecular mechanisms into the WHO classification of glioma, the treatment of glioma is developing a multidisciplinary, individualized, functional and preventive comprehensive treatment strategy, including surgery, postoperative radiotherapy, chemotherapy, immunotherapy and tumor-treating field (TTF), which can improve the outcome and survival of patients with glioma (2–6). Surgery is still the core method of comprehensive treatment, and many studies have proven that increasing the extent of resection (EOR) can prolong survival against glioma (7, 8). However, more aggressive resection may cause injury to normal brain tissue, especially eloquent areas, and their injury will lead to neurological deficits postoperatively. Language is an important neurological function of human, so maximal safe resection is the goal when removing the gliomas involving language areas (GILAs). Thus, the language cortices and tracts should be protected well while the maximal EOR is achieved.

Although direct electrical stimulation (DES) under awake craniotomy is the method of gold standard in mapping language areas when removing GILAs, multimodal techniques (neuronavigation based on multimodal imaging, intraoperative MRI [iMRI] and intraoperative neuromonitoring [IONM]) make maximal safe resection of GILAs possible under general anesthesia (9). An increasing number of studies believe that resection assisted by multimodal techniques under general anesthesia can achieve similar outcomes to awake craniotomy for patients with GILAs and takes less time with lower intraoperative risk (10, 11). We began to use multimodal techniques to remove GILAs under general anesthesia since 2009, and this surgery approach was proved to be effective and safe in our previous studies (12–14). According to our previous experience, some pre-, intra- and postoperative factors may be associated with temporary or permanent language deficits (TLD or PLD). In this study, we aimed to identify significant factors associated with TLD and PLD. Then based on these factors, a predictive model can be established to predict the occurrence of TLD and PLD. This model is expected to help surgeon and patients make appropriate choice on intraoperative techniques.

Methods

Patient selection

Retrospective clinical data were reviewed from electronic medical records in the Department of Neurosurgery at our center between January 2009 and December 2020. This study was approved by our institutional ethics committee. Written informed consent was signed by all patients or their relatives before surgery. These data were treated with privacy and reviewed to identify GILAs according to the following inclusion criteria, 1) pathology confirmed as supratentorial glioma based on the WHO classification of tumors of the central nervous system (3); 2) patients older than 6 years who can be assessed for language completely; 3) the tumor within 2 cm of language areas (language cortices and/or tracts) on preoperative MRI; 4) resection under general anesthesia; 5) pre/postoperative language function assessment and follow-up were completed. The exclusion criteria were as follows: 1) infratentorial glioma; 2) <6 years old; 3) biopsy only; and 4) loss of pre/postoperative MRI data; 5) loss of follow-up.

Patient grouping

The patients were divided into occurrence group (TLD/PLD occurred) and non-occurrence group (TLD/PLD did not occur). The patients were also divided into conventional group

(neuronavigation alone), and multimodal group (combined use of neuronavigation, iMRI, with/without DES/IONM).

Preoperative variables

Preoperative general variables included age, sex, left or right-hander, symptoms, aphasia quotient (AQ) by Western Aphasia Battery testing (AQ≥93.8 and <93.8 were defined as normal and aphasia, respectively) (15–17), seizures (divided into no seizures, drug-controlled seizures and drug intractable seizures) and KPS.

Tumor-related variables included location, recurrent tumor or not, volume (cm^3), language cortices invaded or not, shortest distance to language cortices or tracts (mm), supplementary motor area or premotor area (SMA/PMA) involved or not, histopathology, WHO grade. If the tumor was near language area but did not invaded it directly, the nearest distance was from border of tumor to language area. If the tumor invaded it directly, the nearest distance was 0.

Outcome variables

The outcome variables included EOR, postoperative 3-month/6-month AQ and KPS, other surgery-related complications (intracranial infection, hemorrhage, ischemia, severe brain edema, hydrocephalus and leakage of cerebrospinal fluid, etc.), seizures and their control, temporary and permanent language deficits, postoperative radiotherapy (or not), cycles of TMZ chemotherapy, progression-free survival (PFS) and overall survival (OS). Language deficit was defined as the deterioration of postoperative language function at different time points compared to preoperative functional status of patients. According to De Witt Hamer 2012, the time point of TLD was defined as within 3 months postoperatively (18). The time point of PLD ranged from 2 weeks to 6 months in previous studies. Because the language function still improved after 3 months, according the definition of some studies we defined the time point of PLD as >6 months postoperatively (19–21). Furthermore in order to avoid the situation of language deficit caused by recurrent tumor, the patients of PFS ≤ 3 months were excluded when counting the cases of TLD up, the patients of PFS ≤ 6 months were excluded when counting the cases of PLD up.

Surgery process and language areas preservation

All patients underwent preoperative MRI on a 1.5-T scanner (Siemens Espree, Erlangen, Germany). During the preoperative BOLD-fMRI scanning, the patients were asked to perform tasks of "number counting", "picture naming" and "word/sentence making". So that the language cortices can be activated on MRI. The MRI data were imported into the Brainlab software, iPlan 3.0 was used to perform preoperative surgical plan. All delineations of the region of interest (ROI) were completed by a board-certified neuroradiologist with 8 years of experience and a surgeon. The ROIs included tumor and language areas. The delineation of language cortices was based on anatomy and activated regions of BOLD-fMRI; then according to these seed areas, the language tracts were reconstructed. We depicted Broca area, Wernicke area and arcuate fasciculus for all patients. Because these areas were associated with language most directly, the preservation of them was enough for most patients. Sometimes we also depicted the angular gyrus, supramarginal gyrus, ventral premotor cortex and reconstructed inferior occipito-frontal tract, frontal aslant tract, etc. The 3 dimensional images of tumor and language cortices and tracts can be reconstructed and presented on screen, so that the shortest geodesic distance to language areas (cortices or tracts) can be calculated by measuring tools of iPlan. Finally, the surgical plan data were imported into neuronavigation. We performed most surgeries assisted by neuronavigation, iMRI and DES/IONM (multimodal group). The use of multimodal techniques can guide the surgeon to remove tumor and preserve language areas in real time. Some patients were performed resection guided by neuronavigation alone (conventional group). The choice of multimodal techniques was based on the volume and location of tumor, difficulty of resection, possibility of intraoperative residual tumor and language damage, patients' wishes and surgeon's experience.

Tumor measurements

Tumor volume were measured with iPlan in Brainlab (Feldkirchen, Germany). The EOR was defined as (preoperative tumor volume – postoperative residual tumor volume)/preoperative tumor volume × 100. Gross total resection (GTR) was defined as EOR=100% in this study.

Postoperative treatment and follow-up

Patients with LGG were recommended to receive postoperative radiotherapy (60 Gy) and adjuvant TMZ chemotherapy (150-200 mg/m^2/day). Patients with HGG were recommended to receive radiotherapy plus concomitant (60 Gy + TMZ 75 mg/m^2/day) and adjuvant TMZ chemotherapy (150-200 mg/m^2/day). Regular MRI scanning was performed for patients every 3 months. The patients were followed up by an outpatient service or telephone every 3 months, and the follow-up time was up to December 2021.

Statistical analysis

SPSS 21.0 was used to perform the statistical analysis. The Shapiro–Wilk test was used to test the normality of the data, and

Levene's test was used to test the homogeneity of variance of the samples. The Student's t and χ^2 (or Fisher's exact test) tests were used to compare continuous parametric and categorical variables between groups, respectively. The Mann–Whitney *U* test was used to compare continuous nonparametric variables. Logistic regression was used to perform univariate and multivariate analysis. The predictive model was as follows: ln (P/1-P) = β0+β1X1+β2X2+…+βmXm (P was the occurrence probability of language deficits, β0 was a constant, Xm was the value of the variable, and βm was the regression coefficient). The accuracy of model was assessed by receiver operating characteristic (ROC) curve. A P value <0.05 was considered statistically significant. The univariate analysis set P<0.1 as the significance level.

Results

Among 682 GILAs, 530 patients were included finally. One hundred and fifty-two patients were excluded because of age (<6 years old), biopsy only, loss of MRI data, awake craniotomy or loss of follow-up. Among these included patients, 498 patients were eligible to assess TLD because their PFS were longer than 3 months, 441 patient were eligible to assess PLD because their PFS were longer than 6 months. Among the 530 patients, 363 (355 [97.8%] right-handers) were performed surgery assisted by multimodal techniques and 167 (162 [97.0%] right-handers) were performed surgery assisted by neuronavigation alone.

Comparison between occurrence group and non-occurrence group

Four hundred and ninety-eight patients with GILAs were assessed for the occurrence of TLD. One hundred and sixteen patients had TLD and 382 did not have TLD within 3 months postoperatively. Clinical and tumor factors were compared between the occurrence group and non-occurrence group (Supplementary Table 1). Compared to non-occurrence group, the occurrence group had shorter median distance between tumor and language areas (0.47mm versus 2.11mm, P=0.03), higher median preoperative AQ (100 versus 91.3, P=0.001) and lower rate of using multimodal techniques (56.0% versus 74.1%, P<0.001).

Four hundred and forty-one patients with GILAs were assessed for the occurrence of PLD. Seventy-seven patients had PLD and 364 did not have PLD on 6 months postoperatively. The comparison results between the occurrence group and non-occurrence group were presented in Supplementary Table 2. Compared to non-occurrence group, the occurrence group had shorter median distance between tumor and language areas (0mm versus 2.26mm, P=0.01), higher preoperative AQ (P=0.02), higher rate of SMA/PMA involved (18.2% versus 8.5%, P=0.02) and lower rate of using multimodal techniques (54.5% versus 74.7%, P<0.001).

Comparison between conventional group and multimodal group

The multimodal group had the higher median EOR and rate of GTR than conventional group. The incidence of PLD was 13.4% in multimodal group, which was much lower than that (27.6%, P<0.001) in conventional group. The multimodal group also had higher KPS than conventional group on 3 and 6 months postoperatively. The incidences of other complications and seizure were similar in both groups (Table 1).

Factors associated with TLD

Univariate analysis showed that 4 factors were associated with the occurrence of TLD (P<0.1) (Table 2).

The optimal shortest distance threshold was 1.5mm in differentiating TLD with no TLD, thus if the tumor located

TABLE 1 Comparison of outcomes between multimodal and conventional groups.

Variables	Multimodal group (N=363)	Conventional group (N=167)	P
EOR (%), median (IQR)	100 (98.43-100)	94.97 (90.14-100)	**<0.001**
GTR (EOR=100%)	264 (72.7)	71 (42.5)	**<0.001**
Other complications, N (%)	21 (5.8)	12 (7.2)	0.54
Seizures, N (%)	35 (9.6)	14 (8.4)	0.64
KPS, within 3 months, mean±sd	81.6 ± 15.0	77.9 ± 16.7	**0.02**
KPS, within 6 months, mean±sd	84.9 ± 14.6	82.1 ± 14.7	**0.04**
Temporary language deficit, N (%)	65 (18.7)	51 (34.0)	**<0.001**
Permanent language deficit, N (%)	42 (13.4)	35 (27.6)	**<0.001**

Boldface type indicated statistical significance.

within 1.5mm of language areas, the patient tended to have postoperative TLD (Table 3). The optimal AQ threshold was 52 in differentiating TLD with no TLD, thus if the AQ was more than 52, the patient tended to have postoperative TLD (Table 4).

Multivariate analysis indicated that 3 factors were associated with TLD significantly, including shortest distance to language areas (OR=0.85, P<0.001), preoperative AQ (OR=1.04, P<0.001) and multimodal techniques used (OR=0.41, P<0.001) (Table 5). The predictive model of the probability of TLD was ln (P/1-P) = -1.78 -0.16X1 +0.037X2 -0.884X4, and the range of P was [4.8%, 87.2%].

The ROC analysis showed that the area under curve (AUC) of ROC was 0.70 (95%CI: 0.65-0.75). The cutoff

TABLE 2 Factors for temporary language deficit by univariate analysis.

Factors	OR (95%CI)	P
Sex (Male vs Female)	1.08 (0.71-1.66)	0.72
Age	1.00 (0.98-1.01)	0.52
Recurrent tumor vs primary tumor	0.68 (0.38-1.22)	0.19
WHO grade (HGG vs LGG)	0.95 (0.59-1.52)	0.82
Tumor volume	1.00 (1.00-1.01)	0.23
Tumor location (reference: Frontal/Frontal insular)		
Temporal/Temporal insular	0.94 (0.58-1.53)	0.81
Frontal temporal/Frontotemporal insular	0.84 (0.46-1.54)	0.57
Insular/Parietal/Parietal temporal/Parietooccipital/Other locations	0.58 (0.27-1.27)	0.18
Shortest distance to language areas	0.92 (0.85-0.99)	**0.03**
Language cortices involved vs not involved	0.85 (0.56-1.29)	0.45
SMA/PMA invaded vs not invaded	1.45 (0.75-2.82)	0.27
Preoperative AQ	1.03 (1.01-1.04)	**<0.001**
Preoperative seizure (Yes vs No)	1.05 (0.67-1.64)	0.83
Drug intractable seizures (Yes vs No)	1.16 (0.50-2.66)	0.73
Preoperative KPS	1.01 (0.99-1.03)	0.26
EOR	0.97 (0.96-0.99)	**0.002**
Other complications (Yes vs No)	1.52 (0.80-2.90)	0.20
Multimodal techniques (used vs not used)	0.45 (0.29-0.69)	**<0.001**

Boldface type indicated statistical significance.

TABLE 3 Optimal shortest distance threshold in differentiating TLD with no TLD by reduction of 0.5mm.

Univariate analysis	Shortest distance (≤3mm)	Shortest distance (≤2mm)	Shortest distance (≤1.5mm)	Shortest distance (≤1mm)
OR for TLD (95%CI)	1.48 (0.97-2.26)	1.50 (0.98-2.29)	1.52 (1.00-2.32)	1.57 (1.04-2.39)
P value	0.07	0.06	**0.049**	**0.034**

Boldface type indicated statistical significance.

TABLE 4 Optimal AQ threshold in differentiating TLD with no TLD by increments of 1 AQ.

Univariate analysis	AQ (≥50)	AQ (≥51)	AQ (≥52)	AQ (≥53)	AQ (≥55)	AQ (≥60)
OR for TLD (95%CI)	7.37 (0.98-55.16)	7.37 (0.98-55.16)	8.40 (1.13-62.58)	9.10 (1.22-67.60)	11.60 (1.57-85.62)	13.08 (1.78-96.25)
P value	0.052	0.052	**0.038**	**0.031**	**0.016**	**0.012**

Boldface type indicated statistical significance.

TABLE 5 Factors for temporary language deficit by multivariate analysis.

Factors	OR (95%CI)	P
Shortest distance to language areas (X1)	0.85 (0.78-0.93)	**<0.001**
Preoperative AQ (X2)	1.04 (1.02-1.06)	**<0.001**
EOR (X3)	0.98 (0.96-1.00)	0.06
Multimodal techniques (used vs not used) (X4)	0.41 (0.26-0.65)	**<0.001**

Boldface type indicated statistical significance.

predictive probability of TLD was 23.7%. In this case the sensitivity (Sen) was 0.66, the specificity (Spe) was 0.66, the diagnostic odds ratio (DOR) was 3.64, the positive predictive value (+PV) was 0.37, and the negative predictive value (-PV) was 0.86 (Figure 1).

Factors associated with PLD

Univariate analysis showed that 6 factors were associated with the occurrence of TLD (P<0.1) (Table 6).

The optimal shortest distance threshold was 4mm in differentiating PLD with no PLD, thus if the tumor located within 4mm of language areas, the patient tended to have postoperative PLD (Table 7). The optimal AQ threshold was 61 in differentiating PLD with no PLD, thus if the AQ was more than 61, the patient tended to have postoperative PLD (Table 8).

Multivariate analysis indicated 4 factors were associated with PLD significantly, including shortest distance to language areas (OR=0.83, P=0.001), SMA/PMA involved (OR=3.04, P=0.007), preoperative AQ (OR=1.03, P=0.002) and multimodal techniques used (OR=0.35, P<0.001) (Table 9). The predictive model of the probability of PLD was ln (P/1-P) = -2.098 -0.186X2 +1.112X3 +0.032X4 -1.046X6, and the range of P was [0.1%, 90.2%].

The ROC analysis showed that the AUC of ROC was 0.72 (95%CI: 0.66-0.79). The cutoff of predictive probability of PLD was 16.1%. In this case the Sen was 0.75, the Spe was 0.64, the DOR was 5.49, the positive +PV was 0.31, and the -PV was 0.92 (Figure 1).

Discussion

Maximal safe resection is the goal of surgery of glioma involving eloquent areas. The preservation of language is an important factor that should be considered in the resection of GILAs in the dominant hemisphere. DES combined with awake craniotomy has been the gold standard method for the surgery of GILAs and it continuously develops and innovates (22). Many methods have been developed to increase the accuracy of MRI in functional area localization, for example, a combination of seed-based correlation mapping and spatially independent component analysis, a combination of tb-fMRI and rs-MRI, and optimization of the DTI tract reconstruction algorithm. Furthermore, various intraoperative imaging techniques, especially intraoperative MRI (iMRI), can overcome brain drift defects and increase EOR. Therefore, an increasing number of studies have indicated that neuronavigation based on multimodal imaging, iMRI, DES and IONM (multimodal techniques) can achieve maximal safe resection of GILAs under general anesthesia (23, 24). Our center began to use neuronavigation in glioma surgery in 2002 and has used

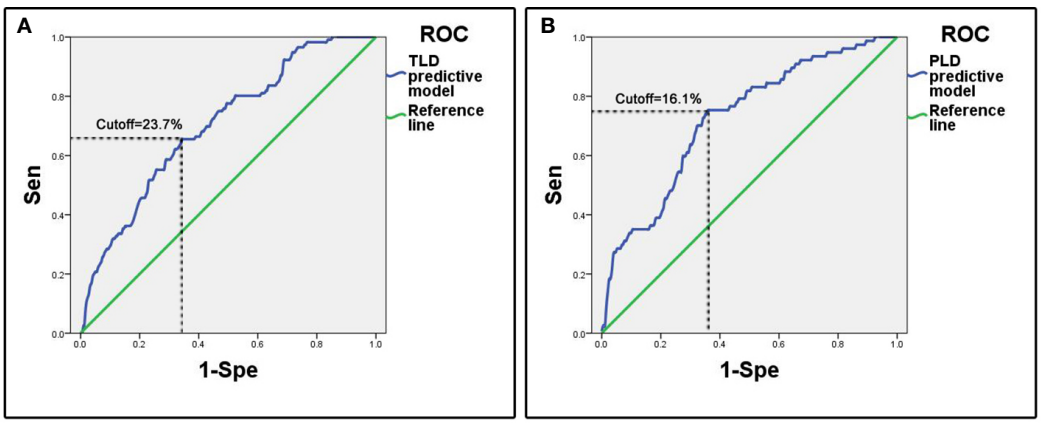

FIGURE 1
ROC curves of predictive models. **(A)** Predictive model of temporary language deficit, the cutoff value of predictive probability of TLD was 23.7%, the Sen was 0.66 and the Spe was 0.66. **(B)** Predictive model of permanent language deficit, the cutoff value of predictive probability of PLD was 16.1%, the Sen was 0.75 and the Spe was 0.64.

TABLE 6 Factors for permanent language deficit by univariate analysis.

Factors	OR (95%CI)	P
Sex (Male vs Female)	1.10 (0.66-1.82)	0.72
Age	1.00 (0.98-1.02)	0.70
Recurrent tumor vs primary tumor	0.75 (0.38-1.50)	0.42
WHO grade (HGG vs LGG)	1.17 (0.67-2.04)	0.58
Tumor volume	1.00 (1.00-1.01)	0.76
Tumor location (reference: Frontal/Frontal insular)		
Temporal/Temporal insular	0.69 (0.39-1.24)	0.22
Frontal temporal/Frontotemporal insular	0.61 (0.29-1.26)	0.57
Insular/Parietal/Parietal temporal/ Parietooccipital/Other locations	0.39 (0.15-1.05)	**0.06**
Shortest distance to language areas	0.91 (0.84-1.00)	**0.05**
Language cortices involved vs not involved	1.01 (0.62-1.66)	0.96
SMA/PMA invaded vs not invaded	2.39 (1.20-4.74)	**0.01**
Preoperative AQ	1.02 (1.00-1.04)	**0.02**
Preoperative seizure (Yes vs No)	1.41 (0.85-2.33)	0.18
Drug intractable seizures (Yes vs No)	1.20 (0.47-3.04)	0.71
Preoperative KPS	1.01 (1.00-1.03)	0.24
EOR	0.98 (0.96-1.00)	**0.07**
Complications (Yes vs No)	0.65 (0.25-1.72)	0.39
Multimodal techniques (used vs not used)	0.41 (0.24-0.67)	**<0.001**

Boldface type indicated statistical significance.

intraoperative multimodal techniques since 2009. Previous studies reported the incidences of PLD ranged from 0 to 14.8% when removing GILAs under awake craniotomy, the incidence was around 8% in most studies. Although our multimodal group of general anesthesia had a little higher incidence of PLD (13.4%) than previous studies of awake craniotomy, we achieved much higher rate of GTR (72.7%) than all previous studies of awake craniotomy (ranged from 25.5% to 72.0%, most around 50%) (24–36). Thus when the patients were underwent surgery assisted by multimodal techniques under general anesthesia, their outcome was not inferior to those under awake craniotomy. However many factors may also cause temporary or permanent language deficits after surgery under general anesthesia. What factors are associated with TLD or PLD remains unclear. In this study, we tried to identify significant factors of TLD and PLD based on our large cohort of patients.

Shortest distance to language areas was both associated with TLD (OR=0.85) and PLD (OR=0.83), which indicated that the shorter the distance between tumor and language areas was, the higher probability of occurrence of TLD and PLD was. This phenomenon was obvious to be explained, if the tumor was close to language areas, it may more likely invade and destroy the language function. Meanwhile preoperative AQ was both associated with TLD (OR=1.04) and PLD (OR=1.03), which demonstrated that a higher AQ of the patient meant a higher probability of occurrence of TLD and PLD. This result can be explained by the more obvious change effect of language function tested by us in patients with higher AQ. Optimal shortest distance threshold for detecting TLD was 1.5mm and for detecting PLD was 4mm. Optimal AQ threshold for detecting TLD was 52 and for detecting PLD was 61. This result indicates that if the border of tumor is less than 4mm from language areas and the AQ is more than 61, the patients tend to have the higher probability of occurrence of PLD. In this case, multimodal techniques should be suggested to be used, in addition awake craniotomy combined with DES can preserve the language function more effectively for this kind of patients (31). The iMRI can both benefit the preservation of temporary and permanent language function. The iMRI was a valuable tool to correct brain drift by updating neuronavigation and reconstructing language cortices and tracts. It can also detect residual tumor and update surgical plan, the further resection can increase the EOR significantly (37, 38). So for all patients with GILAs, iMRI should be suggested.

Tumor location was associated with PLD in univariate analysis. Compared with the tumors of frontal/frontal insular lobes, the tumors of insular and parietal lobes were associated with a lower probability of PLD by univariate analysis (OR=0.39, P=0.06). As we know, frontal lobe, especially inferior frontal gyrus and its related tracts played a main role in language. While some part of insular and parietal lobes also participated

TABLE 7 Optimal shortest distance threshold in differentiating PLD with no PLD by reduction of 0.5mm.

Univariate analysis	Shortest distance (≤5mm)	Shortest distance (≤4.5mm)	Shortest distance (≤4mm)	Shortest distance (≤3mm)
OR for PLD (95% CI)	1.41 (0.72-2.74)	1.84 (0.97-3.49)	1.83 (1.01-3.31)	1.78 (1.05-3.03)
P value	0.32	0.06	**0.046**	**0.033**

Boldface type indicated statistical significance.

TABLE 8 Optimal AQ threshold in differentiating PLD with no PLD by increments of 1 AQ.

Univariate analysis	AQ (≥55)	AQ (≥60)	AQ (≥61)	AQ (≥62)	AQ (≥63)	AQ (≥65)
OR for PLD (95%CI)	6.58 (0.88-49.05)	7.33 (0.99-54.45)	7.83 (1.06-58.10)	8.60 (1.16-63.66)	9.12 (1.23-67.43)	2.91 (1.02-8.30)
P value	0.07	0.052	**0.044**	**0.035**	**0.03**	**0.046**

Boldface type indicated statistical significance.

in language function, for example, angular gyrus and supramarginal gyrus were located in inferior parietal lobe, the insular lobe had efferent and afferent connections with temporal lobe (39, 40). Our result indicated that gliomas of frontal lobe may have more impact on postoperative language function, which can cause more PLD of patients. However this association was not significant in multivariate analysis. We considered it was because the use of intraoperative multimodal techniques for many patients reduced the influence of tumor location on PLD, and tumor location was not more important than other factors.

Many previous studies had proved the influence of SMA and PMA on language function. Language function was considered controlled by a network that involving many cortical and subcortical areas. SMA and PMA were two important areas that took part in language function. Hertrich 2016 reported that SMA was associated with both speech motor control and language processing (41). Bathla 2019 reported that the central SMA can participate in the connectivity with both motor and language networks (42). Van Geemen 2014 reported that the ventral PMA played a role in language production and fluency and its plasticity was limited (43). Another study Duffau, 2004 also proved the relevance between language function and ventral PMA (including its descending subcortical tract) (44). So our result supported the importance of SMA/PMA on language function of previous studies. Our result showed that SMA or PMA involved was associated with the occurrence of PLD, but was not associated with the occurrence of TLD. This phenomenon may be explained by the long-term effects of destroyed SMA/PMA. The AQ test may not have the ability to detect the subtle change of advanced language in a short-term, so the AQ may not change a lot, which caused no association between SMA/PMA involved and TLD. This phenomenon should be testified by studies in future.

To the authors' knowledge, this study is the largest series utilizing a multimodal approach guiding GILAs resection under general anesthesia. We established predictive model based on clinical factors and identified the cutoff values of predictive probability for TLD and PLD respectively. If a patient has a high preoperative AQ and the tumor is close to language areas and involves SMA/PMA, the predictive probability for TLD/PLD is higher than the cutoff, he/she will have a high predictive probability of TLD/PLD. In this case, we should use multimodal techniques (especially iMRI) under general anesthesia to preserve language more effectively. In addition, awake craniotomy combined with DES can be used for patients having a very high predictive probability of TLD/PLD. Although our predictive model had a moderate accuracy, it can still guide surgeon and patients of GILAs to choose an appropriate surgery strategy and avoid unnecessary techniques used. Furthermore, the model for TLD and PLD both had the high -PV (0.86 and 0.92) and low +PV (0.37 and 0.31). Thus, if a patient had a calculated probability less than cutoff value,

TABLE 9 Factors for permanent language deficit by multivariate analysis.

Factors	OR (95%CI)	P
Tumor location (X1, reference: Frontal/Frontal insular)		
Temporal/Temporal insular	0.84 (0.43-1.62)	0.60
Frontal temporal/Frontotemporal insular	0.75 (0.33-1.69)	0.49
Insular/Parietal/Parietal temporal/Parietooccipital/Other locations	0.53 (0.19-1.51)	0.23
Shortest distance to language areas (X2)	0.83 (0.75-0.93)	**0.001**
SMA/PMA invaded vs not invaded (X3)	3.04 (1.35-6.84)	**0.007**
Preoperative AQ (X4)	1.03 (1.01-1.05)	**0.002**
EOR (X5)	0.99 (0.96-1.01)	0.33
Multimodal techniques (used vs not used) (X6)	0.35 (0.20-0.61)	**<0.001**

Boldface type indicated statistical significance.

resection under general anesthesia can ensure a low incidence of TLD/PLD. So this model can provide surgeon and patients a reference of incidence of TLD/PLD to help them make decision of what intraoperative techniques to be used.

Some limitations existed in this study. (1) Retrospective studies have inherent limitations that may cause selection bias, recall bias and loss to follow-up bias. (2) In order to facilitate data analysis, tumor location cannot be classified too many categories, we only classified 4 main categories in our cohort. But the language network was complex, gliomas involving different language areas can cause different types of language deficits. In further study, the tumor location should be divided in detail to explore its association with postoperative language function of GILAs. (3) The predictive model was based on cohort of patients under general anesthesia, so it was only applicable to patients underwent surgery under general anesthesia. The model should be validated with further prospective studies. Awake craniotomy should be also added as a factor that associated with language deficit to improve this model in future, which will make this model have a wider applied range.

Conclusion

The use of multimodal techniques can reduce the risk of postoperative TLD/PLD after removing GILAs under general anesthesia. The established predictive model indicated that higher AQ, shorter distance to language areas, SMA/PMA invaded and multimodal techniques not used were associated with the higher probability of occurrence of language deficit after resection of GILAs under general anesthesia. The optimal AQ threshold and shortest distance threshold in detecting TLD/PLD were also identified. The model had a moderate accuracy in predicting the occurrence of TLD/PLD. We can provide the surgeon and patients a guide to choose appropriate surgery strategy and techniques. The model should be validated with further prospective studies.

Data availability statement

The raw data supporting the conclusions of this article will be made available by the authors, without undue reservation.

Ethics statement

Retrospective clinical data were reviewed from electronic medical records in the Department of Neurosurgery at our center between January 2009 and December 2020. This study was approved by our institutional ethics committee. Written informed consent was signed by all patients or their relatives before surgery.

Author contributions

MC: conceptualization, data collection, data analysis, data visualization, literature review, and manuscript writing and editing; QG, YC: data collection, data analysis, data visualization; MZ, HY, XG, HC, YL: data collection, data curation, reviewed speech and language. XM: conceptualization, methodology, supervision, and manuscript reviewing. All authors contributed to the article and approved the submitted version.

Acknowledgments

Thanks to the members of the Department of Neurosurgery, PLA General Hospital (Xiuying Wang, MD; Zhizhong Zhang, MBBS) for their collaboration.

Conflict of interest

YC was employed by the company Xian Janssen Pharmaceutical Ltd.

The remaining authors declare that the research was conducted in the absence of any commercial or financial relationships that could be construed as a potential conflict of interest.

Publisher's note

Supplementary material

The Supplementary Material for this article can be found online at: https://www.frontiersin.org/articles/10.3389/fonc.2022.1090170/full#supplementary-material

References

1. Ostrom QT, Bauchet L, Davis FG, Deltour I, Fisher JL, Langer CE, et al. The epidemiology of glioma in adults: A "state of the science" review. *Neuro Oncol* (2014) 16(7):896–913. doi: 10.1093/neuonc/nou087

2. Stupp R, Mason WP, van den Bent MJ, Weller M, Fisher B, Taphoorn MJ, et al. Radiotherapy plus concomitant and adjuvant temozolomide for glioblastoma. *N Engl J Med* (2005) 352(10):987–96. doi: 10.1056/NEJMoa043330

3. Louis DN, Perry A, Reifenberger G, von Deimling A, Figarella-Branger D, Cavenee WK, et al. The 2016 world health organization classification of tumors of the central nervous system: A summary. *Acta Neuropathol* (2016) 131(6):803–20. doi: 10.1007/s00401-016-1545-1

4. Nabors LB, Portnow J, Ammirati M, Baehring J, Brem H, Butowski N, et al. NCCN guidelines insights: Central nervous system cancers, version 1.2017. *J Natl Compr Canc Netw* (2017) 15(11):1331–45. doi: 10.6004/jnccn.2017.0166

5. Fabian D, Guillermo Prieto Eibl MDP, Alnahhas I, Sebastian N, Giglio P, Puduvalli V, et al. Treatment of glioblastoma (GBM) with the addition of tumor-treating fields (TTF): A review. *Cancers (Basel)* (2019) 11(2):174–185. doi: 10.3390/cancers11020174

6. Louis DN, Perry A, Wesseling P, Brat DJ, Cree IA, Figarella-Branger D, et al. The 2021 WHO classification of tumors of the central nervous system: a summary. *Neuro Oncol* (2021) 23(8):1231–51. doi: 10.1093/neuonc/noab106

7. Smith JS, Chang EF, Lamborn KR, Chang SM, Prados MD, Cha S, et al. Role of extent of resection in the long-term outcome of low-grade hemispheric gliomas. *J Clin Oncol* (2008) 26(8):1338–45. doi: 10.1200/JCO.2007.13.9337

8. Sanai N, Polley MY, McDermott MW, Parsa AT, Berger MS. An extent of resection threshold for newly diagnosed glioblastomas. *J Neurosurg* (2011) 115 (1):3–8. doi: 10.3171/2011.2.JNS10998

9. Sagar S, Rick J, Chandra A, Yagnik G, Aghi MK. Functional brain mapping: overview of techniques and their application to neurosurgery. *Neurosurg Rev* (2019) 42(3):639–47. doi: 10.1007/s10143-018-1007-4

10. Gravesteijn BY, Keizer ME, Vincent A, Schouten JW, Stolker RJ, Klimek M. Awake craniotomy versus craniotomy under general anesthesia for the surgical treatment of insular glioma: Choices and outcomes. *Neurol Res* (2018) 40(2):87–96. doi: 10.1080/01616412.2017.1402147

11. Chowdhury T, Gray K, Sharma M, Mau C, McNutt S, Ryan C, et al. Brain cancer progression: A retrospective multicenter comparison of awake craniotomy versus general anesthesia in high-grade glioma resection. *J Neurosurg Anesthesiol.* (2022) 34(4):392–400. doi: 10.1097/ANA.0000000000000778

12. Sun GC, Wang F, Chen XL, Yu XG, Ma XD, Zhou DB, et al. Impact of virtual and augmented reality based on intraoperative magnetic resonance imaging and functional neuronavigation in glioma surgery involving eloquent areas. *World Neurosurg* (2016) 96:375–82. doi: 10.1016/j.wneu.2016.07.107

13. Chen LF, Yang Y, Ma XD, Yu XG, Gui QP, Xu BN, et al. Optimizing the extent of resection and minimizing the morbidity in insular high-grade glioma surgery by high-field intraoperative MRI guidance. *Turk Neurosurg* (2017) 27 (5):696–706. doi: 10.5137/1019-5149.JTN.18346-16.1

14. Cui M, Chen H, Sun G, Liu J, Zhang M, Lin H, et al. Combined use of multimodal techniques for the resection of glioblastoma involving corpus callosum. *Acta Neurochirurgica* (2022) 164(3):689–702. doi: 10.1007/s00701-021-05008-6

15. Shewan CM, Kertesz A. Reliability and validity characteristics of the Western aphasia battery (WAB). *J Speech Hear Disord* (1980) 45(3):308–24. doi: 10.1044/jshd.4503.308

16. De Witt Hamer PC, De Witt Hamer PC, Klein M, Hervey-Jumper SL, Wefel JS, Berger MS. Functional outcomes and health-related quality of life following glioma surgery. *Neurosurgery* (2021) 88(4):720–32. doi: 10.1093/neuros/nyaa365

17. Fang S, Weng S, Li L, Guo Y, Fan X, Zhang Z, et al. Association of homotopic areas in the right hemisphere with language deficits in the short term after tumor resection. *J Neurosurg* (2022), 1–10. doi: 10.3171/2022.9.JNS221475

18. De Witt Hamer PC, Robles SG, Zwinderman AH, Duffau H, Berger MS. Impact of intraoperative stimulation brain mapping on glioma surgery outcome: a meta-analysis. *J Clin Oncol* (2012) 30(20):2559–65. doi: 10.1200/JCO.2011.38.4818

19. Brennum J, Engelmann CM, Thomsen JA, Skjøth-Rasmussen J. Glioma surgery with intraoperative mapping-balancing the onco-functional choice. *Acta Neurochir (Wien)* (2018) 160(5):1043–50. doi: 10.1007/s00701-018-3521-0

20. Eseonu CI, Rincon-Torroella J, Lee YM, ReFaey K, Tripathi P, Quinones-Hinojosa A. Intraoperative seizures in awake craniotomy for perirolandic glioma resections that undergo cortical mapping. *J Neurol Surg A Cent Eur Neurosurg* (2018) 79(3):239–46. doi: 10.1055/s-0037-1617759

21. Saito T, Muragaki Y, Tamura M, Maruyama T, Nitta M, Tsuzuki S, et al. Awake craniotomy with transcortical motor evoked potential monitoring for resection of gliomas in the precentral gyrus: utility for predicting motor function. *J Neurosurg* (2019) 132(4):987–97. doi: 10.3171/2018.11.Jns182609

22. Gogos AJ, Young JS, Morshed RA, Hervey-Jumper SL, Berger MS. Awake glioma surgery: Technical evolution and nuances. *J Neurooncol* (2020) 147(3):515–24. doi: 10.1007/s11060-020-03482-z

23. D'Andrea G, Familiari P, Di Lauro A, Angelini A, Sessa G. Safe resection of gliomas of the dominant angular gyrus availing of preoperative FMRI and intraoperative DTI: Preliminary series and surgical technique. *World Neurosurg* (2016) 87:627–39. doi: 10.1016/j.wneu.2015.10.076

24. Pichierri A, Bradley M, Iyer V. Intraoperative magnetic resonance imaging-guided glioma resections in awake or asleep settings and feasibility in the context of a public health system. *World Neurosurg X* (2019) 3:100022. doi: 10.1016/j.wnsx.2019.100022

25. Peraud A, Ilmberger J, Reulen HJ. Surgical resection of gliomas WHO grade II and III located in the opercular region. *Acta Neurochir (Wien)* (2004) 146(1):9–17. doi: 10.1007/s00701-003-0165-4

26. Duffau H, Moritz-Gasser S, Gatignol P. Functional outcome after language mapping for insular world health organization grade II gliomas in the dominant hemisphere: Experience with 24 patients. *Neurosurg Focus* (2009) 27(2):E7. doi: 10.3171/2009.5.Focus0938

27. Chacko AG, Thomas SG, Babu KS, Daniel RT, Chacko G, Prabhu K, et al. Awake craniotomy and electrophysiological mapping for eloquent area tumours. *Clin Neurol Neurosurg* (2013) 115(3):329–34. doi: 10.1016/j.clineuro.2012.10.022

28. Lu J, Wu J, Yao C, Zhuang D, Qiu T, Hu X, et al. Awake language mapping and 3-Tesla intraoperative MRI-guided volumetric resection for gliomas in language areas. *J Clin Neurosci* (2013) 20(9):1280–7. doi: 10.1016/j.jocn.2012.10.042

29. Martino J, Gomez E, Bilbao JL, Duenas JC, Vazquez-Barquero A. Cost-utility of maximal safe resection of WHO grade II gliomas within eloquent areas. *Acta Neurochir (Wien)* (2013) 155(1):41–50. doi: 10.1007/s00701-012-1541-8

30. Tuominen J, Yrjana S, Ukkonen A, Koivukangas J. Awake craniotomy may further improve neurological outcome of intraoperative MRI-guided brain tumor surgery. *Acta Neurochir (Wien)* (2013) 155(10):1805–12. doi: 10.1007/s00701-013-1837-3

31. Ghinda D, Zhang N, Lu J, Yao CJ, Yuan S, Wu JS. Contribution of combined intraoperative electrophysiological investigation with 3-T intraoperative MRI for awake cerebral glioma surgery: Comprehensive review of the clinical implications and radiological outcomes. *Neurosurg Focus* (2016) 40(3):E14. doi: 10.3171/2015.12.FOCUS15572

32. Saito T, Muragaki Y, Maruyama T, Tamura M, Nitta M, Tsuzuki S, et al. Difficulty in identification of the frontal language area in patients with dominant frontal gliomas that involve the pars triangularis. *J Neurosurg* (2016) 125(4):803–11. doi: 10.3171/2015.8.Jns151204

33. Eseonu CI, Rincon-Torroella J, ReFaey K, Lee YM, Nangiana J, Vivas-Buitrago T, et al. Awake craniotomy vs craniotomy under general anesthesia for perirolandic gliomas: Evaluating perioperative complications and extent of resection. *Neurosurgery* (2017) 81(3):481–9. doi: 10.1093/neuros/nyx023

34. Motomura K, Natsume A, Iijima K, Kuramitsu S, Fujii M, Yamamoto T, et al. Surgical benefits of combined awake craniotomy and intraoperative magnetic resonance imaging for gliomas associated with eloquent areas. *J Neurosurg* (2017) 127(4):790–7. doi: 10.3171/2016.9.Jns16152

35. Nakajima R, Kinoshita M, Okita H, Yahata T, Nakada M. Glioma surgery under awake condition can lead to good independence and functional outcome excluding deep sensation and visuospatial cognition. *Neurooncol Pract* (2019) 6 (5):354–63. doi: 10.1093/nop/npy054

36. Zelitzki R, Korn A, Arial E, Ben-Harosh C, Ram Z, Grossman R. Comparison of motor outcome in patients undergoing awake vs general anesthesia surgery for brain tumors located within or adjacent to the motor pathways. *Neurosurgery* (2019) 85(3):E470–6. doi: 10.1093/neuros/nyz007

37. Leroy HA, Delmaire C, Le Rhun E, Drumez E, Lejeune JP, Reyns N. High-field intraoperative MRI and glioma surgery: Results after the first 100 consecutive patients. *Acta Neurochir (Wien)* (2019) 161(7):1467–74. doi: 10.1007/s00701-019-03920-6

38. Yahanda AT, Chicoine MR. Intraoperative MRI for glioma surgery: Present overview and future directions. *World Neurosurg* (2021) 149:267–8. doi: 10.1016/j.wneu.2021.03.011

39. Ibanez A, Gleichgerrcht E, Manes F. Clinical effects of insular damage in humans. *Brain Struct Funct* (2010) 214(5-6):397–410. doi: 10.1007/s00429-010-0256-y

40. Bzdok D, Hartwigsen G, Reid A, Laird AR, Fox PT, Eickhoff SB. Left inferior parietal lobe engagement in social cognition and language. *Neurosci Biobehav Rev* (2016) 68:319–34. doi: 10.1016/j.neubiorev.2016.02.024

41. Hertrich I, Dietrich S, Ackermann H. The role of the supplementary motor area for speech and language processing. *Neurosci Biobehav Rev* (2016) 68:602–10. doi: 10.1016/j.neubiorev.2016.06.030

42. Bathla G, Gene MN, Peck KK, Jenabi M, Tabar V, Holodny AI. Resting state functional connectivity of the supplementary motor area to motor and language networks in patients with brain tumors. *J Neuroimaging* (2019) 29(4):521–6. doi: 10.1111/jon.12624

43. van Geemen K, Herbet G, Moritz-Gasser S, Duffau H. Limited plastic potential of the left ventral premotor cortex in speech articulation: Evidence from intraoperative awake mapping in glioma patients. *Hum Brain Mapp* (2014) 35 (4):1587–96. doi: 10.1002/hbm.22275

44. Duffau H, Capelle L, Denvil D, Gatignol P, Sichez N, Lopes M, et al. The role of dominant premotor cortex in language: A study using intraoperative functional mapping in awake patients. *Neuroimage* (2003) 20(4):1903–14. doi: 10.1016/s1053-8119(03)00203-9

frontiers | Frontiers in Oncology

TYPE Review
PUBLISHED 26 January 2023
DOI 10.3389/fonc.2023.1114450

OPEN ACCESS

EDITED BY
Songbai Xu,
First Affiliated Hospital of Jilin University, Jilin University, China

REVIEWED BY
Tao Xu,
Shanghai Changzheng Hospital, China
Pengfei Ge,
Jilin University, China

*CORRESPONDENCE
Qisheng Tang
tangqisheng@fudan.edu.cn

SPECIALTY SECTION
This article was submitted to Neuro-Oncology and Neurosurgical Oncology, a section of the journal Frontiers in Oncology

RECEIVED 02 December 2022
ACCEPTED 10 January 2023
PUBLISHED 26 January 2023

CITATION
Jiang S, Chai H and Tang Q (2023) Advances in the intraoperative delineation of malignant glioma margin.
Front. Oncol. 13:1114450.
doi: 10.3389/fonc.2023.1114450

Advances in the intraoperative delineation of malignant glioma margin

Shan Jiang, Huihui Chai and Qisheng Tang*

Department of Neurosurgery, Huashan Hospital, Fudan University, Shanghai, China

Surgery plays a critical role in the treatment of malignant glioma. However, due to the infiltrative growth and brain shift, it is difficult for neurosurgeons to distinguish malignant glioma margins with the naked eye and with preoperative examinations. Therefore, several technologies were developed to determine precise tumor margins intraoperatively. Here, we introduced four intraoperative technologies to delineate malignant glioma margin, namely, magnetic resonance imaging, fluorescence-guided surgery, Raman histology, and mass spectrometry. By tracing their detecting principles and developments, we reviewed their advantages and disadvantages respectively and imagined future trends.

KEYWORDS

glioma, intraoperative, MRI, FGS, Raman histology, mass spectrometry

Introduction

At present, the standard treatment for malignant glioma is surgical resection combined with chemotherapy and radiotherapy, which is far from reaching patients' expectations and offers slow progress (1–3). As the first step, surgery plays a critical role in multimodal treatments and its efficacy is highly dependent on the surgeon's skill. Moreover, due to the infiltrative growth, it is difficult to depict the tumor margin and excise the tumor completely (4). Consequently, it contributes to a high local relapse rate, and most recurrences occur near the surgery margins. Therefore, delineating more sophisticated brain tumor margins and improving surgeons' ability to navigate removing the tumor completely are important for the improvement of brain tumor treatments (5).

Therefore, to visualize the tumor margin and assist neurosurgeons in resecting tumors completely, establishing a precise and real-time guiding system has already become an active demand in neurosurgery. Besides the infiltrative growth nature, the requirement of protecting brain functional boundaries emphasizes more importance to improving the resolution of margin demarcation than other solid tumors in the peripheral system. Various techniques in detecting tumor molecular or metabolic markers by physical or chemical methods allow for depicting millimeter-level resolution boundaries (6, 7). Moreover, due to the impact of brain shifting, it is necessary for various techniques to be performed and to amend intraoperative detection (8–10).

Here, we list the developments of several novel intraoperative technologies depicting precise malignant brain tumor margins, that is, magnetic resonance imaging (MRI), fluorescence-

guided surgery (FGS), Raman histology, and mass spectrometry (MS) (Figure 1). Analyzing the advantages and disadvantages of different technologies, we provide a comprehensive review to trace the updated developments of new intraoperative systems.

Intraoperative MRI

MRI is the essential preoperative examination for brain cancer patients and a salient basis for intraoperative navigation. However, due to the presence of brain shift, which is inevitably caused by the loss of cerebrospinal fluid, force-induced deformation of brain tissue, and so on, the utilization of preoperative image data to guide neuronavigation will inevitably lead to deviations (11). These deviations may lead to either residual tumor after resection or over-resection of normal brain tissue. Though various software for correction algorithms based on physical or mathematical models are under research and development, clinical examinations of this software are required (12, 13).

Currently, intraoperative imaging remains the established solution (14). Contributing to its high contrast in soft tissues, precise spatial resolution, and functional brain imaging ability, intraoperative MRI (iMRI) becomes the first option among various intraoperative imaging systems (15, 16). The first public application of iMRI in the neurosurgical community was reported by General Electric and Brigham and Women's Hospital (BWH) of Harvard University in 1996 (17, 18). The past 26 years have witnessed a great development in iMRI systems. Previous generations of iMRI were based on moving the operating table into the MRI examination room. Nowadays, fundamental innovations in the engineering and physics of the magnet and coils allow the movement of MRI scanners. The common characteristic of the newest iMRI systems is the performance of intraoperative imaging without the movement of patients, that is, to be able to perform surgery while the scan is being completed and with the patient in the same position (19). The field strength of iMRI is also increasing, which improves the imaging quality. Moreover, high field strength provides the advantages of less signal acquisition time, high sensitivity of functional imaging, and quantitative analysis of tissue metabolites based on spectrum signal (20, 21). Senft et al. performed a prospective, randomized, parallel-group trial to confirm the efficacy of iMRI application. They found that 96% (23/24) of the patients in the iMRI group and 68% (17/25) of the patients in the control group had complete tumor resection. No patient for whom the use of iMRI led to continued resection of the residual tumor had neurological deterioration. It indicated that imaging helped surgeons provide the optimum extent of resection (22). Huashan Hospital retrospectively analyzed 373 patients with 3T iMRI-guided surgery. The ratio of gross total resection for cerebral gliomas (n = 161) was increased from 55.90% to 87.58% (23). Also, Kuhnt et al. proved the correlation between the extent of tumor resection and glioblastoma multiforme patient survival with high-field iMRI, demonstrating that navigation guidance and iMRI significantly contribute to optimal EOR with low postoperative morbidity, where the extent of resection ≥98% and patient age <65 years are associated with significant survival advantages (22). However, high-field-strength iMRI has its share of problems. Owing to the interference of waves caused by the dielectric effect, the imaging signal is uneven and the center signal is higher than the peripheral one. Also, compared with 1.5 T iMRI, motion artifacts, chemical shift artifacts, and susceptibility artifacts were more obvious on 3.0 T iMRI (24).

Besides the structure imaging ability of iMRI, its functional imaging and molecular imaging show more and more advantages in the operation of malignant glioma. The protection of brain function during operation is a very salient issue in neurosurgery. Different from the peripheral system with more clear structural markers, individual brain functional regions have great differences in details. Therefore, electrophysiological monitoring and intraoperative arousal techniques play critical roles in the resection of tumors located in brain functional areas. Usually, preoperative MRI examination uses blood oxygen level-dependent imaging (BOLD) and diffusion tensor imaging (DTI) technologies to achieve fMRI imaging of brain functional areas, to achieve relatively intuitive and gradual delineation of brain functional area boundaries, and to help design surgical approaches and resection schemes. Lehéricy et al. and Wu et al. both reported that BOLD localization of the motor cortex was in good agreement with the results of controlled studies on direct electrical stimulation during surgery (25–27). Studies by Rutten et al. show that BOLD and electrical stimulation technology have good consistency in locating the language cortex (28). However, the delineation of malignant glioma functional margin based on preoperative MRI has its limitations. Because of the disturbance in the operation, the accuracy of the preoperative functional partition decreases with the operation. The tiny deviations can have serious consequences when it comes to the functional brain regions. Fortunately, iMRI can achieve both fMRI and DTI. Besides the localization of the motor cortex using the task-based intraoperative fMRI technique during awake procedures, the resting state localizing the motor cortex of patients who are under general anesthesia could be detected using intraoperative fMRI (29, 30). Also, D'Andrea et al. reported that they localized white matter tracts participating in language with intraoperative DTI instead of direct electrical cortical stimulation (DCS) and that 78% of patients achieve gross total excision without any postoperative complications (31). However, the inherent flaws in the functional detection ability of MRI may result in limited statistical power, arbitrary data analysis, false-positive results, and lack of independent replications (32). Therefore, though iMRI could improve the precision of fMRI, the fact that it is time-consuming and unstable makes it unlikely to replace DCS, while intraoperative DTI has the potential to increase the safety and excision extension of non-awake surgery.

Not only functional imaging, but also molecular imaging might be a promising development direction. In 2021, the fifth edition of the WHO Central System Tumor Grading Criteria highlighted the importance of tumor molecular markers as an important basis for classification. As for preoperative MRI, it has already shown its potential in detecting the qualitative, quantitative, and localization of specific molecular chemicals. Magnetic resonance spectroscopy (MRS) is a technology that uses the chemical shift of atomic nucleus caused by the external magnetic field to realize a non-invasive *in vivo* study of physiological or pathological metabolic changes. The hydrogen proton (^{1}H-MRS) is the most commonly used one. Compared with conventional MRI, ^{1}H-MRS can determine the nature and value-added activity of lesions from the aspect of

metabolism (33). In the process of occurrence and development of many diseases, the metabolic changes are earlier than the pathological changes (34). Therefore, MRS can distinguish and classify gliomas at the biochemical level (35–37). Roder et al. reported the feasibility of intraoperative MRS and its potential usage in an extended tumor resection (38). However, due to the low spatial resolution, the long examination time, and interference of fat and skull, there is slow progress in the application of intraoperative MRS during surgery. Currently, the mainstream application is to register preoperative MRS imaging into intraoperative MRI, so as to achieve more targeted biopsy or excision guidance (39, 40). More convincing research evidence is needed to support the necessity of carrying out intraoperative MRS.

The application of iMRI also has other limitations. The utilization of iMRI significantly increases operative time compared with traditional operation. It requires additional time for setup, registration, draping, and redraping of patients, as well as the transport of the patient into and out of the scanner (41, 42). It is necessary to take into consideration the additional time needed for patient selection and the scheduling of the operating room. Lastly, the huge cost of iMRI equipment purchase ranges from $3 million to $7 million, not including the inconvenient cost of renovating the operative suite (43). Meanwhile, considerable costs are required for the maintenance of iMRI instruments and to employ specialized staff to assist in surgery. Though there was a study demonstrating the potential economic advantages of less hospital stay and lower total hospital costs from using iMRI (44), there is no doubt that the high cost of purchasing an iMRI system has become a major hindrance to universal implementation (43, 45).

Overall, the iMRI system has already been widely applied and exhibits a fantastic prospect. Its high spatial resolution and the depiction of brain function and metabolism margin improve the effect of surgical removal of brain tumors. The future development of iMRI relies on the amelioration of devices and computational performance, including higher magnetic field intensity, higher gradient performance, and multi-channel signal acquisition. The digitally integrated neurosurgical operation center based on iMRI could contribute to interactively integrating a variety of minimally invasive new technologies, to achieve less surgical trauma and more complete surgical resection. Compared with mechanical design, the effect of algorithms and high-performance computers would play a more important role. It is possible to enhance the spatiotemporal resolution of iMRI without the need for magnetic field strength improvement (46, 47). Besides the imaging resolution of brain structures, it is mainly used for determining functional and metabolic boundaries to guide more sophisticated surgical resection.

Intraoperative fluorescence

Another approach to maximize the extent of resection and avoid neurological damage is to use fluorescence dyestuff to highlight tumor regions and improve visual contrast. In recent decades, several fluorescence contrast agents, such as 5-aminolevulinic acid (5-ALA), indocyanine green (ICG), and fluorescein sodium (FLS), have been available for intraoperative use in clinical settings (48, 49).

5-ALA is the precursor of heme synthesis, which can generate protoporphyrin IV (PpIV) during metabolism (50). PpIV has strong photosensitive activity. In malignant tumor cells, the activity of enzymes involved in PpIV production is stronger than that in normal cells, while the activity of enzymes catalyzing the conversion of PpIV to hemochrome is weaker than that in normal cells. Therefore, a large amount of PpIV is accumulated in tumor cells (51, 52). Using this characteristic, the PpIV-rich tumor tissue can emit red fluorescence (635–705 nm) after being irradiated by an appropriate spectrum (407 nm) during the operation. Thus, tumors can be distinguished from normal tissues under the microscope. Therefore, 5-ALA has the advantages of convenient administration (oral administration before surgery), favorable visualization, and repeated administration (53, 54). It was reported that the sensitivity and specificity of 5-ALA in dense HGG tissue were above 90% (55). However, different studies show varying sensitivities (from 21% to 95%) and specificities (from 53% to 100%) (56–60). Meanwhile, 5-ALA is prone to show false-positive results in low-grade glioma, edema, and inflammatory tissues, and the fluorescence signal of deep tumors may also be covered by normal tissues (61–63).

FLS is a fluorescent compound used for obtaining diagnostic biopsies initially. It could be excited by light in the 460- to 500-nm range and send out the yellow-green part of the spectrum between 540 and 690 nm (64). Its application in neurosurgery was pioneered by Moore et al. in 1947 (65). FLS could be intravenously injected and visualized in the tumor tissue through the blood–brain barrier (66). Since the development of microscopes, the dose of FLS frequently used has been 1–2 mg/kg, guaranteeing safety and tolerability (67). Because of its low cost and simple operation, FLS is easy to promote in clinical practice (68). However, it is not directly bound to glioma cells but only accumulates in the tumor tissue; thus, the specificity is lower than that of 5-ALA (69, 70).

Intraoperative Raman histology

Raman histology is a label-free imaging method that uses intrinsic biochemical markers to distinguish tumor tissues (71, 72). In 1928, the Indian physicist Raman found that the inelastic scattering phenomenon occurs when the frequency of an incident photon is shifted after being scattered by a molecule. Therefore, it is possible to identify specific agents according to their unique Raman scattering spectrum (73). Since tumor cells have the ability to change metabolism to promote their rapid proliferation, Raman histology testing the chemical changes (e.g., protein, lipids, nucleic acids, and pH) could assess the tumor margin to guide the resection, based on the chemical composition of both inorganic and biological specimens. Hollon et al. reported that the diagnostic accuracy using stimulated Raman histology in 48 glioma patients was 95.8%. They concluded that the utilization of stimulated Raman histology improved the intraoperative detection of glioma recurrence in near-real time (74).

Considering its characteristics of real-time and rapid detection, intraoperative Raman histology has already shown its potential to achieve real-time molecular pathological level of tumor boundary detection (75). Surface-enhanced Raman scattering (SERS) is a spectroscopic technique based on the plasmon-assisted scattering of molecules absorbed on the noble metal surface, which has high

photostability, sensitivity, and potential for the simultaneous detection of up to 10 compounds (76, 77). Jin et al. reported an intelligent SERS Navigation System to guide brain tumor resection. They detected tumor tissues' metabolic acidosis (pH 6.2–6.9) caused by glucose metabolism shifting from oxidative phosphorylation to aerobic glycolysis. The efficiency had been examined in both animal models and patients. This system accelerates the clinical translation of acidic margin-guided surgery and avoids exogenous imaging probes. Also, concerning its detection of extracellular acidification, which is a common marker in solid tumors and does not rely on specific genetic phenotypes, SERS depiction of solid tumor margin testing metabolic acidosis might have a broader and universal application prospect (78).

However, intraoperative Raman histology has its drawbacks. Firstly, through the spatial resolution at the millimeter level, a small area of each detection range (mm^2) increased the number of repeated operations and the workload of neurosurgeons (79). Meanwhile, *ex vivo* imaging requires tissue removal, which also limits its further clinical application (80). The future development of Raman histology depends on the feasibility of rapid wide-ranging examination and instrument combination with integration and miniaturization.

Intraoperative mass spectrometry

Mass spectrometry is a method of detecting moving ions by separating them according to their mass-to-charge ratios using electric and magnetic fields. The composition of ions can be determined by measuring the exact mass of ions. It is widely used in the laboratory to qualitatively and quantitatively analyze the composition, molecular phenotype, and content of the samples, which has the advantages of high detection speed and high sensitivity (81). The commonly used indicators of glioma detected by mass spectrometry include N-acetylaspartic acid (NAA), 2-hydroxyglutaric acid (2-HG), choline, creatine (Cr), myoinositol (mI), lactic acid (Lac), and lipid (Lip). According to quantitative analysis of certain contents, neurosurgeons could not only distinguish tumor tissue from normal brain tissue but also identify molecular subtypes of brain tumors (82, 83). For example, the content of NAA reflects the number of neurons and axons, and the concentration of NAA often decreases significantly in brain tumor tissues. 2-HG is the metabolite of *isocitrate dehydrogenase* (*IDH*) gene mutant glioma; the concentration in *IDH-mutant* tumor samples could be more than 100 times the size of a normal brain tissue (84, 85). The detection of such chemical indicators by intraoperative mass spectrometry provided the ability to characterize the molecular and metabolic boundaries of tumors. Considering its operating principles, the technique applies to a wide range of chemicals and promises high-throughput analysis.

Moreover, in 2004, desorption electrospray ionization mass spectrometry (DESI-MS) made it possible to direct intraoperative sampling analysis without the need for sample preprocessing (86). In 2015, Alan et al. reported that the DESI-MS detections of 158 glioma samples, 223 gray matter samples, and 66 white matter samples could effectively distinguish glioma from white matter and gray matter, and the overall sensitivity and specificity reached 97.4% and 98.5%, respectively (87). Moreover, with the development of techniques, the detection time is reduced to 3 min according to Pirro et al.'s report in 2017 (88).

In a nutshell, intraoperative mass spectrometry has shown the potential to redefine the maximum resection of glioma. Despite its rapid development, the clinical application of iMS remains limited in the operating room, which is essential to complete validation of large-sample-size data. The limitation of spatial resolution and detection accuracy required the development of the ionization technique. The miniaturization of intraoperative simple testing instruments and the establishment of rapid intraoperative testing procedures are the key to accelerate clinical popularization. Also, future development requires more stable biomarkers, a mass spectrometry library, and integrated equipment.

Discussion

We summarized different intraoperative techniques for delineating the precise boundaries of brain tumors, including MRI,

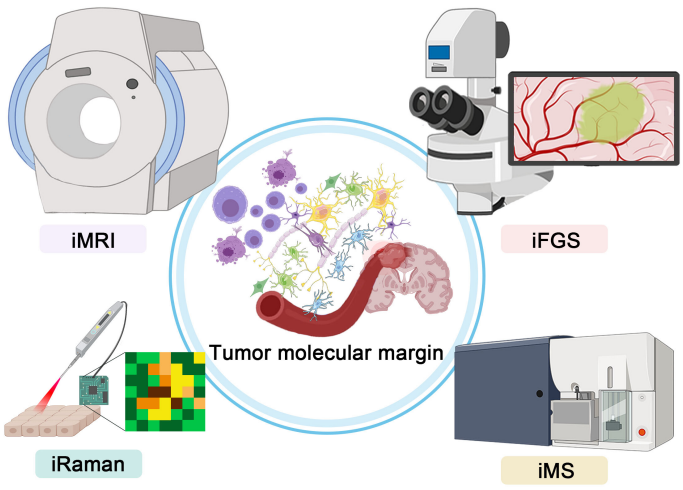

FIGURE 1
Graphical abstract showing the four intraoperative technologies for precise depictions of malignant glioma margin.

fluorescence-guided surgery, Raman histology, and mass spectrometry. Considering their inability to depict precise boundaries, especially molecular and metabolic margins, we did not include intraoperative computerized tomography and ultrasound in this review. The principle and development of each technique are briefly introduced, and their advantages and disadvantages are analyzed. Regardless of the differences in imaging methods, the ultimate goal of accurate delineation of tumor molecular boundaries is to improve the gross total resection and the surgical benefits for brain tumor patients on the premise of protecting normal brain tissues. At the same time, the delineation of tumor molecular boundaries is helpful to further improve the judgment of molecular classification of brain tumors and guide the subsequent diagnosis and treatment. Though we illustrated them respectively, different techniques were not mutually exclusive; for example, intraoperative mass spectrometry could also be used in conjunction with intraoperative MRI (89). The necessity and priority of the use of different techniques need to be explored and verified. Also, how to interact and fuse multiple methods to form multimodal delineation of tumor boundaries is an important direction for future research and development.

At present, the application of these new technologies is hindered by their high cost. ElGamal et al. have analyzed the effectiveness and cost-effectiveness of intraoperative fluorescence, intraoperative ultrasound, and intraoperative MRI (90). All approaches have been shown to significantly improve the gross total resection and progression-free survival of high-grade gliomas, while the high cost of these new techniques has significantly hindered the progress and prevalence of these techniques. Therefore, cost reduction and the improvement of integrated and miniaturized intraoperative detection equipment are urgent problems that need to be solved in future engineering and manufacturing development. To promote the popularization of these new technology, it requires to be compatible with common operating rooms. One possible solution to strike balance between accuracy and economic efficiency is to establish a large-sample multimodal database and use artificial intelligence algorithms to improve the original imaging resolution (91–93).

Based on the criteria of intraoperative real-time imaging and delineation of tumor boundaries at the molecular level, we selected intraoperative MRI, fluorescence-guided surgery, Raman histology, and mass spectrometry for review. Due to the rapid development of technology and the differences in different regions, inevitably, the tracking of new technologies is not timely. Based on physical and chemical principles, advances in mechanical engineering and computer technology make it possible to apply these theories to delineate tumor molecular boundaries in operating rooms. We firmly believe that these multidisciplinary advances and integrated applications drive the continuous progress of medical treatment. The continuous cultivation of these methods also continuously updates our understanding of cancer and innovates our diagnosis and treatment methods, to effectively protect the life and health of patients.

Author contributions

SJ wrote the first draft of the manuscript. HC revised the manuscript and was in charge of language editing. QT reviewed and edited the final manuscript. All authors contributed to the article and approved the submitted version.

Funding

This article was supported by the Shanghai Science and Technology Committee Rising-Star Program(20QA1401900) and National Natural Science Foundation of China (82072020).

Conflict of interest

The authors declare that the research was conducted in the absence of any commercial or financial relationships that could be construed as a potential conflict of interest.

Publisher's note

References

1. McBain C, Lawrie TA, Rogozinska E, Kernohan A, Robinson T, Jefferies S. Treatment options for progression or recurrence of glioblastoma: A network meta-analysis. *Cochrane Database Syst Rev* (2021) 5:CD013579. doi: 10.1002/14651858.CD013579.pub2

2. Stupp R, Hegi ME, Gilbert MR, Chakravarti A. Chemoradiotherapy in malignant glioma: Standard of care and future directions. *J Clin Oncol* (2007) 25(26):4127–36. doi: 10.1200/JCO.2007.11.8554

3. Weller M, Wick W, Aldape K, Brada M, Berger M, Pfister SM, et al. Glioma. *Nat Rev Dis Primers* (2015) 1:15017. doi: 10.1038/nrdp.2015.17

4. Krivosheya D, Prabhu SS, Weinberg JS, Sawaya R. Technical principles in glioma surgery and preoperative considerations. *J Neurooncol* (2016) 130(2):243–52. doi: 10.1007/s11060-016-2171-4

5. Brown TJ, Brennan MC, Li M, Church EW, Brandmeir NJ, Rakszawski KL, et al. Association of the extent of resection with survival in glioblastoma: A systematic review and meta-analysis. *JAMA Oncol* (2016) 2(11):1460–9. doi: 10.1001/jamaoncol.2016.1373

6. Cakmakci D, Kaynar G, Bund C, Piotto M, Proust F, Namer IJ, et al. Targeted metabolomics analyses for brain tumor margin assessment during surgery. *Bioinformatics* (2022) 38(12):3238–44. doi: 10.1093/bioinformatics/btac309

7. Alieva M, Leidgens V, Riemenschneider MJ, Klein CA, Hau P, van Rheenen J. Intravital imaging of glioma border morphology reveals distinctive cellular dynamics and contribution to tumor cell invasion. *Sci Rep* (2019) 9(1):2054. doi: 10.1038/s41598-019-38625-4

8. Gerard IJ, Kersten-Oertel M, Petrecca K, Sirhan D, Hall JA, Collins DL. Brain shift in neuronavigation of brain tumors: A review. *Med Image Anal* (2017) 35:403–20. doi: 10.1016/j.media.2016.08.007

9. Phillips HW, Maniquis CAB, Chen JS, Duby SL, Nagahama Y, Bergeron D, et al. Midline brain shift after hemispheric surgery: Natural history, clinical significance, and association with cerebrospinal fluid diversion. *Oper Neurosurg (Hagerstown)* (2022) 22 (5):269–76. doi: 10.1227/ons.0000000000000134

10. Pallavaram S, Dawant BM, Remple MS, Neimat JS, Kao C, Konrad PE, et al. Effect of brain shift on the creation of functional atlases for deep brain stimulation surgery. *Int J Comput Assist Radiol Surg* (2010) 5(3):221–8. doi: 10.1007/s11548-009-0391-1

11. Luo M, Narasimhan S, Larson PS, Martin AJ, Konrad PE, Miga MI. Impact of brain shift on neural pathways in deep brain stimulation: A preliminary analysis *Via* multi-physics finite element models. *J Neural Eng* (2021) 18(5). doi: 10.1088/1741-2552/abf066

12. Lesage AC, Simmons A, Sen A, Singh S, Chen M, Cazoulat G, et al. Viscoelastic biomechanical models to predict inward brain-shift using public benchmark data. *Phys Med Biol* (2021) 66(20). doi: 10.1088/1361-6560/ac22dc

13. Hu J, Jin X, Lee JB, Zhang L, Chaudhary V, Guthikonda M, et al. Intraoperative brain shift prediction using a 3d inhomogeneous patient-specific finite element model. *J Neurosurg* (2007) 106(1):164–9. doi: 10.3171/jns.2007.106.1.164

14. Kuhnt D, Bauer MH, Nimsky C. Brain shift compensation and neurosurgical image fusion using intraoperative mri: Current status and future challenges. *Crit Rev BioMed Eng* (2012) 40(3):175–85. doi: 10.1615/critrevbiomedeng.v40.i3.20

15. Villanueva-Meyer JE, Mabray MC, Cha S. Current clinical brain tumor imaging. *Neurosurgery* (2017) 81(3):397–415. doi: 10.1093/neuros/nyx103

16. Fink JR, Muzi M, Peck M, Krohn KA. Multimodality brain tumor imaging: Mr imaging, pet, and Pet/Mr imaging. *J Nucl Med* (2015) 56(10):1554–61. doi: 10.2967/jnumed.113.131516

17. Black PM, Moriarty T, Alexander E3rd, Stieg P, Woodard EJ, Gleason PL, et al. Development and implementation of intraoperative magnetic resonance imaging and its neurosurgical applications. *Neurosurgery* (1997) 41(4):831–42. doi: 10.1097/00006123-199710000-00013

18. Black P, Jolesz FA, Medani K. From vision to reality: The origins of intraoperative Mr imaging. *Acta Neurochir Suppl* (2011) 109:3–7. doi: 10.1007/978-3-211-99651-5_1

19. Rogers CM, Jones PS, Weinberg JS. Intraoperative mri for brain tumors. *J Neurooncol* (2021) 151(3):479–90. doi: 10.1007/s11060-020-03667-6

20. Hespel AM, Cole RC. Advances in high-field mri. *Vet Clin North Am Small Anim Pract* (2018) 48(1):11–29. doi: 10.1016/j.cvsm.2017.08.002

21. Cattarinussi G, Delvecchio G, Maggioni E, Bressi C, Brambilla P. Ultra-high field imaging in major depressive disorder: A review of structural and functional studies. *J Affect Disord* (2021) 290:65–73. doi: 10.1016/j.jad.2021.04.056

22. Senft C, Bink A, Franz K, Vatter H, Gasser T, Seifert V. Intraoperative mri guidance and extent of resection in glioma surgery: A randomised, controlled trial. *Lancet Oncol* (2011) 12(11):997–1003. doi: 10.1016/S1470-2045(11)70196-6

23. Qiu TM, Yao CJ, Wu JS, Pan ZG, Zhuang DX, Xu G, et al. Clinical experience of 3t intraoperative magnetic resonance imaging integrated neurosurgical suite in shanghai huashan hospital. *Chin Med J (Engl)* (2012) 125(24):4328–33.

24. Roder C, Haas P, Tatagiba M, Ernemann U, Bender B. Technical limitations and pitfalls of diffusion-weighted imaging in intraoperative high-field mri. *Neurosurg Rev* (2021) 44(1):327–34. doi: 10.1007/s10143-019-01206-0

25. Lehericy S, Duffau H, Cornu P, Capelle L, Pidoux B, Carpentier A, et al. Correspondence between functional magnetic resonance imaging somatotopy and individual brain anatomy of the central region: Comparison with intraoperative stimulation in patients with brain tumors. *J Neurosurg* (2000) 92(4):589–98. doi: 10.3171/jns.2000.92.4.0589

26. Leclercq D, Duffau H, Delmaire C, Capelle L, Gatignol P, Ducros M, et al. Comparison of diffusion tensor imaging tractography of language tracts and intraoperative subcortical stimulations. *J Neurosurg* (2010) 112(3):503–11. doi: 10.3171/2009.8.JNS09558

27. Ghinda D, Zhang N, Lu J, Yao CJ, Yuan S, Wu JS. Contribution of combined intraoperative electrophysiological investigation with 3-T intraoperative mri for awake cerebral glioma surgery: Comprehensive review of the clinical implications and radiological outcomes. *Neurosurg Focus* (2016) 40(3):E14. doi: 10.3171/2015.12.FOCUS15572

28. Rutten GJ, Ramsey NF, van Rijen PC, Noordmans HJ, van Veelen CW. Development of a functional magnetic resonance imaging protocol for intraoperative localization of critical temporoparietal language areas. *Ann Neurol* (2002) 51(3):350–60. doi: 10.1002/ana.10117

29. Gasser T, Ganslandt O, Sandalcioglu E, Stolke D, Fahlbusch R, Nimsky C. Intraoperative functional mri: Implementation and preliminary experience. *Neuroimage* (2005) 26(3):685–93. doi: 10.1016/j.neuroimage.2005.02.022

30. Qiu TM, Gong FY, Gong X, Wu JS, Lin CP, Biswal BB, et al. Real-time motor cortex mapping for the safe resection of glioma: An intraoperative resting-state fmri study. *AJNR Am J Neuroradiol* (2017) 38(11):2146–52. doi: 10.3174/ajnr.A5369

31. D'Andrea G, Familiari P, Di Lauro A, Angelini A, Sessa G. Safe resection of gliomas of the dominant angular gyrus availing of preoperative fmri and intraoperative dti: Preliminary series and surgical technique. *World Neurosurg* (2016) 87:627–39. doi: 10.1016/j.wneu.2015.10.076

32. Poldrack RA, Baker CI, Durnez J, Gorgolewski KJ, Matthews PM, Munafo MR, et al. Scanning the horizon: Towards transparent and reproducible neuroimaging research. *Nat Rev Neurosci* (2017) 18(2):115–26. doi: 10.1038/nrn.2016.167

33. Rich LJ, Bagga P, Wilson NE, Schnall MD, Detre JA, Haris M, et al. (1)H magnetic resonance spectroscopy of (2)H-to-(1)H exchange quantifies the dynamics of cellular metabolism in vivo. *Nat BioMed Eng* (2020) 4(3):335–42. doi: 10.1038/s41551-019-0499-8

34. Nakahara T, Tsugawa S, Noda Y, Ueno F, Honda S, Kinjo M, et al. Glutamatergic and gabaergic metabolite levels in schizophrenia-spectrum disorders: A meta-analysis of (1)H-magnetic resonance spectroscopy studies. *Mol Psychiatry* (2022) 27(1):744–57. doi: 10.1038/s41380-021-01297-6

35. Branzoli F, Marjanska M. Magnetic resonance spectroscopy of isocitrate dehydrogenase mutated gliomas: Current knowledge on the neurochemical profile. *Curr Opin Neurol* (2020) 33(4):413–21. doi: 10.1097/WCO.0000000000000833

36. Ruiz-Rodado V, Brender JR, Cherukuri MK, Gilbert MR, Larion M. Magnetic resonance spectroscopy for the study of cns malignancies. *Prog Nucl Magn Reson Spectrosc* (2021) 122:23–41. doi: 10.1016/j.pnmrs.2020.11.001

37. Hwang JH, Choi CS. Use of in vivo magnetic resonance spectroscopy for studying metabolic diseases. *Exp Mol Med* (2015) 47:e139. doi: 10.1038/emm.2014.101

38. Roder C, Skardelly M, Ramina KF, Beschorner R, Honneger J, Nagele T, et al. Spectroscopy imaging in intraoperative Mr suite: Tissue characterization and optimization of tumor resection. *Int J Comput Assist Radiol Surg* (2014) 9(4):551–9. doi: 10.1007/s11548-013-0952-1

39. Grech-Sollars M, Vaqas B, Thompson G, Barwick T, Honeyfield L, O'Neill K, et al. An Mrs- and pet-guided biopsy tool for intraoperative neuronavigational systems. *J Neurosurg* (2017) 127(4):812–818. doi: 10.3171/2016.7.JNS16106

40. Zhang J, Zhuang DX, Yao CJ, Lin CP, Wang TL, Qin ZY, et al. Metabolic approach for tumor delineation in glioma surgery: 3d Mr spectroscopy image-guided resection. *J Neurosurg* (2016) 124(6):1585–93. doi: 10.3171/2015.6.JNS142651

41. Lu CY, Chen XL, Chen XL, Fang XJ, Zhao YL. Clinical application of 3.0 T intraoperative magnetic resonance combined with multimodal neuronavigation in resection of cerebral eloquent area glioma. *Med (Baltimore)* (2018) 97(34):e11702. doi: 10.1097/MD.0000000000011702

42. Berkow LC. Anesthetic management and human factors in the intraoperative mri environment. *Curr Opin Anaesthesiol* (2016) 29(5):563–7. doi: 10.1097/ACO.0000000000000366

43. Abraham P, Sarkar R, Brandel MG, Wali AR, Rennert RC, Lopez Ramos C, et al. Cost-effectiveness of intraoperative mri for treatment of high-grade gliomas. *Radiology* (2019) 291(3):689–97. doi: 10.1148/radiol.2019182095

44. Hall WA, Kowalik K, Liu H, Truwit CL, Kucharezyk J. Costs and benefits of intraoperative Mr-guided brain tumor resection. *Acta Neurochir Suppl* (2003) 85:137–42. doi: 10.1007/978-3-7091-6043-5_19

45. Bettmann MA. Intraoperative mri for treatment of high-grade glioma: Is it cost-effective? *Radiology* (2019) 291(3):698–9. doi: 10.1148/radiol.2019190337

46. Zhao C, Dewey BE, Pham DL, Calabresi PA, Reich DS, Prince JL. Smore: A self-supervised anti-aliasing and super-resolution algorithm for mri using deep learning. *IEEE Trans Med Imaging* (2021) 40(3):805–17. doi: 10.1109/TMI.2020.3037187

47. Johnson PM, Recht MP, Knoll F. Improving the speed of mri with artificial intelligence. *Semin Musculoskelet Radiol* (2020) 24(1):12–20. doi: 10.1055/s-0039-3400265

48. Orillac C, Stummer W, Orringer DA. Fluorescence guidance and intraoperative adjuvants to maximize extent of resection. *Neurosurgery* (2021) 89(5):727–36. doi: 10.1093/neuros/nyaa475

49. Shen B, Zhang Z, Shi X, Cao C, Zhang Z, Hu Z, et al. Real-time intraoperative glioma diagnosis using fluorescence imaging and deep convolutional neural networks. *Eur J Nucl Med Mol Imaging* (2021) 48(11):3482–92. doi: 10.1007/s00259-021-05326-y

50. Rehani PR, Iftikhar H, Nakajima M, Tanaka T, Jabbar Z, Rehani RN. Safety and mode of action of diabetes medications in comparison with 5-aminolevulinic acid (5-ala). *J Diabetes Res* (2019) 2019:4267357. doi: 10.1155/2019/4267357

51. Bunk EC, Wagner A, Stummer W, Senner V, Brokinkel B. 5-ala kinetics in meningiomas: Analysis of tumor fluorescence and ppix metabolism in vitro and comparative analyses with high-grade gliomas. *J Neurooncol* (2021) 152(1):37–46. doi: 10.1007/s11060-020-03680-9

52. Jones PS, Yekula A, Lansbury E, Small JL, Ayinon C, Mordecai S, et al. Characterization of plasma-derived protoporphyrin-Ix-Positive extracellular vesicles following 5-ala use in patients with malignant glioma. *EBioMedicine* (2019) 48:23–35. doi: 10.1016/j.ebiom.2019.09.025

53. Diez Valle R, Hadjipanayis CG, Stummer W. Established and emerging uses of 5-ala in the brain: An overview. *J Neurooncol* (2019) 141(3):487–94. doi: 10.1007/s11060-018-03087-7

54. Michael AP, Watson VL, Ryan D, Delfino KR, Bekker SV, Cozzens JW. Effects of 5-ala dose on resection of glioblastoma. *J Neurooncol* (2019) 141(3):523–31. doi: 10.1007/s11060-019-03100-7

55. Hadjipanayis CG, Widhalm G, Stummer W. What is the surgical benefit of utilizing 5-aminolevulinic acid for fluorescence-guided surgery of malignant gliomas? *Neurosurgery* (2015) 77(5):663–73. doi: 10.1227/NEU.0000000000000929

56. Gessler F, Forster MT, Duetzmann S, Mittelbronn M, Hattingen E, Franz K, et al. Combination of intraoperative magnetic resonance imaging and intraoperative fluorescence to enhance the resection of contrast enhancing gliomas. *Neurosurgery* (2015) 77(1):16–22. doi: 10.1227/NEU.0000000000000729

57. Coburger J, Scheuerle A, Pala A, Thal D, Wirtz CR, Konig R. Histopathological insights on imaging results of intraoperative magnetic resonance imaging, 5-

aminolevulinic acid, and intraoperative ultrasound in glioblastoma surgery. *Neurosurgery* (2017) 81(1):165–74. doi: 10.1093/neuros/nyw143

58. Valdes PA, Jacobs V, Harris BT, Wilson BC, Leblond F, Paulsen KD, et al. Quantitative fluorescence using 5-aminolevulinic acid-induced protoporphyrin ix biomarker as a surgical adjunct in low-grade glioma surgery. *J Neurosurg* (2015) 123 (3):771–80. doi: 10.3171/2014.12.JNS14391

59. Kiesel B, Mischkulnig M, Woehrer A, Martinez-Moreno M, Millesi M, Mallouhi A, et al. Systematic histopathological analysis of different 5-aminolevulinic acid-induced fluorescence levels in newly diagnosed glioblastomas. *J Neurosurg* (2018) 129(2):341–53. doi: 10.3171/2017.4.JNS162991

60. Valdes PA, Roberts DW, Lu FK, Golby A. Optical technologies for intraoperative neurosurgical guidance. *Neurosurg Focus* (2016) 40(3):E8. doi: 10.3171/2015.12.FOCUS15550

61. Kiesel B, Freund J, Reichert D, Wadiura L, Erkkilae MT, Woehrer A, et al. 5-ala in suspected low-grade gliomas: Current role, limitations, and new approaches. *Front Oncol* (2021) 11:699301. doi: 10.3389/fonc.2021.699301

62. Almekkawi AK, El Ahmadieh TY, Wu EM, Abunimer AM, Abi-Aad KR, Aoun SG, et al. The use of 5-aminolevulinic acid in low-grade glioma resection: A systematic review. *Oper Neurosurg (Hagerstown)* (2020) 19(1):1–8. doi: 10.1093/ons/opz336

63. Hosmann A, Millesi M, Wadiura LI, Kiesel B, Mercea PA, Mischkulnig M, et al. 5-ala fluorescence is a powerful prognostic marker during surgery of low-grade gliomas (Who grade ii)-experience at two specialized centers. *Cancers (Basel)* (2021) 13(11):2540. doi: 10.3390/cancers13112540

64. Waqas M, Shamim MS. Sodium fluorescein guided resection of malignant glioma. *J Pak Med Assoc* (2018) 68(6):968–70.

65. Schebesch KM, Brawanski A, Hohenberger C, Hohne J. Fluorescein sodium-guided surgery of malignant brain tumors: History, current concepts, and future project. *Turk Neurosurg* (2016) 26(2):185–94. doi: 10.5137/1019-5149.JTN.16952-16.0

66. Folaron M, Strawbridge R, Samkoe KS, Filan C, Roberts DW, Davis SC. Elucidating the kinetics of sodium fluorescein for fluorescence-guided surgery of glioma. *J Neurosurg* (2018) 131(3):724–34. doi: 10.3171/2018.4.JNS172644

67. Fan C, Jiang Y, Liu R, Wu G, Wu G, Xu K, et al. Safety and feasibility of low-dose fluorescein-guided resection of glioblastoma. *Clin Neurol Neurosurg* (2018) 175:57–60. doi: 10.1016/j.clineuro.2018.10.011

68. Bowden SG, Neira JA, Gill BJA, Ung TH, Englander ZK, Zanazzi G, et al. Sodium fluorescein facilitates guided sampling of diagnostic tumor tissue in nonenhancing gliomas. *Neurosurgery* (2018) 82(5):719–27. doi: 10.1093/neuros/nyx271

69. Schwake M, Stummer W, Suero Molina EJ, Wolfer J. Simultaneous fluorescein sodium and 5-ala in fluorescence-guided glioma surgery. *Acta Neurochir (Wien)* (2015) 157(5):877–9. doi: 10.1007/s00701-015-2401-0

70. Hansen RW, Pedersen CB, Halle B, Korshoej AR, Schulz MK, Kristensen BW, et al. Comparison of 5-aminolevulinic acid and sodium fluorescein for intraoperative tumor visualization in patients with high-grade gliomas: A single-center retrospective study. *J Neurosurg* (2019) 133(5):1324-1331. doi: 10.3171/2019.6.JNS191531

71. Di L, Eichberg DG, Huang K, Shah AH, Jamshidi AM, Luther EM, et al. Stimulated raman histology for rapid intraoperative diagnosis of gliomas. *World Neurosurg* (2021) 150:e135–e43. doi: 10.1016/j.wneu.2021.02.122

72. Hollon T, Orringer DA. Label-free brain tumor imaging using raman-based methods. *J Neurooncol* (2021) 151(3):393–402. doi: 10.1007/s11060-019-03380-z

73. Yui H. Electron-enhanced raman scattering: A history of its discovery and spectroscopic applications to solution and interfacial chemistry. *Anal Bioanal Chem* (2010) 397(3):1181–90. doi: 10.1007/s00216-010-3703-y

74. Hollon TC, Pandian B, Urias E, Save AV, Adapa AR, Srinivasan S, et al. Rapid, label-free detection of diffuse glioma recurrence using intraoperative stimulated raman histology and deep neural networks. *Neuro Oncol* (2021) 23(1):144–55. doi: 10.1093/neuonc/noaa162

75. Hollon TC, Pandian B, Adapa AR, Urias E, Save AV, Khalsa SSS, et al. Near real-time intraoperative brain tumor diagnosis using stimulated raman histology and deep neural networks. *Nat Med* (2020) 26(1):52–8. doi: 10.1038/s41591-019-0715-9

76. Spedalieri C, Kneipp J. Surface enhanced raman scattering for probing cellular biochemistry. *Nanoscale* (2022) 14(14):5314–28. doi: 10.1039/d2nr00449f

77. Vendrell M, Maiti KK, Dhaliwal K, Chang YT. Surface-enhanced raman scattering in cancer detection and imaging. *Trends Biotechnol* (2013) 31(4):249–57. doi: 10.1016/j.tibtech.2013.01.013

78. Jin Z, Yue Q, Duan W, Sui A, Zhao B, Deng Y, et al. Intelligent sers navigation system guiding brain tumor surgery by intraoperatively delineating the metabolic acidosis. *Adv Sci (Weinh)* (2022) 9(7):e2104935. doi: 10.1002/advs.202104935

79. Hollon T, Stummer W, Orringer D, Suero Molina E. Surgical adjuncts to increase the extent of resection: Intraoperative mri, fluorescence, and raman histology. *Neurosurg Clin N Am* (2019) 30(1):65–74. doi: 10.1016/j.nec.2018.08.012

80. Hubbard TJE, Shore A, Stone N. Raman spectroscopy for rapid intra-operative margin analysis of surgically excised tumour specimens. *Analyst* (2019) 144(22):6479–96. doi: 10.1039/c9an01163c

81. Santilli AML, Ren K, Oleschuk R, Kaufmann M, Rudan J, Fichtinger G, et al. Application of intraoperative mass spectrometry and data analytics for oncological margin detection, a review. *IEEE Trans BioMed Eng* (2022) 69(7):2220–32. doi: 10.1109/TBME.2021.3139992

82. Neidert MC, Bozinov O. Mass spectrometry-based intraoperative tissue identification in neurosurgery. *World Neurosurg* (2013) 80(6):683–4. doi: 10.1016/j.wneu.2013.10.027

83. Parry PV, Engh JA. Ambient mass spectrometry for the intraoperative molecular diagnosis of human brain tumors. *Neurosurgery* (2013) 72(4):N17–8. doi: 10.1227/01.neu.0000428422.82081.62

84. Chen R, Brown HM, Cooks RG. Metabolic profiles of human brain parenchyma and glioma for rapid tissue diagnosis by targeted desorption electrospray ionization mass spectrometry. *Anal Bioanal Chem* (2021) 413(25):6213–24. doi: 10.1007/s00216-021-03593-0

85. Radoul M, Hong D, Gillespie AM, Najac C, Viswanath P, Pieper RO, et al. Early noninvasive metabolic biomarkers of mutant idh inhibition in glioma. *Metabolites* (2021) 11(2):109. doi: 10.3390/metabo11020109

86. Takats Z, Wiseman JM, Gologan B, Cooks RG. Mass spectrometry sampling under ambient conditions with desorption electrospray ionization. *Science* (2004) 306 (5695):471–3. doi: 10.1126/science.1104404

87. Jarmusch AK, Pirro V, Baird Z, Hattab EM, Cohen-Gadol AA, Cooks RG. Lipid and metabolite profiles of human brain tumors by desorption electrospray ionization-Ms. *Proc Natl Acad Sci U S A* (2016) 113(6):1486–91. doi: 10.1073/pnas.1523306113

88. Pirro V, Alfaro CM, Jarmusch AK, Hattab EM, Cohen-Gadol AA, Cooks RG. Intraoperative assessment of tumor margins during glioma resection by desorption electrospray ionization-mass spectrometry. *Proc Natl Acad Sci U S A* (2017) 114 (26):6700–5. doi: 10.1073/pnas.1706459114

89. Letertre MPM, Dervilly G, Giraudeau P. Combined nuclear magnetic resonance spectroscopy and mass spectrometry approaches for metabolomics. *Anal Chem* (2021) 93 (1):500–18. doi: 10.1021/acs.analchem.0c04371

90. Eljamel MS, Mahboob SO. The effectiveness and cost-effectiveness of intraoperative imaging in high-grade glioma resection; a comparative review of intraoperative ala, fluorescein, ultrasound and mri. *Photodiagnosis Photodyn Ther* (2016) 16:35–43. doi: 10.1016/j.pdpdt.2016.07.012

91. Leclerc P, Ray C, Mahieu-Williame L, Alston L, Frindel C, Brevet PF, et al. Machine learning-based prediction of glioma margin from 5-ala induced ppix fluorescence spectroscopy. *Sci Rep* (2020) 10(1):1462. doi: 10.1038/s41598-020-58299-7

92. Cakmakci D, Karakaslar EO, Ruhland E, Chenard MP, Proust F, Piotto M, et al. Machine learning assisted intraoperative assessment of brain tumor margins using hrmas nmr spectroscopy. *PLoS Comput Biol* (2020) 16(11):e1008184. doi: 10.1371/journal.pcbi.1008184

93. Marsden M, Weyers BW, Bec J, Sun T, Gandour-Edwards RF, Birkeland AC, et al. Intraoperative margin assessment in oral and oropharyngeal cancer using label-free fluorescence lifetime imaging and machine learning. *IEEE Trans BioMed Eng* (2021) 68 (3):857–68. doi: 10.1109/TBME.2020.3010480

frontiers | Frontiers in Oncology

TYPE Original Research
PUBLISHED 03 February 2023
DOI 10.3389/fonc.2023.1089787

OPEN ACCESS

EDITED BY
Songbai Xu,
First Affiliated Hospital of Jilin University, Jilin University, China

REVIEWED BY
Tommaso Sciortino,
Galeazzi Orthopedic Institute (IRCCS), Italy
Xiang Wang,
West China Fourth Hospital of Sichuan University, China

*CORRESPONDENCE
Sanzhong Li
sunny_3c@126.com
Zhou Fei
feizhou@fmmu.edu.cn

†These authors have contributed equally to this work and share first authorship

SPECIALTY SECTION
This article was submitted to Neuro-Oncology and Neurosurgical Oncology, a section of the journal Frontiers in Oncology

RECEIVED 04 November 2022
ACCEPTED 20 January 2023
PUBLISHED 03 February 2023

CITATION
Li S, Mu Y, Rao Y, Sun C, Li X, Liu H, Yu X, Yan X, Ding Y, Wang Y and Fei Z (2023) Preoperative individual-target transcranial magnetic stimulation demonstrates an effect comparable to intraoperative direct electrical stimulation in language-eloquent glioma mapping and improves postsurgical outcome: A retrospective fiber-tracking and electromagnetic simulation study. *Front. Oncol.* 13:1089787. doi: 10.3389/fonc.2023.1089787

Preoperative individual-target transcranial magnetic stimulation demonstrates an effect comparable to intraoperative direct electrical stimulation in language-eloquent glioma mapping and improves postsurgical outcome: A retrospective fiber-tracking and electromagnetic simulation study

Sanzhong Li[1*†], Yunfeng Mu[2†], Yang Rao[3†], Chuanzhu Sun[3], Xiang Li[3,4], Huan Liu[5], Xun Yu[6], Xiao Yan[3], Yunxia Ding[3], Yangtao Wang[3] and Zhou Fei[1*]

[1]Department of Neurosurgery, Xijing Hospital, Air Force Medical University, Xi'an, Shaanxi, China, [2]Department of Gynecological Oncology, Shaanxi Provincial Cancer Hospital, Xi'an, China, [3]Shaanxi Brain Modulation and Scientific Research Center, Xi'an, Shaanxi, China, [4]The Key Laboratory of Biomedical Information Engineering of Ministry of Education, Institute of Health and Rehabilitation Science, School of Life Science and Technology, Xi'an Jiaotong University, Xi'an, Shaanxi, China, [5]School of Mathematics and Statistics, Xi'an Jiaotong University, Xi'an, Shaanxi, China, [6]Product Department, Solide Brain Medical Technology, Ltd., Xi'an, Shaanxi, China

Background: Efforts to resection of glioma lesions located in brain-eloquent areas must balance the extent of resection (EOR) and functional preservation. Currently, intraoperative direct electrical stimulation (DES) is the gold standard for achieving the maximum EOR while preserving as much functionality as possible. However, intraoperative DES inevitably involves risks of infection and epilepsy. The aim of this study was to verify the reliability of individual-target transcranial magnetic stimulation (IT-TMS) in preoperative mapping relative to DES and evaluate its effectiveness based on postsurgical outcomes.

Methods: Sixteen language-eloquent glioma patients were enrolled. Nine of them underwent preoperative nTMS mapping (n=9, nTMS group), and the other seven were assigned to the non-nTMS group and did not undergo preoperative nTMS mapping (n=7). Before surgery, online IT-TMS was performed during a language task in the nTMS group. Sites in the cortex at which this task was disturbed in three consecutive trials were recorded and regarded as positive and designated nTMS hotspots (HS_{nTMS}). Both groups then underwent awake surgery and intraoperative DES mapping. DES hotspots (HS_{DES}) were also determined in a manner analogous to HS_{nTMS}. The spatial distribution of HS_{nTMS} and HS_{DES} in the nTMS group was

recorded, registered in a single brain template, and compared. The center of gravity (CoG) of HS_{nTMS} ($HS_{nTMS\text{-}CoG}$)-based and $HS_{DES\text{-}CoG}$-based diffusion tensor imaging-fiber tracking (DTI-FT) was performed. The electromagnetic simulation was conducted, and the values were then compared between the nTMS and DES groups, as were the Western Aphasia Battery (WAB) scale and fiber-tracking values.

Results: HS_{nTMS} and HS_{DES} showed similar distributions (mean distance 6.32 ± 2.6 mm, distance range 2.2-9.3 mm, 95% CI 3.9-8.7 mm). A higher fractional anisotropy (FA) value in nTMS mapping (P=0.0373) and an analogous fiber tract length (P=0.2290) were observed. A similar distribution of the electric field within the brain tissues induced by nTMS and DES was noted. Compared with the non-nTMS group, the integration of nTMS led to a significant improvement in language performance (WAB scores averaging 78.4 in the nTMS group compared with 59.5 in the non-nTMS group, P=0.0321 < 0.05) as well as in brain-structure preservation (FA value, P=0.0156; tract length, P=0.0166).

Conclusion: Preoperative IT-TMS provides data equally crucial to DES and thus facilitates precise brain mapping and the preservation of linguistic function.

KEYWORDS

transcranial magnetic stimulation, language mapping, fiber-tracking, electromagnetic simulation, deep electrical stimulation

1 Introduction

Gliomas, the most common type of brain tumor, are highly infiltrative and diffusive and display migrative ability (1). Generally, the optimal surgical treatment involves achievement of the maximum extent of resection (EOR) while preserving as much functionality as possible (2, 3). Because the risk of postoperative language deficits significantly increases when brain tumor surgery involves the language-dominant area, it is crucial to determine language dominance as part of surgical planning (4, 5). Linguistic maps provide surgeons with a visualized distribution of language-eloquent brain lesions. In particular, knowledge of the spatial relationship between a tumor and the language area serves to distinguish the safe and vulnerable areas for precise resection. Currently, awake surgery in combination with direct electrical stimulation (DES) is the gold standard for brain functional mapping (6, 7), but the operation time for awake surgery is substantial. For example, recently Rossi et al. investigated the mean duration of awake surgery, including intraoperative tasks and functional mapping, in 95 glioma patients (8). The average time is (280 ± 30) min, about (4.67 ± 0.5) h. Maldaun et al. also reported that the mean duration of awake surgery was 7.3 hours (range 4.0-13.9 hours), in an analysis of 42 glioma awake craniotomy cases for both motor and speech mapping (9). Accordingly, the risk of intraoperative infection is greater, as operation time is a known risk factor for surgical site infection (10). In addition, Valentini et al. also reported that this risk was increased with duration of surgery > 2 hours, and a further relative risk increase for surgeries lasting 3–4 hours according (11). When precise localization by preoperative methods is achieved, the time required for awake surgery and intraoperative cortical mapping may be less, and attendant risks may be reduced (12).

In order to map the language cortex preoperatively, a new technique combining advanced imaging and electrophysiology, namely navigated transcranial magnetic stimulation (nTMS), has been introduced (13, 14). Transcranial magnetic stimulation (TMS) is a non-invasive stimulating technique that generates an alternating magnetic field, thereby inducing transient electric fields within the targeted brain cortex that, in turn, alters neural plasticity, restores synaptic connections, and finally excites/inhibits neurons (15). In cognitive studies, TMS is used to interfere with neural circuits in a temporally precise manner to create what is known as "virtual lesion". Researchers then study the effect of this lesion on a certain behavior (16). Consequently, online nTMS mapping may provide information about the brain functional boundary in a reliable noninvasive manner, anticipating information that otherwise may be available to surgeons only during an operation using DES. Many previous studies have compared TMS to DES to test if eloquent areas can also be reliably predicted in a noninvasive manner (17–21), and reported that nTMS provided mapping effects equivalent to those that DES provided, especially with respect to target location (22), and outperformed DES in functional preservation (23). These studies have provided valuable insights into the prediction accuracy of TMS for neurosurgical guidance (24) and established TMS as a useful tool for presurgical planning. However, direct evidence of the elucidating mechanisms, such as induced electric fields in the cortex and subcortical fiber tracts, has been lacking.

Individual target (IT)-TMS, a novel form of nTMS that combines the personalized stimulation site and dose with precise robotic targeting, has already been shown to increase the remission rates of major depressive disorders significantly compared with intermittent theta burst stimulation (25) as well as improve primary insomnia (26), postpartum depression (27), and Meige's syndrome (28). The term "individual" refers in this context to the construction of unique brain regions in each subject and selection of stimulation sites, that is, location. The term "target" refers to the navigated stimulation of the selected site with the help of robotic TMS equipment sets, that is, positioning. It is as yet unclear whether IT-TMS enhances the reliability of preoperative mapping results. The main aim of this study was, accordingly, to compare the reliability and effectiveness of IT-TMS with those of DES with respect to language mapping in patients with glioma, so as to provide evidence that matches with the evidence provided by DES and, therefore, reduces the time required for and risks associated with the operation.

2 Materials and methods

2.1 Subjects

This study included sixteen patients, 6 men and 10 women aged 28–69 (mean 52.69 ± 12.7 years, all right-handed), with brain glioma located in areas surrounding classic Broca's area, inferior frontal gyrus and ventral precentral gyrus. All surgeries were performed by the same surgeon, who commonly finishes about 150 glioma surgeries every year in his department. All of the subjects provided written informed consent. All of the procedures in this study were approved by the ethics committee of Xijing Hospital and conducted under the guidelines of the Declaration of Helsinki.

2.2 Magnetic resonance imaging

The subjects received preoperative and postoperative awake MRI scans, including T1, T2, and DTI. The scans were performed using a 3.0 T scanner equipped with a 32-channel head coil. T1-weighted sagittal anatomical images were obtained with the following parameters: sagittal slices = 192; repetition time (TR) = 7.24 ms; echo time (TE) = 3.10 ms; slice thickness/gap = 0.5/0 mm; in-plane resolution = 512 × 512; inversion time (TI) = 750 ms; flip angle = 10°; field of view (FOV) = 256 × 256 mm; voxel size = 0.5 × 0.5 × 1 mm; and T2 with TR/TE/FOV/voxel size/slice number 2,500 ms/236 ms/240 mm/1 mm × 1 mm × 1 mm/200. The DTI data were acquired with the repetition time (TR) = 12,676 ms; echo time (TE) = 88.6 ms, slice thickness = 2 mm, flip angle = 90°. All subjects wore earplugs to reduce the noise and possible head motion.

2.3 Preoperative IT-TMS mapping

We used the Black Dolphin Navigation Robot (S-50, a sub-millimeter smart positioning system, Solide Medical Sci. & Tech. Co., Ltd., Xi'an, Shaanxi, China) with a figure-of-8 coil (Yingchi Tech, Shenzhen, China) to perform the IT-TMS. An infrared camera and a three-dimensional individual mask were used for precise navigation of the coil over the target area under real-time visualization. The possible individual language sites close to the lesions of each subject in the nTMS group were marked prior to the experiments. Briefly, based on individual MRI brain images, the predefined targets were integrated into the operation system, in which a 3D restoration of the brain images and targets was visualized that allowed for the visual selection and monitoring of the immediate targets selection and monitoring. Next, online continuous theta burst stimulation (cTBS) examining these sites was performed before the subjects entered the operation room, with a number-counting task being performed in the meantime. When language was disturbed, the site was regarded as an nTMS hotspot (HS_{nTMS}). The resting motor threshold (rMT, defined as the lowest TMS intensity capable of eliciting a 50 μV MEP amplitude in at least 5 out of 10 consecutive trials) was measured over the abductor pollicis brevis (APB).

2.4 Intraoperative DES mapping

For each subject in the two groups, an awake craniotomy was performed to gain access to the tumor regions near the language areas, during which procedure the language task and DES targeting the language cortex were conducted to test whether language was disturbed. The DES was guided by the results of the preoperative data provided by the nTMS and nTMS-based DTI-FT (when available). A single anodal square pulse (pulse duration 0.2 ms) was employed. The minimum intensities from 1 mA, 2 mA to maximally 6 mA were applied when no response was achieved. When language was disturbed in three consecutive trials (29, 30), the site was regarded as DES hotspots (HS_{DES}).

2.5 Language task

Given the uniformity of enrolled subjects, we aimed to identify language-eloquent sites for speech production. Hence, only number-counting task was performed during the nTMS and DES procedures (2, 31, 32). Briefly, each was asked to count from 1 to 20 in succession while the nTMS and DES mapping were being conducted. Once counting was interrupted in three consecutive trials, this stimulation site and parameter were recorded as positive and deserving of further analysis.

2.6 Electromagnetic simulation

SimNIBS software (Version 3.2.4) served to generate for each subject the finite element mesh model based on the T1 images. A 3Dslicer served to segment the tumor using the intensity threshold method, and manual correction was performed. The isotropic tissue conductivity was as follows: σ_{skin}=0.465 S/m, σ_{skull}=0.010 S/m, σ_{CSF}=1.654 S/m, σ_{GM}=0.2765 S/m, σ_{WM}=0.126 S/m The electrical

conductivity of glioma tissue was consistent with that of surrounding gray matter.

For the nTMS, SimNIBS software again served to simulate the electric field. The coil model was established by measuring the magnetic field from the center of gravity (CoG). For the DES, the monopolar electrical stimulation was modeled by applying a Dirichlet boundary condition (33) for the electric potential at the stimulation point on the grey matter surface and a remote large return electrode at the inferior end of the FEM model. Two small balls with a radius of 1 mm served as the positive and negative electrodes of the electrode pen, and the distance between the centers was 4.4 mm. A realistic head model served to simulate the electric field generated during the intraoperative stimulation.

2.7 TMS-DES comparison

To compare the extent of the simulated TMS electric field stimulation area that coincided with the DES stimulation area, we computed the percentage of the area on the grey matter surface of the nTMS-induced electric field (E_{nTMS}) included in the area of the DES-induced electric field (E_{DES}) in a DES-determined region of interest (ROI). In the next step we computed the CoG of HS_{nTMS} ($HS_{nTMS\text{-}CoG}$) and $HS_{DES\text{-}CoG}$ for each subject as described previously (34). This method reduces the electric field maps to a single point. In the following analysis, we computed the Euclidian distance between the two CoG points for each subject.

2.8 Diffusion tensor imaging (DTI)-based fiber tracking (DTI-FT)

All language-positive $HS_{nTMS\text{-}CoG}$ and $HS_{DES\text{-}CoG}$ sites were transferred to DSI Studio software to determine the DTI-FT. First, the group of language-positive sites was fused with the MRI sequences preoperatively acquired. Next, these sites were defined as a region of interest, and tractography was conducted. The minimum fiber length was set at 20 mm for all of the trackings. Fractional anisotropy (FA) values were predefined as 0.1 as well as 50% of the individual FA threshold, as is conventionally done for the purpose of fiber tracking (35–37). We then saved the resulting data set consisting of preoperative MRI sequences, language-positive sites, and nTMS-based tractography.

2.9 Outcome measurements

A detailed case history and neurological examination, including the Western Aphasia Battery (WAB) scale (38) as the primary outcome, was conducted both preoperatively and postoperatively for each subject in the nTMS and non-nTMS groups.

2.10 Statistical analysis

The parameters assessed in this study are presented as means ± standard deviations and calculated using SPSS software. GraphPad Prism software served to generate the values and graphs. We performed all of the computations described here for each subject individually and then calculated the mean over all of the subjects.

3 Results

3.1 Preoperative and intraoperative language mapping

First, preoperative IT-TMS mapping was performed on one subject, as shown in Figure 1. Briefly, a TMS coil exporting the cTBS signal was used to target the language-eloquent cortical areas so as to examine the positive sites during the number-counting task for each subject in the nTMS group. No side effects were reported. Figure 1 shows the positive mapping results. The yellow dots indicate language-interrupted areas, and the grey dots indicate the peritumoral mouth and facial motor area. The location of the glioma is shown in red. Figure 1 shows the subsequent intraoperative functional boundary derived from the DES in the same subject. Again, the yellow numbers indicate the language area, and the white numbers indicate the peritumoral mouth and facial motor

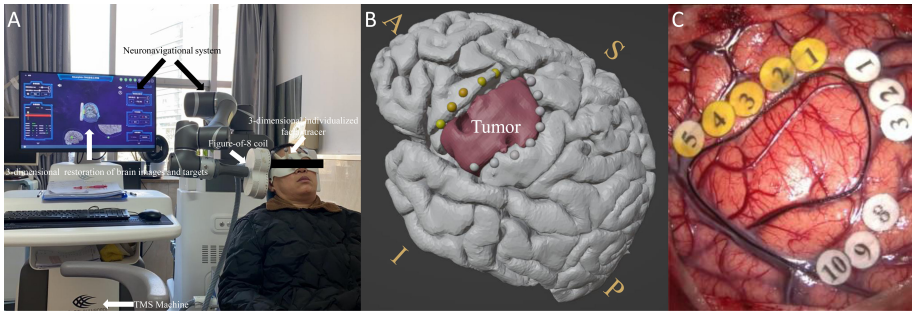

FIGURE 1
(A) Experimental set-up with labeled devices with picture of the IT-TMS system used for preoperative functional mapping prior to brain tumor surgery. The monitor shows a 3D-reconstruction of the brain with coil localization. **(B)** Preoperative language-positive mapping sites in one patient. **(C)** The intraoperative functional boundary in the same patient. The yellow dots and numbers indicate language-interrupted areas; the grey dots and white numbers indicate the peritumoral mouth and facial motor areas. The red color indicates the area of the tumor. A similar distribution of positive language-related sites was observed between pre-operation and intra-operation. S, superior; I, inferior; A, anterior; P, posterior.

area. Figures 1B, C show the similar distribution of positive language-related sites.

3.2 Distance between $HS_{nTMS\text{-}CoG}$ and $HS_{DES\text{-}CoG}$

The distribution of positive nTMS language mapping sites was similar to those of DES (Figure 2), reporting a mean distance of 6.32 ± 2.6 mm (distance range 2.2-9.3 mm, 95% CI 3.9-8.7 mm). The green dots indicate the nTMS-positive sites, and the yellow dots indicate the DES-positive sites. The red dot indicates the CoG of the nTMS-positive sites ($HS_{nTMS\text{-}CoG}$), and the blue dot indicates the $HS_{DES\text{-}CoG}$.

3.3 Comparison of $HS_{nTMS\text{-}CoG}$-based and $HS_{DES\text{-}CoG}$-based DTI-FT

As Figure 3 shows, the tractography results of arcuate fasciculus (AF) and superior longitudinal fasciculus II and III (SLF-II + III) derived from CoG-based DTI-FT were similar between nTMS and DES mapping. No significant difference in tract length was found between the two groups (P=0.2290, Table 1). In addition, the FA value was significantly higher in the nTMS mapping than in the DES mapping (P=0.0373, Table 1), suggesting that the former may provide extra assistance in language mapping and functional preservation.

3.4 Distribution of electric field induced by nTMS and DES

To analyze the accuracy of the nTMS mapping, we compared the computationally predicted stimulation area in $HS_{nTMS\text{-}CoG}$ with the $HS_{DES\text{-}CoG}$ area for each subject in the nTMS group (Figure 4). The high electric field strengths of E_{nTMS} were restricted to the inferior frontal gyrus. The E_{DES} was considerably more spatially restricted and decreased rapidly as the area increased. Over 90% overlap of the E_{nTMS} stimulation area fell within the DES electric field (Figure 4, see more data in Supplementary Material section).

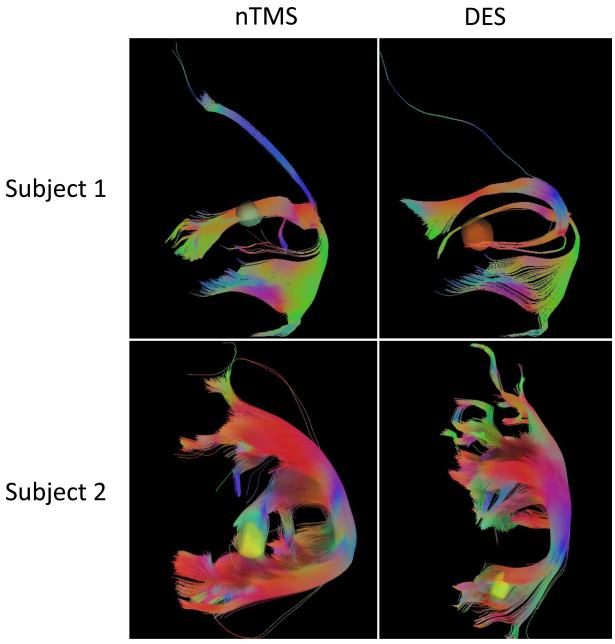

FIGURE 3
The tractography results of arcuate fasciculus **(AF)** and superior longitudinal fasciculus II and III (SLF-II + III) derived from CoG-based DTI-FT of two subjects, in nTMS and DES, respectively.

3.5 Effectiveness of the nTMS mapping compared with the non-nTMS group

As shown in Figure 5, the members of the nTMS group demonstrated significantly higher postoperative WAB scores than the members of the non-nTMS group, suggesting that the preoperative mapping generated a better result with respect to linguistic preservation. To be specific, preoperative WAB score in nTMS group was (97.14 ± 2.56, n=9), and in non-nTMS group (97.7 ± 2.5, n=7). The independent-samples t-test demonstrated no significance (P=0.658>0.05). Postoperatively, the mean WAB score in nTMS group was (78.4 ± 10.4, n=9), and in non-nTMS group (59.5 ± 8.8, n=7). The independent-samples t-test between these two groups showed a P value of 0.0321 (less than 0.05). Moreover, according to the DTI-FT of AF and SLF-II + III results shown in Table 2, greater

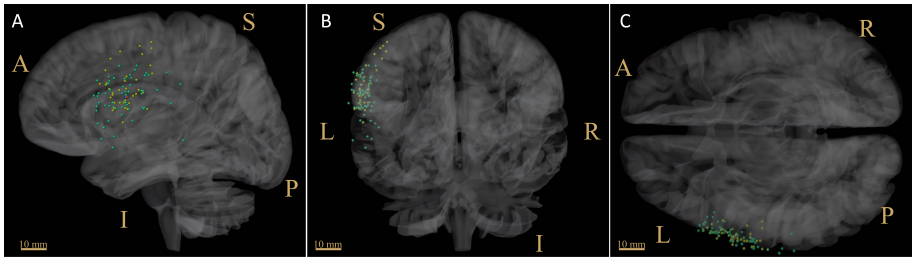

FIGURE 2
Distribution of language-positive sites derived from nTMS and DES. The green dots indicate the nTMS-positive sites, among which the CoG is shown in red. The yellow dots indicate the DES-positive sites, among which the CoG is shown in blue. **(A)** sagittal view; **(B)** coronal view; **(C)** cross view. CoG = center of gravity; scale bar = 10 mm; L, left; R, right; S, superior; I, inferior; A, anterior; P, posterior.

10.3389/fonc.2023.1089787

TABLE 1 Analysis of fiber-tracking results between nTMS and DES.

Group	FA value			Tract length		
	Mean	SD	*P* value	Mean	SD	*P* value
nTMS	0.35	0.09	0.0373	63.75	36.05	0.2290
DES	0.30	0.09		45.62	11.59	

FA, fractional anisotropy; nTMS, navigated transcranial magnetic stimulation; DES, deep electrical stimulation; SD, standard deviation.

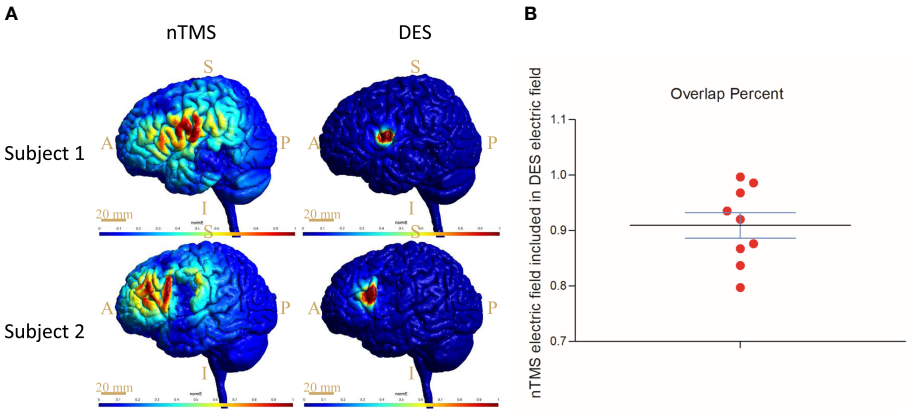

FIGURE 4
Results of electromagnetic simulation and quantification through computational modeling targeting the CoG sites. **(A)** The distribution of the electric field induced by nTMS and DES, respectively, in two subjects. Scale bar = 20 mm; S, superior; I, inferior; A, anterior; P, posterior. **(B)** Percent overlap of E_{nTMS} and E_{DES}; more than 90% overlap of the E_{nTMS} stimulation area fell within the DES electric field. CoG = center of gravity.

postoperative integrity and structure were observed in the nTMS group than in the non-nTMS group.

4 Discussion

The management of gliomas close to functional areas is challenging because of the risk of surgery-related morbidity (6). Thus, functional mapping is increasingly used for resection (17). The aim of this study was to verify the reliability and effectiveness of nTMS in the preoperative period for language mapping, which surgeons routinely perform during awake craniotomy (39). These findings provide direct evidence that preoperative nTMS language mapping is comparable to intraoperative DES mapping in brain tumor patients. Though intraoperative DES mapping is the gold standard (6, 7), preoperative language evaluation can be of great value because the investigation of cortical language functions beforehand surgery tends to result in safer and more efficient surgeries (40). In other words, nTMS provided valuable results that may have otherwise become available only by DES intraoperatively.

Other researchers have explored the effective use of nTMS mapping in surgical techniques with respect to such considerations as the scope of craniotomy (22), gross total resection (1), and duration of operations (41). However, the actual effects and mechanisms of nTMS mapping on the brain cortex remain unclear. As shown in Figure 1, online IT-TMS targeting of the left language-eloquent area was performed to output the interference signal during the number-counting task (32). The stimulation sites that disturbed language behavior were detected (Figure 1) and compared with DES-positive sites (Figure 1). As shown in Figure 2, the comparison between spatial distribution of nTMS-positive sites and DES-positive sites was completed in nTMS group (n=9). The mean distance between nTMS-positive sites and DES-positive sites was 6.32 ± 2.6 mm (distance range 2.2-9.3 mm, 95% CI 3.9-8.7 mm). Compared with the results from Opitz et al. (the minimum distance between nTMS-positive sites and DES-positive sites was 6.3 ± 0.7 mm) (42), we can draw a conclusion that in our study nTMS-positive sites were close to those of DES. Hence, the mapping results acquired from DES and nTMS are similar. These results

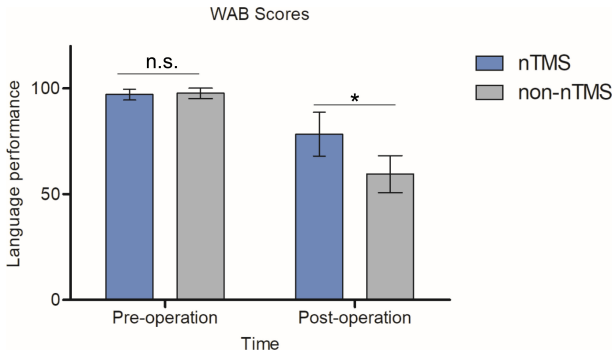

FIGURE 5
WAB scores for the nTMS and non-nTMS groups preoperatively and postoperatively. No significance was observed preoperatively (*P*=0.658). We observed a significant postoperative improvement in the nTMS group relative to the non-nTMS group (*P*=0.0321). The independent-samples t-test was employed. n.s. indicates no significant difference; *indicates $P < 0.05$.

TABLE 2 Analysis of fiber-tracking results between nTMS and non-nTMS.

Group		FA value			Tract length		
		Mean	SD	*P* value	Mean	SD	*P* value
Preoperative	nTMS	0.39	0.06	0.550	64.35	36.32	0.971
	Non-nTMS	0.30	0.09		64.33	36.73	
Postoperative	nTMS	0.34	0.08	0.0156	57.45	31.71	0.0166
	Non-nTMS	0.27	0.06		39.29	10.82	

FA, fractional anisotropy; nTMS, navigated transcranial magnetic stimulation; non-nTMS, non-navigated transcranial magnetic stimulation; SD, standard deviation.

provided evidences for the reliability of nTMS mapping, because DES is the current gold standard for brain mapping.

The fiber tracts, AF and SLF-II + III overlap in the classic Broca's area and ventral precentral gyrus, are the main structures responsible for language production (43, 44). DES of SLF-II + III induces anarthria or speech arrest (45), and interference with AF causes phonemic paraphasia (44, 46). The fiber-tracking results of AF and SLF-II + III, as Figure 3 shows, reflect the degree of functional preservation after surgery. We observed a significantly higher FA value with better protection in the nTMS group, but no difference in tract length. In fact, these DTI data were collected immediately after tumor resection, once the subject had been allowed to do so. This procedure can detect the structural preservation of fiber tracts as soon as possible because an instant comparison between nTMS and DES DTI-FT is needed before the dynamic reorganization of the brain. Hence, higher FA values could reflect better functional and linguistic preservation, as described in previous studies (22).

The analysis of the distribution of the electric fields that nTMS and DES induce yielded another key finding from this study. In fact, the cortical and subcortical currents, namely virtual lesions (16), originating from the induced electric field disturb cortical functions and, ultimately, language behavior (31). We found the distributions (Figure 4) of the electric fields in nTMS and DES to be similar, showing an overlap of up to 90% (Figure 4). Opitz et al. reported a similar overlap of the TMS- and DES-induced electric fields in a realistic head model and spherical model, respectively (42), thus verifying the similarities in the simulation model between TMS and DES, but the actual effects on the brain cortex remained unclear. Our results showed the surface electric fields in living subjects, thus complementing the direct evidence of preoperative localization by nTMS. In short, the preoperative nTMS mapping proved reliable.

Regarding effectiveness, the findings of a higher WAB score and better DTI-FT value (Figure 5, Table 2) demonstrated that less impairment of the language area and linguistic function occurred in the nTMS group, owing to the precise mapping by nTMS. Because DES is a local stimulation method for mapping structure-function relationships in the brain, its application is typically limited to patients undergoing brain surgery. According to our results, with the availability of an additional preoperative nTMS map, a surgeon is able to address intrinsic functional brain lesions more easily to more aggressively, thereby optimizing EOR while maintaining quality of life. Notably, we did not directly compare the advantages and disadvantages of nTMS and DES, and nTMS did not serve as an adjunct of DES during our mapping procedures. In other words, nTMS and DES are parallel approaches.

This study thus provides evidence that preoperative nTMS correlates well with intraoperative DES in language-eloquent mapping and, therefore, contributes to good language performance for language-eloquent glioma patients after surgery. The electromagnetic simulation results reveal a comparison between nTMS and DES, demonstrating that the brain tissues on or beneath the cortex receive the equivalent level of electric energy. Above all, preoperative nTMS mapping is a specific non-invasive method which does not require a lengthy operation and might significantly reduce the surgical risk of infections and limitations of other complications.

5 Limitations and conclusion

This study has several limitations. First, the small sample size and restriction of the population to glioma patients may have introduced bias. For precise brain-mapping validation, future research could be conducted with larger samples that include healthy subjects and/or subjects with other brain diseases. Second, we did not determine whether IT-TMS-based language mapping alone improves clinical outcomes. Lastly, we did not compare mapping based on IT-TMS only and DES only in this study because of a problem with the ethical review.

In conclusion, we have described here the reliability and effectiveness of preoperative IT-TMS-based brain functional language mapping. In doing so, we provide novel evidence of fiber-tracking and electromagnetic simulation for the preoperative neurophysiological mapping of language sites prior to surgery to treat intrinsic brain tumors located in or near eloquent networks.

Data availability statement

The original contributions presented in the study are included in the article/Supplementary Material. Further inquiries can be directed to the corresponding authors.

Ethics statement

The studies involving human participants were reviewed and approved by the ethnic review board of Xijing Hospital. The patients/participants provided their written informed consent to participate in this study.

Author contributions

SL and YR designed this study and directed the trial. CS collected and analyzed the MRI data. XL and HL prepared the algorithm. XuY recruited the subjects and collected the clinical information. XiY performed the electromagnetic simulation. YD conducted the DTI-FT and statistical analysis. YW and YR prepared the manuscript. ZF and SL are the co-corresponding authors; they directed the research program, revised the draft of the manuscript, and submitted this article. All authors contributed to the article and approved the submitted version.

Conflict of interest

Author XuY is employed by Solide Brain Medical Technology, Ltd. The remaining authors declare that the research was conducted in the absence of any commercial or financial relationships that could be construed as a potential conflict of interest.

Publisher's note

Supplementary material

The Supplementary Material for this article can be found online at: https://www.frontiersin.org/articles/10.3389/fonc.2023.1089787/full#supplementary-material

References

1. Takakura T, Muragaki Y, Tamura M, Maruyama T, Nitta M, Niki C, et al. Navigated transcranial magnetic stimulation for glioma removal: Prognostic value in motor function recovery from postsurgical neurological deficits. *J Neurosurg* (2017) 127(4):877–91. doi: 10.3171/2016.8.Jns16442

2. Sanai N, Mirzadeh Z, Berger MS. Functional outcome after language mapping for glioma resection. *New Engl J Med* (2008) 358(1):18–27. doi: 10.1056/NEJMoa067819

3. Wijnenga MM, French PJ, Dubbink HJ, Dinjens WN, Atmodimedjo PN, Kros JM, et al. The impact of surgery in molecularly defined low-grade glioma: An integrated clinical, radiological, and molecular analysis. *Neuro Oncol* (2018) 20(1):103–12. doi: 10.1093/neuonc/nox176

4. Knecht S, Dräger B, Deppe M, Bobe L, Lohmann H, Flöel A, et al. Handedness and hemispheric language dominance in healthy humans. *Brain* (2000) 123(12):2512–8. doi: 10.1093/brain/123.12.2512

5. Bonelli SB, Thompson PJ, Yogarajah M, Vollmar C, Powell RH, Symms MR, et al. Imaging language networks before and after anterior temporal lobe resection: Results of a longitudinal fmri study. *Epilepsia* (2012) 53(4):639–50. doi: 10.1111/j.1528-1167.2012.03433.x

6. Duffau H, Lopes M, Arthuis F, Bitar A, Sichez J, Van Effenterre R, et al. Contribution of intraoperative electrical stimulations in surgery of low grade gliomas: A comparative study between two series without (1985–96) and with (1996–2003) functional mapping in the same institution. *J Neurology Neurosurg Psychiatry* (2005) 76(6):845–51. doi: 10.1136/jnnp.2004.048520

7. Soffietti R, Baumert B, Bello L, Von Deimling A, Duffau H, Frénay M, et al. Guidelines on management of low-grade gliomas: Report of an efns–eano* task force. *Eur J Neurol* (2010) 17(9):1124–33. doi: 10.1111/j.1468-1331.2010.03151.x

8. Rossi M, Gay L, Conti Nibali M, Sciortino T, Ambrogi F, Leonetti A, et al. Challenging giant insular gliomas with brain mapping: Evaluation of neurosurgical, neurological, neuropsychological, and quality of life results in a Large mono-institutional series. *Front Oncol* (2021) 11:629166. doi: 10.3389/fonc.2021.629166

9. Maldaun MVC, Khawja SN, Levine NB, Rao G, Lang FF, Weinberg JS, et al. Awake craniotomy for gliomas in a high-field intraoperative magnetic resonance imaging suite: Analysis of 42 cases: Clinical article. *J Neurosurg JNS* (2014) 121(4):810–7. doi: 10.3171/2014.6.JNS132285

10. Viken H, Iversen I, Jakola A, Sagberg L, Solheim O. When are complications after brain tumor surgery detected? *World Neurosurg* (2018) 112:E702–10. doi: 10.1016/j.wneu.2018.01.137

11. Valentini LG, Casali C, Chatenoud L, Chiaffarino F, Uberti-Foppa C, Broggi G. Surgical site infections after elective neurosurgery: A survey of 1747 patients. *Neurosurgery* (2008) 62(1):88–96. doi: 10.1227/01.NEU.0000311065.95496.C5

12. Takahashi S, Vajkoczy P, Picht T. Navigated transcranial magnetic stimulation for mapping the motor cortex in patients with rolandic brain tumors. *Neurosurgical Focus* (2013) 34(4):E3. doi: 10.3171/2013.1.Focus133

13. Picht T, Mularski S, Kuehn B, Vajkoczy P, Kombos T, Suess O. Navigated transcranial magnetic stimulation for preoperative functional diagnostics in brain tumor surgery. *Operative Neurosurg* (2009) 65(suppl_6):ons93–ons9. doi: 10.1227/01.NEU.0000348009.22750.59

14. Raffa G, Germanò A, Tomasello F. Letter to the Editor regarding" first united kingdom experience of navigated transcranial magnetic stimulation in preoperative mapping of brain tumors". *World Neurosurg* (2019) 125:549–50. doi: 10.1016/j.wneu.2018.12.111

15. Siebner H, Rothwell J. Transcranial magnetic stimulation: New insights into representational cortical plasticity. *Exp Brain Res* (2003) 148(1):1–16. doi: 10.1007/s00221-002-1234-2

16. Pascual-Leone A. Transcranial magnetic stimulation: Studying the brain–behaviour relationship by induction of 'Virtual lesions'. *Philos Trans R Soc London Ser B: Biol Sci* (1999) 354(1387):1229–38. doi: 10.1098/rstb.1999.0476

17. Krieg SM, Sollmann N, Obermueller T, Sabih J, Bulubas L, Negwer C, et al. Changing the clinical course of glioma patients by preoperative motor mapping with navigated transcranial magnetic brain stimulation. *BMC Cancer* (2015) 15:231. doi: 10.1186/s12885-015-1258-1

18. Picht T, Schmidt S, Brandt S, Frey D, Hannula H, Neuvonen T, et al. Preoperative functional mapping for rolandic brain tumor surgery: Comparison of navigated transcranial magnetic stimulation to direct cortical stimulation. *Neurosurgery* (2011) 69(3):581–9. doi: 10.1227/NEU.0b013e3182181b89

19. Vitikainen A-M, Salli E, Lioumis P, Mäkelä JP, Metsähonkala L. Applicability of ntms in locating the motor cortical representation areas in patients with epilepsy. *Acta Neurochirurgica* (2013) 155(3):507–18. doi: 10.1007/s00701-012-1609-5

20. Sollmann N, Hauck T, Obermüller T, Hapfelmeier A, Meyer B, Ringel F, et al. Inter- and intraobserver variability in motor mapping of the hotspot for the abductor policis brevis muscle. *BMC Neurosci* (2013) 14(1):94. doi: 10.1186/1471-2202-14-94

21. Tarapore PE, Findlay AM, Honma SM, Mizuiri D, Houde JF, Berger MS, et al. Language mapping with navigated repetitive tms: Proof of technique and validation. *NeuroImage* (2013) 82:260–72. doi: 10.1016/j.neuroimage.2013.05.018

22. Frey D, Schilt S, Strack V, Zdunczyk A, Rösler J, Niraula B, et al. Navigated transcranial magnetic stimulation improves the treatment outcome in patients with brain tumors in motor eloquent locations. *Neuro Oncol* (2014) 16(10):1365–72. doi: 10.1093/neuonc/nou110

23. Hendrix P, Dzierma Y, Burkhardt BW, Simgen A, Wagenpfeil G, Griessenauer CJ, et al. Preoperative navigated transcranial magnetic stimulation improves gross total resection rates in patients with motor-eloquent high-grade gliomas: A matched cohort study. *Neurosurgery* (2021) 88(3):627–36. doi: 10.1093/neuros/nyaa486

24. Picht T, Schulz J, Hanna M, Schmidt S, Suess O, Vajkoczy P. Assessment of the influence of navigated transcranial magnetic stimulation on surgical planning for tumors in or near the motor cortex. *NeuroSurgery* (2012) 70(5):1248–57. doi: 10.1227/NEU.0b013e318243881e

25. Tang N, Sun C, Wang Y, Li X, Liu J, Chen Y, et al. Clinical response of major depressive disorder patients with suicidal ideation to individual target-transcranial magnetic stimulation. *Front Psychiatry* (2021) 12:768819. doi: 10.3389/fpsyt.2021.768819

26. Qi S, Zhang Y, Li X, Sun C, Ma X, Li S, et al. Improved functional organization in patients with primary insomnia after individually-targeted transcranial magnetic stimulation. *Front Neurosci* (2022) 16. doi: 10.3389/fnins.2022.859440

27. Zhang Y, Mu Y, Li X, Sun C, Ma X, Li S, et al. Improved interhemispheric functional connectivity in postpartum depression disorder: Associations with individual target-transcranial magnetic stimulation treatment effects. *Front Psychiatry* (2022) 13. doi: 10.3389/fpsyt.2022.859453

28. Song C-G, Shi X-J, Jiang B, Shi R, Guo X, Qi S, et al. Successful treatment of the meige's syndrome with navigated repetitive transcranial magnetic stimulation: A case report. *Brain Stimulation: Basic Translational Clin Res Neuromodulation* (2022) 15(1):96–8. doi: 10.1016/j.brs.2021.11.013

29. Ille S, Sollmann N, Hauck T, Maurer S, Tanigawa N, Obermueller T, et al. Combined noninvasive language mapping by navigated transcranial magnetic stimulation and functional mri and its comparison with direct cortical stimulation. *J Neurosurg JNS* (2015) 123(1):212–25. doi: 10.3171/2014.9.jns14929

30. Ille S, Sollmann N, Hauck T, Maurer S, Tanigawa N, Obermueller T, et al. Impairment of preoperative language mapping by lesion location: A functional magnetic resonance imaging, navigated transcranial magnetic stimulation, and direct cortical stimulation study. *J Neurosurg* (2015) 123(2):314–24. doi: 10.3171/2014.10.JNS141582

31. Wu J, Lu J, Zhang H, Zhang J, Yao C, Zhuang D, et al. Direct evidence from intraoperative electrocortical stimulation indicates shared and distinct speech production center between Chinese and English languages. *Hum Brain Mapp* (2015) 36(12):4972–85. doi: 10.1002/hbm.22991

32. Lu J, Zhao Z, Zhang J, Wu B, Zhu Y, Chang EF, et al. Functional maps of direct electrical stimulation-induced speech arrest and anomia: A multicentre retrospective study. *Brain* (2021) 144(8):2541–53. doi: 10.1093/brain/awab125

33. Joucla S, Yvert B. Modeling extracellular electrical neural stimulation: From basic understanding to mea-based applications. *J Physiology-Paris* (2012) 106(3-4):146–58. doi: 10.1016/j.jphysparis.2011.10.003

34. Sollmann N, Krieg SM, Säisänen L, Julkunen P. Mapping of motor function with neuronavigated transcranial magnetic stimulation: A review on clinical application in brain tumors and methods for ensuring feasible accuracy. *Brain Sci* (2021) 11(7):897. doi: 10.3390/brainsci11070897

35. Frey D, Strack V, Wiener E, Jussen D, Vajkoczy P, Picht T. A new approach for corticospinal tract reconstruction based on navigated transcranial stimulation and standardized fractional anisotropy values. *NeuroImage* (2012) 62(3):1600–9. doi: 10.1016/j.neuroimage.2012.05.059

36. Krieg SM, Buchmann NH, Gempt J, Shiban E, Meyer B, Ringel F. Diffusion tensor imaging fiber tracking using navigated brain stimulation–a feasibility study. *Acta Neurochirurgica* (2012) 154(3):555–63. doi: 10.1007/s00701-011-1255-3

37. Sollmann N, Wildschuetz N, Kelm A, Conway N, Moser T, Bulubas L, et al. Associations between clinical outcome and navigated transcranial magnetic stimulation characteristics in patients with motor-eloquent brain lesions: A combined navigated transcranial magnetic stimulation–diffusion tensor imaging fiber tracking approach. *J Neurosurg JNS* (2018) 128(3):800–10. doi: 10.3171/2016.11.jns162322

38. Dekhtyar M, Braun EJ, Billot A, Foo L, Kiran S. Videoconference administration of the Western aphasia battery–revised: Feasibility and validity. *Am J Speech-Language Pathol* (2020) 29(2):673–87. doi: 10.1044/2019_AJSLP-19-00023

39. Aonuma S, Gomez-Tames J, Laakso I, Hirata A, Takakura T, Tamura M, et al. A high-resolution computational localization method for transcranial magnetic stimulation mapping. *NeuroImage* (2018) 172:85–93. doi: 10.1016/j.neuroimage.2018.01.039

40. Raffa G, Quattropani MC, Germanò A. When imaging meets neurophysiology: The value of navigated transcranial magnetic stimulation for preoperative neurophysiological mapping prior to brain tumor surgery. *Neurosurgical Focus* (2019) 47(6):E10. doi: 10.3171/2019.9.FOCUS19640

41. Sollmann N, Kelm A, Ille S, Schröder A, Zimmer C, Ringel F, et al. Setup presentation and clinical outcome analysis of treating highly language-eloquent gliomas *Via* preoperative navigated transcranial magnetic stimulation and tractography. *Neurosurgical Focus* (2018) 44(6):E2. doi: 10.3171/2018.3.FOCUS1838

42. Opitz A, Zafar N, Bockermann V, Rohde V, Paulus W. Validating computationally predicted tms stimulation areas using direct electrical stimulation in patients with brain tumors near precentral regions. *NeuroImage: Clin* (2014) 4:500–7. doi: 10.1016/j.nicl.2014.03.004

43. Duffau H. Stimulation mapping of white matter tracts to study brain functional connectivity. *Nat Rev Neurol* (2015) 11(5):255–65. doi: 10.1038/nrneurol.2015.51

44. Bu L, Lu J, Zhang J, Wu J. Intraoperative cognitive mapping tasks for direct electrical stimulation in clinical and neuroscientific contexts. *Front Hum Neurosci* (2021) 15:612891. doi: 10.3389/fnhum.2021.612891

45. van Geemen K, Herbet G, Moritz-Gasser S, Duffau H. Limited plastic potential of the left ventral premotor cortex in speech articulation: Evidence from intraoperative awake mapping in glioma patients. *Hum Brain Mapp* (2014) 35(4):1587–96. doi: 10.1002/hbm.22275

46. Porto de Oliveira JVM, Raquelo-Menegassio AF, Maldonado IL. What's your name again? a review of the superior longitudinal and arcuate fasciculus evolving nomenclature. *Clin Anat* (2021) 34(7):1101–10. doi: 10.1002/ca.23764

frontiers | Frontiers in Oncology

TYPE Original Research
PUBLISHED 21 February 2023
DOI 10.3389/fonc.2023.1089139

OPEN ACCESS

EDITED BY
Yasuo Iwadate,
Chiba University, Japan

REVIEWED BY
Ji Peigang,
Fourth Military Medical University, China
Jianping Song,
Fudan University, China

*CORRESPONDENCE
Hongmin Bai
baihmfmmu@vip.163.com

†These authors have contributed equally to this work

SPECIALTY SECTION
This article was submitted to Neuro-Oncology and Neurosurgical Oncology, a section of the journal Frontiers in Oncology

RECEIVED 03 November 2022
ACCEPTED 07 February 2023
PUBLISHED 21 February 2023

CITATION
Yao S, Yang R, Du C, Jiang C, Wang Y, Peng C and Bai H (2023) Maximal safe resection of diffuse lower grade gliomas primarily within central lobe using cortical/subcortical direct electrical stimulation under awake craniotomy.
Front. Oncol. 13:1089139.
doi: 10.3389/fonc.2023.1089139

Maximal safe resection of diffuse lower grade gliomas primarily within central lobe using cortical/subcortical direct electrical stimulation under awake craniotomy

Shujing Yao†, Ruixin Yang†, Chenggang Du, Che Jiang, Yang Wang, Chongqi Peng and Hongmin Bai*

Department of Neurosurgery, General Hospital of Southern Theater Command of PLA, Guangzhou, China

Background: Diffuse lower-grade glioma (DLGG) in the central lobe is a challenge for safe resection procedures. To improve the extent of resection and reduce the risk of postoperative neurological deficits, we performed an awake craniotomy with cortical-subcortical direct electrical stimulation (DES) mapping for patients with DLGG located primarily within the central lobe. We investigated the outcomes of cortical-subcortical brain mapping using DES in an awake craniotomy for central lobe DLGG resection.

Methods: We performed a retrospective analysis of clinical data of a cohort of consecutively treated patients from February 2017 to August 2021 with diffuse lower-grade gliomas located primarily within the central lobe. All patients underwent awake craniotomy with DES for cortical and subcortical mapping of eloquent brain areas, neuronavigation, and/or ultrasound to identify tumor location. Tumors were removed according to functional boundaries. Maximum safe tumor resection was the surgical objective for all patients.

Results: Thirteen patients underwent 15 awake craniotomies with intraoperative mapping of eloquent cortices and subcortical fibers using DES. Maximum safe tumor resection was achieved according to functional boundaries in all patients. The pre-operative tumor volumes ranged from 4.3 cm^3 to 137.3 cm^3 (median 19.2 cm^3). The mean extent of tumor resection was 94.6%, with eight cases (53.3%) achieving total resection, four (26.7%) subtotal and three (20.0%) partial. The mean tumor residue was 1.2 cm^3. All patients experienced early postoperative neurological deficits or worsening conditions. Three patients (20.0%) experienced late postoperative neurological deficits at the 3-month follow-up, including one moderate and two mild neurological deficits. None of the patients experienced late onset severe neurological impairments post-operatively. Ten patients with 12 tumor resections (80.0%) had resumed activities of daily living at the 3-month follow-up. Among 14 patients with pre-operative epilepsy, 12 (85.7%) were seizure-free after treatment with antiepileptic drugs 7 days after surgery up to the last follow-up.

Conclusions: DLGG located primarily in the central lobe deemed inoperable can be safely resected using awake craniotomy with intraoperative DES without severe permanent neurological sequelae. Patients experienced an improved quality of life in terms of seizure control.

KEYWORDS

lower-grade glioma, central lobe, awake craniotomy, direct electrical stimulation, maximal safe resection

1 Introduction

Diffuse lower grade glioma (DLGG) is one of the most common primary brain tumors, and includes tumors classified as Grade 2–3 astrocytoma by the World Health Organization (WHO), oligodendroglioma, and types with no or slight enhancement on pre-operative magnetic resonance imaging (MRI) studies where postoperative pathology demonstrates focal anaplasia. Conversely, these types of tumors, especially those in or near the eloquent brain areas, are difficult to treat and are often considered inoperable due to their propensity for deep infiltration of the surrounding parenchyma and malignant transformation. However, patients with DLGG achieve long-term survival if they receive early and successful surgical treatment. Furthermore, there has been compelling evidence that an increased extent of resection (EOR) of DLGG could prolong the survival of patients (1–6). Individuals with at least 90% EOR achieved 5-year survival rates of 97%, while patients with less than 90% EOR achieved 5-year survival rates of 76% (1). Therefore, the goal of DLGG surgery should be to maximize the extent of tumor resection while minimizing the risk of postoperative neurological deficits to improve overall survival (OS) and quality of life.

Currently, multiple image-based techniques can be used pre-operatively to help identify eloquent brain areas and define their relationship with brain lesions, including functional magnetic resonance imaging (fMRI), diffusion tensor imaging (DTI), and magnetoencephalography (MEG). Intraoperative aids, such as functional neuronavigation, intraoperative MRI, intraoperative ultrasound, and fluorescent tumor markers, have also been applied to maximize the safety of aggressive resection around eloquent areas. However, these techniques have limited sensitivity and specificity for cortical or subcortical functional mapping (2–5). Consequently, surgeons often face difficulties in distinguishing compensable areas that can be resected and critical areas that must be surgically preserved.

Direct electrical stimulation (DES) mapping is considered the gold standard for neurosurgical planning and can provide a more direct assessment of neuronal function. A recent large meta-analysis that included more than 8000 patients found that glioma resections using intraoperative stimulation mapping were associated with fewer severe late neurologic deficits and more extensive resection, although lesions were more frequent in eloquent areas (6–10).

In this study, we summarized our surgical experience in 15 cases of awake craniotomy with intraoperative DES for DLGG located primarily in the central lobe to explore the efficacy of maximal safe glioma resection using intraoperative cortical and subcortical mapping by DES under awake craniotomy.

2 Methods

2.1 Patient enrollment

From February 2017 to August 2021, a total of 13 patients (15 operations) suspected of DLGG in the central lobe based on pre-operative MRI were successively treated with awake craniotomy. All the patients recruited had no severe pre-operative neurological deficits or mental disorientation.

Clinical, radiological and histopathological characteristics were collected during admission, including sex, age, symptoms, neurological deficits, Karnofsky performance scale, seizure attacks, tumor location, and pathological grades and subtypes were revised according to the WHO Classification of Tumors of the Central Nervous System, Fifth Edition (CNS 5). The regional ethics committee approved the procedures and all subjects provided their informed written consent prior to participation in this study.

2.2 Pre-operative examinations

All patients underwent detailed neurological and psychological evaluations before surgery. Two neurosurgeons completed a neurological function assessment and motor function was scored using a standard muscle strength score ranging from 0 to 5 (0, complete paralysis; 5, entirely normal strength). Neuropsychologists evaluated the general cognitive function of the patients using a brief psychiatric examination. All patients were assessed for handedness using a standardized questionnaire (Edinburgh Handedness Inventory) and were examined with the Mini-Mental State Examination (MMSE). Language function was assessed using an aphasia screening chart, a dysarthria chart, and naming of images. Aphasia screening included oral, written, and sign language comprehension and expression. The dysarthria chart was evaluated by orofacial movement, vowels, and consonant articulation, with a

total score of 14 points. The picture naming task was to name 80 black and white pictures with a naming accuracy rate ≥95% being normal. The grade of neurological deficits are presented in Table 1. Within 3 days before surgery, MRI was performed using a 3.0-T scanner (GE HealthCare, Chicago, IL, USA) to obtain T1, T2, T2-fluid attenuated inversion recovery (FLAIR), gadolinium enhanced diffuse tensor imaging (DTI), magnetic resonance spectrum (MRS) and perfusion-weighted sequences. All patients were informed in detail about the risks of surgery and the intraoperative stimulation monitoring procedure was performed by a trained nurse responsible for intraoperative motor and language testing.

2.3 Surgical procedure

As previously described (11), the critical points of awake surgery include patient position, awake anesthesia, neuronavigation, intraoperative ultrasound, DES mapping, and tumor resection. All patients were anesthetized by administration of propofol and remifentanil by target-controlled infusion, using a laryngeal mask airway for intubation during the craniotomy. The ipsilateral critical sensory scalp nerves, pin insertion, and scalp incision sites were injected with local anesthetic (0.67% lidocaine and 0.33% ropivacaine) with 1:200,000 adrenaline to provide rapid and long-lasting local anesthesia while reducing bleeding. Anesthesia was withdrawn to wake up the patient. The location of the tumor was detected intraoperatively using ultrasound before brain mapping and tumor resection. DES mapping was performed using a 5-mm interval bipolar electrical nerve stimulator (Osiris NeuroStimulator; inomed Medizintechnik GmbH, Emmendingen, Germany) with a frequency of 60 Hz, a pulse duration of 1 ms, a current of 2–6 mA (usually 3–4 mA), and a duration of 1 s for motor and sensory tasks and 4 s for language or other cognitive tasks. Positive motor area stimulation was assumed when movements of the contralateral limb or face were induced. Positive stimulation affecting sensory areas was considered when an abnormal feeling was generated in the contralateral limb or face. Positive stimulation of language areas was considered when the patient exhibited counting arrest, anomia, speech repetition, or other language disturbances without twitching of the mouth. After cortical mapping, the lesion was removed by alternating resection and regular subcortical stimulation.

To protect functional pathways, the patient was asked to continue to move their arm and hand or leg, count numbers, or name pictures when the resection moved closer to the subcortical structures. If the patient experienced weakness of the limb, abnormal language, or abnormal sensation, subcortical DES was performed immediately with the same stimulation parameters. If the above-mentioned positive reaction occurred, it was confirmed to be an essential subcortical conduction pathway. The resection was then interrupted in this direction and was continued in other directions. If no positive response occurred, after the patient's function recovered, resection was continued until the subcortical areas (positive stimulation) or normal meninges (such as the falx cerebri, fissures), ventricles, or arachnoid borders were encountered, or when more than 1 cm outside of normal white matter surrounding the tumor could be visualized. Tumors were resected 2 mm from the sulci near the eloquent brain areas and then were resected inside the pia mater to avoid damage to the vital supplying arteries in the subarachnoid space. Lesions were safely removed to the greatest extent possible to preserve the cortical and subcortical structures of critical functional areas, drainage veins, and supplying arteries.

2.4 Postoperative evaluation

Detailed neurological examinations and cognitive function assessments, such as language, were performed 1 day and 5 days after surgery, at discharge, and 3 months after surgery. Neurological dysfunction within 3 months was defined as the early onset stage and after 3 months was defined as the late onset stage. Neurological dysfunction was defined as mild, moderate, or severe based on the assessments described above, which included muscle strength, aphasia detection, articulation disorder detection, and picture naming. Cranial MRI was completed 48 hours after surgery, T2-weighted images or FLAIR imaging was used as a reference, and tumor volume was calculated using 3D Slicer software (v4.6; http://www.slicer.org) (12). Total resection was defined as 100% resection, with 90–100% resection and residual tumor volume < 10 cm^3 as subtotal resection and < 90% resection and residual tumor volume ≥ 10 cm^3 considered partial resection.

3 Results

3.1 Demographic, clinical, and tumor characteristics

From February 2017 to August 2021, a total of 13 patients (15 cases) met the inclusion criteria for this study, including two patients who underwent awake surgery twice in our hospital due

TABLE 1 Grading of neurological deficits.

Neurological Deficit	Normal	Mild	Moderate	Severe
Muscle strength (Grade)	5	5-	4	≤3
Aphasia Screening (correct rate, %)	100	75	50	≤25
Articulation Screening (scores)	14	≥10,<14	≥5,<10	<5
Naming Screening (correct rate, %)	≥95	≥75,<95	≥25,<75	<25

to tumor recurrence 3 to 4 years after the first surgery. The patient sample included 7 men and 8 women, aged 24–62 years (average 36.3 years). Twelve patients had experienced seizures before admission, and the other patient also experienced seizures before the second operation. Two patients presented headaches. All patients had MMSE scores ≥ 28. Twelve patients were right-handed and only one patient was ambidextrous.

Pre-operative tumor volumes ranged from 4.3 to 137.3 cm^3, with a median of 19.2 cm^3. In all cases, the tumor was primarily in the central lobe (including precentral and postcentral gyri and paracentral lobule) or invaded the central lobe (66.7% of the cases on the left side, 33.3% on the right side). There was involvement of the frontal lobe in nine cases, involvement of the frontoparietal and parietal lobe in two cases and involvement of the insular lobe and parieto-occipital lobe in one case. The exact gyri invaded by the tumors are shown in Table 2.

3.2 Intraoperative DES mapping, tumor EOR, and pathological diagnoses

An awake craniotomy was successfully performed in all cases. After DES in all cases reached a certain intensity (2.0–4.0 mA, median 3.0 mA), DES-induced movement was observed in 13 cases,

TABLE 2 Demographic data, clinical features, intraoperative mapping, extent of resection, postoperative deficits, and oncological features.

Case N.	Age (year)/ sex	Pre-operative symptoms	Lesion location (side)	Lesion volume (cm^3)	Residual lesion volume (cm^3)/ EOR (%)	Pathology (WHO Grade)
1	62/F	Seizure	Posterior central gyrus and superior parietal lobule (L)	44.1	4.3/90.2	Astrocytoma (2)/IDH(+)
2	53/F	Seizure	Posterior central gyrus and superior parietal lobule (L)	16.8	2.4/85.7	Oligoastrocytoma (3)/IDH(+), 1p19q LOH
3	28/M	Headache	Middle part of the precentral gyrus (L)	4.3	0/100	Astrocytoma (2)/IDH(+)
4	37/F	Seizure	Superior part of the precentral gyrus and posterior central gyrus (R)	19.2	3.7/80.8	Astrocytoma (2)/IDH(+)
5	25/M	Seizure	Inferior precentral gyrus and posterior inferior frontal gyrus (R)	36.2	0/100	Astrocytoma (2)/IDH(+)
6	28/F	Seizure	Inferior precentral gyrus and posterior of inferior frontal gyrus (L)	26.9	0/100	Oligoastrocytoma (2)/IDH(+), 1p19q LOH
7	28/F	Headache, seizure	Posterior central gyrus and superior and inferior parietal lobule (L)	118.9	0/100	Oligoastrocytoma (2)/IDH(+), 1p19q LOH
8	54/M	Seizure	Posterior central gyrus and superior parietal lobule (R)	137.3	0/100	Oligoastrocytoma (2)/IDH(+), 1p19q LOH
9	27/F	Seizure,	Inferior precentral gyrus (L)	13.0	0/100	Oligoastrocytoma (3)/IDH(+), 1p19q LOH
10/4	40/F	Seizure	Superior precentral gyrus and posterior central gyrus (R)	12.8	1.2/90.6	Astrocytoma (2)/IDH(+)

(Continued)

TABLE 2 Continued

Case N.	Age (year)/ sex	Pre-operative symptoms	Lesion location (side)	Lesion volume (cm^3)	Residual lesion volume (cm^3)/ EOR (%)	Pathology (WHO Grade)
11	38/M	Seizure	Hand knob of the precentral gyrus (R)	16.8	0/100	Astrocytoma (2)/IDH(+)
12	35/M	Seizure	Inferior precentral gyrus and posterior of inferior frontal gyrus (L)	27.4	0/100	Astrocytoma (3)/IDH (–) NEC
13	34/F	Seizure	Inferior precentral gyrus and posterior of inferior frontal gyrus (L)	26.2	1.4/94.7	Oligoastrocytoma (3)/IDH(+), 1p19q LOH
14/3	32/M	Seizure	Middle part of the precentral gyrus (L)	5.9	0.5/91.5	Astrocytoma (2)/IDH(+)
15	24/M	Seizure	Inferior precentral gyrus and posterior of inferior frontal gyrus (L)	34.7	4.8/86.2	Oligoastrocytoma (2)/IDH(+), 1p19q LOH

Case n.	Cortical sites for motor (n)	Subcortical site for motor (n)	Cortical sites for sensory (n)	Subcortical sites for Sensory (n)	Cortical sites for language (n)	Subcortical sites for language (n)	Early neurological deficits	Late neurological deficits
1	2	1	2	1	0	0	Severe paralysis	Moderate paralysis
2	3	1	1	0	2	0	Moderate paralysis	Normal
3	2	0	2	0	2	1	Severe paralysis and aphasia	Normal
4	2	1	2	0	0	0	Severe paralysis	Normal
5	2	2	1	0	0	0	Moderate aphasia	Normal
6	0	1	1	0	1	0	Moderate aphasia	Normal
7	2	1	3	2	0	2	Severe paralysis	Normal
8	0	0	1	1	0	0	Moderate paralysis	Normal
9	1	2	3	1	1	0	Moderate aphasia	Normal
10/5	1	2	1	0	0	0	Severe paralysis	Normal
11	1	2	3	0	0	0	Moderate paralysis	Normal
12	0	0	0	0	2	1	Severe paralysis and aphasia	Mild paralysis
13	2	0	2	0	3	0	Severe aphasia	Mild aphasia
14/3	1	1	2	0	3	1	Severe paralysis and aphasia	Normal
15	1	0	0	0	1	1	Severe aphasia	Normal

n, number; F, female; M, male; L, left; R, right; EOR, extent of resection; +, mutation; -, wild-type.

including 20 cortical sites in 12 cases and 14 subcortical sites in 10 cases. Stimulation-induced sensation was observed in 13 cases, including 24 cortical sites in 13 cases and five subcortical sites in four cases. Twenty-one sites showed language responses in 9 cases (15 cortical areas in 8 cases and 6 subcortical regions in 5 cases). Pyramidal tracts, suprathalamic radiation, or fibers of white matter related to language were identified surrounding the tumor in all patients. Maximum safe tumor resection was achieved according to functional boundaries in all patients.

The mean extent of tumor resection was 94.6%, with 8 cases (53.3%) achieving total resection, 4 (26.7%) subtotal, and three (20.0%) partial resections. The mean residual tumor volume was 1.2 cm^3. In terms of pathology, tumor grades and subtypes were revised according to the WHO CNS 5. There were 7 cases of diffuse astrocytoma with IDH mutation (Grade 2), 1 case of diffuse astrocytoma with wild-type IDH (Grade 3, NEC), 4 cases of oligodendroglioma with IDH mutation and 1p19q LOH (Grade 2), and 3 cases of oligodendroglioma with IDH mutation 1p19q LOH (Grade 3).

3.3 Complications

During surgery, no adverse events related to awake craniotomy were observed. One patient experienced partial DES-induced seizures during resection, which was controlled by cold normal saline irrigation for about 3 minutes.

All patients experienced early postoperative neurological deficits or worsening of symptoms. Nine cases presented severe neurological deficits and 6 showed moderate deficits. Three patients (20.0%) experienced late postoperative neurological deficits at the 3-month follow-up, including one case of mild Broca's aphasia and 2 cases of inflexible movements (one mild, one moderate). One patient (6.7%) experienced moderate late neurological sequelae after awake craniotomy for DLGG in the central lobe. None of the patients experienced post-operative late onset severe neurological impairments. Ten patients with 12 tumor resections (80.0%) had resumed normal activities of daily living at the 3-month follow-up.

Among the 14 cases of pre-operative epilepsy, 12 (85.7%) were seizure-free after receiving antiepileptic drugs from 7 days after surgery up to the last follow-up.

3.4 Illustrative cases

3.4.1 Case 1

A 27-year-old right-handed woman (case 9) presented a two-week history of transient language disruptions accompanied by loss of consciousness. Physical examination revealed no neurological impairments, and pre-operative MRI revealed a low-grade glioma in the left central lobe (Figures 1A–E). DTI-based fiber tracking showed that the arcuate fasciculus and the pyramidal tract were below and medial to the lesion, respectively (Figures 1F, G). After revealing the dura, intraoperative ultrasound showed a tumor in the inferior part of the left precentral gyrus. Eloquent cortices, including sensory, motor, and language areas, were found by cortical mapping (Figure 1H). Three subcortical sensory and motor sites were detected during tumor resection using DES (Figure 1I). Postoperative MRI revealed total tumor resection (Figures 1J–L). The patient experienced moderate aphasia about one week after surgery, with normal language function at discharge.

3.4.2 Case 2

A 28-year-old right-handed man (case 3) presented with a headache. A surface rendering of pre-operative T1-weighted MRI revealed a tumor located entirely within the precentral gyrus (Figures 2A–E). The surface rendering of the functional areas overlapped with T1-weighted MRI and fMRI identified the active sites for hand grasping and naming tasks (Figure 2F). DTI-based fiber tracking showed a close relationship between the tumor and white matter fibers (Figures 2G, H). Under awake craniotomy using cortical and subcortical DES, the maximum safe tumor resection was achieved with an EOR of 100% (Figures 2I–L). The patient experienced paralysis of the right hand and Broca aphasia three days after surgery, but resumed normal life 3 months after surgery. The histological diagnosis was astrocytoma with IDH mutation (Grade 2). This patient presented seizures 40 months after surgery, with MRI revealing a recurrent tumor anterior to the residual surgical cavity (Figures 2M, N). Thus, we performed a second awake craniotomy (case 14), with subtotal tumor resection and an EOR of 91.5% (Figures 2O, P). Following surgery, the patient experienced severe paralysis and aphasia, but recovered to normal at the 3-month follow-up.

3.4.3 Case 3

A 38-year-old man (case 11) experienced recurrent left hand convulsions one month before admission. MRI revealed a low-grade glioma located precisely in the hand knob of the right precentral gyrus (Figures 3A–D). The pre-operative physical examination showed normal muscle strength in all limbs. To achieve maximum safe tumor resection, the patient underwent awake craniotomy (Figures 3E, F), resulting in total tumor resection with cortical and subcortical boundaries (Figures 3G, H) and moderate transient postoperative paralysis at one week after surgery.

4 Discussion

DLGG frequently occurs in young patients and life expectancy is longer in patients with active social and professional lives (1, 13). The first-line therapeutic option for DLGG is maximum safe resection, with EOR being a significant independent prognostic factor. Studies have shown that higher EOR is associated with better progression-free survival and OS (1–6, 14–18). Even some cases with grade 3 or 4 transformation foci with a grade 2 background do not necessarily require immediate adjuvant therapy following a radical maximal safe resection under awake craniotomy. Therefore, we selected patients with DLGG having a grade 2 background, which included four cases presenting

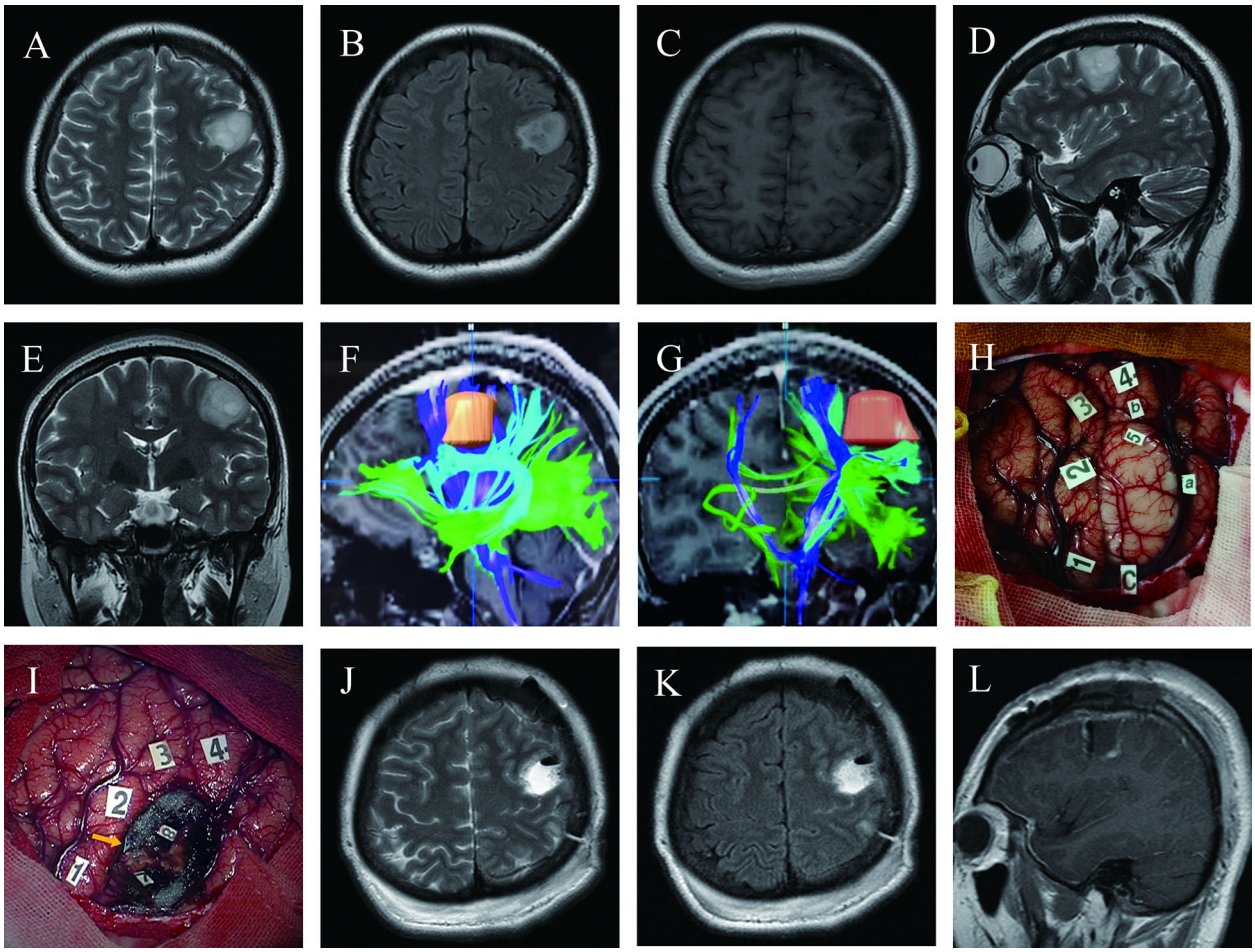

FIGURE 1
Maximum safe resection of oligodendroglioma harboring IDH mutation and 1P/19Q codeletion (WHO Grade 3) in the inferior left precentral gyrus under awake craniotomy in a 27-year-old woman presenting with seizures (Case 9); **(A–E)** Pre-operative T2 axial, T2 FLAIR axial, T1-weighted gadolinium-enhanced axial, T2 sagittal, and T2 coronal MRI revealed the tumor's location precisely in the inferior lateral left hand knob of the precentral gyrus. **(F, G)** DTI-based reconstructed fibers showed arcuate fasciculus beneath the lesion and slightly distorted, and the pyramidal tract was medial to the lesion; **(H)** Intraoperative view before tumor resection; Tumor borders marked by letters (a, anterior; b, superior; c, inferior). Number of tags denotes positive DES mappings (1, paresthesia of the right little and ring fingers; 2, numbness of the right thumb; 3, paresthesia of the right corner of mouth; 4, motor responses in the right corner of mouth; tag 5 is on the surface of the tumor, where speech arrest and convulsions of the right corner of the mouth were induced during DES); **(I)** Intraoperative view after tumor resection based on the functional boundary; The tumor was removed until DES mapping encountered eloquent brain areas at cortical and subcortical levels (Tag 7, movement of the right hand during DES; 8, movement of the right corner of the mouth; 9 with a yellow arrow, an electrifying sensation of the right index finger); **(J–L)** Twenty-four hours postoperative T2 axial, T2 FLAIR axial, and T1-weighted gadolinium-enhanced sagittal MRI demonstrated total tumor resection.

focal grade 3 anaplasia as our cohort (19). Furthermore, because oligodendroglioma is sensitive to radiotherapy and chemotherapy, some clinicians have a conservative attitude toward surgical resection. When oligodendroglioma is located in eloquent brain areas, to avoid postoperative neurological deficits, some clinicians sustain that excessive resection is not necessary, and elect only partial resection or biopsy as the therapeutic option. It is challenging to classify tumors as oligodendroglioma or astrocytoma pre-operatively. Furthermore, recent research has also confirmed that the EOR of oligodendroglioma is closely related to prognosis. Studies registered in the extensive Surveillance, Epidemiology and End Results database and in the National Cancer Database revealed that the extent of resection was associated with an increase in OS for both histologically confirmed oligodendrogliomas and molecularly defined tumors (IDH mutations with 1p/19q-codeletion) (17, 20). However, the major challenge in neurosurgery is to eradicate the tumor as much as possible while maximally preserving neurological functions. Various techniques have been introduced to achieve this goal, such as fluorescence-guided surgery, intraoperative ultrasound, intraoperative MRI combined with functional neuronavigation, and Raman spectroscopy (21–27).

Although fMRI, a noninvasive mapping method, is becoming increasingly applied in neurosurgery, its precision remains controversial and the parameters used in different studies vary significantly (9, 19, 21–23, 28). Recently, Weng et al. (21) performed a systematic review that included ten studies with a total of 214 patients with brain tumors to assess the accuracy of fMRI for language mapping with direct cortical stimulation and found that, per patient, the pooled sensitivity and specificity of fMRI was 44%

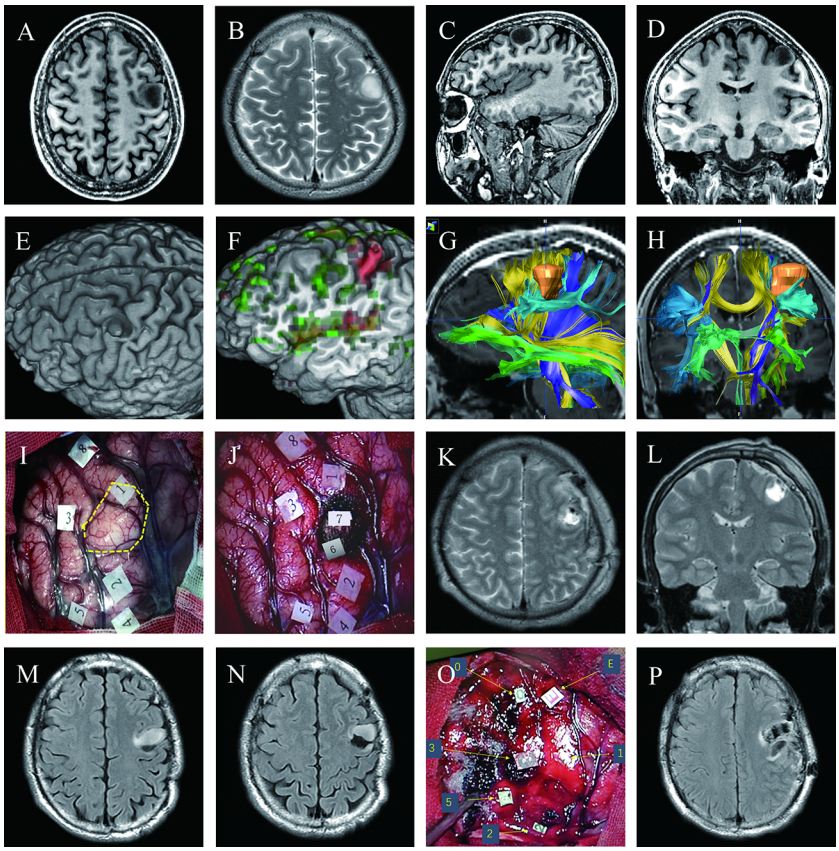

FIGURE 2
Maximum safe resection of astrocytoma with IDH mutation (WHO Grade 2) in the inferior left precentral gyrus in two successive awake craniotomies over four years (Cases 3 and 14); **(A–D)** Pre-operative T1 axial, T2 axial, T1 sagittal, and T1 coronal MRI; **(E)** Surface rendering of pre-operative T1-weighted MRI revealed a tumor in the middle of the left precentral gyrus, which was separated into the dorsal and ventral parts by the tumor; **(F)** Surface rendering of functional areas overlapped with T1-weighted MRI and fMRI; Red denotes active sites for hand grasp task; green represents active sites for naming task; **(G, H)** Pre-operative planning using neuro-navigation showed a close relationship between the tumor and white matter fibers; **(I)** Intraoperative view before tumor resection; An ultrasonic tumor border is marked with the dotted yellow circle. Numbers on tags denote zones of positive DES mapping (2 and 4, finger movement; 3, mouth sensation; 5, finger sensation; 1, speech arrest during counting; 8, anomia during naming) **(J)** Intraoperative view after tumor resection; glioma was removed until eloquent neural structures were encountered at cortical and subcortical levels using subcortical DES; Tag 6, pyramidal tract for right thumb movement; 7, area responsible for speech arrest during counting; Postoperative axial **(K)** and coronal **(L)** T2 FLAIR-weighted MRI demonstrated total tumor resection; **(M, N)** Follow-up MRI revealed a recurrent tumor anterior to the previous surgical residual cavity; **(O)** Intraoperative view of the second surgery before tumor resection; Number and letter tags denote zones of positive DES mapping (2, thumb movement; 3, mouth sensation; 5, finger sensation; 0, 1, and E, both speech arrest and interrupt of hand grasp during a dual coordinate task); **(P)** Postoperative axial T2 FLAIR MRI showed subtotal tumor resection with a residue of 0.5 cm^3.

and 80%, respectively; per tag, the pooled sensitivity and specificity were 67% and 55%, respectively. Another meta-analysis by Metwali et al. (23) included six studies of language activation and two of motor activation. The study concluded that fMRI alone (due to neurovascular uncoupling) or analysis of the findings present limitations in reliability compared to direct cortical stimulation, and using fMRI alone for surgical planning could lead to undesirable outcomes. Additionally, a clinical survey conducted by Stopa et al. on the use and attitudes of neurosurgeons towards fMRI as a surgical planning tool in neurooncology patients revealed that 70% of the responders presented a resected fMRI positive functional site, of which 77% did so because the area was 'cleared' using intraoperative cortical stimulation. If the results of fMRI and intraoperative mapping disagreed, 98% of the respondents would rely on intraoperative mapping (25).

DTI tractography, a noninvasive method for visualizing white matter tracts, can provide clinically relevant information during pre-operative planning and intraoperative mapping for brain tumor resection (8, 21, 25). However, DTI tractography relies only on the indirect reconstruction of fibers based on measuring the diffusion of water molecules. The results depend on many factors, including data acquisition, geometrical models, software programs, and regions of interest (7, 9, 10, 23, 26, 27). Maier-Hein reported that most state-of-the-art algorithms produce tractograms containing 90% of the ground-truth bundles, while the same tractograms have many more invalid than valid bundles. Consequently, DTI tractography is not sufficiently reliable to be the basis for neurosurgical decision making, and the possibility of incorrectly displayed fibers leads to a risk of postoperative deficits for the patient (2).

It should be mentioned that to date, intraoperative DES mapping under awake anesthesia remains the standard goal for brain surgery, especially at the subcortical level (11, 12, 28–37). In the present study, we performed an awake craniotomy in patients

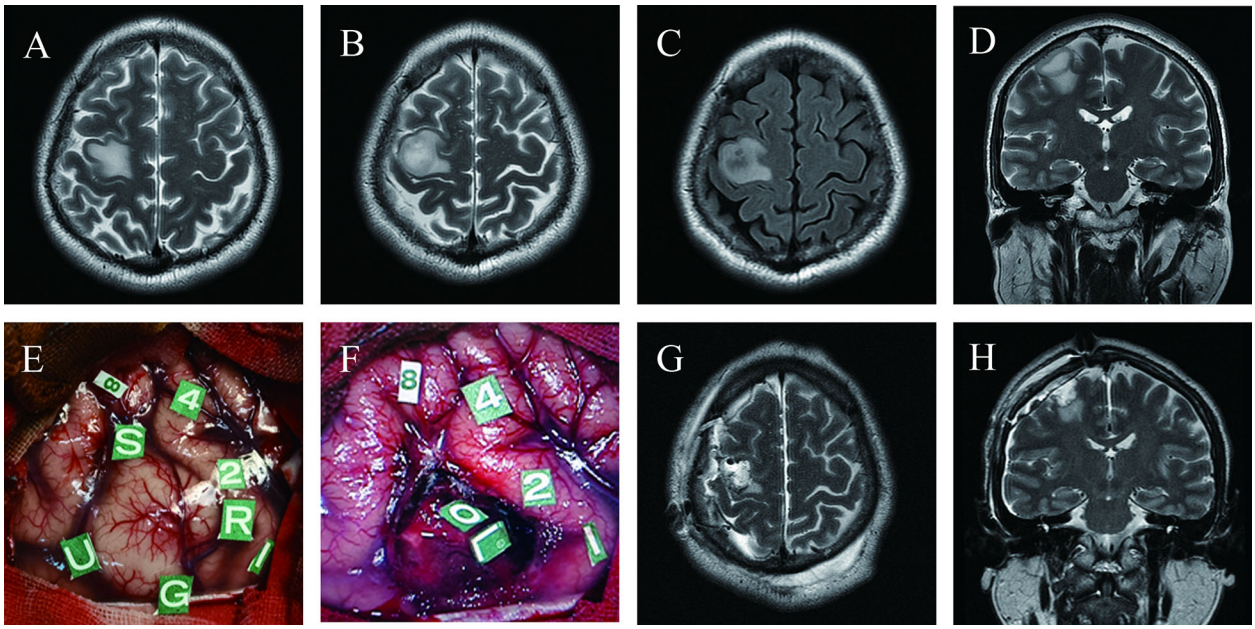

FIGURE 3
Maximum safe resection of astrocytoma with IDH mutation (WHO Grade 3) in the hand knob of the right precentral gyrus under awake craniotomy in a 38-year-old man presenting with seizures (Case 11); Pre-operative T2 axial **(A, B)**, T2 FLAIR axial **(C)** and T2 coronal **(D)** MRI revealed the tumor's location precisely on the hand knob of the right precentral gyrus; **(E)** Intraoperative view before tumor resection; Tumor borders marked with letter tags (Tag U, anterior; G, superior; S, inferior; R, posterior). Number tags show positive points of DES mapping (8, changes in vocal tone; 1, 2, 4, primary sensory cortex, paresthesia of the left forearm, palm, and thumb, respectively); **(F)** Intraoperative view subsequent to tumor removal; Tag L, subcortical area for wrist movement; O, subcortical area for finger movement; Postoperative axial **(G)** and coronal **(H)** T2-weighted MRI demonstrated total tumor resection.

pre-operatively suspected of DLGG located primarily in the central lobe. The postoperative outcomes also illustrated the power of this procedure to detect functional tissue around tumors. From a traditional standpoint, DLGG is considered inoperable in the central lobe, which is composed of the pre- and postcentral gyri and the paracentral lobule, which are the eloquent brain areas (38–41). According to our experience in this study, awake surgery and DES can also achieve maximum safe resection of DLGG when it is located entirely in the central lobe due to functional remodeling of the brain.

In this retrospective report, functional white matter fibers were identified surrounding the tumor in all patients, and maximum safe tumor resection was achieved according to functional limits in all patients. The mean extent of tumor resection was 94.6%. The mean tumor residue was 1.2 cm^3. Only one patient (6.7%) experienced moderate late onset postoperative neurological deficits and none of the patients experienced severe late neurological impairments. Among 14 cases with pre-operative epilepsy, 12 patients (85.7%) were seizure-free after taking antiepileptic drugs starting 7 days post-operatively to the last follow-up after surgery (3 months). Lower-grade glioma located primarily in the central lobe can be safely resected using awake craniotomy with intraoperative DES without severe permanent neurological sequelae. All patients achieved a better quality of life with respect to seizure control.

Although the application of subcortical DES to remove DLGG in functional areas can reduce the incidence of late onset neurological dysfunction, the incidence of early neurological dysfunction is high. All the patients in the present cohort exhibited early neurological dysfunction, which may be related to postoperative tumor cavity edema, ischemia, or damage to some auxiliary functions of the cortical and subcortical fibers. However, early postoperative neurological dysfunction will prolong hospital stays, and most patients require rehabilitation treatment, leading to increased medical costs.

During awake craniotomy procedures, surgeons should pay closer attention to the following details: 1) maintain the integrity of the fiber tracts of white matter as subcortical electrical stimulation is as essential as cortical mapping, and the tumor should be excised using alternating resection and regular subcortical stimulation (42–44); 2) ensure postoperative arterial supply and venous drainage of surrounding normal brain tissue, and some vital blood vessels must be preserved, such as the central sulcus artery, the artery of pre- and post-central sulcus artery, the paracentral artery, and veins of Labbé and Trolard (41, 42); 3) the functional boundaries detected by intraoperative DES and pia mater can be used as essential protective tissue to avoid injury to important blood supply arteries located in the cerebral sulcus.

There are some limitations to this study. First, this was a single-center retrospective study with a small sample size, and patient selection was based on the economic status and intraoperative cooperation of awake craniotomy of the patient. Therefore, to

evaluate the fundamental role of awake craniotomy surgery for DLGG in the central lobe, further prospective and randomized multicenter cohort studies with larger sample sizes are required. Second, in such a clinical study, some mixed factors could lead to potentially biased results. To reduce bias in surgical procedures, surgeries in all cases were performed by the same team composed of experienced neurosurgeons, anesthetists, and trained nurses. Third, we attempted to analyze the relationship between seizure control after surgery and LGG EOR. However, no definitive conclusion could be drawn due to the small sample size, although the incidence of seizure after tumor total resection was seemingly lower than that of nontotal resection.

5 Conclusions

Based on our experience in this study, DLGG located exclusively in the central lobe and considered inoperable can be safely resected with a mean EOR of nearly 95% under awake anesthesia with intraoperative DES. Although numerous non-invasive imaging techniques are becoming increasingly popular and accurate, their validity in identifying eloquent cortical areas and white matter tracts is still inferior to intraoperative DES. However, a prospective and more extensive randomized cohort studies are needed to evaluate the fundamental role of awake craniotomy surgery for DLGG in the central lobe.

Data availability statement

The raw data supporting the conclusions of this article will be made available by the authors, without undue reservation.

Ethics statement

The studies involving human participants were reviewed and approved by the ethics committee of the General Hospital of Southern Theater Command of PLA. The patients/participants provided their written informed consent to participate in this study. Written informed consent was obtained from the individual(s) for the publication of any potentially identifiable images or data included in this article.

Author contributions

SY, RY, and CP participated in data collection and analysis, and writing of the paper. CJ and YW participated in the pre- and post-operative evaluation. HB participated in brain mapping and data interpretation. HB and CD reviewed and edited the manuscript. All authors contributed to the article and approved the submitted version.

Funding

The study was supported by National Natural Science Foundation of China (U1201257) and the Science and Technology Planning Projects of Guangdong Province, China (2017B020210008).

Acknowledgments

We thank the patients and their families. We thank the nurses (Ruiqin Tian and Hongyu Sun) and linguist (Yan Cai) of the Department of Neurosurgery, General Hospital of Southern Theater Command of PLA for intraoperative photography and neurological function monitoring. We also thank Genetron Health (Beijing) Co., Ltd. for providing sequencing services for this study.

Conflict of interest

The authors declare that the research was conducted in the absence of any commercial or financial relationships that could be construed as a potential conflict of interest.

Publisher's note

References

1. Hervey-Jumper SL, Berger MS. Maximizing safe resection of low- and high-grade glioma. *J Neurooncol* (2016) 130:269–82. doi: 10.1007/s11060-016-2110-4

2. Maier-Hein KH, Neher PF, Houde JC, Côté MA, Garyfallidis E, Zhong J, et al. The challenge of mapping the human connectome based on diffusion tractography. *Nat Commun* (2017) 8(1):1349. doi: 10.1038/S41467-017-01285-X

3. Feigl GC, Hiergeist W, Fellner C, Schebesch KMM, Doenitz C, Finkenzeller T, et al. Magnetic resonance imaging diffusion tensor tractography: Evaluation of anatomic accuracy of different fiber tracking software packages. *World Neurosurg* (2014) 81:144–50. doi: 10.1016/J.WNEU.2013.01.004

4. Duffau H. The dangers of magnetic resonance imaging diffusion tensor tractography in brain surgery. *World Neurosurg* (2014) 81:56–8. doi: 10.1016/J.WNEU.2013.01.116

5. Jones DK, Knösche TR, Turner R. White matter integrity, fiber count, and other fallacies: the do's and don'ts of diffusion MRI. *Neuroimage* (2013) 73:239–54. doi: 10.1016/J.NEUROIMAGE.2012.06.081

6. Staub-Bartelt F, Radtke O, Hänggi D, Sabel M, Rapp M. Impact of anticipated awake surgery on psychooncological distress in brain tumor patients. *Front Oncol* (2022) 11:795247/PDF. doi: 10.3389/FONC.2021.795247/PDF

7. de Witt Hamer PC, Robles SG, Zwinderman AH, Duffau H, Berger MS. Impact of intraoperative stimulation brain mapping on glioma surgery outcome: A meta-analysis. *J Clin Oncol* (2012) 30:2559–65. doi: 10.1200/JCO.2011.38.4818

8. Sanai N, Berger MS. Intraoperative stimulation techniques for functional pathway preservation and glioma resection. *Neurosurg Focus* (2010) 28(2):E1. doi: 10.3171/2009.12.FOCUS09266

9. Keles GE, Lundin DA, Lamborn KR, Chang EF, Ojemann G, Berger MS. Intraoperative subcortical stimulation mapping for hemispherical perirolandic gliomas located within or adjacent to the descending motor pathways: Evaluation of morbidity and assessment of functional outcome in 294 patients. *J Neurosurg* (2004) 100:369–75. doi: 10.3171/JNS.2004.100.3.0369

10. Duffau H. Awake mapping with transopercular approach in right insular-centered low-grade gliomas improves neurological outcomes and return to work. *Neurosurgery* (2022) 91:182–90. doi: 10.1227/neu.0000000000001966

11. Bai HM, Wang WM, Li TD, He H, Shi C, Guo XF, et al. Three core techniques in surgery of neuroepithelial tumors in eloquent areas: Awake anaesthesia, intraoperative direct electrical stimulation and ultrasonography. *Chin Med J (Engl)* (2011) 124:3035–41. doi: 10.3760/cma.j.issn.0366-6999.2011.19.015

12. Kikinis R, Pieper SD, Vosburgh K. 3D slicer: A platform for subject-specific image analysis, visualization, and clinical support. *Intraoperative Imaging Image-Guided Ther* (2014) 3(19):277–89. doi: 10.1007/978-1-4614-7657-3_19

13. McGirt MJ, Chaichana KL, Attenello FJ, Weingart JD, Than K, Burger PC, et al. Extent of surgical resection is independently associated with survival in patients with hemispheric infiltrating low-grade gliomas. *Neurosurgery* (2008) 63:700–7. doi: 10.1227/01.NEU.0000325729.41085.73

14. Berger MS, Deliganis AV, Dobbins J, Keles GE. The effect of extent of resection on recurrence in patients with low grade cerebral hemisphere gliomas. *Cancer* (1994) 74:1784–91. doi: 10.1002/1097-0142(19940915)74:6<1784::aid-cncr2820740622>3.0.co;2-d

15. Blobner J, Tonn JC. Resection of glioma - feeding the beast? *Neuro Oncol* (2022) 24:1088–9. doi: 10.1093/neuonc/noac078

16. Tang OY, Pugacheva A, Bajaj AI, Rivera Perla KM, Weil RJ, Toms SA. The national inpatient sample: A primer for neurosurgical big data research and systematic review. *World Neurosurg* (2022) 162:e198–217. doi: 10.1016/j.wneu.2022.02.113

17. Garton ALA, Kinslow CJ, Rae AI, Mehta A, Pannullo SC, Magge RS, et al. Extent of resection, molecular signature, and survival in 1p19q-codeleted gliomas. *J Neurosurg* (2020) 134(5):1357–67. doi: 10.3171/2020.2.jns192767

18. Smith JS, Chang EF, Lamborn KR, Chang SM, Prados MD, Cha S, et al. Role of extent of resection in the long-term outcome of low-grade hemispheric gliomas. *J Clin Oncol* (2008) 26:1338–45. doi: 10.1200/JCO.2007.13.9337

19. Al-Tamimi YZ, Palin MS, Patankar T, MacMullen-Price J, O'Hara DJ, Loughrey C, et al. Low-grade glioma with foci of early transformation does not necessarily require adjuvant therapy after radical surgical resection. *World Neurosurg* (2018) 110:e346–54. doi: 10.1016/j.wneu.2017.10.172

20. Kinslow CJ, Garton ALA, Rae AI, Marcus LP, Adams CM, McKhann GM, et al. Extent of resection and survival for oligodendroglioma: A U.S. population-based study. *J Neurooncol* (2019) 144:591–601. doi: 10.1007/s11060-019-03261-5

21. Weng H-H, Noll KR, Johnson JM, Prabhu SS, Tsai Y-H, Chang S-WW, et al. Accuracy of presurgical functional MR imaging for language mapping of brain tumors: A systematic review and meta-analysis. *Radiology* (2018) 286:512–23. doi: 10.1148/radiol.2017162971

22. Lu J, Zhao Z, Zhang J, Wu B, Zhu Y, Chang EF, et al. Functional maps of direct electrical stimulation-induced speech arrest and anomia: A multicentre retrospective study. *Brain* (2021) 144:2541–53. doi: 10.1093/brain/awab125

23. Metwali H, Raemaekers M, Kniese K, Kardavani B, Fahlbusch R, Samii A. Reliability of functional magnetic resonance imaging in patients with brain tumors: A critical review and meta-analysis. *World Neurosurg* (2019) 125:183–90. doi: 10.1016/j.wneu.2019.01.194

24. Schilling KG, Nath V, Hansen C, Parvathaneni P, Blaber J, Gao Y, et al. Limits to anatomical accuracy of diffusion tractography using modern approaches. *Neuroimage* (2019) 185:1–11. doi: 10.1016/j.neuroimage.2018.10.029

25. Stopa BM, Senders JT, Broekman MLD, Vangel M, Golby AJ. Preoperative functional MRI use in neurooncology patients: A clinician survey. *Neurosurg Focus* (2020) 48:E11. doi: 10.3171/2019.11.FOCUS19779

26. Ellis DG, White ML, Hayasaka S, Warren DE, Wilson TW, Aizenberg MR. Accuracy analysis of fMRI and MEG activations determined by intraoperative mapping. *Neurosurg Focus* (2020) 48:E13. doi: 10.3171/2019.11.FOCUS19784

27. Azad TD, Duffau H. Limitations of functional neuroimaging for patient selection and surgical planning in glioma surgery. *Neurosurg Focus* (2020) 48:E12. doi: 10.3171/2019.11.FOCUS19769

28. Aghi MK, Nahed BV, Sloan AE, Ryken TC, Kalkanis SN, Olson JJ. The role of surgery in the management of patients with diffuse low grade glioma: A systematic review and evidence-based clinical practice guideline. *J Neurooncol* (2015) 125:503–30. doi: 10.1007/s11060-015-1867-1

29. Albuquerque LAF, Almeida JP, de Macêdo Filho LJM, Joaquim AF, Duffau H. Extent of resection in diffuse low-grade gliomas and the role of tumor molecular signature-a systematic review of the literature. *Neurosurg Rev* (2021) 44:1371–89. doi: 10.1007/S10143-020-01362-8

30. Potgieser ARE, Wagemakers M, van Hulzen ALJ, de Jong BM, Hoving EW, Groen RJM. The role of diffusion tensor imaging in brain tumor surgery: A review of the literature. *Clin Neurol Neurosurg* (2014) 124:51–8. doi: 10.1016/J.CLINEURO.2014.06.009

31. Pujol S, Wells W, Pierpaoli C, Brun C, Gee J, Cheng G, et al. The DTI challenge: Toward standardized evaluation of diffusion tensor imaging tractography for neurosurgery. *J Neuroimaging* (2015) 25:875–82. doi: 10.1111/JON.12283

32. Kurian J, Pernik MN, Traylor JI, Hicks WH, el Shami M, Abdullah KG. Neurological outcomes following awake and asleep craniotomies with motor mapping for eloquent tumor resection. *Clin Neurol Neurosurg* (2022) 213:107128. doi: 10.1016/J.CLINEURO.2022.107128

33. Duffau H. Awake surgery for left posterior insular low-grade glioma through the parietorolandic operculum: The need to preserve the functional connectivity. *A Case Series. Front Surg* (2022) 8:824003/PDF. doi: 10.3389/FSURG.2021.824003/PDF

34. Duffau H. What direct electrostimulation of the brain taught us about the human connectome: A three-level model of neural disruption. *Front Hum Neurosci* (2020) 14:315. doi: 10.3389/fnhum.2020.00315

35. Rahimpour S, Haglund MM, Friedman AH, Duffau H. History of awake mapping and speech and language localization: From modules to networks. *Neurosurg Focus* (2019) 47:E4. doi: 10.3171/2019.7.FOCUS19347

36. Duffau H, Capelle L, Sichez J, Faillot T, Abdennour L, Law Koune JD, et al. Intra-operative direct electrical stimulations of the central nervous system: The salpêtrière experience with 60 patients. *Acta Neurochir (Wien)* (1999) 141:1157–67. doi: 10.1007/s007010050413

37. de Benedictis A, Moritz-Gasser S, Duffau H. Awake mapping optimizes the extent of resection for low-grade gliomas in eloquent areas. *Neurosurgery* (2010) 66 (6):1074–84. doi: 10.1227/01.NEU.0000369514.74284.78

38. Frigeri T, Paglioli E, de Oliveira E, Rhoton AL. Microsurgical anatomy of the central lobe. *J Neurosurg* (2015) 122:483–98. doi: 10.3171/2014.11.JNS14315

39. Magill ST, Han SJ, Li J, Berger MS. Resection of primary motor cortex tumors: Feasibility and surgical outcomes. *J Neurosurg* (2018) 129:961–72. doi: 10.3171/2017.5.JNS163045

40. Yang R, Bai H. Maximal safe resection of diffuse low-grade gliomas within/near motor areas using awake craniotomy with intraoperative cortical/subcortical mapping *via* direct electrical stimulation: A narrative review. *Glioma* (2020) 3:126. doi: 10.4103/glioma.glioma_14_20

41. Certo F, Baldoncini M, Bykanov A, Burdenko NN, Moiraghi A, Isolan GR. Avoiding vascular complications in insular glioma surgery. *A microsurgical Anat study Crit reflections regarding intraoperative findings* (2022) 9:906466. doi: 10.3389/fsurg.2022.906466

42. Menjot De Champfleur N, Lima Maldonado I, Moritz-Gasser S, MacHi P, le Bars E, Bonafé A, et al. Middle longitudinal fasciculus delineation within language pathways: A diffusion tensor imaging study in human. *Eur J Radiol* (2013) 82:151–7. doi: 10.1016/j.ejrad.2012.05.034

43. Duffau H. Diffuse low-grade glioma, oncological outcome and quality of life: a surgical perspective. *Curr Opin Oncol* (2018) 30:383–9. doi: 10.1097/CCO.0000000000000483

44. Pallud J, Blonski M, Mandonnet E, Audureau E, Fontaine D, Sanai N, et al. Velocity of tumor spontaneous expansion predicts long-term outcomes for diffuse low-grade gliomas. *Neuro Oncol* (2013) 15(5):595–606. doi: 10.1093/neuonc/nos331

frontiers | Frontiers in Oncology

TYPE Original Research
PUBLISHED 22 February 2023
DOI 10.3389/fonc.2023.1086118

OPEN ACCESS

EDITED BY
Songbai Xu,
First Affiliated Hospital of Jilin University, Jilin University, China

REVIEWED BY
Adrià Rofes,
University of Groningen, Netherlands
Fang Liu,
Changzhou No.2 People's Hospital, China

*CORRESPONDENCE
Liang Wang
drwangliang@126.com
Peigang Ji
doctorjipg@163.com

†These authors have contributed equally to this work

SPECIALTY SECTION
This article was submitted to Neuro-Oncology and Neurosurgical Oncology, a section of the journal Frontiers in Oncology

RECEIVED 01 November 2022
ACCEPTED 09 February 2023
PUBLISHED 22 February 2023

CITATION
Wang Y, Guo S, Wang N, Liu J, Chen F, Zhai Y, Wang Y, Jiao Y, Zhao W, Fan C, Xue Y, Gao G, Ji P and Wang L (2023) The clinical and neurocognitive functional changes with awake brain mapping for gliomas invading eloquent areas: Institutional experience and the utility of The Montreal Cognitive Assessment. *Front. Oncol.* 13:1086118. doi: 10.3389/fonc.2023.1086118

The clinical and neurocognitive functional changes with awake brain mapping for gliomas invading eloquent areas: Institutional experience and the utility of The Montreal Cognitive Assessment

Yuan Wang[1†], Shaochun Guo[1†], Na Wang[1], Jinghui Liu[1], Fan Chen[1], Yulong Zhai[1], Yue Wang[2], Yang Jiao[1], Wenjian Zhao[1], Chao Fan[1], Yanrong Xue[3,4], GuoDong Gao[1], Peigang Ji[1*] and Liang Wang[1*]

[1]Department of Neurosurgery, Tangdu Hospital, Fourth Military Medical University, Xi'an, Shaanxi, China, [2]Department of Health Statistics, Fourth Military Medical University, Xi'an, Shaanxi, China, [3]National Time Service Center, Chinese Academy of Sciences, Xi'an, Shaanxi, China, [4]School of Optoelectronics, University of Chinese Academy of Sciences, Beijing, China

Objective: Awake craniotomy with intraoperative brain functional mapping effectively reduces the potential risk of neurological deficits in patients with glioma invading the eloquent areas. However, glioma patients frequently present with impaired neurocognitive function. The present study aimed to investigate the neurocognitive and functional outcomes of glioma patients after awake brain mapping and assess the experience of a tertiary neurosurgical center in China over eight years.

Methods: This retrospective study included 80 patients who underwent awake brain mapping for gliomas invading the eloquent cortex between January 2013 and December 2021. Clinical and surgical factors, such as the extent of resection (EOR), perioperative Karnofsky Performance Score (KPS), progression-free survival (PFS), and overall survival (OS), were evaluated. We also used the Montreal Cognitive Assessment (MoCA) to assess the neurocognitive status changes.

Results: The most frequently observed location of glioma was the frontal lobe (33/80, 41.25%), whereas the tumor primarily invaded the language-related cortex (36/80, 45%). Most patients had supratotal resection (11/80, 13.75%) and total resection (45/80, 56.25%). The median PFS was 43.2 months, and the median OS was 48.9 months in our cohort. The transient (less than seven days) neurological deficit rate was 17.5%, whereas the rate of persistent deficit (lasting for three months) was 15%. At three months of follow-up, most patients (72/80, 90%) had KPS scores > 80. Meanwhile, compared to the preoperative baseline

tests, the changes in MoCA scores presented significant improvements at discharge and three months follow-up tests.

Conclusion: Awake brain mapping is a feasible and safe method for treating glioma invading the eloquent cortex, with the benefit of minimizing neurological deficits, increasing EOR, and extending survival time. The results of MoCA test indicated that brain mapping plays a critical role in preserving neurocognitive function during tumor resection.

KEYWORDS

glioma, awake brain mapping, extent of resection (EOR), Karnofsky Performance Status (KPS), neurocognitive status, Montreal Cognitive Assessment (MoCA)

Introduction

Balancing maximal tumor removal and neurological functional preservation is always a challenge for patients with glioma infiltrating the eloquent regions of the cortex. Surgical resection is considered the first-line treatment for glioma management, with the benefit of reducing tumor volume and increasing survival time (1). However, when glioma is identified in the eloquent areas, the potential risk of neurological function disturbances increases significantly (2). Therefore, awake surgery, which allows for intraoperative brain mapping of motor-sensory and language functions by directly stimulating cortical and subcortical areas, has been adopted to improve the safety of surgical interventions (3–5). Evidence has suggested that awake surgery could maximize the extent of resection (EOR) of tumors and relieve the symptoms caused by tumor mass effect, particularly in low-grade gliomas (LGG) (2, 6).

More glioma patients benefit from longer survival durations as glioma treatment regimens advance (7). However, glioma patients frequently present with impaired neurocognitive functions, such as memory, language, attention, and executive functions (7–9). Meanwhile, medical providers and patients have paid recent attention to neurological and neurocognitive status (7, 10, 11). Previous research has also indicated that neurocognitive function is an important predictor for glioma patients, providing insight into overall survival (OS), progression-free survival, and further tumor management (12, 13). Therefore, assessing the neurocognitive status is crucial for optimal surgical and oncological management.

The Montreal Cognitive Assessment (MoCA) is a brief screening tool that helps medical service providers make more informed medical decisions to assess a patient's cognitive health (14, 15). Compared to comprehensive neuropsychological assessment batteries, which are too long and sophisticated for most patients in routine care, MoCA provides a short and sensitive enough tool to detect cognitive impairment, particularly in people with brain metastases (16, 17). However, the utility and feasibility of MoCA for glioma patients receiving awake surgery have seldom been reported (10, 18, 19).

In the present study, we aimed to evaluate the experience of one tertiary neurosurgical center over eight years, performing awake brain mapping for glioma patients using direct cortical and subcortical stimulation to preserve neurological functions. We presented the clinical outcomes and evaluated the effect of awake mapping techniques on perioperative cognitive changes using MoCA tests.

Methods and materials

Patients and study design

As an observational retrospective study, we reviewed a cohort of 80 patients who underwent awake surgery with intraoperative direct electrical mapping for dominant and nondominant hemispheres. All patients were treated at Department of Neurosurgery, Tangdu Hospital, Airforce Medical University, from January 2013 to December 2021. The inclusion criteria were (1) age ≥ 18 years, (2) newly diagnosed glioma, including astrocytoma, oligodendroglioma, anaplastic oligodendroglioma, anaplastic astrocytoma, anaplastic oligoastrocytoma, and glioblastoma, based on the WHO 2007 classification. The WHO 2016 classification was applied in 2017-2019 (31 cases), and the WHO 2021 classification of glioma was applied in 2021 (18 cases). The exclusion criteria included biopsy and incomplete MRI data calculating the tumor volume.

Demographic, clinical, and histological data were collected and analyzed from patients and neurocognitive and functional outcomes. The Institutional Review Board at Tangdu Hospital approved the study (TDLL-202210-18).

Perioperative neuroradiological evaluation

Preoperative MRI imaging (T1 and T2-weighted imaging, diffusion-weighted imaging, with and without gadolinium) was performed one week before surgery. Postoperative MRI (T1 and

T2-weighted imaging) was also performed within 72 h to assess the EOR three months later and every three months after that.

The region of interest was delineated manually, and the volumetric analysis was performed according to the thickness of the scanning layer by evaluating pre- and post-operative tumor volumes. EOR was estimated by measuring volumes of perioperative T1-weighted, T2-weighted and T2-fluid-attenuated inversion recovery (T2-FLAIR) images. EOR was defined as follows: (1) supratotal resection, EOR > 100%; (2) gross total resection (GTR), EOR > 95%; (3) subtotal resection (STR), EOR = 85%-95%; and (4) partial resection (PR), EOR < 85% (1).

Preoperative and postoperative neurocognitive assessment

Basic clinical features of patients were obtained through neurological and physical examinations and Karnofsky Performance Score (KPS). KPS was the most applied tool to assess daily functional status, especially for cancer patients (20).

To minimize the test-retest effect, the Chinese version of MoCA test, including Beijing version of MoCA (MoCA-BJ) and Changsha version of MoCA (MoCA-CS), was used for neurocognitive evaluation to assess patients' cognitive health (14, 21, 22). All patients were evaluated with MoCA test at three-time points: 48 h before surgery with MoCA-BJ, discharged from the hospital with MoCA-CS, and clinic follow-up three months after surgery with MoCA-BJ. The MoCA test score ranged from 0 to 30, with a higher score indicating better cognitive function. The MoCA test consisted of seven sections: visuospatial/executive (5 points), naming (3 points), attention, concentration and working memory (6 points), language (3 points), abstraction (2 points), delayed recall (5 points), and orientation (6 points). Subjects with scores > 26 were considered cognitively normal. Scores 18-25 indicated mild cognitive impairment, 10-17 indicated moderate cognitive impairment, and < 10 indicated severe cognitive impairment.

Awake craniotomy and intraoperative mapping tasks

We adopted the asleep-awake-asleep protocol for awake craniotomy with direct brain stimulation, and tumor removal was performed on all 80 patients. After removing the bone flap, the patient was awakened, and cortical mapping was used to identify language and motor areas. The StealthStation S7 neuronavigation (Medtronic Navigation) was applied in each case to plan the surgical incision and identify tumor margins related to brain sulcal and gyral surface structures. Intraoperative ultrasound was also used to help distinguish the tumor boundaries. Before the brain shifts, numerical and letter tags were placed along the cortical tumor margins.

A biphasic current (pulse frequency 60 Hz; single pulse duration 0.5 msec) was delivered through a bipolar stimulator with a 5 mm interelectrode distance for cortical stimulation. The initial setting was 1 mA, gradually increasing the amplitude in 0.5-1 mA increments until reproducible response (motor or sensory function) was obtained or discharge potentials were detected (baseline 1 mA, maximum 8 mA). Stimulation was applied for 4 s at the indicated areas, with a pause of 2-4 s between stimulations. Cortical and subcortical regions were identified using a similar stimulation protocol.

Sensorimotor mapping was first performed to confirm the positive responses (movement and/or paresthesia). Stimulations were repeated at least three times to confirm the positive sites. A negative sensorimotor area was also indicated when no response occurred in the area of interest.

For language mapping, the patient was asked to perform three verbal tasks: counting (regular rhythm, from 1 to 10, repetitively), picture naming (DO80) and word-reading task to identify the essential cortical sites which might be inhibited by stimulation. During the picture naming task, the patient was asked to read a short phrase in Chinese as "this is a ……" before naming each picture to check whether seizures were generated and induced speech arrest if the patient could not name the picture successfully. During the word-reading task, the patient was asked to read Chinese words presented on the computer screen. The duration of each stimulation was also about 4 s. Between each actual stimulus interval, at least one picture was presented without stimulation, and no site was stimulated twice in succession. The types of language disturbances (speech arrest, dysarthria, phonetic/phonemic/semantic paraphasia, anomia, and alexia) found intraoperatively were classified by neuropsychological experts in our department.

By applying the same stimulation parameters, the glioma was removed with alternating resection and electrostimulation for subcortical functional mapping. The patient continuously performed the above tasks throughout glioma resection.

Outcome evaluation

Each patient receiving awake surgery was followed up, and the primary outcome was postoperative KPS, defined as general daily performance status three months after surgery. Secondary outcomes included OS, defined as the duration from diagnosis to death or most recent follow-up, and PFS, defined as the time from diagnosis to disease progression or the latest follow-up imaging study if no progression occurred.

Statistical analysis

One-way ANOVA with Bonferroni's multiple comparisons tests was applied to detect the changes in MoCA total scores and related subdomains. The Kaplan-Meier curves and log-rank tests were used to estimate survival curves. The significance level was set at 0.05, and all tests were performed using SPSS Statistics, Version 25.0 (IBM Corp, Armonk, NY, USA) and GraphPad Prism (version 8.0). The figures were generated by OriginPro 2021 software (OriginLab Corporation, Northampton, MA, USA).

10.3389/fonc.2023.1086118

Results

Patient demographic characteristics

The present study included 80 glioma patients (45 males and 35 females) who underwent awake surgery from January 2013 to December 2021. Table 1 summarizes the clinical and demographic information for each patient. The mean age for the awake surgery was 43.84 years (range: 19–68 years). The frontal lobe (n = 33, 41.25%), temporal lobe (n = 12, 15%) and parietal lobe (n = 12, 15%) were the most common tumor locations. Most patients (44/80, 55%) had seizures when admitted to the hospital, and generalized seizures (26/80, 32.5%) were common among them.

In our cohort, the most common type of glioma histology was WHO grade II diffuse astrocytoma (23/80, 35%). Glioblastoma (19/80, 23.75%), oligodendroglioma (14/80, 17.5%), anaplastic astrocytoma (9/80, 11.25%), and anaplastic oligodendroglioma (7/80, 8.75%) were the other major pathological types. Based on the development of WHO CNS classification, Supplementary Table 1 lists the detailed pathological diagnosis with a different version of WHO CNS classification. We summarized the tumor locations by regions in the eloquent cortex by considering the location differences and the relationship between awake surgery and functional outcome. In our case series, the glioma most invaded language-related cortex (36/80, 45%), followed by the premotor cortex (19/80, 23.75%), the primary motor cortex (14/80, 17.50%) and primary sensory cortex (11/80, 13.75%) (Table 2).

The extent of resection and outcomes

Table 2 summarizes the EOR calculated by volumetry. The mean preoperative tumor volume was 55.01 ± 67.13 mm^3 (range: 0.99–392.1 mm^3). Compared to the preoperative calculation, postoperative imaging demonstrated a mean residual tumor volume of 3.593 ± 10.82 mm^3 (range: 0–69.21 mm^3). The mean EOR measured by volume was 51.41 ± 59.57 mm^3 (range: 0.99–322.9 mm^3). According to EOR definition, 11/80 (13.75%) patients achieved supratotal resection, 45/80 (56.25%) patients achieved GTR and 13/80 (16.25%) with STR.

In our cohort, KPS ≥ 80 was considered good functional status, while KPS < 80 was considered a poor outcome. We presented the dynamic changes in KPS at three different time points: preoperative, discharging, and three months follow-ups (Supplementary Figure 1). Most patients (79/80, 98.75%) performed well on preoperative KPS. Before being discharged from the hospital, 74/80 (92.50%) patients had an excellent KPS status, and three-month follow-up KPS indicated a similar trend, with 72/80 (90%) patients having KPS scores above 80.

In our case series, the mean PFS was 43.2 months (95% CI: 16.81-69.58), and the mean OS was 48.9 months (95% CI: 23.17-74.63) in all patients (Figure 1).

Table 3 summarizes the frequency of transient (less than seven days) or persistent (lasting three months) postoperative

TABLE 1 Patient clinical characteristics and demographic features.

Parameters	Value	Percent
Age		
Mean	43.84	–
Median	43.5	–
Range	19-68	–
Sex		
Male	45	56.25%
Female	35	43.75%
Site of lesion		
Right	14	17.50%
Left	66	82.50%
Main tumor location, n (%)		
Frontal lobe	33	41.25%
Temporal lobe	12	15.00%
Parietal lobe	12	15.00%
Insular	10	12.50%
Frontal insular lobe	7	8.75%
Temporal insular lobe	5	6.25%
Frontotemporal insular lobe	1	1.25%
Seizure history, n (%)		
Yes	44	55.00%
No	36	45.00%
Seizure types, n (%)		
Focal seizures	16	20.00%
Generalized seizures	26	32.50%
Auditory/visual hallucinations	2	2.50%
WHO grade, n (%)		
WHO Grade II	43	53.75%
WHO Grade III	18	22.50%
WHO Grade IV	19	23.75%
WHO classification, n (%)		
Diffuse astrocytoma	28	35.00%
Oligodendroglioma	14	17.50%
Oligoastrocytoma	1	1.25%
Anaplastic astrocytoma	9	11.25%
Anaplastic oligodendroglioma	7	8.75%
Anaplastic oligoastrocytoma	2	2.50%
Glioblastoma	19	23.75%
Comorbidities		

(Continued)

TABLE 1 Continued

Parameters	Value	Percent
Diabetes mellitus	18	22.50%
COPD	13	16.25%
CHD/Hypertension	21	26.25%
Smoker	36	45.00%
Miscellaneous	11	13.75%

WHO, World Health Organization; COPD, chronic obstructive pulmonary disease; CHD, chronic heart diseases.
-, not applicable or none.

TABLE 2 Surgical characteristics of patients receiving awake surgery in eloquent regions.

Parameters	Value	Percent
Tumor locations, n (%)		
Primary motor cortex	14	17.50%
Primary sensory cortex	11	13.75%
Premotor cortex	19	23.75%
Language cortex	36	45.00%
Preoperative tumor volume, ml		
Mean (SD)	55.01 ± 67.13	–
Median (IQR)	34.59 (20.56-58.65)	–
Range	0.99-392.1	–
Postoperative tumor volume, ml		
Mean (SD)	3.593 ± 10.82	–
Median (IQR)	0 (0-2.48)	–
Range	0-69.21	–
Extent of resection by volume		
Mean (SD)	51.41 ± 59.57	–
Median (IQR)	31.62 (19.78-54.83)	–
Range	0.99-322.9	–
Extent of resection		
Supratotal resection	11	13.75%
Gross total resection	45	56.25%
Subtotal resection	13	16.25%
Partial resection	11	13.75%
Mapping and surgical adjuncts		
Intraoperative mapping	80	100.00%
Intraoperative ultrasound	71	88.75%
Preoperative KPS, n (%)		
100	62	77.50%
90	13	16.25%
80	4	5.00%
70	1	1.25%
Discharge KPS, n (%)		
100	60	75.00%
90	10	12.50%
80	4	5.00%
70	4	5.00%
60	2	2.50%
3-month follow-up KPS, n (%)		
100	64	80.00%
90	5	6.25%
80	3	3.75%
70	7	8.75%
60	1	1.25%

SD, Standard deviation; IQR, Interquartile range; KPS, Karnofsky Performance Score.
-, not applicable or none.

neurological deficits, such as motor or language disturbance. Due to brain plasticity after traumatic event of the surgery, we still considered the timepoint of three months after surgery follow-up was in the recovery process. During the postoperative period, 11 patients (13.75%) developed new transient speech and language-related deficits, while 3 (3.75%) presented with transient motor-related symptoms. After removing the tumor, 12 patients developed persistent deficits lasting for three months, including five (6.25%) with motor-related disturbance and seven (8.75%) with speech and language disturbance. No cases of persistent speech and language disturbance were reported among patients with tumors located in the parietal and temporal-insular lobes.

Neurocognitive status with MoCA test

We totally reviewed MoCA test scores from 79 cases, and one case lost post-op and follow-up test. Table 4 summarizes the changes and distribution of MoCA scores at the preoperative baseline test, discharge from the hospital, and three months follow-up. The total MoCA score increased significantly from baseline to 3-month follow-up (19.95 ± 1.99 vs. 26.65 ± 1.41, $p < 0.001$). At the three months follow-up visit, most patients (65/80, 81.25%) achieved normal neurocognitive status with MoCA score > 26. At a 3-month follow-up, we found no cases of moderate-to-severe cognitive impairment (MoCA < 20).

We further analyzed the subdomain score distribution for each MoCA test (Figure 2; Supplementary Table 2). With surgical intervention, we noticed that the scores of subdomains were elevated significantly for most domains in each timepoint (post-op *vs.* pre-op, 3-month follow-up *vs.* pre-op, 3-month follow-up *vs.* post-op), including visuospatial/executive, language, delayed recall,

and naming domains. For example, in the language domain, the patients demonstrated favorable recovery outcomes as evidenced by post-operative and follow-up assessments. This may be attributed to the measures employed during intraoperative surgical manipulations. However, no significant improvement was observed in the abstraction domain test.

Due to the glioma invading the eloquent area, we divided patients into the functionally related cortex, including the primary motor cortex, primary sensory cortex, premotor cortex, and language cortex (Supplementary Figure 2). In general, our findings demonstrated that MoCA scores of patients at three months follow-ups were significantly higher than the baseline MoCA scores in the present cohort. Specifically, for gliomas invading the primary motor cortex and primary sensory cortex, each domain in MoCA test indicated a significant increase from preoperative to three months test ($p < 0.001$). Whereas, for gliomas invading the premotor and language cortex, most domains in MoCA test presented similar increments at all three-time points, except for the abstraction domain. Although the scores in the domain of abstraction improved in both groups, no significant difference was observed between the preoperative and three months follow-up tests (for premotor cortex, improved score: 0.16 ± 0.69, range:-1~1, $p = 0.3306$; for language cortex, improved score: 0.00 ± 0.69, range: -1~1, $p > 0.99$). Supplementary Table 3 indicates the detailed MoCA scores and subdomain distribution stratified by glioma locations.

In this study, we applied 26 points as the cut-off value to distinguish normal and cognitive impairment cases. We did not observe severe impairment patients but with eight moderate cognitive impairment cases in pre-op tests. To further clarify the relationship between pre-op MoCA status with patients' clinical features, we established Kaplan-Meier curve and performed the survival analysis. In Supplementary Figure 3, we presented PFS and OS for normal and mild cognitive impairments. In Supplementary Figure 4, we stratified the WHO pathological categorical classification and presented the OS of each grade glioma case. However, no significant difference was observed in PFS/OS with different MoCA statuses. We also presented the dynamic changes in MoCA scores according to WHO grades (Supplementary Figure 5). Based on our current data, although WHO classification grades, including Grade II, III and IV, did not show the survival benefit by MoCA scores stratification, the rate of normal MoCA score was significantly improved, especially at 3-month follow-up test.

TABLE 3 Distribution of patients with transient and persistent neurological deficits.

Impairment	Transient deficit (%)		Persistent deficit (%)	
	No.	Percent	No.	Percent
Motor-related	5	6.25%	3	3.75%
Frontal lobe	2	2.50%	1	1.25%
Parietal lobe	–	–	2	2.50%
Insular	1	1.25%	2	2.50%
Language-related	11	13.75%	7	8.75%
Frontal lobe	3	3.75%	5	6.25%
Parietal lobe	4	5.00%	–	–
Insular	1	1.25%	2	2.50%
Tempo-insular	3	3.75%	–	–
Total	14	17.50%	12	15.00%

Transient deficits: less than seven days; persistent deficits: lasting three months.
-, not applicable or none.

Discussion

Awake brain mapping, a technique for functional preservation, has been widely adopted by neurosurgical institutions in recent years (8, 10, 23, 24). Despite advancements in intraoperative MRI, neuro-navigation systems, and intraoperative imaging techniques, intraoperative direct electrical stimulation for patients with gliomas in eloquent areas remains the gold standard for eloquent cortex localization (25). Studies have indicated that awake brain mapping could improve tumor EOR and OS and reduce the rate of persistent postoperative neurofunctional deficits (6, 26–28). We retrospectively reviewed our institutional experiences with awake surgery in this study. We applied MoCA test to assess the neurocognitive status of patients with glioma in eloquent areas. Our findings confirmed the safety and feasibility of awake surgery in treating gliomas in the eloquent cortex. The awake functional

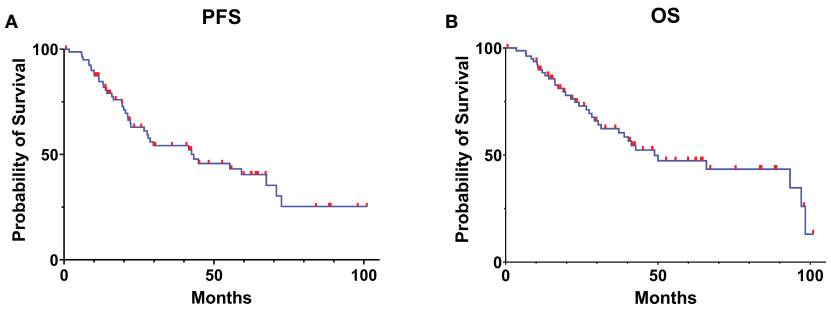

FIGURE 1
Kaplan-Meier curve estimates of progress-free survival **(A)** and overall survival **(B)** for the patients with glioma receiving awake brain mapping surgery in our cohort.

TABLE 4 Treatments and neurological deficit and general performance scores.

Parameter	Value	Percent
Postoperative adjuvant therapy		
Radiotherapy only	4	5.00%
Chemotherapy only	16	20.00%
Both radiotherapy & chemotherapy	37	46.25%
With TTF	3	3.75%
None	23	28.75%
Pre-operative MoCA score		
Mean (SD)	19.95 ± 1.99	–
Median (IQR)	20	–
Range	16-26	–
Discharging MoCA score		
Mean (SD)	21.87 ± 1.89	–
Median (IQR)	22	–
Range	18-26	–
3 months follow-up MoCA score		
Mean (SD)	26.65 ± 1.41	–
Median (IQR)	27	–
Range	23-30	–
3 months follow-up MoCA score		
Normal	65	81.25%
Abnormal	14	17.50%
Median progression-free survival, months (95% CI)	43.2	16.81-69.58
Median overall survival, months (95% CI)	48.9	23.17-74.63

TTF, Tumor treating field; MoCA, The Montreal Cognitive Assessment; SD, Standard deviation; IQR, Interquartile range; KPS, Karnofsky Performance Score; CI, Confidence interval.
-, not applicable or none.

mapping enabled favorable functional and neurocognitive outcomes with MoCA test.

Evidence suggests that EOR > 78% of the contrast-enhanced portion of glioma is an important prognostic factor (29). However, whether awake surgery can improve EOR and OS remains debatable. Gerritsen et al. demonstrated that awake surgery could improve EOR, but the treatment did not affect the patient's OS (30). Another study found comparable EOR and OS for awake surgery and general anesthesia craniotomy (31). Considering the limited number of cases from previous studies and the difference in technique application between institutions, most surgeons planned to perform the resection based on the preoperative daily status of the patient and intraoperative real-time stimulation feedback. In this study, total resection was achieved in more than half cases (45/80, 56.25%), consistent with previous studies (30, 32).

In addition, supratotal resection (11/80, 13.75%) was achieved for selected cases. Supratotal resection was still defined differently by neurosurgical oncologists. Generally, resection beyond 1-2 cm for contrast-enhanced tumors or 1-2 cm beyond the boundary in Flair images for non-enhanced tumors could be considered acceptable supratotal resection (33). Evidence indicated that supratotal resection might improve EOR and prolong the progression-free as well as OS in glioma patients (34). Our findings also suggested that awake brain mapping enabled surgeons to achieve supratotal resection with favorable neurological and clinical outcomes while preserving the neurocognitive function.

As the primary purpose of brain mapping, neurosurgeons in the operation room always prioritize minimizing the risk of postoperative neurological deficits. Previous studies reported varied morbidity rates. A meta-analysis revealed that with stimulation mapping, the early neurological deficit rate could be 47.8%, and the late neurological deficit rate could be 6.4% (27). Li et al. demonstrated that early and late deficit rates were 19.6% and 10.7%, respectively (35). In contrast, Trinh et al. reported 38% and 13%, respectively (36). This study revealed that the transient deficit rate was 17.5%, significantly lower than previous studies, while the persistent deficit was 15%, which was consistent with most studies.

Notably, language-related deficits accounted for the most significant proportion of transient and persistent morbidities (13.75% and 8.75%, respectively). Considering the similar proportion of glioma in the premotor cortex (35/80) and language cortex (36/80), the differences in morbidity rate between these two groups suggested that awake brain mapping for the language cortex required more sophisticated intraoperative monitoring and evaluation. Meanwhile, previous research indicated that awake surgery with brain mapping could reduce late severe persistent neurological deficits.

This cohort observed early transient speech and motor disturbances in 11/80 and 5/80 patients. In contrast, the late persistent speech and motor disturbance rates were 7/80 and 3/80, respectively. Most transient deficits were recovered within a few weeks after resolving tissue swelling and reducing stress responses. Consequently, awake mapping enabled tumor resection by more precisely identifying the critical structures to avoid persistent functional deficits, which significantly helped intraoperative tumor resection manipulation control (2).

Neurological performance status is a prerequisite for awake mapping (35). Several studies have found that postoperative KPS scores were significantly improved in awake craniotomy than in general anesthesia (35, 37). The preoperative baseline KPS score in the present cohort was good (KPS ≥ 80, 79/80). Most patients returned to their preoperative KPS score after the awake mapping and tumor resection. However, a small portion of cases experienced transient neurological deficits. At the three-month follow-up visit, most cases indicated an improvement in KPS between pre-and postoperative periods, corresponding to the improvement in neurological deficits.

10.3389/fonc.2023.1086118

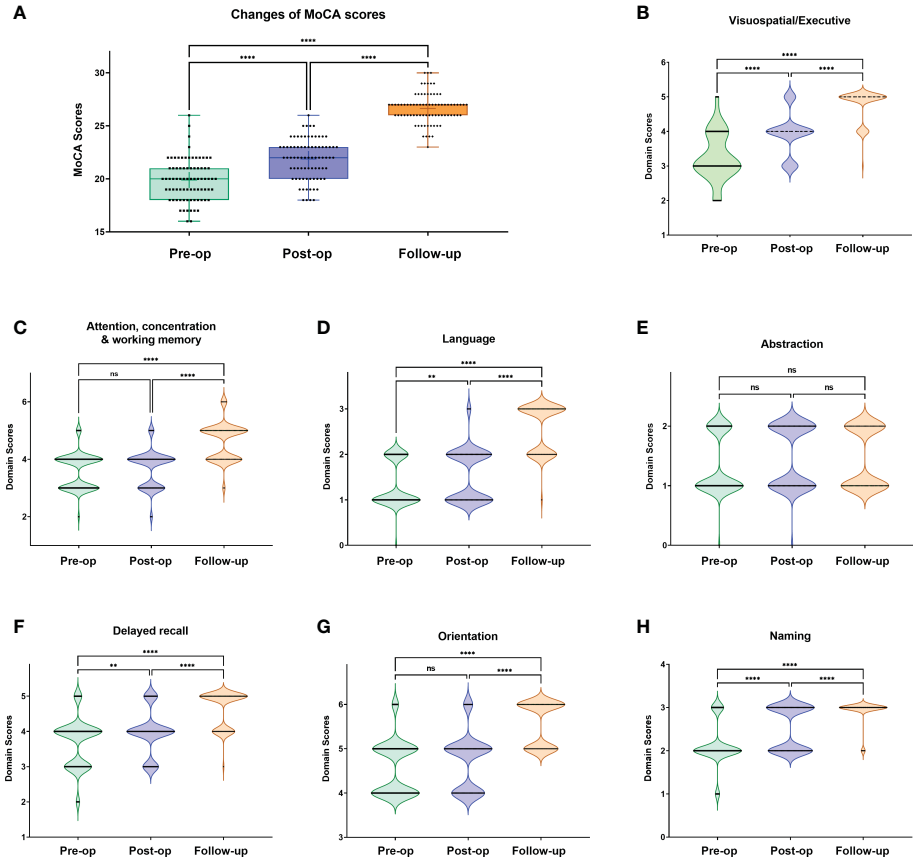

FIGURE 2
Changes of total MoCA scores **(A)** and subdomain score distribution **(B-H)** at each MoCA test timepoint. One-way ANOVA with Bonferroni's multiple comparisons tests. **: <0.001; ****:<0.0001; ns, not significant.

Although MoCA was initially designed for patients with mild cognitive impairment (MCI) and Alzheimer's disease, the evidence suggests that it is superior to Mini-Mental State Examination (MMSE) in detecting cognitive impairment in patients with brain metastases (38, 39). The sensitivity of MoCA was lower compared to a comprehensive neuropsychological battery in sensitivity to detecting cognitive deficits (40). However, due to the intrinsic nature of a comprehensive battery, the comprehensive battery administration process may take several hours, and the presence of fatigue may interfere with the patient's performance (41). In addition, the results of comprehensive battery may be affected by the professional expertise and level of experience of the evaluators, limiting the scope of its application as routine tests. Therefore, researchers tried to investigate the use of MoCA in the primary brain tumor population, especially in the setting of global COVID-19 pandemic (16, 42).

In our case series, we identified that MoCA has a surprisingly high sensitivity in neurocognitive impairments detection. The overall MoCA score improvements (preoperative baseline vs. three-month follow-up test) indicated that surgical intervention had a clinical benefit in terms of neurocognitive improvement. In this study, several patients presented with lower baseline MoCA scores (median: 20; range: 16-26; Normal: 1 case; Mild: 70 cases). When the patients were discharged from the hospital, they revealed a trend of improvement (median: 22; range: 18-26; Normal: 1 case; Mild: 79 cases), while a three-month follow-up test demonstrated a significant increase in MoCA score (median: 27; range: 23-30; Normal: 65 cases; Mild: 14 cases; Supplementary Figure 6).

Detailed analysis of MoCA domains supported the improvement of cognitive conditions in most cases. For abstraction domain, we did not observe any significant improvement during the whole hospitalization and 3-month follow-up. According to Zhang et al., the scores of memory function and abstract thinking were significantly different presented for grade III glioma patients, and their results implied that patients with IDHwt-astrocytoma/anaplastic astrocytoma are more susceptible to suffering from neurocognitive function decline than those with other subgroups of grade II and III gliomas (43). Our current data did not further support the relationship between the cognitive status of MoCA scores and the pathological classification (Supplementary Figures 3–5). More concern should be paid to this issue in future work.

Other studies suggested that KPS, age, education, and previous treatment were associated with patient MoCA outcomes and that the cutoff score appropriate for neuro-oncology establishment required further validation (16, 40). Therefore, based on our results, MoCA administration for neurocognitive monitoring was feasible and convenient for patients undergoing awake surgeries.

Since we applied MoCA tests three times during the study, it was inevitable that the test-retest effects could influence the data and results. Several factors might impact the test-retest effect, such as the number of test administrations, test speed, test form, and test-retest interval (44). Considering our current study design, an alternative of applying MoCA test with Beijing version and Changsha version could greatly minimize the retest effect. In addition, though MoCA-Beijing was applied twice, the test interval was almost more than three months. We suggest that this setting up of MoCA tests diminishes the size of retest effect, as the patients are less likely to remember the test contents.

Other new tools for language deficit assessments were reported recently. *El Hachioui et al.* reported ScreeLing application for assessing the presence and severity of aphasia and linguistic deficits 12 days after stroke (45). The ScreeLing aimed at the basic linguistic components (semantics, phonology, and syntax) and has been adopted as an important tool for assessing long-term post-stroke aphasia patients (46) (47). Currently, there is no evidence supporting ScreeLing in language function prediction for glioma patients. Language Screening Test (LAST) was another important screening tool (48), and recently its Chinese version, CLAST, has been developed and reported as an efficient and time-saving bedside aphasia screening tool for stroke patients in the acute phase (49). New evidence also implied that CLAST is suitable for Chinese post-stroke patients with high reliability, validity, sensitivity, and specificity (50). Meanwhile, in the background of Covid-19, TeleLanguage test has drawn special attention. A short telephone-based language test battery for pre- and postoperative language assessments was developed and piloted for 14 brain tumor patients. Preliminary results showed that TeleLanguage battery could provide convenient, optimized patient care and enable longitudinal clinical research (42). For MoCA tests, Jammula et al. also reported a pilot study on the feasibility and utility of telehealth and in-person clinical assessments (16). Considering the unique nature of awake surgery, it is necessary to further evaluate the patients' language status with more specific tools to better help their neurofunctional recovery process in our future work.

Limitations

The current study has several limitations. First, the pathological classification of glioma has changed several times due to the time span of the current cohort. Almost half of the cases were diagnosed using previous versions of diagnosis criteria, which correlated with the patient's prognosis. Second, due to institutional constraints, the comprehensive neurocognitive battery was not applied until 2019, which constrained us to compare the findings of other tests. Third, the test-retest effect was inevitable since MoCA test was performed three times for each patient. We managed to diminish the size of retest effect by adopting two versions of MoCA test. Especially for MoCA-BJ test, the test interval was more than three months. In addition, considering the unique nature of awake surgery, it is necessary to further evaluate the patients' cognitive status, such as language status, with more specific tools to better help their neurofunctional recovery process in our future work.

Conclusion

In conclusion, the present study investigated the role of awake functional mapping in the surgical treatment of glioma invading the eloquent cortex. The technique reduced the risk of neurological deficit while providing clinical benefits such as better KPS, increased EOR, and longer survival time. Notably, the postoperative and follow-up neurological and cognitive status on MoCA assessment was improved compared to preoperative status. Our findings demonstrated that awake functional mapping could achieve favorable neurological, neurocognitive, and functional outcomes for glioma patients.

MoCA statement

The MoCA test is a screening instrument used to facilitate the assessment of mild cognitive impairment. The MoCA copyright permission was obtained for the current research.

Data availability statement

The raw data supporting the conclusions of this article will be made available by the authors, without undue reservation.

Ethics statement

The studies involving human participants were reviewed and approved by Ethics Committee at Tangdu Hospital. Written informed consent for participation was not required for this study in accordance with the national legislation and the institutional requirements.

Author contributions

YuanW and SG wrote the main manuscript text. YuanW and LW designed the study. NW, JL, FC, YZ, YX, and CF conducted the study and collected and analyzed data. YueW, YJ, and WZ provided the service and technical support for this study. PJ and GG supervised this study. NW, LW, and YuanW prepared tables. All authors contributed to the article and approved the submitted version.

Funding

This work was supported by National Natural Science Foundation of China (81601100 and 81772661). Special thanks to Mr. Kai Yao for their contributions to the management and coordination of the study.

Conflict of interest

The authors declare that the research was conducted in the absence of any commercial or financial relationships that could be construed as a potential conflict of interest.

Publisher's note

Supplementary material

The Supplementary Material for this article can be found online at: https://www.frontiersin.org/articles/10.3389/fonc.2023.1086118/full#supplementary-material

SUPPLEMENTARY FIGURE 1
The perioperative changes of KPS for patients with gliomas receiving awake brain mapping surgery at preoperative baseline **(A)**, discharging from hospitalization **(B)** and 3 months follow-up **(C)** evaluations. KPS, Karnofsky Performance Score.

SUPPLEMENTARY FIGURE 2
The domain distribution and changes of MoCA score in perioperative period and 3 months follow-up, stratified by the glioma functional locations: total changes **(A, B)**, primary motor cortex **(C, D)**, primary sensory cortex **(E, F)**; premotor cortex **(G, H)**; language cortex **(I, J)**. MoCA, the Montreal Cognitive Assessment.

SUPPLEMENTARY FIGURE 3
Kaplan-Meier curve estimates of progress-free survival **(A)** and overall survival **(B)** for the patients with different preoperative MoCA score status.

SUPPLEMENTARY FIGURE 4
Kaplan-Meier curve of overall survival for the patients with different preoperative MoCA score status, stratified by WHO glioma grades.

SUPPLEMENTARY FIGURE 5
The dynamic changes of cumulative MoCA status by different WHO glioma grades.

SUPPLEMENTARY FIGURE 6
The Sankey diagram of the dynamic flow of neurocognitive status (normal, mild and moderate) by MoCA scores. The number indicates the cases in each MoCA test timepoint.

References

1. Li YC, Chiu HY, Lin YJ, Chen KT, Hsu PW, Huang YC, et al. The merits of awake craniotomy for glioblastoma in the left hemispheric eloquent area: One institution experience. *Clin Neurol Neurosurg* (2021) 200:106343. doi: 10.1016/j.clineuro.2020.106343

2. Motomura K, Chalise L, Ohka F, Aoki K, Tanahashi K, Hirano M, et al. Neurocognitive and functional outcomes in patients with diffuse frontal lower-grade gliomas undergoing intraoperative awake brain mapping. *J Neurosurg* (2019) 132:1683–91. doi: 10.3171/2019.3.JNS19211

3. Brown T, Shah AH, Bregy A, Shah NH, Thambuswamy M, Barbarite E, et al. Awake craniotomy for brain tumor resection: The rule rather than the exception? *J Neurosurg Anesthesiol* (2013) 25:240–7. doi: 10.1097/ANA.0b013e318290c230

4. Quinones-Hinojosa A, Ojemann SG, Sanai N, Dillon WP, Berger MS. Preoperative correlation of intraoperative cortical mapping with magnetic resonance imaging landmarks to predict localization of the broca area. *J Neurosurg* (2003) 99:311–8. doi: 10.3171/jns.2003.99.2.0311

5. Rofes A, Mandonnet E, de Aguiar V, Rapp B, Tsapkini K, Miceli G. Language processing from the perspective of electrical stimulation mapping. *Cognit Neuropsychol* (2019) 36:117–39. doi: 10.1080/02643294.2018.1485636

6. Gerritsen JKW, Arends L, Klimek M, Dirven CMF, Vincent AJE. Impact of intraoperative stimulation mapping on high-grade glioma surgery outcome: a meta-analysis. *Acta Neurochir (Wien)* (2019) 161:99–107. doi: 10.1007/s00701-018-3732-4

7. Sierpowska J, Rofes A, Dahlslatt K, Mandonnet E, Ter Laan M, Polczynska M, et al. The aftercare survey: Assessment and intervention practices after brain tumor surgery in Europe. *Neurooncol Pract* (2022) 9:328–37. doi: 10.1093/nop/npac029

8. Santini B, Talacchi A, Squintani G, Casagrande F, Capasso R, Miceli G. Cognitive outcome after awake surgery for tumors in language areas. *J Neurooncol* (2012) 108:319–26. doi: 10.1007/s11060-012-0817-4

9. Rofes A, Talacchi A, Santini B, Pinna G, Nickels L, Bastiaanse R, et al. Language in individuals with left hemisphere tumors: Is spontaneous speech analysis comparable to formal testing? *J Clin Exp Neuropsychol* (2018) 40:722–32. doi: 10.1080/13803395.2018.1426734

10. Racine CA, Li J, Molinaro AM, Butowski N, Berger MS. Neurocognitive function in newly diagnosed low-grade glioma patients undergoing surgical resection with awake mapping techniques. *Neurosurgery* (2015) 77:371–9. doi: 10.1227/NEU.0000000000000779

11. Rofes A, Mandonnet E, Godden J, Baron MH, Colle H, Darlix A, et al. Survey on current cognitive practices within the European low-grade glioma network: Towards a European assessment protocol. *Acta Neurochir (Wien)* (2017) 159:1167–78. doi: 10.1007/s00701-017-3192-2

12. Zarino B, Di Cristofori A, Fornara GA, Bertani GA, Locatelli M, Caroli M, et al. Long-term follow-up of neuropsychological functions in patients with high grade gliomas: Can cognitive status predict patient's outcome after surgery? *Acta Neurochir (Wien)* (2020) 162:803–12. doi: 10.1007/s00701-020-04230-y

13. Noll KR, Sullaway C, Ziu M, Weinberg JS, Wefel JS. Relationships between tumor grade and neurocognitive functioning in patients with glioma of the left temporal lobe prior to surgical resection. *Neuro Oncol* (2015) 17:580–7. doi: 10.1093/neuonc/nou233

14. Huang YY, Qian SX, Guan QB, Chen KL, Zhao QH, Lu JH, et al. Comparative study of two Chinese versions of Montreal cognitive assessment for screening of mild cognitive impairment. *Appl Neuropsychol Adult* (2021) 28:88–93. doi: 10.1080/23279095.2019.1602530

15. Yu J, Li J, Huang X. The Beijing version of the Montreal cognitive assessment as a brief screening tool for mild cognitive impairment: A community-based study. *BMC Psychiatry* (2012) 12:156. doi: 10.1186/1471-244X-12-156

16. Jammula V, Rogers JL, Vera E, Christ A, Leeper HE, Acquaye A, et al. The Montreal cognitive assessment (MoCA) in neuro-oncology: A pilot study of feasibility and utility in telehealth and in-person clinical assessments. *Neurooncol Pract* (2022) 9:429–40. doi: 10.1093/nop/npac038

17. Renovanz M, Reitzug L, Messing L, Scheurich A, Gruninger S, Ringel F, et al. Patient reported feasibility and acceptance of Montreal cognitive assessment (MoCA) screening pre- and postoperatively in brain tumour patients. *J Clin Neurosci* (2018) 53:79–84. doi: 10.1016/j.jocn.2018.04.034

18. Cui M, Chen H, Sun G, Liu J, Zhang M, Lin H, et al. Combined use of multimodal techniques for the resection of glioblastoma involving corpus callosum. *Acta Neurochir (Wien)* (2022) 164:689–702. doi: 10.1007/s00701-021-05008-6

19. Gao H, Bai HM, Han LX, Li TD, Wang GL, Wang WM. Brain cancer surgery in the language areas of mandarin-Cantonese bilinguals. *J Cancer Res Ther* (2015) 11:415–9. doi: 10.4103/0973-1482.151932

20. Mor V, Laliberte L, Morris JN, Wiemann M. The karnofsky performance status scale. an examination of its reliability and validity in a research setting. *Cancer* (1984) 53:2002–7. doi: 10.1002/1097-0142(19840501)53:9<2002::AID-CNCR2820530933>3.0.CO;2-W

21. Li F, Kong X, Zhu H, Xu H, Wu B, Cao Y, et al. The moderating effect of cognitive reserve on cognitive function in patients with acute ischemic stroke. *Front Aging Neurosci* (2022) 14:1011510. doi: 10.3389/fnagi.2022.1011510

22. Zhou L, Lin Z, Jiao B, Liao X, Zhou Y, Li H, et al. Consistency analysis and conversion model establishment of mini-mental state examination and montreal cognitive assessment in Chinese patients with alzheimer's disease. *Front Psychol* (2022) 13:990666. doi: 10.3389/fpsyg.2022.990666

23. Duffau H. Mapping the connectome in awake surgery for gliomas: An update. *J Neurosurg Sci* (2017) 61:612–30. doi: 10.23736/S0390-5616.17.04017-6

24. Duffau H. Brain connectomics applied to oncological neuroscience: From a traditional surgical strategy focusing on glioma topography to a meta-network approach. *Acta Neurochir (Wien)* (2021) 163:905–17. doi: 10.1007/s00701-021-04752-z

25. Gogos AJ, Young JS, Morshed RA, Hervey-Jumper SL, Berger MS. Awake glioma surgery: technical evolution and nuances. *J Neurooncol* (2020) 147:515–24. doi: 10.1007/s11060-020-03482-z

26. Chang EF, Clark A, Smith JS, Polley MY, Chang SM, Barbaro NM, et al. Functional mapping-guided resection of low-grade gliomas in eloquent areas of the brain: improvement of long-term survival. *Clin article J Neurosurg* (2011) 114:566–73. doi: 10.3171/2010.6.JNS091246

27. De Witt Hamer PC, Robles SG, Zwinderman AH, Duffau H, Berger MS. Impact of intraoperative stimulation brain mapping on glioma surgery outcome: A meta-analysis. *J Clin Oncol* (2012) 30:2559–65. doi: 10.1200/JCO.2011.38.4818

28. Lima GLO, Dezamis E, Corns R, Rigaux-Viode O, Moritz-Gasser S, Roux A, et al. Surgical resection of incidental diffuse gliomas involving eloquent brain areas. rationale, functional, epileptological and oncological outcomes. *Neurochirurgie* (2017) 63:250–8. doi: 10.1016/j.neuchi.2016.08.007

29. Sanai N, Polley MY, McDermott MW, Parsa AT, Berger MS. An extent of resection threshold for newly diagnosed glioblastomas. *J Neurosurg* (2011) 115:3–8. doi: 10.3171/2011.2.JNS10998

30. Fukui A, Muragaki Y, Saito T, Nitta M, Tsuzuki S, Asano H, et al. Impact of awake mapping on overall survival and extent of resection in patients with adult diffuse gliomas within or near eloquent areas: A retrospective propensity score-matched analysis of awake craniotomy vs. general anesthesia. *Acta Neurochir (Wien)* (2022) 164:395–404. doi: 10.1007/s00701-021-04999-6

31. Pichierri A, Bradley M, Iyer V. Intraoperative magnetic resonance imaging-guided glioma resections in awake or asleep settings and feasibility in the context of a public health system. *World Neurosurg X* (2019) 3:100022. doi: 10.1016/j.wnsx.2019.100022

32. Bloch O, Han SJ, Cha S, Sun MZ, Aghi MK, McDermott MW, et al. Impact of extent of resection for recurrent glioblastoma on overall survival: Clinical article. *J Neurosurg* (2012) 117:1032–8. doi: 10.3171/2012.9.JNS12504

33. Rakovec M, Khalafallah AM, Wei O, Day D, Sheehan JP, Sherman JH, et al. A consensus definition of supratotal resection for anatomically distinct primary glioblastoma: An AANS/CNS section on tumors survey of neurosurgical oncologists. *J Neurooncol* (2022) 159:233–42. doi: 10.1007/s11060-022-04048-x

34. Motomura K, Ohka F, Aoki K, Saito R. Supratotal resection of gliomas with awake brain mapping: Maximal tumor resection preserving motor, language, and neurocognitive functions. *Front Neurol* (2022) 13:874826. doi: 10.3389/fneur.2022.874826

35. Li YC, Chiu HY, Wei KC, Lin YJ, Chen KT, Hsu PW, et al. Using cortical function mapping by awake craniotomy dealing with the patient with recurrent glioma in the eloquent cortex. *BioMed J* (2021) 44:S48–53. doi: 10.1016/j.bj.2020.06.004

36. Trinh VT, Fahim DK, Shah K, Tummala S, McCutcheon IE, Sawaya R, et al. Subcortical injury is an independent predictor of worsening neurological deficits following awake craniotomy procedures. *Neurosurgery* (2013) 72:160–9. doi: 10.1227/NEU.0b013e31827b9a11

37. Gupta DK, Chandra PS, Ojha BK, Sharma BS, Mahapatra AK, Mehta VS. Awake craniotomy versus surgery under general anesthesia for resection of intrinsic lesions of eloquent cortex–a prospective randomised study. *Clin Neurol Neurosurg* (2007) 109:335–43. doi: 10.1016/j.clineuro.2007.01.008

38. Olson RA, Chhanabhai T, McKenzie M. Feasibility study of the Montreal cognitive assessment (MoCA) in patients with brain metastases. *Support Care Cancer* (2008) 16:1273–8. doi: 10.1007/s00520-008-0431-3

39. Olson R, Tyldesley S, Carolan H, Parkinson M, Chhanabhai T, McKenzie M. Prospective comparison of the prognostic utility of the mini mental state examination and the Montreal cognitive assessment in patients with brain metastases. *Support Care Cancer* (2011) 19:1849–55. doi: 10.1007/s00520-010-1028-1

40. Robinson GA, Biggs V, Walker DG. Cognitive screening in brain tumors: short but sensitive enough? *Front Oncol* (2015) 5:60. doi: 10.3389/fonc.2015.00060

41. Ng JCH, See AAQ, Ang TY, Tan LYR, Ang BT, King NKK. Effects of surgery on neurocognitive function in patients with glioma: A meta-analysis of immediate post-operative and long-term follow-up neurocognitive outcomes. *J Neurooncol* (2019) 141:167–82. doi: 10.1007/s11060-018-03023-9

42. De Witte E, Piai V, Kurteff G, Cai R, Marien P, Dronkers N, et al. A valid alternative for in-person language assessments in brain tumor patients: Feasibility and validity measures of the new TeleLanguage test. *Neurooncol Pract* (2019) 6:93–102. doi: 10.1093/nop/npy020

43. Zhang Z, Jin Z, Yang X, Zhang L, Zhang Y, Liu D, et al. Pre-operative neurocognitive function was more susceptible to decline in isocitrate dehydrogenase wild-type subgroups of lower-grade glioma patients. *Front Neurol* (2020) 11:591615. doi: 10.3389/fneur.2020.591615

44. Scharfen J, Jansen K, Holling H. Retest effects in working memory capacity tests: A meta-analysis. *Psychon Bull Rev* (2018) 25:2175–99. doi: 10.3758/s13423-018-1461-6

45. El Hachioui H, Sandt-Koenderman MW, Dippel DW, Koudstaal PJ, Visch-Brink EG. The ScreeLing: Occurrence of linguistic deficits in acute aphasia post-stroke. *J Rehabil Med* (2012) 44:429–35. doi: 10.2340/16501977-0955

46. Jiskoot LC, Panman JL, van Asseldonk L, Franzen S, Meeter LHH, Donker Kaat L, et al. Longitudinal cognitive biomarkers predicting symptom onset in presymptomatic frontotemporal dementia. *J Neurol* (2018) 265:1381–92. doi: 10.1007/s00415-018-8850-7

47. Nouwens F, Visch-Brink EG, El Hachioui H, Lingsma HF, van de Sandt-Koenderman M, Dippel DWJ, et al. Validation of a prediction model for long-term outcome of aphasia after stroke. *BMC Neurol* (2018) 18:170. doi: 10.1186/s12883-018-1174-5

48. Flamand-Roze C, Falissard B, Roze E, Maintigneux L, Beziz J, Chacon A, et al. Validation of a new language screening tool for patients with acute stroke: The language screening test (LAST). *Stroke* (2011) 42:1224–9. doi: 10.1161/STROKEAHA.110.609503

49. Yang H, Tian S, Flamand-Roze C, Gao L, Zhang W, Li Y, et al. A Chinese version of the language screening test (CLAST) for early-stage stroke patients. *PloS One* (2018) 13:e0196646. doi: 10.1371/journal.pone.0196646

50. Sun M, Zhan Z, Chen B, Xin J, Chen X, Yu E, et al. Development and application of a Chinese version of the language screening test (CLAST) in post-stroke patients. *Med (Baltimore)* (2020) 99:e22165. doi: 10.1097/MD.0000000000022165

frontiers | Frontiers in Oncology

TYPE Review
PUBLISHED 16 March 2023
DOI 10.3389/fonc.2023.1088484

OPEN ACCESS

EDITED BY
Zhifeng Shi,
Fudan University, China

REVIEWED BY
Hailiang Tang,
Fudan University, China
Jianping Song,
Fudan University, China

*CORRESPONDENCE
Xuan Chen
chen_xuan@jlu.edu.cn

SPECIALTY SECTION
This article was submitted to Neuro-Oncology and Neurosurgical Oncology, a section of the journal Frontiers in Oncology

RECEIVED 03 November 2022
ACCEPTED 24 February 2023
PUBLISHED 16 March 2023

CITATION
Yang Z, Zhao C, Zong S, Piao J, Zhao Y and Chen X (2023) A review on surgical treatment options in gliomas. *Front. Oncol.* 13:1088484. doi: 10.3389/fonc.2023.1088484

A review on surgical treatment options in gliomas

Zhongxi Yang[1], Chen Zhao[1], Shan Zong[2], Jianmin Piao[1], Yuhao Zhao[1] and Xuan Chen[1]*

[1]Department of Neurosurgery, The First Hospital of Jilin University, Jilin, China, [2]Department of Gynecology Oncology, The First Hospital of Jilin University, Jilin, China

Gliomas are one of the most common primary central nervous system tumors, and surgical treatment remains the principal role in the management of any grade of gliomas. In this study, based on the introduction of gliomas, we review the novel surgical techniques and technologies in support of the extent of resection to achieve long-term disease control and summarize the findings on how to keep the balance between cytoreduction and neurological morbidity from a list of literature searched. With modern neurosurgical techniques, gliomas resection can be safely performed with low morbidity and extraordinary long-term functional outcomes.

KEYWORDS

review, intraoperative techniques, extent of resection (EOR), gliomas, imaging technologies, intraoperative stimulation mapping, awake craniotomy, augmented reality high-definition fiber tractography and fluorescein

Introduction

Gliomas stem from glial cells of the central nervous system (CNS), and they are the most common primary CNS tumors. According to the 2021 World Health Organization (WHO) classification of CNS tumors, gliomas are classified as low-grade gliomas (LGGs; WHO grades I or II) and high-grade gliomas (HGGs; WHO grades III or IV). Supratentorial gliomas account for approximately 30% of all adult primary intracranial tumors, and more than 50% of these are high-grade gliomas (HGGs) (1). Several clinical features (both pathological and non-pathological) determine the grade, with pathological features including nuclear atypia, mitotic activity, vascular proliferation, necrosis, and so on, and non-pathological ones including clinical course and treatment outcome (2). Glioma is more common in whites and blacks, and the incidence of it in men is 1.5 times that in women (3).

China is one of the countries with the largest prevalence and death rates of CNS tumors (4). Overall incidence rates with adjusted age for all gliomas range from 4.67 to 5.73 per 100,000 persons (5, 6). The median overall survival (OS) times were 78.1, 37.6, and 14.4 months for low-grade gliomas, anaplastic gliomas, and glioblastomas, respectively (7). Most cases of gliomas are of sporadic onset, although some are related to Mendelian disorders such as tuberous sclerosis, neurofibromatosis type 1 or type 2, and so on (8). There are several factors that influence prognosis, including the Karnofsky Performance Status Scale at diagnosis, histology, and molecular markers. Age and tumor histology have

been identified as primary predictors of patient prognosis (9, 10). Irradiated brain or scalp in the past may increase the risk of developing gliomas (11, 12).

Gliomas have variable presenting symptoms depending on tumor size and location. A systemic review summarizes the symptom prevalence and concludes several symptoms, of which the most prevalent ones are seizures, cognitive deficits, drowsiness, and dysphagia during different phases (13). In these tumors, seizures are the most common presenting symptom since they tend to be highly epileptogenic. It is common in low- and high-grade gliomas. The risk of seizures varies between 60% and 100% among low-grade gliomas and between 40% and 60% among glioblastomas (14). Seizure control and decreasing neurocognitive deficits are the two main purposes for some of the patients diagnosed with gliomas, which they always pursue.

The principle of surgical treatment of gliomas is necessary to reduce the mass effect caused by the tumors, maximize the extent of resection, and in the meantime reduce the damage to the surrounding tissue structure, especially the gliomas located in the eloquent area, to protect neurological function. The treatment procedures are different depending on the grade of the gliomas. We will introduce LGGs, HGGs, and recurrent gliomas separately.

Low-grade gliomas

LGGs account for up to 15% of all brain tumors in adults (15). Some volumetric studies support the idea of "extent of resection" (EOR) to improve survival in patients with LGGs. These ones illustrated mean survival time variation (61.1 to 90.5 months) with maximal resection (10, 16, 17). Low-grade gliomas are the most common and uniformly fatal disease in young adults (mean age 41 years), with survival averaging approximately 7 years (18). EOR is a statistically significant predictor of overall survival. The data from these studies emphasize the importance of achieving a complete resection, cannot be overstated. LGGs have a diverse anatomical, histopathological, and molecular profile, which reflect the clinical outcome (19). In addition to affecting overall survival in LGG patients, the EOR also influences the malignant transformation rate and seizure-free status (20). A retrospective study including 153 glioma patients followed by "watch and wait" and early surgical resection, respectively, demonstrated that patients with LGGs who underwent early surgery had a higher chance of survival, which suggested that the timing of resection was crucial (21).

High-grade gliomas

For patients with primary HGGs such as glioblastoma, retrospective analysis from a randomized trial has concluded that survival and progression-free survival are highly influenced by the extent of tumor resection; the fact that incomplete resections result in more rapid neurological deterioration also attests to the importance of complete resections on progression-free survival (22–24).

One retrospective study on the comparison of "gross total" and "subtotal" resection data demonstrated that the gross total section of HGGs had a greater survival rate for 1 year follow-up, which decreased to 19% at 2 years, than subtotal resection (25). Some MRI scans of these patients diagnosed as HGGs always show a noncontrast-enhancing surrounding abnormality, so the study of the resection rate on the abnormality's surroundings remains unclear. Li reported the results that the group that underwent gross total resection of ≥53.21% of the surrounding FLAIR abnormality beyond the 100% contrast-enhancing resection was associated with a significant prolongation of survival compared with that following less extensive resection ($p < 0.001$) (26).

In the discussion of the extent and rate of resection, Sanai reported that for glioblastoma multiforme (GBM), aggressive EOR equated to improvement in overall survival, even at the highest levels of resection. A significant survival advantage was seen with as little as 78% EOR, and stepwise improvement in survival was evident even in the 95%–100% EOR range (27).

Recurrent gliomas

No matter which classification the recurrent gliomas (LGGs or HGGs) are, many patients accept repeat resection as a common treatment option to pursue a good quality of life (28). A significant benefit had been seen in 52 patients with reoperated LGGs; the principle of undergoing reoperation demonstrated an overall 10-year survival rate of 57%; variable prognostic factors such as the use of upfront radiation and pathology at recurrence influenced the overall survival rate (29). A large study on recurrent HGGs reported to date that the median overall survival duration was 19 months with a median progression-free survival following re-resection of 5.2 months, suggesting that the survival benefit of microsurgical resection did not diminish despite biological progression (30). At present, the clinical benefit of reoperation for both recurrent LGGs and HGGs demonstrates that the extent of resection can be the strongest predictor of overall survival in each individual patient.

Advances in surgical techniques and neurosurgical tools make neuro-oncology practice easier, meanwhile improving favorable outcomes and maximizing cytoreduction for patients with gliomas. Advanced neurosurgical imaging technologies, including intraoperative neuronavigation (31, 32), DTI tractography (33), intraoperative MRI (IoMRI) (34, 35), intraoperative ultrasonography (IoUS) (36, 37), fluorescence-guided surgery (38, 39), intraoperative stimulation mapping (IoSM), the awake craniotomy (AC) approach (40, 41), augmented reality high-definition fiber tractography and fluorescein (AR HDFT-F) (42, 43), intraoperative hand-held microscopy, and intraoperative mutational analysis have improved the complete radiographic resection rate of gliomas.

Neuronavigation systems

Neuronavigation systems have been widely used in the operative management of gliomas and offer lots of advantages to surgeons. Preoperatively precise planning of the craniotomy in real time and the identification of small intracranial lesions are some of

the principal benefits. In addition to the basic settings, it is also now possible to add functional MRI (fMRI) and DTI tractography information as an overlay available to the surgeon intraoperatively. fMRI does not rely on the use of radiation; it can produce images with high spatial resolution by the millimeter and poor temporal resolution because of a 5-second lag between initial neural activity and image; it can capture a clear picture of brain activity picture only if the patient stays still but not moment-to-moment brain activity. Neuronavigation can generate relationships between mass lesions and functional areas. A randomized controlled trial on the study of the effectiveness of neuronavigation demonstrated that the mean amount of residual tumor tissue was 13.8% for surgery involving neuronavigation compared with 28.9% for standard surgery, although there was no rationale for the use of neuronavigation to improve the extent of tumor resection because of the size or location of the lesion (33).

DTI tractography

DTI is utilized to plan major fibro-parcel pathways in 3D and keep away from significant white-matter packages. The imagined white-matter groups are integrated into a 3D model to limit the level of careful dreariness brought about by disturbance of significant white-matter packs.

Nevertheless, some perioperative trials about the effect of DTI neuronavigation on reducing morbidity did not show clear evidence because of tumor infiltration and edema (31, 44, 45). Given the insufficient approximation of functional sites, DTI itself cannot be used as a tool for surgical decision-making. Diffusion-weighted MRI as a novel technique is being used to overcome the previous issue of accurately mapping peritumoral edema tissue (46).

Intraoperative MRI

Intraoperative MRI (IoMRI) changes the way we deal with gliomas. IoMRI not only helps us to solve the problem of brain shift but also assists the neurosurgeon to highlight the tumor remnants and reach a higher EOR. In one prospective study including 100 adult patients operated on for gliomas using IoMRI with neuronavigation, Leroy reported that the median EOR was 100% whatever the type of glioma and location. It was only in the insula area that residue levels were higher. There was no difference between LGGs and HGGs in the median KPS at different follow-up times after surgery. “Staged volume” surgery was also introduced by him to ensure a high level of security for the surgeon and low morbidity for the patients (47). Several other nonrandomized studies also indicate that IoMRI can increase the resection rate of LGGs and HGGs, preserve neurofunction, and prolong patient survival (48–50).

Intraoperative ultrasound

Intraoperative ultrasound (IoUS) is an affordable tool that can be easily incorporated into existing infrastructure and operative workflows. IoUS has dramatically evolved with well-integrated navigation tools and improvements in image quality compared with the previous artifact-prone image quality of ultrasound (51). However, it is difficult to detect residuals below 1 cm in diameter when using IoUS (52), and the cone-shaped field of view can sometimes make it hard to see the lesion.

Fluorescence-guided surgery

Recently, intraoperative fluorescence surgery using 5-aminolevulinic acid (5-ALA) has been widely adopted (22, 53). 5-ALA as a prodrug to heme can be converted to protoporphyrin IX (PpIX), and PpIX can be accumulated preferentially in tumor cells and epithelial tissues when 5-ALA is administered through the intact blood–brain barrier (BBB) (53, 54). The properties of PpIX, which emits fluorescence of red-violet light, have been used for the detection of tumor tissues during glioma resection (38, 39).

The sensitivity of 5-ALA to gliomas has been demonstrated up to 95% in one study as a growing technology (55). Specificity for 5-ALA in predicting malignant tissues has a wide degree of variance, and in most studies it can be above 70% (56–58). The visible fluorescence varies depending on the grade of glioma, which is 95.4% in glioblastomas compared with 24.1%–26.3% in grade I and II gliomas (59). Alessandro reported the resection outcome guided by 5-ALA fluorescence: overall gross total resection of >98% was achieved in 93% of HGG patients, and the boundaries of fluorescent tissue exceeded those of tumoral tissue by neuronavigation in 43% of the patients (60).

Intraoperative 5-ALA fluorescence is ineffective at guiding LGGs because they do not produce a level of fluorescence that is visible to the naked eye (38). Hence, the approaches of intraoperative confocal microscopy have been developed and used to visualize 5-ALA-based tumor fluorescence in LGGs when exposed to resection procedures. With this microscopy, PpIX fluorescence has been detected in cellular infiltration identified at the tumor margins of WHO grade I and II gliomas (61).

Intraoperative stimulation mapping and awake craniotomy approach

Because it allows for a more precise identification of functional areas (especially in the dominant hemisphere), intraoperative stimulation (IS) mapping has emerged as the standard treatment of choice for eloquent tumors. This allows surgeons to achieve higher extents of resection (EOR) and reduce postoperative morbidity.

This technique involves electrical stimulation to depolarize a focal area of the functional cortex. An electrode precisely stimulates the focal neurons to depolarize, passes the signal within the area of interest, and causes local excitation, inhibition, or perhaps diffusion to distant areas (40). The whole procedure can be monitored by an electrophysiologist if the patient is performing a motor or language task. With the help of a bipolar probe, the neurosurgeon can perform more precise mapping.

Sometimes the nidus of gliomas is located within functional cortical areas of the brain. Neurosurgeons cannot use the classic anatomy of the central nervous system (CNS) to predict functional areas (such as language or motor sites) because of individual cortical heterogeneity (62, 63). The mass effects of gliomas can distort the topography of the brain, and the brain's plasticity can cause functional networks to be rearranged (64).

A meta-analysis of IoSM enrolled patients diagnosed with supratentorial gliomas; the result showed that the gross total resections were 75% of the patients whose resection was guided by IoSM, compared with 58% of the patients without intraoperative mapping; the IoSM did not influence the extent of the resection (65). Another meta-analysis shared similar results, especially the outcome of delayed severe deficits, which demonstrated a lower incidence (3.4%) in patients with IoSM significantly (63), and the deficits were always transient because of brain structures adjacent to the resection cavity. The use of IoSM during resection surgery reduces late, severe neurological deficits (65). The recommendation for awake craniotomy (AC) guided surgery is for gliomas affecting the dominant mid-to-posterior frontal, temporal, and mid-to-anterior parietal lobes. AC techniques can monitor more complex cognitive functions such as spatial and emotional recognition more effectively (41).

Based on some experience, the maximum duration that patients can stay conscious and complete mapping tasks is about 1 h. During this period there are several task series for IoSM, such as language tasks (the major tasks are number counting and picture naming) and non-language tasks (vision and other higher cognitive functions include calculation, working memory, and music) (66, 67). When tumors are near language or motor networks, it is recommended that direct cortical stimulation be used to help preserve function in appropriately selected patients. This often involves proceeding with an awake craniotomy, for which technical nuances and anesthesia considerations have been previously reported (68). If the gliomas are located within the area associated with severe complications, the rate of permanent complications will be about 10% with the use of AC mapping techniques (69).

A random-effects meta-analysis showed that AC (90.1%) had a higher mean EOR than general anesthesia (GA) (81.7%), which was found to be the case ($p = 0.06$). For analysis, neurological deficits were divided according to their severity and timing. Early neurological deficits, late neurological deficits, and non-severe and severe morbidity were not significantly different between patients who underwent AC and GA, respectively. The results suggested that IoSM when resecting gliomas located in the eloquent area can be carried out safely and effectively with AC (70).

Other adjunct IoSM methods

There are some other adjunct IoSM methods. Functional MRI (fMRI) mainly provides vital information regarding the location of sensory and motor pathways, but it is unable to map language sites (71). Somatosensory-evoked potential (SSEP) phase-reversal techniques can be used to identify the location of the primary sensory cortex. However, the level of SSEP is only useful for locating the primary somatosensory cortex (72).

Augmented reality high-definition fiber tractography and fluorescein

As with simulating three-dimensional virtual objects with real objects, the application of augmented reality (AR) in neurosurgery has the potential to change the way neurosurgeons plan and perform surgical procedures. The AR neuronavigation system has been used in surgical planning (73), integrating MR or CT images into the surgical field (74). López et al., in a review, illustrated that as the second most frequent use in brain tumors, AR enabled the neurosurgeon to locate the fiber tracts and guide resection (42). It can improve intraoperative safety. It facilitates and simplifies the selective anatomy of the lesion and adjacent structures, although there is no established method for precise measurement of 3D error and bias in deep injuries.

DTI high-definition fiber tractography (HDFT) has been tested as a useful tool for glioma resection planning and assessment of postoperative connectivity of the fiber tracts (43). Sodium fluorescein (F) has been used as a fluorescent dye in HGGs to increase the EOR (75). Although there is still a wide range of limitations, there are several studies about the combined utility of AR and HDFT-F. AR HDFT-F improves the neurosurgeon's intraoperative spatial location and allows for differential visualization of each tract as needed. Luzzi (1) enrolled 117 patients newly diagnosed as supratentorial HGGs, of whom 54 underwent surgery with the AR HDFT-F technique and 63 with conventional neuronavigation surgery. The results suggested that the AR HDFT-F group had a higher extent of resection and longer progression-free survival, although there was no significant difference in complication rates between the two groups. Surgery with AR HDFT-F is regarded as a safe and effective procedure for patients' neurofunction recovery. However, the present procedures involve only GA patients, and the whole process is still limited by the DTI's only supply of anatomical information (76).

There are some *other intraoperative tools* that have been described to achieve maximal tumor resection, and most of them are still in debate.

(1) Intraoperative hand-held microscopy

This is a technique in which a single optical fiber combined with miniaturized scanning and optical systems supplies high-resolution images (77). It can solve problems at the cellular level. The histological characteristics of gliomas, meningiomas, and central neurocytomas have been distinguished by intraoperative confocal microscopy to visualize fluorescein (78). Further study is needed to determine whether this technique can be used to complement resection procedures and conventional neuropathological diagnostic techniques.

(2) Intraoperative mutational analysis

The analysis can be used in real time to theoretically determine the true tumor margins. All these methods include genotyping for known

TABLE 1 Perioperative treatment options.

Timepoint	Techniques	Advantages
Preoperative	Neuronavigation systems	(1) preoperative precise planning of the craniotomy in real time and the identification of small intracranial lesions. (2) can add functional MRI and DTI tractography information intraoperatively.
Preoperative	DTI tractography	Plan major fibro-parcel pathways in 3D and keeping away from significant white-matter packages.
Intraoperative	Intraoperative MRI (IoMRI)	Solve the problem of the brain shift and increase the rate of EOR.
Intraoperative	Intraoperative ultrasound (IoUS)	The tool that can be easily incorporated into operative workflow to detect the residual above 1cm in diameter.
Intraoperative	Fluorescence-guided surgery	(1) fluorescence of red-violet light: for the detection of tumor tissues during HGGs resection. (2) intraoperative confocal microscopy with fluorescence: for LGGs.
Intraoperative	Intraoperative Stimulation Mapping (IoSM) and Awake craniotomy (AC) approach	Resect gliomas located in the eloquent area can be carried out safely and effectively.
Intraoperative	Augmented reality high-definition fiber tractography and fluorescein (AR HDFT-F)	Improve intraoperative spatial location and allow for differential visualization of each tract.
Intraoperative	Intraoperative hand-held microscopy	Solve problems at cellular resolution with a single optical fiber.
Intraoperative	Intraoperative mutational analysis	Genotyping and mass spectroscopy in real time to determine the true tumor margins.

tumor mutations using PCR-based approaches, such as isocitrate dehydrogenase 1 or 2 (IDH1/2) aberrations (79); mass spectroscopy based on defined tumor spectral profiles, which is similar to magnetic resonance spectroscopy techniques (80); All these methods need to be further tested for specificity and sensitivity in resectioning gliomas.

Conclusions

Preoperative (such as neuronavigation systems and DTI tractography) and intraoperative (including IoMRI, IoUS, fluorescence-guided surgery, IoSM and AC approaches, AR HDFT-F, intraoperative hand-held microscopy, and mutational analysis) surgical options for gliomas therapy supply a lot of choices for neurosurgeons to improve the greater extent of resections of any grade of gliomas (Table 1). The neuronavigation system is always used for preoperatively precise planning. DTI tractography can plan surgical fibro-parcel pathways, keeping away from significant white-matter packages. IoMRI can solve the intraoperative brain shift. IoUS can be easily incorporated into operations to detect residuals above 1 cm in diameter. Fluorescence-guided surgery can detect the tumors in HGGs and LGGs with confocal microscopy and fluorescence. IoSM and AC approaches can be used for gliomas located in the eloquent area. AR HDFT-F can improve intraoperative spatial location and allow for differential visualization of each tract. As the methods need to be further tested, intraoperative hand-held microscopy and mutational analysis also provide the methods for glioma resection. The development of surgical techniques has changed the principles of gliomas and characterized them as accurate, effective, and real-time to maximize tumor resection, preserve neurological function of the eloquent area near the lesion, decrease morbidity, and improve outcomes.

Author contributions

XC is the corresponding author, and he designed the content. ZY works on the analysis selected data and wrote the manuscript. CZ, SZ, JP, and YZ are responsible for collecting the papers focused on the surgical treatment of the gliomas from hundreds of papers. All authors contributed to the article and approved the submitted version.

Funding

This study was supported by Jiapeng Medical Nutrition Technology (Jilin) Co., Ltd (grant no. 3R2220793428).

Conflict of interest

The authors declare that the research was conducted in the absence of any commercial or financial relationships that could be construed as a potential conflict of interest.

Publisher's note

References

1. Luzzi S, Giotta Lucifero A, Martinelli A, Maestro MD, Savioli G, Simoncelli A, et al. Supratentorial high-grade gliomas: Maximal safe anatomical resection guided by augmented reality high-definition fiber tractography and fluorescein. *Neurosurg Focus* (2021) 51(2):E5. doi: 10.3171/2021.5.FOCUS21185

2. Louis DN, Ohgaki H, Wiestler OD, Cavenee WK, Burger PC, Jouvet A, et al. The 2007 WHO classification of tumours of the central nervous system. *Acta Neuropathol (Berl)* (2007) 114:97–109. doi: 10.1007/s00401-007-0243-4

3. Ostrom QT, Gittleman H, Stetson L, Virk SM, Barnholtz-Sloan JS. Epidemiology of gliomas. *Cancer Treat Res* (2015) 163:1–14. doi: 10.1007/978-3-319-12048-5_1

4. Chen W, Zheng R, Baade PD, Zhang S, Zeng H, Bray F, et al. Cancer statistics in China, 2015. *CA Cancer J Clin* (2016) 66:115–32. doi: 10.3322/caac.21338

5. Larjavaara S, Mantyla R, Salminen T, Haapasalo H, Raitanen J, Jääskeläinen J, et al. Incidence of gliomas by anatomic location. *Neuro Oncol* (2007) 9(3):319–25. doi: 10.1215/15228517-2007-016

6. Gousias K, Markou M, Voulgaris S, Goussia A, Voulgari P, Bai M, et al. Descriptive epidemiology of cerebral gliomas in northwest Greece and study of potential predisposing factors, 2005-2007. *Neuroepidemiology* (2009) 33(2):89–95. doi: 10.1159/000222090

7. Yang P, Wang Y, Peng X, You G, Zhang W, Yan W, et al. Management and survival rates in patients with glioma in China (2004-2010): A retrospective study from a single-institution. *J Neuro-Oncol* (2013) 113(2):259–66. doi: 10.1007/s11060-013-1103-9

8. Ostrom QT, Bauchet L, Davis FG, Deltour I, Fisher JL, Langer CE, et al. The epidemiology of glioma in adults: A "state of the science" review. *Neuro-oncol* (2014) 16:896–913. doi: 10.1093/neuonc/nou087

9. Sanai N, Chang S, Berger MS. Low-grade gliomas in adults. *J Neurosurg* (2011) 115:948–65. doi: 10.3171/2011.7.JNS101238

10. Sanai N, Berger MS. Glioma extent of resection and its impact on patient outcome. *Neurosurgery* (2008) 62:753–64. doi: 10.1227/01.neu.0000318159.21731.cf

11. Preston DL, Ron E, Yonehara S, Kobuke T, Fujii H, Kishikawa M, et al. Tumors of the nervous system and pituitary gland associated with atomic bomb radiation exposure. *J Natl Cancer Inst* (2002) 94:1555–63. doi: 10.1093/jnci/94.20.1555

12. Sadetzki S, Chetrit A, Freedman L, Stovall M, Modan B, Novikov I. Long-term follow-up for brain tumor development after childhood exposure to ionizing radiation for tinea capitis. *Radiat Res* (2005) 163:424–32. doi: 10.1667/RR3329

13. IJzerman-Korevaar M, Snijders TJ, de Graeff A, Teunissen SCCM, de Vos FYF. Prevalence of symptoms in glioma patients throughout the disease trajectory: A systematic review. *J Neurooncol* (2018) 140(3):485–96. doi: 10.1007/s11060-018-03015-9

14. Vecht CJ, Kerkhof M, Duran-Pena A. Seizure prognosis in brain tumors: new insights and evidence-based management. *Oncologist* (2014) 19(7):751–9. doi: 10.1634/theoncologist.2014-0060

15. Guthrie BL, Laws ERJr. Supratentorial low-grade gliomas. *Neurosurg Clin N Am* (1990) 1:37–48. doi: 10.1016/S1042-3680(18)30822-2

16. Hollon T, Nguyen V, Smith BW, Lewis S, Junck L, Orringer DA. Supratentorial hemispheric ependymomas: An analysis of 109 adults for survival and prognostic factors. *J Neurosurg* (2016) 8:1–9. doi: 10.3171/2015.7.JNS151187

17. Incekara F, Olubiyi O, Ozdemir A, Lee T, Rigolo L, Golby A. The value of pre- and intraoperative adjuncts on the extent of resection of hemispheric low-grade gliomas: A retrospective analysis. *J Neurol Surg A Cent Eur Neurosurg* (2016) 77(2):79–87. doi: 10.1055/s-0035-1551830

18. Claus EB, Walsh KM, Wiencke JK, Molinaro AM, Wiemels JL, Schildkraut JM, et al. Survival and low-grade glioma: The emergence of genetic information. *Neurosurg Focus* (2015) 38(1):E6. doi: 10.3171/2014.10.FOCUS12367

19. Reifenberger G, Wirsching HG, Knobbe Thomsen CB, Weller M. Advances in the molecular genetics of gliomas — implications for classification and therapy. *Nat Rev Clin Oncol* (2017) 14:434–52. doi: 10.1038/nrclinonc.2016.204

20. Xu DS, Awad AW, Mehalechko C, Wilson JR, Ashby LS, Coons SW, et al. An extent of resection threshold for seizure freedom in patients with low-grade gliomas. *J Neurosurg* (2018) 128(4):1084–90. doi: 10.3171/2016.12.JNS161682

21. Jakola AS, Myrmel KS, Kloster R, Torp SH, Lindal S, Unsgård G, et al. Comparison of a strategy favoring early surgical resection versus a strategy favoring watchful waiting in low-grade gliomas. *JAMA* (2012) 308:1881–8. doi: 10.1001/jama.2012.12807

22. Stummer W, Pichlmeier U, Meinel T, Wiestler OD, Zanella F, Reulen H-J. Fluorescence-guided surgery with 5-aminolevulinic acid for resection of malignant glioma: A randomised controlled multicentre phase III trial. *Lancet Oncol* (2006) 7:392–401. doi: 10.1016/S1470-2045(06)70665-9

23. Stummer W, Tonn JC, Mehdorn HM, Nestler U, Franz K, Goetz C, et al. Counterbalancing risks and gains from extended resections in malignant glioma surgery: A supplemental analysis from the randomized 5-aminolevulinic acid glioma resection study. *Clin Article J Neurosurg* (2011) 114:613–23. doi: 10.3171/2010.3.JNS097

24. Stummer W, Reulen HJ, Meinel T, Pichlmeier U, Schumacher W, Tonn JC, et al. Extent of resection and survival in glioblastoma multiforme: Identification of and adjustment for bias. *Neurosurgery* (2008) 62:564–76. doi: 10.1227/01.neu.0000317304.31579.17

25. Brown TJ, Brennan MC, Li M, Church EW, Brandmeir NJ, Rakszawski KL, et al. Association of the extent of resection with survival in glioblastoma: A systematic review and meta-analysis. *JAMA Oncol* (2016) 2:1460–9. doi: 10.1001/jamaoncol.2016.1373

26. Li YM, Suki D, Hess K, Sawaya R. The influence of maximum safe resection of glioblastoma on survival in 1229 patients: Can we do better than gross-total resection? *J Neurosurg* (2016) 124:977–88. doi: 10.3171/2015.5.JNS142087

27. Sanai N, Polley MY, McDermott MW, Parsa AT, Berger MS. An extent of resection threshold for newly diagnosed glioblastomas. *J Neurosurg* (2011) 115:3–8. doi: 10.3171/2011.2.JNS10998

28. Chaichana KL, Jusue-Torres I, Navarro-Ramirez R, Raza SM, Pascual-Gallego M, Ibrahim A, et al. Establishing percent resection and residual volume thresholds affecting survival and recurrence for patients with newly diagnosed intracranial glioblastoma. *Neuro Oncol* (2014) 16:113–22. doi: 10.1093/neuonc/not137

29. Ramakrishna R, Hebb A, Barber J, Rostomily R, Silbergeld D. Outcomes in reoperated low-grade gliomas. *Neurosurgery* (2015) 77:175–84. doi: 10.1227/NEU.0000000000000753

30. Oppenlander ME, Wolf AB, Snyder LA, Bina R, Wilson JR, Coons SW, et al. An extent of resection threshold for recurrent glioblastoma and its risk for neurological morbidity. *J Neurosurg* (2014) 120:846–53. doi: 10.3171/2013.12.JNS13184

31. Wu JS, et al. Clinical evaluation and follow-up outcome of diffusion tensor imaging-based functional neuronavigation: A prospective, controlled study in patients with gliomas involving pyramidal tracts. *Neurosurgery* (2007) 61:935–48. doi: 10.1227/01.neu.0000303189.80049.ab

32. Fountain DM, Bryant A, Barone DG, Waqar M, Hart MG, Bulbeck H, et al. Intraoperative imaging technology to maximise extent of resection for glioma: a network meta-analysis. *Cochrane Database Syst Rev* (2021) 1(1):CD013630. doi: 10.1002/14651858.CD013630.pub2

33. Willems PW, Taphoorn MJ, Burger H, Berkelbach van der Sprenkel JW, Tulleken CA. Effectiveness of neuronavigation in resecting solitary intracerebral contrast-enhancing tumors: A randomized controlled trial. *J Neurosurg* (2006) 104 (3):360–8. doi: 10.3171/jns.2006.104.3.360

34. Pamir MN, Ozduman K, Dinçer A, Yildiz E, Peker S, Ozek MM. First intraoperative, shared-resource, ultrahigh-field 3-Tesla magnetic resonance imaging system and its application in low-grade glioma resection. *J Neurosurg* (2010) 112:57–69. doi: 10.3171/2009.3.JNS081139

35. Matsumae M, Nishiyama J, Kuroda K. Intraoperative MR imaging during glioma resection. *Magn Reson Med Sci* (2022) 21(1):148–67. doi: 10.2463/mrms.rev.2021-0116

36. Coenen VA, Krings T, Weidemann J, Hans FJ, Reinacher P, Gilsbach JM, et al. Sequential visualization of brain and fiber tract deformation during intracranial surgery with three-dimensional ultrasound: An approach to evaluate the effect of brain shift. *Neurosurgery* (2005) 56:133–41. doi: 10.1227/01.neu.0000144315.35094.5f

37. Shi J, Zhang Y, Yao B, Sun P, Hao Y, Piao H, et al. Application of multiparametric intraoperative ultrasound in glioma surgery. *BioMed Res Int* (2021) 2021:6651726. doi: 10.1155/2021/6651726

38. Ishihara R, Katayama Y, Watanabe T, Yoshino A, Fukushima T, Sakatani K. Quantitative spectroscopic analysis of 5-aminolevulinic acid-induced protoporphyrin IX fluorescence intensity in diffusely infiltrating astrocytomas. *Neurol Med Chir* (2007) 47:53–7. doi: 10.2176/nmc.47.53

39. Zhang RR, Schroeder AB, Grudzinski JJ, Rosenthal EL, Warram JM, Pinchuk AN, et al. Beyond the margins: Real-time detection of cancer using targeted fluorophores. *Nat Rev Clin Oncol* (2017) 14:347–64. doi: 10.1038/nrclinonc.2016.212

40. Kunieda T, Yamao Y, Kikuchi T, Matsumoto R. New approach for exploring cerebral functional connectivity: Review of cortico-cortical evoked potential. *Neurol Med Chir* (2015) 55:374–82. doi: 10.2176/nmc.ra.2014-0388

41. Duffau H. Stimulation mapping of white matter tracts to study brain functional connectivity. *Nat Rev Neurol* (2015) 11:255–65. doi: 10.1038/nrneurol.2015.51

42. Contreras López WO, Navarro PA, Crispin S. Intraoperative clinical application of augmented reality in neurosurgery: A systematic review. *Clin Neurol Neurosurg* (2019) 177:6–11. doi: 10.1016/j.clineuro.2018.11.018

43. Henderson F, Abdullah KG, Verma R, Brem S. Tractography and the connectome in neurosurgical treatment of gliomas: the premise, the progress, and the potential. *Neurosurg Focus* (2020) 48(2):E6. doi: 10.3171/2019.11.FOCUS19785

44. Mickevicius NJ, Carle AB, Bluemel T, Santarriaga S, Schloemer F, Shumate D, et al. Location of brain tumor intersecting white matter tracts predicts patient prognosis. *J Neurooncol* (2015) 125:393–400. doi: 10.1007/s11060-015-1928-5

45. Nimsky C, Bauer M, Carl B. Merits and limits of tractography techniques for the uninitiated. *Adv Tech Stand Neurosurg* (2016) 43:37–60. doi: 10.1007/978-3-319-21359-0_2

46. McDonald CR, White NS, Farid N, Lai G, Kuperman JM, Bartsch H, et al. Recovery of white matter tracts in regions of peritumoral FLAIR hyperintensity with use of restriction spectrum imaging. *AJNR Am J Neuroradiol* (2013) 34:1157–63. doi: 10.3174/ajnr.A3372

47. Leroy HA, Delmaire C, Le Rhun E, Drumez E, Lejeune JP, Reyns N. High-field intraoperative MRI and glioma surgery: Results after the first 100 consecutive patients. *Acta Neurochir* (2019) 161:1467–74. doi: 10.1007/s00701-019-03920-6

48. Kuhnt D, Ganslandt O, Schlaffer SM, Buchfelder M, Nimsky C. Quantification of glioma removal by intraoperative highfield magnetic resonance imaging: An update. *Neurosurgery* (2011) 69:852–62. doi: 10.1227/NEU.0b013e318225ea6b

49. Mohammadi AM, Sullivan TB, Barnett GH, Recinos V, Angelov L, Kamian K, et al. Use of high-field intraoperative magnetic resonance imaging to enhance the extent of resection of enhancing and nonenhancing gliomas. *Neurosurgery* (2014) 74:339. doi: 10.1227/NEU.0000000000000278

50. Reins N, Leroy HA, Delmaire C, Derre B, Le-Rhun E, Lejeune JP. Intraoperative MRI for the management of brain lesions adjacent to eloquent areas. *Neurochirurgie* (2017) 63:181–8. doi: 10.1016/j.neuchi.2016.12.006

51. Dixon L, Lim A, Grech-Sollars M, Nandi D, Camp S. Intraoperative ultrasound in brain tumor surgery: A review and implementation guide. *Neurosurg Rev* (2022) 45:2503–15. doi: 10.1007/s10143-022-01778-4

52. Gerganov VM, Samii A, Akbarian A, Stieglitz L, Samii M, Fahlbusch R. Reliability of intraoperative high-resolution 2D ultrasound as an alternative to high-field strength MR imaging for tumor resection control: A prospective comparative study. *J Neurosurg* (2009) 111:512–9. doi: 10.3171/2009.2.JNS08535

53. Stummer W, Stocker S, Simon W, Herbert S, Clemens F, Claudia G, et al. Intraoperative detection of malignant gliomas by 5-aminolevulinic acid-induced porphyrin fluorescence. *Neurosurgery* (1998) 42:518–26. doi: 10.1097/00006123-199803000-00017

54. Duffner F, Ritz R, Freudenstein D, Weller M, Dietz K, Wessels J. Specific intensity imaging for glioblastoma and neural cell cultures with 5-aminolevulinic acid-derived protoporphyrin IX. *J Neurooncol* (2005) 71:107–11. doi: 10.1007/s11060-004-9603-2

55. Yamada S, Muragaki Y, Maruyama T, Komori T, Okada Y. Role of neurochemical navigation with 5-aminolevulinic acid during intraoperative MRI-guided resection of intracranial malignant gliomas. *Clin Neurol Neurosurg* (2015) 130:134–9. doi: 10.1016/j.clineuro.2015.01.005

56. Coburger J, Engelke J, Scheuerle A, Thal D, Hlavac M, Wirtz CR, et al. Tumor detection with 5-aminolevulinic acid fluorescence and Gd-DTPA–enhanced intraoperative MRI at the border of contrast-enhancing lesions: A prospective study based on histopathological assessment. *Neurosurg Focus* (2014) 36:E3. doi: 10.3171/2013.11.FOCUS13463

57. Panciani PP, Fontanella M, Garbossa D, Agnoletti A, Ducati A, Lanotte M. 5-aminolevulinic acid and neuronavigation in high-grade glioma surgery: Results of a combined approach. *Neurocirugía* (2012) 23:23–8. doi: 10.1016/j.neucir.2012.04.003

58. Roberts DW, Valdés PA, Harris BT, Fontaine KM, Hartov A, Fan X, et al. Coregistered flfluorescence-enhanced tumor resection of malignant glioma: Relationships between δ-aminolevulinic acid–induced protoporphyrin IX flfluorescence, magnetic resonance imaging enhancement, and neuropathological parameters. *J Neurosurg* (2011) 114:595–603. doi: 10.3171/2010.2.JNS091322

59. Ji SY, Kim JW, Park C-K. Experience profifiling of fluorescence-guided surgery I: Gliomas. *Brain Tumor Res Treat* (2019) 7:98–104. doi: 10.14791/btrt.2019.7.e38

60. Della Puppa A, Ciccarino P, Lombardi G, Rolma G, Cecchin D, Rossetto M. 5-aminolevulinic acid fluorescence in high grade glioma surgery: Surgical outcome, intraoperative findings, and fluorescence patterns. *BioMed Res Int* (2014) 2014:232561. doi: 10.1155/2014/232561

61. Sanai N, Snyder LA, Honea NJ, Coons SW, Eschbacher JM, Smith KA, et al. Intraoperative confocal microscopy in the visualization of 5-aminolevulinic acid fluorescence in lowgrade gliomas. *J Neurosurg* (2011) 115:740–8. doi: 10.3171/2011.6.JNS11252

62. Herholz K, Thiel A, Wienhard K, Pietrzyk U, von Stockhausen HM, Karbe H, et al. Individual functional anatomy of verb generation. *Neuroimage* (1996) 3:185–94. doi: 10.1006/nimg.1996.0020

63. Skirboll SS, Ojemann GA, Berger MS, Lettich E, Winn HR. Functional cortex and subcortical white matter located within gliomas. *Neurosurgery* (1996) 38:678–84. doi: 10.1227/00006123-199604000-00008

64. Duffau H. Brain plasticity: From pathophysiological mechanisms to therapeutic applications. *J Clin Neurosci* (2006) 13:885–97. doi: 10.1016/j.jocn.2005.11.045

65. De Witt Hamer PC, Robles GS, Zwinderman A, Duffau H, Berger MS. Impact of intraoperative stimulation brain mapping on glioma surgery outcome: A meta-analysis. *J Clin Oncol* (2012) 30:1–7. doi: 10.1200/JCO.2011.38.4818

66. Mandonnet E, Herbet G, Dufffau H. A letter: Introducing new tasks for intraoperative mapping in awake glioma surgery: Clearing the line between patient care and scientific research. *Neurosurgery* (2019) 86:E256–7. doi: 10.1093/neuros/nyz447

67. Bu L, Lu J, Zhang J, Wu J. Intraoperative cognitive mapping tasks for direct electrical stimulation in clinical and neuroscientific contexts. *Front Hum Neurosci* (2021) 15:612891. doi: 10.3389/fnhum.2021.612891

68. Hervey-Jumper SL, Li J, Lau D, Molinaro AM, Perry DW, Meng L, et al. Awake craniotomy to maximize glioma resection: methods and technical nuances over a 27-year period. *J Neurosurg* (2015) 123:325–39. doi: 10.3171/2014.10.JNS141520

69. Rolston JD, Englot DJ, Benet A, Li J, Cha S, Berger MS. Frontal operculum gliomas: Language outcome following resection. *J Neurosurg* (2015) 122:725–34. doi: 10.3171/2014.11.JNS132172

70. Suarez-Meade P, Marenco-Hillembrand L, Prevatt C, Murguia-Fuentes R, Mohamed A, Alsaeed T, et al. Awake vs. asleep motor mapping for glioma resection: A systematic review and meta-analysis. *Acta Neurochir (Wien)* (2020) 162 (7):1709–20. doi: 10.1007/s00701-020-04357-y

71. Cochereau J, Deverdun J, Herbet G, Charroud C, Boyer A, Moritz-Gasser S, et al. Comparison between resting state fMRI networks and responsive cortical stimulations in glioma patients. *Hum Brain Mapp* (2016) 37:3721–32. doi: 10.1002/hbm.23270

72. Romstock J, Fahlbusch R, Ganslandt O, Nimsky C, Strauss C. Localisation of the sensorimotor cortex during surgery for brain tumours: Feasibility and waveform patterns of somatosensory evoked potentials. *J Neurol Neurosurg Psychiatry* (2002) 72:221–9. doi: 10.1136/jnnp.72.2.221

73. Deng W, Li F, Song Z. Easy-to-use augmented reality neuronavigation using wireless tablet PC. *Stereotact Funct Neurosurg* (2014) 92:17–24. doi: 10.1159/000354816

74. Mahvash M, Tabrizi LB. A novel augmented reality system of image projection for image-guided neurosurgery. *Acta Neurochir* (2013) 155:943–7. doi: 10.1007/s00701-013-1668-2

75. Acerbi F, Broggi M, Eoli M, Anghileri E, Cavallo C, Boffano C, et al. Is fluorescein-guided technique able to help in resection of high-grade gliomas? *Neurosurg Focus* (2014) 36(2):E5. doi: 10.3171/2013.11.FOCUS13487

76. Duffau H. The dangers of magnetic resonance imaging diffusion tensor tractography in brain surgery. *World Neurosurg* (2014) 81(1):56–8. doi: 10.1016/j.wneu.2013.01.116

77. Sanai N, Eschbacher J, Hattendorf G, Coons SW, Preul MC, Smith KA, et al. Intraoperative confocal microscopy for brain tumors: A feasibility analysis in humans. *Neurosurgery* (2011) 68:282–90. doi: 10.1227/NEU.0b013e318212464e

78. Kubben PL, ter Meulen KJ, Schijns OE, ter Laak-Poort MP, van Overbeeke JJ, van Santbrink H. Intraoperative MRI-guided resection of glioblastoma multiforme: A systematic review. *Lancet Oncol* (2011) 12:1062–70. doi: 10.1016/S1470-2045(11)70130-9

79. Kanamori M, Kikuchi A, Watanabe M, Shibahara I, Saito R, Yamashita Y, et al. Rapid and sensitive intraoperative detection of mutations in the isocitrate dehydrogenase 1 and 2 genes during surgery for glioma. *J Neurosurg* (2014) 120:1288–97. doi: 10.3171/2014.3.JNS131505

80. Eberlin LS, Norton I, Orringer D, Dunn IF, Liu X, Ide JL, et al. Ambient mass spectrometry for the intraoperative molecular diagnosis of human brain tumors. *Proc Natl Acad Sci USA* (2013) 110:1611–6. doi: 10.1073/pnas.1215687110

frontiers | Frontiers in Oncology

TYPE Original Research
PUBLISHED 24 March 2023
DOI 10.3389/fonc.2023.1089923

OPEN ACCESS

EDITED BY
Yan Qu,
Air Force Military Medical University, China

REVIEWED BY
Laura Mancini,
University College London Hospitals NHS Foundation Trust, United Kingdom
Haining Zhen,
Fourth Military Medical University, China

*CORRESPONDENCE
Ching-Po Lin
chingpolin@gmail.com
Jianping Song
neurosurgerysong@foxmail.com

†These authors have contributed equally to this work

SPECIALTY SECTION
This article was submitted to Neuro-Oncology and Neurosurgical Oncology, a section of the journal Frontiers in Oncology

RECEIVED 04 November 2022
ACCEPTED 03 March 2023
PUBLISHED 24 March 2023

CITATION
Yuan Y, Qiu T, Chong ST, Hsu SP-C, Chu Y-H, Hsu Y-C, Xu G, Ko Y-T, Kuo K-T, Yang Z, Zhu W, Lin C-P and Song J (2023) Automatic bundle-specific white matter fiber tracking tool using diffusion tensor imaging data: A pilot trial in the application of language-related glioma resection. *Front. Oncol.* 13:1089923. doi: 10.3389/fonc.2023.1089923

Automatic bundle-specific white matter fiber tracking tool using diffusion tensor imaging data: A pilot trial in the application of language-related glioma resection

Yifan Yuan[1,2,3,4,5,6†], Tianming Qiu[1,2,3,4,5,6†], Shin Tai Chong[7†], Sanford Pin-Chuan Hsu[8], Ying-Hua Chu[9], Yi-Cheng Hsu[9], Geng Xu[1,2,3,4,5,6], Yu-Ting Ko[7], Kuan-Tsen Kuo[7], Zixiao Yang[1,2,3,4,5,6], Wei Zhu[1,2,3,4,5,6], Ching-Po Lin[7*] and Jianping Song[1,2,3,4,5,6,10*]

[1]Department of Neurosurgery, Huashan Hospital, Shanghai Medical College, Fudan University, Shanghai, China, [2]National Center for Neurological Disorders, Shanghai, China, [3]Neurosurgical Institute of Fudan University, Shanghai, China, [4]Shanghai Clinical Medical Center of Neurosurgery, Shanghai, China, [5]Shanghai Key Laboratory of Brain Function Restoration and Neural Regeneration, Shanghai, China, [6]Research Units of New Technologies of Micro-Endoscopy Combination in Skull Base Surgery, Chinese Academy of Medical Sciences (CAMS), Shanghai, China, [7]Institute of Neuroscience, National Yang Ming Chiao Tung University, Hsinchu, Taiwan, [8]Department of Neurosurgery, Neurological Institute, Taipei Veterans General Hospital, Taipei, Taiwan, [9]Magnetic Resonance (MR) Collaboration, Siemens Healthineers Ltd., Shanghai, China, [10]Department of Neurosurgery, National Regional Medical Center, Fudan University Huashan Hospital, Fuzhou, Fujian, China

Cerebral neoplasms like gliomas may cause intracranial pressure increasing, neural tract deviation, infiltration, or destruction in peritumoral areas, leading to neuro-functional deficits. Novel tracking technology, such as DTI, can objectively reveal and visualize three-dimensional white matter trajectories; in combination with intraoperative navigation, it can help achieve maximum resection whilst minimizing neurological deficit. Since the reconstruction of DTI raw data largely relies on the technical engineering and anatomical experience of the operator; it is time-consuming and prone to operator-induced bias. Here, we develop new user-friendly software to automatically segment and reconstruct functionally active areas to facilitate precise surgery. In this pilot trial, we used an in-house developed software (DiffusionGo) specially designed for neurosurgeons, which integrated a reliable diffusion-weighted image (DWI) preprocessing pipeline that embedded several functionalities from software packages of FSL, MRtrix3, and ANTs. The preprocessing pipeline is as follows: 1. DWI denoising, 2. Gibbs-ringing removing, 3. Susceptibility distortion correction (process if opposite polarity data were acquired), 4. Eddy current and motion correction, and 5. Bias correction. Then, this fully automatic multiple assigned criteria algorithms for fiber tracking were used to achieve easy modeling and assist precision surgery. We demonstrated the application with three language-related cases in three different centers, including a left frontal, a left temporal, and a left frontal-temporal glioma, to achieve a favorable surgical

outcome with language function preservation or recovery. The DTI tracking result using DiffusionGo showed robust consistency with direct cortical stimulation (DCS) finding. We believe that this fully automatic processing pipeline provides the neurosurgeon with a solution that may reduce time costs and operating errors and improve care quality and surgical procedure quality across different neurosurgical centers.

KEYWORDS

awake neurosurgery, brain mapping, diffusion tensor imaging, functional neuroimaging, white matter tracts fiber tracking software for neurosurgeon

1 Introduction

Glioma is the most common malignant intradural tumor, with a new incidence of about 4 per 100,000 people worldwide every year (1). Surgery is the first-line treatment for debulking tumors and obtaining tissues for pathology analysis. It has widely been agreed that the extent of tumor removal is positively correlated with patient survival and that residues surrounding the tumor margin always lead to early recurrence (2, 3). However, glioma grows infiltratively along fiber tracts, making it difficult to determine the tumor boundary only according to surgeons' experiences. Extended resection may impair eloquent brain areas and cause functional disorders such as hemiplegia and aphasia. Therefore, precise tracing of tumor boundary is the key to balancing the survival and quality of life of glioma patients (4).

Diffusion tensor imaging (DTI) is a noninvasive technique that can probe the molecular diffusivity of water within the white matter to reflect the intravoxel architecture by measuring the water self-diffusion tensor (5, 6). Linking the anisotropic orientation determined by the principal eigenvector of the tensor has been widely applied to map neuronal tracts (7, 8). This method has been used to reveal and visualize three-dimensional white matter trajectories and provides crucial information to neurosurgeons for neurosurgical planning and navigation (9, 10). Thus, DTI tractography has been considered routine for many neurosurgical procedures.

Many imaging techniques and surgical adjuncts, such as integrated neuro-navigation with DTI or blood oxygen level-dependent functional magnetic resonance imaging (BOLD-fMRI), have been developed to delineate the tumor margin and protect eloquent areas to avoid increasing postoperative deficits during aggressive tumor resection (11). Currently, these techniques are routinely applied in many neurosurgical procedures for cortical eloquence and white matter assessment. However, the complexity of imaging processing will increase the clinical burden, and insufficient experience in imaging processing in some clinical centers may misguide the surgical procedure, leading to consequent complications. Therefore, a simple, automatic, less time-consuming, high-accuracy imaging processing and easy-to use software is needed to reduce the clinical burden for the neurosurgeon and narrow the gap between different clinical centers.

Imaging quality and preprocessing procedures are crucial to obtain robust and reliable tractography for neurosurgery. Despite having a few helpful workstations provided by the magnetic resonance imaging (MRI) machine vendors and powerful software (such as MRtrix3, FSL, DSI-studio, 3D-Slicer, etc.) used for reconstructing neural tractography, complicated processing procedures, and reconstructing reliability have hindered its clinical applications, especially for neurosurgery (12). A well-trained technician or surgeon must integrate different software programs for surgical planning based on prior anatomical knowledge, which is time-consuming and prone to operator-induced bias (13). Thus, an automatic imaging processing pipeline and fiber tractography segmentation tool are necessary.

Here, we develop an in-house software, "DiffusionGo" that integrates a fully automatic preprocessing pipeline for diffusion MRI data and a boosted tractography algorithm to achieve efficient and reliable modeling. In this pilot trial, the surgical plan of three language-related cases from multicenter, including one left frontal-temporal-insular glioma, one left temporal glioma, and one left frontal-insular glioma, was reconstructed by DiffusionGo, and favorable surgical outcomes with language function preservation was achieved.

2 Materials and methods

2.1 Study design and patient recruitment

This was a multicenter, observational, prospective pilot trial. We report three patients with preoperatively imaging-diagnosed gliomas who underwent surgical resection at Huashan Hospital (Shanghai, China), Taipei Veterans General Hospital (Taipei, Taiwan), and the First Affiliated Hospital of Fujian Medical University (Fujian, China) between December 2020 and March 2022. We collected clinical, imaging, treatment, and outcome data. This study was approved by the local Hospital Ethics Committee (Approval No. KY2021-452 and KY2019-008) and was conducted under the Declaration of Helsinki. All patients were verbally informed, and the signature of a specific informed consent was obtained.

2.2 Imaging acquisition

As a pilot trial, three typical cases from three different centers, respectively, with completed MRI and clinical assessment, were described here. The MRI images of the first case were acquired on a 3.0 Tesla MRI scanner (Magnetom Verio; Siemens, Erlangen, Germany) with a 12-channel head coil at Huashan Hospital, Shanghai, China, including high-resolution three-dimensional T1-weighted images (T1WI, TR = 1630 ms; TE = 2.9 ms; flip angle = 9°; field of view (FOV) = 172 x 250 x 176 mm^3; voxel size = 1 x 1 x 1 mm^3), diffusion-weighted images (DWI, TR = 6500 ms; TE = 95 ms; FOV = 220 x 220 x 140 mm^3; voxel size = 2 x 2 x 2 mm^3, 30 directions of b value = 1000 s/mm^2; average = 2).

The MRI images of the second case were acquired on a 3.0 Tesla MRI scanner (Siemens Magnetom Tim Trio, Erlangen, Germany) at National Yang Ming Chiao Tung University, Taipei, Taiwan, using a 12-channel head array coil. High-resolution T1W images were acquired using a 3D magnetization-prepared rapid gradient echo sequence (MPRAGE, TR/TE = 2530/3.5 ms; TI = 1100 ms; FOV = 256 mm; voxel size = 1 x1 x 1 mm^3; flip angle = 7°) for image segmentation, registration, and brain mask extraction. Multishelled, multiband DWIs were acquired using a single-shot spin-echo planar imaging sequence (monopolar scheme; TR = 3525 ms; TE = 109.2 ms; FOV = 240 x 240 x 144 mm^3; voxel size: 2 × 2 × 2 mm^3; multiband factor = 3; phase encoding: anterior to posterior) with two b-values of 1000 s/mm^2 (30 diffusion directions) and 3000 s/mm^2 (60 diffusion directions), in which b0 images were interleaved in every six volumes. Data with the same DWI protocol using an opposite polarity (phase encoding from posterior to anterior) were also acquired for three B_0 images.

The MRI images of the third case were acquired on a 3.0 Tesla MRI scanner (Siemens Magnetom Prisma, Erlangen, Germany) at the First Affiliated Hospital of Fujian Medical University, Fuzhou, Fujian, China, using a 64-channel head array coil. High-resolution T1W images with a 3D MPRAGE sequence (TR/TE = 2300/2.32 ms; TI = 946 ms; FOV = 240 mm; voxel size = 0.94 x0.94 x 0.90 mm^3; flip angle = 8) and DWI with a single shot spin-echo planar imaging sequence (monopolar scheme; TR = 3700 ms; TE = 92 ms; FOV = 220 x 220 x 130 mm^3; voxel size: 1.72 × 1.72 × 5.2 mm^3 with 20 diffusion directions and b-values of 1000 s/mm^2) were acquired.

2.3 Automatic bundle-specific neuro-fiber tractography by DiffusionGo

DiffusionGo integrates a reliable preprocessing pipeline with a fully automatic multiple assigned criteria algorithm for bundle-specific tractography using DTI data based on anatomical connectivity (14). First, structural (typo) images were coregistered with DWI by using Advanced Normalization Tools (ANTs, http://stnava.github.io/ANTs/). All DWIs underwent diffusion preprocessing pipeline and DTI model fitting with MRtrix3 (https://www.mrtrix.org) (15) and FSL (https://fsl.fmrib.ox.ac.uk/fsl/fslwiki) (16): 1. DWI denoising (17–19), 2. Gibbs-ringing removing (20), 3. Susceptibility distortion correction (process if opposite polarity data were acquired), 4. Eddy current and motion correction (21), 5. Bias correction (22), and 6. DTI fitting. A patent-protected multiple assigned criteria (MAC) algorithm (14) for fiber tracking was used. The motor pathway (corticospinal tract, CST), language pathway (arcuate fasciculus, AF, superior longitudinal fasciculus, SLF, frontal aslant tract, FAT, inferior longitudinal fasciculus, ILF, inferior fronto-occipital fasciculus, IFOF, and uncinate fasciculus, UF), and visual pathway (optic radiation, OR) were segmented automatically. The potential false-positive tracts were identified and manually removed by experiences neurosurgeon. The workflow is demonstrated in Figure 1. Validation results for the DiffusionGo automatic fiber tractography are summarised in the Supplementary Material.

2.4 Three-dimensional visualization

The cortical surface was reconstructed by FreeSurfer (version 7.1, https://surfer.nmr.mgh.harvard.edu) (23) and integrated into DiffusionGo with DTI tractography to build 3D model visualization.

3 Case study

Here, three exemplary cases from three different neurosurgical centers were demonstrated respectively. The first case was a 42-year-old woman with left frontal-temporal-insular lobe astrocytoma in Huashan Hospital. The lesion was about 79mm in diameter with high signal in T2 and not enhanced after contrast; and had a close relationship to the speech output language area with high surgical risk. Considering the tumor might not be highly aggressive and malignant and was more sensitive to subsequent radiotherapy and chemotherapy, we focused more on functional protection to maintain a relatively high living quality for the patient. DTI fiber tractography and conventional MRI sequences were integrated with DiffusionGo for surgical planning (Figure 2). Multimodality-guided awake surgery under electrophysiology monitoring for language function mapping and preservation was used. Speech arrest was defined as discontinuing number counting without simultaneous motor response by direct cortical stimulation (DCS). In the language mapping phase, we found that the eloquent area of speech arrest was located in the classical Broca's area as the terminal territory of our reconstructed AF. The surgery was conducted under awake surgery, and the tumor subtotally resected. There was no language dysfunction during the whole procedure. The patients was finally diagnosed as astrocytoma, WHO grade 2, IDH mutant. For this case, the automatic algorithm was used to reconstruct the AF and SLF-II, which were considered the major white matter tracts adjacent to the lesion.

The second case was diagnosed and treated at Taipei Veterans General Hospital. This 41-year-old woman suffered from intermittent headaches, which progressed gradually. In addition, she could not write or read words that she knew. Ignoring the objects on her right side was also noted. She went to the clinic, and MRI of the brain showed a heterogeneous mass, 55 mm in diameter,

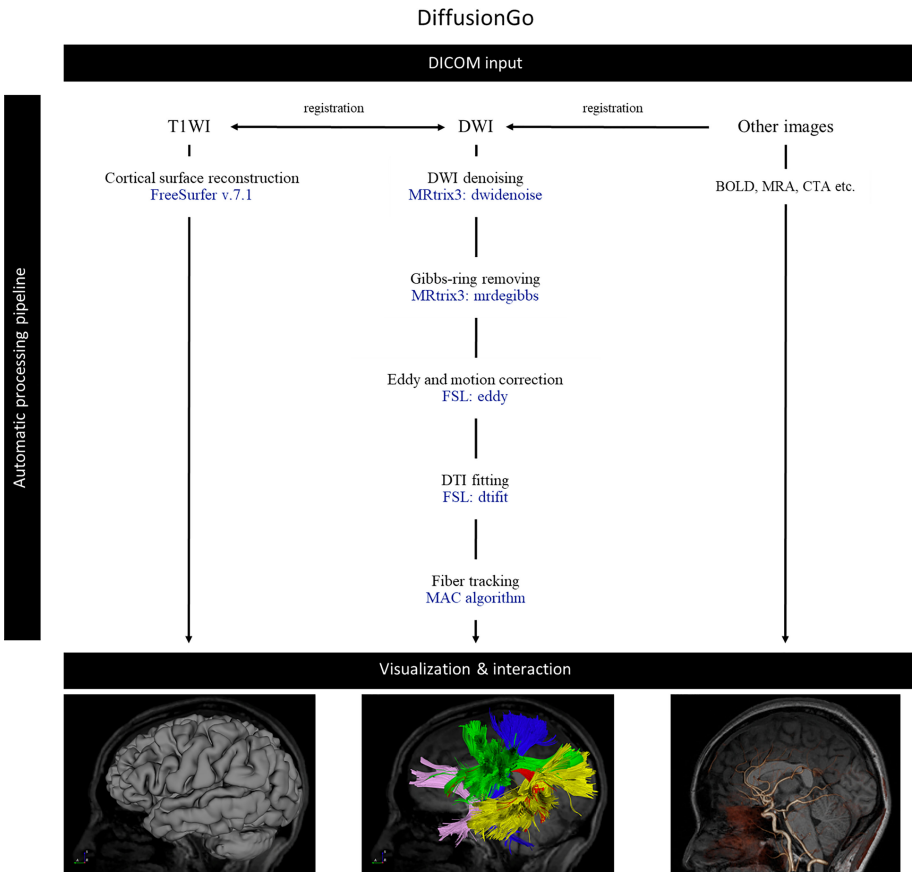

FIGURE 1
The automatic pipeline of DiffusionGo. MAC, multiple assigned criteria; DICOM, digital imaging and communications in medicine; DSA, digital subtraction angiography; DWI, diffusion weighted image; DTI, diffusion tensor imaging; BOLD, blood oxygen level-dependent.

over the left temporal lobe with mild perifocal edema. DTI fiber tractography of the language-related pathways (AF, and SLF-II) was reconstructed and displayed in DiffusionGo. Superior displacement of the left Wernicke's area was identified with intact AF projecting to the left premotor and left Broca areas (Figure 3). After a complete survey, since the patient could not endure an awake surgery, tumor removal was performed under general anesthesia without any neurological deficits postoperatively. MRI of the brain revealed total gross removal without residual tumor. Unfortunately, glioblastoma was diagnosed.

The third case was recently conducted at the First Affiliated Hospital of Fujian Medical University. This 41-year-old female suffered from recurrent seizures attack for 4 years. Conventional MR indicates a left frontal-insular lesion of 3.8 cm, with high signal in T2WI and not enhanced after contrast. Preoperative DTI showed the AF and SLF were located below and behind the tumor, respectively (Figure 4). Considering the close relationship between the lesion and Broca's region, multimodality-guided awake surgery under electrophysiology monitoring for language function mapping and preservation was conducted. After craniotomy, in the language mapping phase using DCS, we found that the eloquent area of speech arrest was located in the terminal territory of our reconstructed AF and SLF. The surgery was conducted under awake surgery. Since there was no clear boundary between the tumor and the eloquent area and SLF behind the tumor, a subtotal resection of tumor was achieved. There was no language dysfunction during the whole procedure. The pathology showed anaplastic astrocytoma, and the patient was discharged for adjuvant radiotherapy.

4 Discussion

Sensorimotor and language eloquence are considered higher brain function, and even mild impairment causes poor outcomes (24). Unlike the sensorimotor area, the eloquent language area is more diverse, and currently, researchers have revealed that it is quite different from classical canonical classification (25, 26). Classic language eloquent models posited that motor and sensory language cortex existed in Broca's area (including pars triangularis and pars opercularis) and Wernicke's area, respectively (26). However, cortical maps generated with intraoperative direct cortical stimulation (DCS) data revealed extraordinary variability in language localization in the dominant hemisphere, and the eloquent language areas are quite different from the classical canonical models (27). The expression tasks are best mapped in the frontal lobe, with 100% of sensitivity and 66% of specificity with a 5-mm resolution (28). Tate et al. found that speech arrest regions

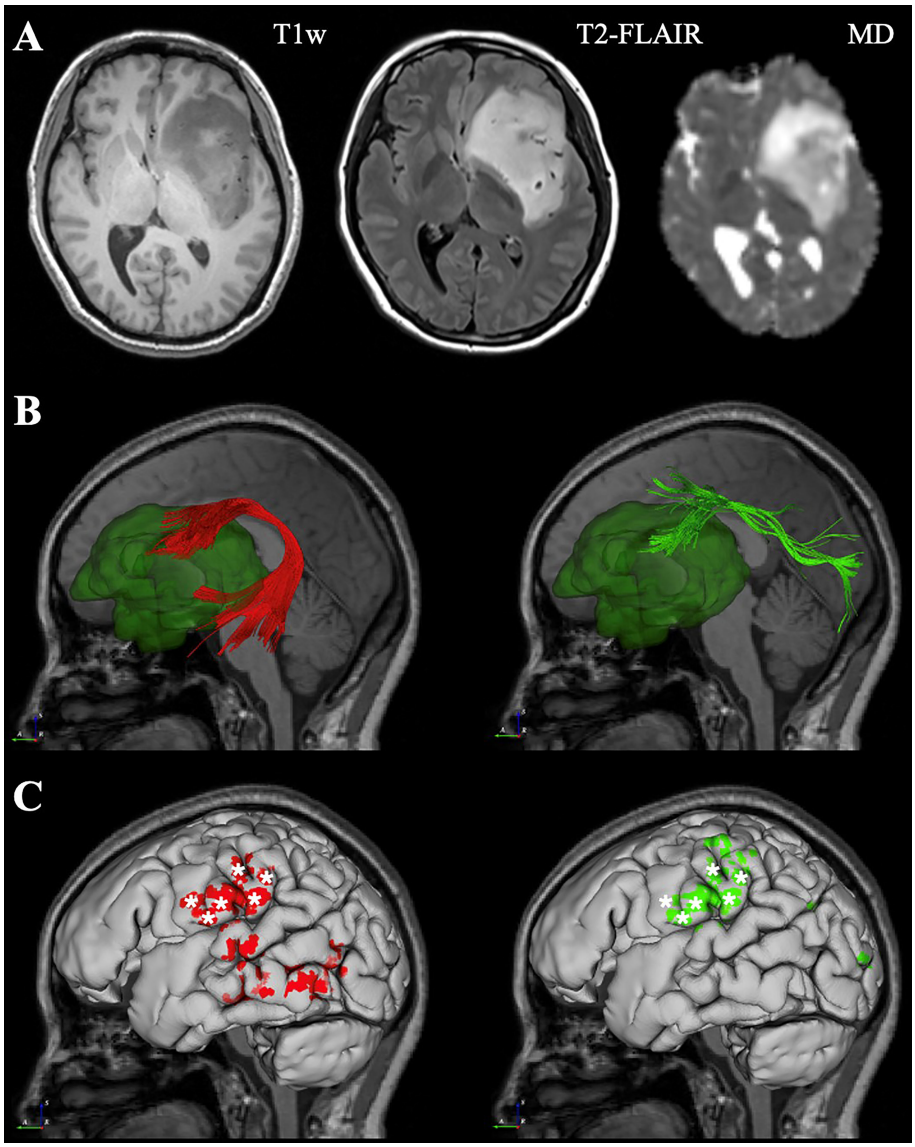

FIGURE 2
Representive imaging of a patient with left frontal-temporal lobe astrocytoma. Case 1, a 42-year-old woman with left frontal-temporal lobe astrocytoma (WHO grade II) in MR images **(A)**. The relationship between language-related fiber tracts (AF in red and SLF-II in green color) and tumor (dark green color) were shown in **(B)**. The cortical termination of each tract was projected on the cortical surface **(C)**. The eloquent area of intro-operative speech arrest (DCS) was marked with stars. (MD, Mean Diffusivity).

(or the speech output region) seemed to be localized in the ventral premotor cortex rather than the classical Broca's area (29). According to Wu et al. study, most Chinese speech arrest areas were located at specific language production sites, which 50% positive sites in the ventral precentral gyrus, 28% in the pars opercularis and pars triangularis. Additionally, the left middle frontal gyrus (Brodmann's areas 6/9) was found to be unique for Chinese production. Moreover, Chinese speakers' inferior ventral precentral gyrus (Brodmann's area 6) was used more often than English speakers (30). Therefore, the combinational speech arrest map can be divided into four clusters: Cluster 1 was mainly located in the ventral precentral gyrus and the pars opercularis, which contained the peak of speech arrest in the ventral precentral gyrus; Cluster 2 was in the ventral and dorsal precentral gyrus; Cluster 3 was in the supplementary motor area; Cluster 4 was in the posterior superior temporal gyrus and supramarginal gyrus (31).

The white matter tracts transmit information between different cortical regions, and their connectivity enables the central nervous system to function normally. Hence, the idea of "eloquent areas" should be expanded to include deep structures rather than a purely cortical concept. BOLD-fMRI and DTI tractography have been routinely applied in many neurosurgical procedures for cortical eloquence and white matter assessment.

However, conventional DTI tractography methods rely on the technician to manually select the region of interest based on prior knowledge of anatomy, then generate the fibers from there, then clean

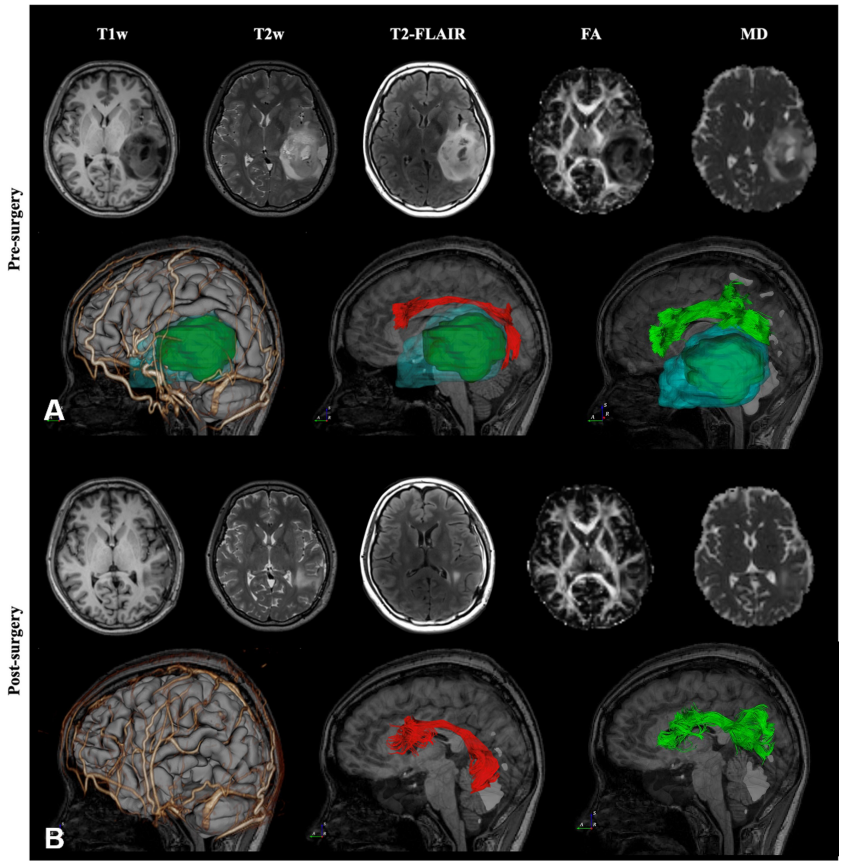

FIGURE 3
Preoperative and post-operative imaging of a patient with left temporal lobe astrocytoma. Case 2, A 41-year-old woman with temporal lobe glioblastoma over the left temporal lobe with mild perifocal edema was reconstructed and displayed in DiffusionGo **(A)**. The AF (red) and SLF-II (green) were automatically reconstructed and integrated with the cortical surface (gray), arteries and veins (gold), tumor (dark green), and peritumoral edema (light blue with translucent). Superior displacement of the left Wernicke's area was identified with intact AF projecting to the left premotor and left Broca's areas. After a complete survey, since the patient could not endure an awake surgery, tumor removal was performed under general anesthesia without any neurological deficits postoperatively. Two months later, MRI of the brain revealed total gross removal without residual tumor, and DTI showed preservation of the AF (red) and SLF-II (green) **(B)**. (FA, Fractional Anisotropy).

and refine the bundle obtained. This approach is time-consuming, prone to operator-induced deviation, and without any "gold standard" (32). Therefore, the training of a specialized technician does need a learning curve. Unfortunately, most hospitals in China do not even provide this technician position due to the huge inequalty of medical resources among different neurosurgery centers (33). Although there are several automatic algorithms for whole-brain tractography, tracts derived from these algorithms can deviate significantly from each other, making it difficult to identify the most accurate one (12). A feasible automatic bundle-specific neurofiber tractography algorithm is not yet available.

Given this, we have developed an automatic bundle-specific white matter fiber tracking tool (DiffusionGo) with a fully automatic multiple assigned criteria (MAC) algorithm for bundle-specific neurofiber reconstruction (14) to achieve multimodality modeling and visualization for precision surgical planning with minimal human processing error. Previous bundle-specific tractography studies mostly used manually tractography but faced significant challenges in identifying accurate tracts, especially in cases with apparent lesion effects for neurosurgical implementation (34–36). In contrast, DiffusionGo was developed based on anatomical connectivity from clinical and autopsy data.

Modern neuroscience research has revealed a dorsal language pathway (arcuate fasciculus, AF, and superior longitudinal fasciculus II, SLF-II) using DTI tractography responsible for verbal repetition by integrating sensory-motor information. The SLF/AF system is the most comprehensive association fiber system at the lateral surface, connecting the frontal, temporal, parietal, and occipital lobes. AF was considered to connect the classic Broca's area and Wernicke's area. Specifically, the SLF connects the frontal and parietal lobes, allowing communication between the dorsal premotor and prefrontal cortices to the angular gyrus. The SLF also contains frontal-to-parietal connections terminating within the supramarginal gyrus (26).

In these three cases, both AF and SLF were automatically generated using DiffusionGo. In Case 1, the actual speech arrest

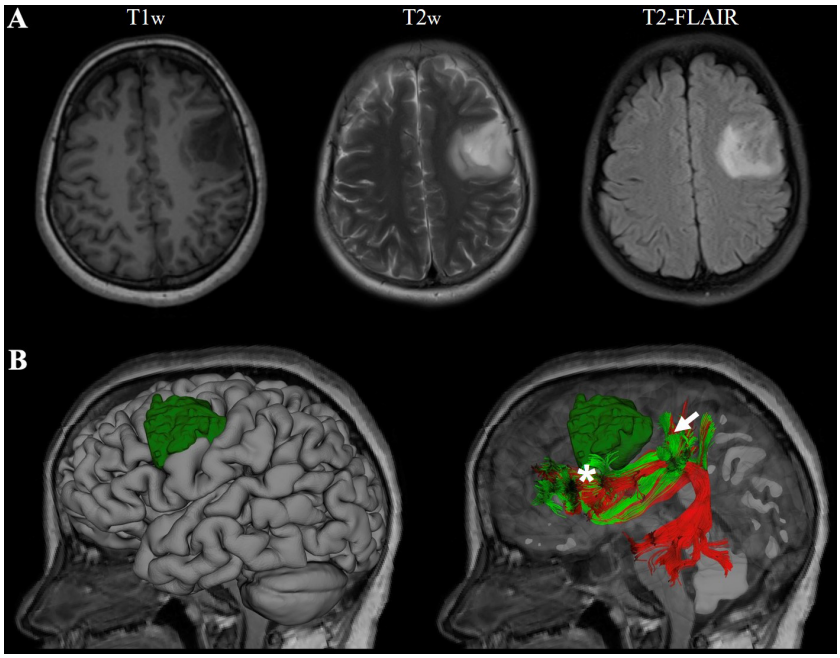

FIGURE 4
Representive imaging of a patient with left frontal lobe astrocytoma. Case 3, a 41-year-old female with left frontal lobe astrocytoma (WHO grade III) in MR images **(A)**. The relationship between language-related fiber tracts (AF in red and SLF-II in green color) and tumor (dark green) were shown in **(B)**; the eloquent area of intro-operative speech arrest (DCS) was marked with a star(Projecting terminal territory of AF) and an arrow (Projecting terminal territory of SLF-II).

areas were located at the tract-based cortical termination of SLF-II. Independently, our glioma team's study of language mapping in glioma surgery showed that in Chinese people the goodness of fit between the terminal territories of the manually tracked AF and SLF and the DSC-mapped eloquent speech output area in the pars opercularis and ventral premotor cortex was 82% and 86%, respectively (25). For Case 2 treated in another institute, although nonawake surgery was performed, the automatic tracked neurofibers still augmented surgical plans, with an exceptionally safe approach design, for removing highly invasive gliomas by analyzing the relationship between the tumor and white matter tracts. Similar results were reported previously (37) and as in Case 3.

The major limitation of this pilot study was its limited sample size and lack of a control group. However, these results did show the promising value of the clinical implementation of DiffusionGO. We are now pursuing a multicenter clinical trial of this automatic DTI tractography pipeline to prove its potential role as an efficient, clinically applicable bundle-specific tractography tool to augment technical equality and improve surgical planning precision across different hospitals in China.

5 Conclusion

We demonstrated the application of DiffusionGo in three language-related cases. The fully automatic processing pipeline may provide the technician or surgeon with a solution to reduce time cost and operating error. We believe that this promising technique can improve care quality and surgical procedure quality across different facilities.

Data availability statement

The raw data supporting the conclusions of this article will be made available by the authors, without undue reservation.

Ethics statement

The studies involving human participants were reviewed and approved by IRB of Huashan Hospital, Fudan University (KY2021-452 and KY2019-008). The patients/participants provided their written informed consent to participate in this study. Written informed consent was obtained from the individual(s) for the publication of any potentially identifiable images or data included in this article.

Author contributions

Conceptualization, JS and C-PL. Methodology, YY, TQ, SC and S-PC. Software, Y-HC, Y-CH, Y-TK and K-TK. Validation, GX, YY and ZY. Investigation, YY and TQ. Resources, WZ and C-PL. Data curation, YY and TQ. Writing—original draft preparation, YY and

SC. Writing—review and editing, SC, JS and C-PL. Visualization, YY, GX, Y-TK and K-TK. Supervision, JS and C-PL. Funding acquisition, JS. All authors contributed to the article and approved the submitted version.

Funding

This study was supported and granted by the CAMS Innovation Fund for Medical Sciences (CIFMS, 2019-I2M-5-008), Fujian Province Science and Technology Innovation Joint Fund (2021Y9135) and Shanghai Municipal Science and Technology Major Project (No.2018SHZDZX01) and ZJLab and Ministry of Science and Technology (MOST) of Taiwan (MOST 111-2321-B-A49-003).

Conflict of interest

Author Y-HC and Y-CH were employed by the company Siemens Healthineers Ltd.

The remaining authors declare that the research was conducted in the absence of any commercial or financial relationships that could be construed as a potential conflict of interest.

Publisher's note

Supplementary material

The Supplementary Material for this article can be found online at: https://www.frontiersin.org/articles/10.3389/fonc.2023.1089923/full#supplementary-material

References

1. Bray F, Ferlay J, Soerjomataram I, Siegel RL, Torre LA, Jemal A. Global cancer statistics 2018: GLOBOCAN estimates of incidence and mortality worldwide for 36 cancers in 185 countries. *CA Cancer J Clin* (2018) 68:394–424. doi: 10.3322/caac.21492

2. Weller M, van den Bent M, Preusser M, Le Rhun E, JC T, Minniti G, et al. EANO guidelines on the diagnosis and treatment of diffuse gliomas of adulthood. *Nat Rev Clin Oncol* (2021) 18:170–86. doi: 10.1038/s41571-020-00447-z

3. Molinaro AM, Hervey-Jumper S, Morshed RA, Young J, Han SJ, Chunduru P, et al. Association of maximal extent of resection of contrast-enhanced and non-Contrast-Enhanced tumor with survival within molecular subgroups of patients with newly diagnosed glioblastoma. *JAMA Oncol* (2020) 6:495–503. doi: 10.1001/jamaoncol.2019.6143

4. Yuan Y, Yu Y, Guo Y, Chu Y, Chang J, Hsu Y, et al. Noninvasive delineation of glioma infiltration with combined 7T chemical exchange saturation transfer imaging and MR spectroscopy: A diagnostic accuracy study. *Metabolites* (2022) 12. doi: 10.3390/metabo12100901

5. Basser PJ, Mattiello J, LeBihan D. MR diffusion tensor spectroscopy and imaging. *Biophys J* (1994) 66:259–67. doi: 10.1016/S0006-3495(94)80775-1

6. Basser PJ. Inferring microstructural features and the physiological state of tissues from diffusion-weighted images. *NMR BioMed* (1995) 8:333–44. doi: 10.1002/nbm.1940080707

7. Mori S, van Zijl PC. Fiber tracking: Principles and strategies - a technical review. *NMR BioMed* (2002) 15:468–80. doi: 10.1002/nbm.781

8. Mori S, BJ C, VP C, van Zijl PC. Three-dimensional tracking of axonal projections in the brain by magnetic resonance imaging. *Ann Neurol* (1999) 45:265–9. doi: 10.1002/1531-8249(199902)45:2<265::aid-ana21>3.0.co;2-3

9. Bello L, Gambini A, Castellano A, Carrabba G, Acerbi F, Fava E, et al. Motor and language DTI fiber tracking combined with intraoperative subcortical mapping for surgical removal of gliomas. *NEUROIMAGE* (2008) 39:369–82. doi: 10.1016/j.neuroimage.2007.08.031

10. Berman JI, Berger MS, Mukherjee P, Henry RG. Diffusion-tensor imaging-guided tracking of fibers of the pyramidal tract combined with intraoperative cortical stimulation mapping in patients with gliomas. *J Neurosurg* (2004) 101:66–72. doi: 10.3171/jns.2004.101.1.0066

11. Wu JS, Zhang J, Zhuang DX, Yao CJ, Qiu TM, Lu JF, et al. Current status of cerebral glioma surgery in China. *Chin Med J (Engl)* (2011) 124:2569–77.

12. Maier-Hein KH, Neher PF, Houde JC, Cote MA, Garyfallidis E, Zhong J, et al. The challenge of mapping the human connectome based on diffusion tractography. *Nat Commun* (2017) 8:1349. doi: 10.1038/s41467-017-01285-x

13. Pujol S, Wells W, Pierpaoli C, Brun C, Gee J, Cheng G, et al. The DTI challenge: Toward standardized evaluation of diffusion tensor imaging tractography for neurosurgery. *J Neuroimaging* (2015) 25:875–82. doi: 10.1111/jon.12283

14. Lin C-P, Chong S-T, Lo C, Huang C. *Method and apparatus of fiber tracking, and non-transitory computer-readable medium thereof.* (2019).

15. Tournier JD, Smith R, Raffelt D, Tabbara R, Dhollander T, Pietsch M, et al. MRtrix3: A fast, flexible and open software framework for medical image processing and visualisation. *NEUROIMAGE* (2019) 202:116137. doi: 10.1016/j.neuroimage.2019.116137

16. Jenkinson M, Beckmann CF, Behrens TE, Woolrich MW, Smith SM. FSL. *NEUROIMAGE* (2012) 62:782–90. doi: 10.1016/j.neuroimage.2011.09.015

17. Veraart J, Fieremans E, Novikov DS. Diffusion MRI noise mapping using random matrix theory. *Magn Reson Med* (2016) 76:1582–93. doi: 10.1002/mrm.26059

18. Cordero-Grande L, Christiaens D, Hutter J, Price AN, Hajnal JV. Complex diffusion-weighted image estimation *via* matrix recovery under general noise models. *NEUROIMAGE* (2019) 200:391–404. doi: 10.1016/j.neuroimage.2019.06.039

19. Veraart J, Novikov DS, Christiaens D, Ades-Aron B, Sijbers J, Fieremans E. Denoising of diffusion MRI using random matrix theory. *NEUROIMAGE* (2016) 142:394–406. doi: 10.1016/j.neuroimage.2016.08.016

20. Kellner E, Dhital B, Kiselev VG, Reisert M. Gibbs-Ringing artifact removal based on local subvoxel-shifts. *Magn Reson Med* (2016) 76:1574–81. doi: 10.1002/mrm.26054

21. Graham MS, Drobnjak I, Jenkinson M, Zhang H. Quantitative assessment of the susceptibility artefact and its interaction with motion in diffusion MRI. *PLoS One* (2017) 12:e185647. doi: 10.1371/journal.pone.0185647

22. Tustison NJ, Avants BB, Cook PA, Zheng Y, Egan A, Yushkevich PA, et al. N4ITK: improved N3 bias correction. *IEEE Trans Med Imaging* (2010) 29:1310–20. doi: 10.1109/TMI.2010.2046908

23. Fischl B. FreeSurfer. *NEUROIMAGE* (2012) 62:774–81. doi: 10.1016/j.neuroimage.2012.01.021

24. Mascitelli JR, Yoon S, Cole TS, Kim H, Lawton MT. Does eloquence subtype influence outcome following arteriovenous malformation surgery? *J Neurosurg* (2018) 131:876–83. doi: 10.3171/2018.4.JNS18403

25. Wu J, Lu J, Zhang H, Zhang J, Mao Y, Zhou L. Probabilistic map of language regions: Challenge and implication. *BRAIN* (2015) 138:e337. doi: 10.1093/brain/awu247

26. Chang EF, Raygor KP, Berger MS. Contemporary model of language organization: An overview for neurosurgeons. *J Neurosurg* (2015) 122:250–61. doi: 10.3171/2014.10.JNS132647

27. Sanai N, Mirzadeh Z, Berger MS. Functional outcome after language mapping for glioma resection. *N Engl J Med* (2008) 358:18–27. doi: 10.1056/NEJMoa067819

28. Gamble AJ, Schaffer SG, Nardi DJ, Chalif DJ, Katz J, Dehdashti AR. Awake craniotomy in arteriovenous malformation surgery: The usefulness of cortical and subcortical mapping of language function in selected patients. *World Neurosurg* (2015) 84:1394–401. doi: 10.1016/j.wneu.2015.06.059

29. Tate MC, Herbet G, Moritz-Gasser S, Tate JE, Duffau H. Probabilistic map of critical functional regions of the human cerebral cortex: Broca's area revisited. *BRAIN* (2014) 137:2773–82. doi: 10.1093/brain/awu168

30. Wu J, Lu J, Zhang H, Zhang J, Yao C, Zhuang D, et al. Direct evidence from intraoperative electrocortical stimulation indicates shared and distinct speech

production center between Chinese and English languages. *Hum Brain MAPP* (2015) 36:4972–85. doi: 10.1002/hbm.22991

31. Lu J, Zhao Z, Zhang J, Wu B, Zhu Y, Chang EF, et al. Functional maps of direct electrical stimulation-induced speech arrest and anomia: A multicentre retrospective study. *BRAIN* (2021) 144:2541–53. doi: 10.1093/brain/awab125

32. Rathore RK, Gupta RK, Agarwal S, Trivedi R, Tripathi RP, Awasthi R. Principal eigenvector field segmentation for reproducible diffusion tensor tractography of white matter structures. *Magn Reson Imaging* (2011) 29:1088–100. doi: 10.1016/j.mri.2011.04.014

33. Shi A, Zhou X, Xie Z, Mou H, Ouyang Q, Wang D. Internet Plus health care's role in reducing the inequality of high-quality medical resources in China. *Asia Pacific J Public Health* (2021) 33(8):997–8. doi: 10.1177/10105395211044954

34. Nazem-Zadeh MR, Davoodi-Bojd E, Soltanian-Zadeh H. Atlas-based fiber bundle segmentation using principal diffusion directions and spherical harmonic coefficients. *NEUROIMAGE* (2011) 54(Suppl 1):S146–64. doi: 10.1016/j.neuroimage.2010.09.035

35. Li H, Xue Z, Guo L, Liu T, Hunter J, Wong ST. A hybrid approach to automatic clustering of white matter fibers. *NEUROIMAGE* (2010) 49:1249–58. doi: 10.1016/j.neuroimage.2009.08.017

36. Fillard P, Descoteaux M, Goh A, Gouttard S, Jeurissen B, Malcolm J, et al. Quantitative evaluation of 10 tractography algorithms on a realistic diffusion MR phantom. *NeuroImage* (2011) 56:220–34. doi: 10.1016/j.neuroimage.2011.01.032

37. Yang Z, Song J, Zhu W. How I do it? Anatomical multifocal high-grade glioma resection. *Acta Neurochir (Wien)* (2021) 163:953–7. doi: 10.1007/s00701-020-04637-7

frontiers | Frontiers in Neurology

TYPE Methods
PUBLISHED 21 April 2023
DOI 10.3389/fneur.2023.1170045

OPEN ACCESS

EDITED BY
Zhifeng Shi,
Fudan University, China

REVIEWED BY
Hailiang Tang,
Fudan University, China
Ranjith Kumar Kankala,
Huaqiao University, China

*CORRESPONDENCE
Motoki Tanikawa
✉ mtnkw@med.nagoya-cu.ac.jp

RECEIVED 20 February 2023
ACCEPTED 03 April 2023
PUBLISHED 21 April 2023

CITATION
Sakata T, Tanikawa M, Yamada H, Fujinami R, Nishikawa Y, Yamada S and Mase M (2023) Minimally invasive treatment for glioblastoma through endoscopic surgery including tumor embolization when necessary: a technical note.
Front. Neurol. 14:1170045.
doi: 10.3389/fneur.2023.1170045

Minimally invasive treatment for glioblastoma through endoscopic surgery including tumor embolization when necessary: a technical note

Tomohiro Sakata, Motoki Tanikawa*, Hiroshi Yamada, Ryota Fujinami, Yusuke Nishikawa, Shigeki Yamada and Mitsuhito Mase

Department of Neurosurgery, Nagoya City University Graduate School of Medical Sciences, Nagoya, Japan

Background: Although there have been some reports on endoscopic glioblastoma surgery, the indication has been limited to deep-seated lesions, and the difficulty of hemostasis has been a concern. In that light, we attempted to establish an endoscopic procedure for excision of glioblastoma which could be applied even to hypervascular or superficial lesions, in combination with pre-operative endovascular tumor embolization.

Methods: Medical records of six consecutive glioblastoma patients who received exclusive endoscopic removal between September and November 2020 were analyzed. Preoperative tumor embolization was performed in cases with marked tumor stain and proper feeder arteries having an abnormal shape, for instance, tortuous or dilated, without passing through branches to the normal brain. Endoscopic tumor removal through a key-hole craniotomy was performed by using an inside-out excision for a deep-seated lesion, with the addition of an outside-in extirpation for a shallow portion when needed.

Results: Endoscopic removal was successfully performed in all six cases. Before resection, endovascular tumor embolization was performed in four cases with no resulting complications, including ischemia or brain swelling. Gross total resection was achieved in three cases, and near total resection in the other three cases. Intraoperative blood loss exceeded 1,000ml in only one case, whose tumor showed a prominent tumor stain but no proper feeder artery for embolization. In all patients, a smooth transition to adjuvant therapy was possible with no surgical site infection.

Conclusion: Endoscopic removal for glioblastoma was considered to be a promising procedure with minimal invasiveness and a favorable impact on prognosis.

KEYWORDS

endoscope, glioblastoma, tumor embolization, cylinder surgery, key-hole surgery

Introduction

Glioblastoma, one of the most common primary brain neoplasms, comprises 15% of all intracranial neoplasms and 60–75% of astrocytic tumors (1). Its treatment outcomes have improved only incrementally over the last several decades, with a tragic course, having a mean survival time fewer than 2 years after diagnosis, despite many efforts having been made in various fields, including surgical resection, radiation therapy, chemotherapy, and treatments based on novel concepts (2–4). Regarding surgical treatment, maximizing the extent of resection, which must be balanced finely with minimizing morbidities, has been confirmed to be essential for extending patients' survival time (1, 5, 6). A broad variety of refinements to achieve optimal resection have been made through the utilization of multiple modalities, including preoperative techniques such as diffusion tensor imaging (7), functional magnetic resonance imaging (MRI) (8–10), or magnetoencephalography (11), and intraoperative modalities such as image guidance (12), photodynamic diagnosis, for instance using 5-aminolevulinic acid (13), functional mapping *via* awake surgery, intraoperative ultrasound imaging, or intraoperative MRI (14, 15). Nevertheless, the prognosis of this devastating disease has not been substantially improved. Given this state of affairs, anything that can contribute to ameliorating the bleak prognosis of this disease is to be greatly desired.

Current neurosurgical procedure is undergoing what could be considered a transitional era, with a conventional operating microscope (OM), an endoscope, or an exoscope employed divergently according to the lesion or to surgeons' preferences. The OM, which appeared in the 1960s, revolutionized improvement in neurosurgical outcomes (16, 17) by providing a stable, illuminated, magnified, 3-dimensional view, though at the cost of sacrificing the surgeon's ergonomic comfort insofar as a bulky object between the operative field and the surgeon's eyes (18). In contrast, an exoscope, developed through advances in digital imaging, offers an operative view equivalent to an OM and superior ergonomics, though even experts in microsurgery require a certain amount of practice to attain a level clinically comparable to maneuvering under an OM (19). Since an exoscope, as with OM, utilizes illumination from the outside, a sufficiently large opening is necessitated; nevertheless, blind spots are still likely to occur in the deep areas (18). On the other hand, an endoscopic procedure with superior ergonomics can be performed through a narrow opening and corridor and reduce blind spots in deep areas (20). However, its maneuverability is limited by space, and in comparison to other devices, some time is required to acquire a sufficient level of skill. In addition, the current technology of endoscope provides inferior images of the operative field compared to other devices.

Introducing endoscopic surgery through a small opening for glioblastoma removal might benefit patients by virtue of limiting the invasiveness of the procedure, reducing the burden on patients, simplifying wound healing, decreasing the chance of infection, and contributing to the smooth transition to adjuvant treatment. In fact, some reports have described the utilization of an endoscope for glioblastoma surgery through a narrow transparent sheath, and it has been confirmed that endoscopic procedures could be performed as efficaciously as with an OM (21, 22). However, the same reports recommended that the procedure be essentially limited to deep-seated lesions. Moreover, the procedure necessitates initially entering the middle of a lesion, which can sometimes be vascular-rich, creating difficulty in achieving hemostasis through a limited corridor. Therefore, in this study, we attempted to develop an optimal and minimally invasive surgery for glioblastoma, which could be applied even to hypervascular or superficial lesions, by utilizing endovascular tumor embolization and endoscopic removal through an outside-in procedure following inside-out decompression (Figure 1).

Methods

All procedures performed in this study were in accordance with the 1964 Declaration of Helsinki and its later amendments and were reviewed and approved by the Institutional Review Board (IRB) at Nagoya City University (IRB number: 60-20-0187). Additionally, written informed consent was obtained from all the participants or appropriate surrogate decision-makers. Between September and November 2020, 6 consecutive glioblastoma patients, who were set to undergo surgical resection, were enrolled in this study. Data regarding clinical manifestation, neuroimaging, intraoperative videos, and surgical outcomes were analyzed.

Surgical procedure

Endovascular tumor embolization

Tumor embolization was performed if there was a marked tumor stain and prominent feeding arteries with abnormal shapes, for instance, tortuous or dilated, without passing through branches to the normal brain (Figure 2A). A cone-beam computed tomography (CT) was effective for confirming these findings. Under general anesthesia, a 5Fr guiding catheter was inserted into the main trunk, and a flow-guide microcatheter (Marathon; ev3 Neurovascular, Irvine, CA, United States) was advanced into the feeder vessel as close to the tumor as possible. The tumor was embolized with approximately 20% NBCA (Figure 2B). Platinum coils were also used for feeder vessel occlusion to prevent migration of NBCA. After this procedure, tumor removal proceeded continuously, or if time was required until tumor excision, general anesthesia was maintained in the intensive care unit to avoid brain swelling.

Endoscopic tumor removal

Surgical procedures of endoscopic tumor removal were performed with the aid of 4-mm rigid endoscopes with 0 or 30-degree angled lenses fixed with an exclusive holder (HD-EndoArm, Olympus, Tokyo, Japan), a high-speed drill, an ultrasonic surgical aspirator, and a series of endoscopic surgical instruments with a slender or single shaft. Under general anesthesia, patients were placed with their head positioned so that the location of a key-hole craniotomy was highest in the operative field and the axis from there to the center of the tumor was slightly tilted forward, allowing both hands of the surgeon to assume an ergonomically advantageous position. A key-hole craniotomy, which was simulated preoperatively to determine the proper size and location using an image workstation, was set precisely and performed using an image guidance system (SealthStation S8; Medtronic, Minneapolis, MN, United States) (Figure 3A). The lateral edge of the craniotomy was conically widened to allow, to the extent

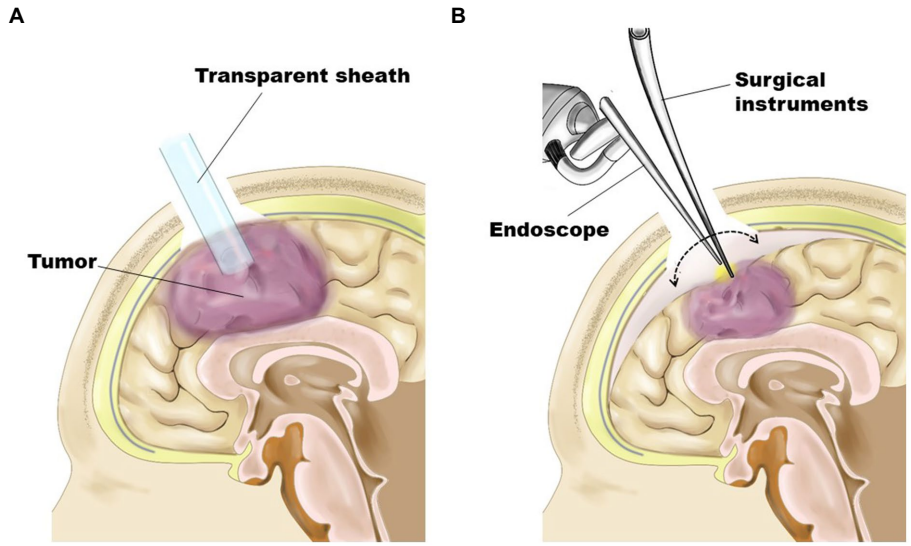

FIGURE 1
Schematic representation demonstrating surgical procedures. **(A)** As the first step, the tumor was removed in an inside-out fashion through a transparent sheath inserted into the tumor's center under the guidance of a neuronavigation system. **(B)** For tumors having a shallow portion, the residual part was removed in an outside-in fashion after obtaining enough space by subsidence of the brain surface through substantial tumor volume reduction.

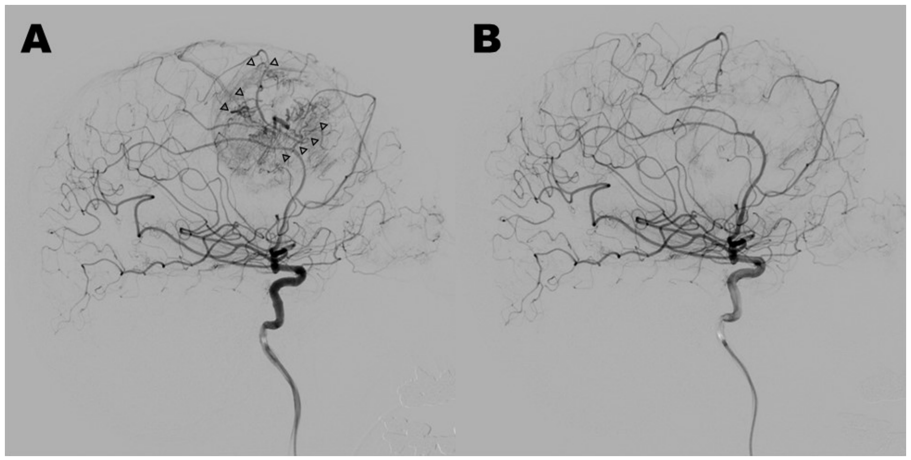

FIGURE 2
Case 4: lateral view of pre-embolization **(A)** and post-embolization **(B)** in digital subtraction angiograms of the right internal carotid artery. Marked tumor stain and prominent feeding arteries with abnormal shapes (arrowheads) disappeared through tumor embolization with 20% NBCA, and normal arteries were preserved.

possible, manipulation over a wide range (Figure 1). After insertion of a transparent sheath with a diameter of 10 mm (NeuroPort; Olympus, Tokyo, Japan) into the center of the tumor, guided by the image guidance system (Figure 3B), an endoscope was introduced. Initially, internal decompression of the tumor was conducted using suction or an ultrasonic surgical aspirator in an inside-out fashion while attaining hemostasis rigorously through cauterization by bipolar forceps with a slender or single shaft, or hemostatic material such as fibrin glue. If a lesion had only a deep-seated portion, it could be entirely removed through repetition of these procedures. For a lesion that also had shallow portions, after obtaining substantial subsidence of the brain surface and sufficient working space by internal decompression, the transparent sheath was taken out (Figure 3C), and the remaining part was resected in an outside-in fashion through a sufficient cortical incision (Figure 3D). Finally, after confirming hemostasis, BCNU wafers were placed over the extent of the tumor bed. The highlights of the procedure can be seen in Supplementary Video S1.

Results

Endoscopic removal was successfully performed in six glioblastoma cases as an initial treatment through a key-hole craniotomy approximately 20 mm in diameter. Clinical features and surgical outcomes of six cases were shown in Table 1. Prior to resection, endovascular tumor embolization was performed in four

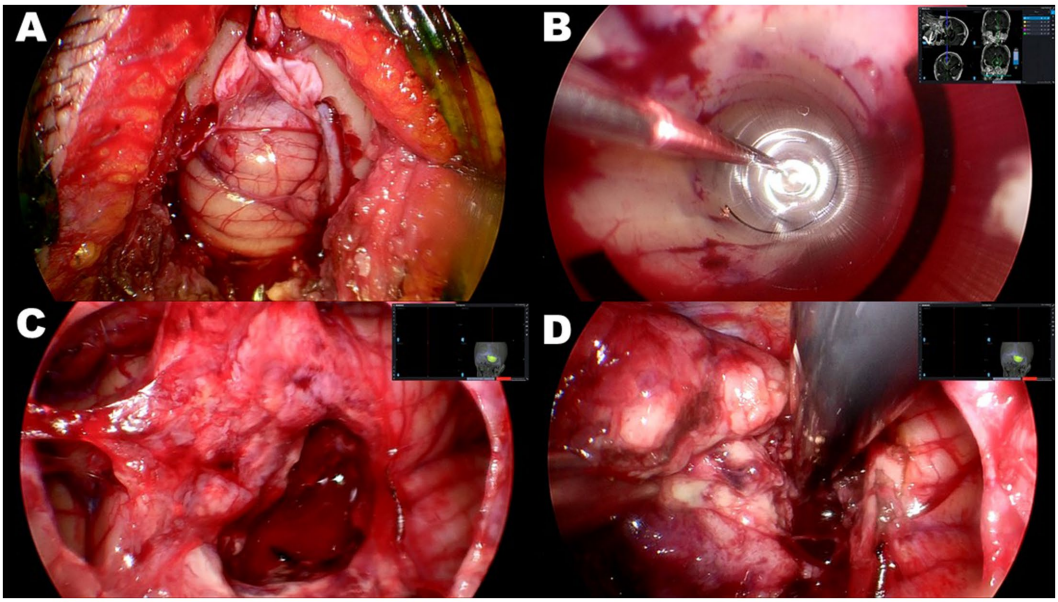

FIGURE 3
Case 2: intraoperative photographs of right cerebellar glioblastoma. **(A)** Key-hole craniotomy approximately 20mm in diameter. **(B)** Insertion of 10mm transparent sheath into center of tumor through guidance of neuronavigation system. The tumor was subsequently removed in an inside-out fashion. **(C)** After obtaining sufficient space by subsidence of brain surface through substantial tumor volume reduction, transparent sheath was removed. **(D)** Residual portion of tumor resected in an outside-in fashion through sufficient cortical incision.

cases, in which marked tumor stain and proper feeding arteries were detected by preoperative angiography. In all four cases, there were no complications related to tumor embolization such as ischemia or brain swelling. In three cases, where tumor developed only in a deep-seated area, the portion identified on gadolinium-enhanced T1-weighted MRI was removed entirely in one and near-totally in two cases, in an inside-out fashion (Figures 4A–C). In the remaining three cases, the procedure was supplemented with outside-in excision, and gross-total resection in two patients (Figures 4D,E) and near-total resection in one patient was achieved (Figure 4F). In two patients where a premotor area was involved, tumor removal could be performed with minimal deterioration of hemiparesis (one grade on MMT) by identifying and preserving the motor strip and pathway through motor-evoked potential mapping, after creating space by initially removing the forward portion of the lesion, a maneuver which was considered to be relatively safe. One other patient had transient upper extremity motor weakness postoperatively. Intraoperative blood loss exceeded 1,000 ml in only one case, where the patient did not receive preoperative tumor embolization due to the lack of a proper feeder for embolization, despite having a prominent tumor stain. In all patients, a smooth transition to adjuvant therapy was possible with no surgical site infection.

Discussion

This study successfully demonstrated the feasibility and effectiveness of an endoscopic excision for glioblastoma not only for the deep-seated portion *via* the inside-out procedure through a narrow transparent sheath, but in addition even for the shallow portion *via* the outside-in procedure. Since the goals of surgical resection of glioblastoma are to provide ample tissue for an accurate histological and genomic diagnosis and continued study of the disease, to relieve symptoms, and to extend patient survival by achieving maximal cytoreduction without morbidity, it was thought that this procedure could realize these aims to nearly the same extent as the ordinary microscopic procedure. Predicted difficulty in manipulation capability through narrow opening and corridor produced virtually no stress even during the inside-out phase through a 10 mm transparent sheath. Furthermore, in the subsequent process preceded by thorough internal decompression, the space through the key-hole craniotomy could be sufficient for adequate removal *via* the outside-in procedure.

Bleeding is one of the most likely complications during the removal of glioblastoma because glioblastoma is often highly vascularized by neoformed vessels, as microvascular proliferation is one of its diagnostic hallmarks (23). Therefore, endovascular tumor embolization was considered indispensable for the smooth and safe progression of an endoscopic glioblastoma excision procedure if the target lesion was vascular-rich. In fact, blood loss relatively increased in the case of hypervascular lesion, which could not be embolized due to a lack of a suitable feeder artery. In such cases, thorough preparation of hemostatic devices and transfusion blood will be required. On the other hand, because glioblastoma is an intraparenchymal tumor, proper selection of intratumoral vessels to be embolized, which were characteristically tortuous and dilated in shape (24), and which ended in the tumor without passing through branches to the normal brain, was considered very important. A cone-beam CT, which does not require particularly exceptional equipment (25), was useful for identifying those findings in this study. In either case, endovascular tumor embolization has not been standard treatment for glioblastoma, and even in this study, it was

10.3389/fneur.2023.1170045

TABLE 1 Clinical characteristics and outcomes of the six patients with fully endoscopic glioblastoma removal.

Case	Age, Sex	Size (mm)	Location	Preoperative embolization	Endoscopic procedure	Extent of resection	Blood loss	Pathological diagnosis	Survival time	Complications
1	70 years, M	32 × 31 × 30	Rt frontal lobe	No	I-O	GTR	336 ml	Glioblastoma, IDH-wildtype	123 weeks, alive	Upper limb motor weakness (transient)
2	59 years, F	40 × 34 × 29	Lt parietal lobe	No	I-O	NTR	1,048 ml	Glioblastoma, IDH-wildtype	49 weeks	None
3	72 years, F	28 × 24 × 36	Rt frontal lobe	Yes	I-O	NTR	106 ml	Glioblastoma, IDH-wildtype	29 weeks	Deterioration of hemiparesis (persistent)
4	68 years, F	53 × 51 × 36	Rt frontal lobe	Yes	O-I following I-O	GTR	580 ml	Glioblastoma, IDH-wildtype	129 weeks, alive	None
5	73 years, F	55 × 31 × 42	Rt cerebellum	Yes	O-I following I-O	GTR	354 ml	Glioblastoma, IDH-wildtype	45 weeks	None
6	66 years, M	69 × 53 × 49	Rt frontal lobe	Yes	O-I following I-O	NTR	651 ml	Glioblastoma, IDH-wildtype	45 weeks	Deterioration of hemiparesis (persistent)

I-O, inside-out style; O-I, outside-in style; GTR, gross total resection; NTR, near total resection.

only performed in four cases. Therefore, a future study including a more significant number of cases will be necessary to establish the efficacy and safety of this technique.

Surgical intervention is confirmed to cause a neurophysiological reflex response involving hypothalamic–pituitary–adrenal axis activation, and results in complex neuroendocrine, inflammatory, metabolic cascade, and immunological responses (26–29). Experimentally, inflammatory mediators, such as CINC1, IL-8, TNF-α, and NO, have also been found to increase proportionately depending on the length of the skin incision experimentally (29). In addition, the reduction of the inflammatory response has been proven with the laparoscopic procedure compared to open surgery (30–32). Therefore, surgical intervention, including skin incision, muscle dissection, and craniotomy, should be minimized not just for the sake of reducing pain and better cosmetic results but also from the standpoint of mitigating the surgical stress response, and the endoscopic procedure was considered to be suitable for its realization even in surgery of glioblastoma.

Surgical site infections (SSI) after cranial surgery, which are an inevitable complication and have been reported to occur in 1–16% of patients (33–42), especially in glioblastoma surgery, would not only lead to the discontinuation of postoperative treatment but would also affect patient survival (33). While various risk factors for SSI have been assumed, e.g., number of operations (34–38, 41), duration of operation (35, 37, 39, 40), emergency operation (37), cerebrospinal fluid leakage (34, 35, 37, 39, 42), CSF drainage (35, 39), and American Society of Anesthesiologists score (>2) including body mass index and diabetes mellitus (34–36, 38, 42), there have also been reports that craniotomy itself could constitute a risk factor (40, 41). Therefore, by using endoscopic resection for glioblastoma through key-hole craniotomy as in this study, it may be possible to reduce SSI to a level similar to that of other organs (43, 44), and facilitate a smooth transition to postoperative therapy.

The largeness of a lesion would not be a contraindicating factor for this procedure since, in principle, the larger the lesion, the larger the space that can hypothetically be secured through an internal decompression. On the other hand, it can be inherently difficult in this procedure, which employs endoscopic surgery through a narrow opening, to remove a lesion which extends widely in a shallow area. Even for such lesions, however, successful removal could be achieved in this study by making space through internal decompression, provided there was the appropriate volume and depth. This study was not able to establish the relationship between the extent of the surface and volume in the deep portion, where this procedure can be successfully utilized. A lesion close to eloquent areas, for which the use of brain mapping would be essential for removal, could be assumed to be another limitation of this procedure. Brain mapping may also be possible if a lesion involving the eloquent area has a significant amount of lesion in the adjacent non-eloquent area, as was the situation in two cases in this study, whose premotor lesions were successfully resected by using motor evoked potential mapping. Moreover, this procedure, performed through small skin incision and craniotomy, may be suitable for awake surgery because of the reduced burden on the patient. Notwithstanding, since the present study is only a preliminary report, including a small number of patients and only a few types of lesions, further studies with more cases are needed to clarify the efficacy and safety of this endoscopic procedure for glioblastoma and to eliminate such limitations.

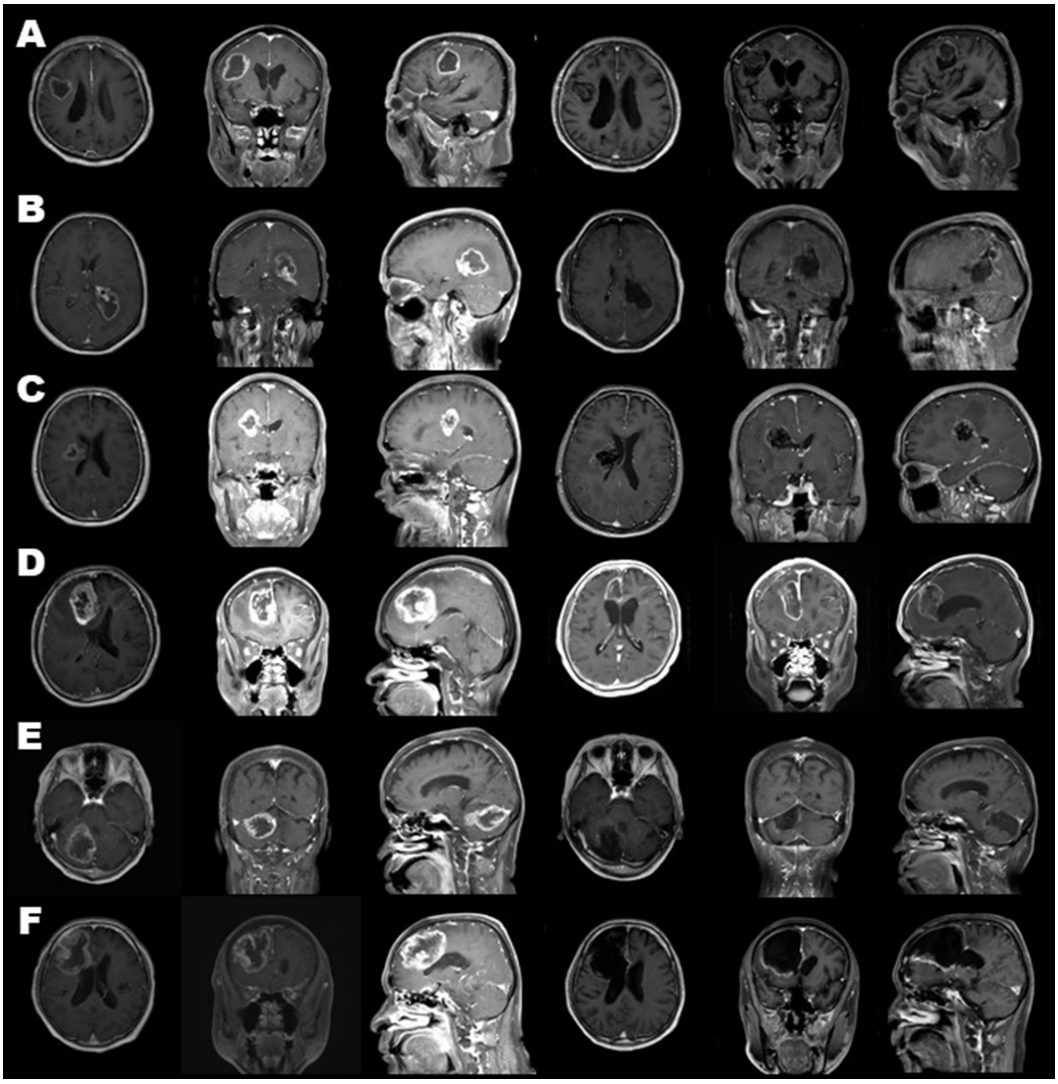

FIGURE 4
Preoperative (three columns on the left) and postoperative (three columns on the right) gadolinium-enhanced magnetic resonance images of all cases. Cases 1, 2, 3 **(A–C)** were treated through tumor removal only in an inside-out fashion. Cases 4, 5, 6 **(D–F)** combined excision in an outside-in fashion. As a result, gross-total resection in cases 1, 4, and 5 **(A,D,E)** and near-total resection in cases 2, 3, and 6 **(B,C,F)** was achieved.

Conclusion

Endoscopic removal of glioblastoma using an inside-out style excision for a deep-seated lesion was considered to be a promising procedure, with the addition of an outside-in style extirpation for a shallow portion if needed. This procedure could be performed *via* small skin incision and key-hole craniotomy less invasively and had a positive effect on patients' prognosis, facilitating a smooth transition to postoperative adjuvant therapy. In addition, endovascular tumor embolization, when it was needed before resection, was also considered beneficial. However, a more extensive number of patients will need to be evaluated in future studies to confirm the efficacy and safety of this procedure.

Data availability statement

The raw data supporting the conclusions of this article will be made available by the authors, without undue reservation.

Ethics statement

The studies involving human participants were reviewed and approved by Institutional Review Board at Nagoya City University. The patients/participants provided their written informed consent to participate in this study. Written informed consent was obtained from the individual(s) for the publication of any potentially identifiable images or data included in this article.

Author contributions

TS: conceptualization, project administration, acquisition, methodology, investigation, resources, data curation, formal analysis, and writing–original draft. MT: methodology, investigation, resources, and writing–review and editing. HY, RF, YN, and SY: methodology, investigation, and resources. MM: conceptualization, funding acquisition, and supervision. All authors contributed to the article and approved the submitted version.

Conflict of interest

The authors declare that the research was conducted in the absence of any commercial or financial relationships that could be construed as a potential conflict of interest.

Publisher's note

Supplementary material

The Supplementary material for this article can be found online at: https://www.frontiersin.org/articles/10.3389/fneur.2023.1170045/full#supplementary-material

References

1. Young RM, Jamshidi A, Davis G, Sherman JH. Current trends in the surgical management and treatment of adult glioblastoma. *Ann Transl Med*. (2015) 3:121. doi: 10.3978/j.issn.2305-5839.2015.05.10

2. Kobayashi T, Nitta M, Shimizu K, Saito T, Tsuzuki S, Fukui A, et al. Therapeutic options for recurrent glioblastoma-efficacy of Talaporfin sodium mediated photodynamic therapy. *Pharmaceutics*. (2022) 14:353. doi: 10.3390/pharmaceutics14020353

3. Wen PY, Weller M, Lee EQ, Alexander BM, Barnholtz-Sloan JS, Barthel FP, et al. Glioblastoma in adults: a Society for Neuro-Oncology (SNO) and European Society of Neuro-Oncology (EANO) consensus review on current management and future directions. *Neuro-Oncology*. (2020) 22:1073–113. doi: 10.1093/neuonc/noaa106

4. Kinzel A, Ambrogi M, Varshaver M, Kirson ED. Tumor treating fields for glioblastoma treatment: patient satisfaction and compliance with the second-generation Optune((R)) system. *Clin Med Insights Oncol*. (2019) 13:1179554918825449. doi: 10.1177/1179554918825449

5. Li YM, Suki D, Hess K, Sawaya R. The influence of maximum safe resection of glioblastoma on survival in 1229 patients: can we do better than gross-total resection? *J Neurosurg*. (2016) 124:977–88. doi: 10.3171/2015.5.JNS142087

6. Sanai N, Polley MY, McDermott MW, Parsa AT, Berger MS. An extent of resection threshold for newly diagnosed glioblastomas. *J Neurosurg*. (2011) 115:3–8. doi: 10.3171/2011.2.JNS10998

7. Zhu FP, Wu JS, Song YY, Yao CJ, Zhuang DX, Xu G, et al. Clinical application of motor pathway mapping using diffusion tensor imaging tractography and intraoperative direct subcortical stimulation in cerebral glioma surgery: a prospective cohort study. *Neurosurgery*. (2012) 71:1170–84. doi: 10.1227/NEU.0b013e318271bc61

8. Kuchcinski G, Mellerio C, Pallud J, Dezamis E, Turc G, Rigaux-Viode O, et al. Three-tesla functional MR language mapping: comparison with direct cortical stimulation in gliomas. *Neurology*. (2015) 84:560–8. doi: 10.1212/WNL.0000000000001226

9. Trinh VT, Fahim DK, Maldaun MV, Shah K, McCutcheon IE, Rao G, et al. Impact of preoperative functional magnetic resonance imaging during awake craniotomy procedures for intraoperative guidance and complication avoidance. *Stereotact Funct Neurosurg*. (2014) 92:315–22. doi: 10.1159/000365224

10. Roux FE, Boulanouar K, Ranjeva JP, Tremoulet M, Henry P, Manelfe C, et al. Usefulness of motor functional MRI correlated to cortical mapping in Rolandic low-grade astrocytomas. *Acta Neurochir*. (1999) 141:71–9. doi: 10.1007/s007010050268

11. Tarapore PE, Tate MC, Findlay AM, Honma SM, Mizuiri D, Berger MS, et al. Preoperative multimodal motor mapping: a comparison of magnetoencephalography imaging, navigated transcranial magnetic stimulation, and direct cortical stimulation. *J Neurosurg*. (2012) 117:354–62. doi: 10.3171/2012.5.JNS112124

12. Wu JS, Zhou LF, Tang WJ, Mao Y, Hu J, Song YY, et al. Clinical evaluation and follow-up outcome of diffusion tensor imaging-based functional neuronavigation: a prospective, controlled study in patients with gliomas involving pyramidal tracts. *Neurosurgery*. (2007) 61:935–49. doi: 10.1227/01.neu.0000303189.80049.ab

13. Stummer W, Pichlmeier U, Meinel T, Wiestler OD, Zanella F, Reulen HJ, et al. Fluorescence-guided surgery with 5-aminolevulinic acid for resection of malignant glioma: a randomised controlled multicentre phase III trial. *Lancet Oncol*. (2006) 7:392–401. doi: 10.1016/S1470-2045(06)70665-9

14. Serra C, Stauffer A, Actor B, Burkhardt JK, Ulrich NH, Bernays RL, et al. Intraoperative high frequency ultrasound in intracerebral high-grade tumors. *Ultraschall Med*. (2012) 33:E306–12. doi: 10.1055/s-0032-1325369

15. Senft C, Bink A, Franz K, Vatter H, Gasser T, Seifert V. Intraoperative MRI guidance and extent of resection in glioma surgery: a randomised, controlled trial. *Lancet Oncol*. (2011) 12:997–1003. doi: 10.1016/s1470-2045(11)70196-6

16. Jamieson KG. Excision of pineal tumors. *J Neurosurg*. (1971) 35:550–3. doi: 10.3171/jns.1971.35.5.0550

17. Stein BM. The infratentorial supracerebellar approach to pineal lesions. *J Neurosurg*. (1971) 35:197–202. doi: 10.3171/jns.1971.35.2.0197

18. Ridge SE, Shetty KR, Lee DJ. Heads-up surgery: endoscopes and exoscopes for otology and Neurotology in the era of the COVID-19 pandemic. *Otolaryngol Clin N Am*. (2021) 54:11–23. doi: 10.1016/j.otc.2020.09.024

19. Pafitanis G, Hadjiandreou M, Alamri A, Uff C, Walsh D, Myers S. The exoscope versus operating microscope in microvascular surgery: A simulation non-inferiority trial. *Arch Plast Surg*. (2020) 47:242–9. doi: 10.5999/aps.2019.01473

20. Tanikawa M, Yamada H, Sakata T, Hayashi Y, Sasagawa Y, Watanabe T, et al. Exclusive endoscopic occipital transtentorial approach for pineal region tumors. *World Neurosurg*. (2019) 131:167–73. doi: 10.1016/j.wneu.2019.08.038

21. Ogura K, Tachibana E, Aoshima C, Sumitomo M. New microsurgical technique for intraparenchymal lesions of the brain: transcylinder approach. *Acta Neurochir*. (2006) 148:779–85. doi: 10.1007/s00701-006-0768-7

22. Kassam AB, Engh JA, Mintz AH, Prevedello DM. Completely endoscopic resection of intraparenchymal brain tumors. *J Neurosurg*. (2009) 110:116–23. doi: 10.3171/2008.7.JNS08226

23. Rajagopalan V, Chouhan RS, Pandia MP, Lamsal R, Rath GP. Effect of intraoperative blood loss on perioperative complications and neurological outcome in adult patients undergoing elective brain tumor surgery. *J Neurosci Rural Pract*. (2019) 10:631–40. doi: 10.1055/s-0039-3399487

24. Jain RK, di Tomaso E, Duda DG, Loeffler JS, Sorensen AG, Batchelor TT. Angiogenesis in brain tumours. *Nat Rev Neurosci*. (2007) 8:610–22. doi: 10.1038/nrn2175

25. Radbruch A, Eidel O, Wiestler B, Paech D, Burth S, Kickingereder P, et al. Quantification of tumor vessels in glioblastoma patients using time-of-flight angiography at 7 tesla: a feasibility study. *PLoS One*. (2014) 9:e110727. doi: 10.1371/journal.pone.0110727

26. Kohl BA, Deutschman CS. The inflammatory response to surgery and trauma. *Curr Opin Crit Care*. (2006) 12:325–32. doi: 10.1097/01.ccx.0000235210.85073.fc

27. Desborough JP. The stress response to trauma and surgery. *Br J Anaesth*. (2000) 85:109–17. doi: 10.1093/bja/85.1.109

28. Watt DG, Horgan PG, McMillan DC. Routine clinical markers of the magnitude of the systemic inflammatory response after elective operation: a systematic review. *Surgery*. (2015) 157:362–80. doi: 10.1016/j.surg.2014.09.009

29. Ioannidis A, Arvanitidis K, Filidou E, Valatas V, Stavrou G, Michalopoulos A, et al. The length of surgical skin incision in postoperative inflammatory reaction. *JSLS*. (2018) 22:e2018.00045. doi: 10.4293/JSLS.2018.00045

30. Novitsky YW, Litwin DE, Callery MP. The net immunologic advantage of laparoscopic surgery. *Surg Endosc*. (2004) 18:1411–9. doi: 10.1007/s00464-003-8275-x

31. Kim TK, Yoon JR. Comparison of the neuroendocrine and inflammatory responses after laparoscopic and abdominal hysterectomy. *Korean J Anesthesiol*. (2010) 59:265–9. doi: 10.4097/kjae.2010.59.4.265

32. Evans C, Galustian C, Kumar D, Hagger R, Melville DM, Bodman-Smith M, et al. Impact of surgery on immunologic function: comparison between minimally invasive techniques and conventional laparotomy for surgical resection of colorectal tumors. *Am J Surg*. (2009) 197:238–45. doi: 10.1016/j.amjsurg.2008.01.021

33. Salle H, Deluche E, Couve-Deacon E, Beaujeux AC, Pallud J, Roux A, et al. Surgical site infections after glioblastoma surgery: results of a multicentric retrospective study. *Infection*. (2021) 49:267–75. doi: 10.1007/s15010-020-01534-0

34. Chiang HY, Kamath AS, Pottinger JM, Greenlee JD, Howard MA 3rd, Cavanaugh JE, et al. Risk factors and outcomes associated with surgical site infections after craniotomy or craniectomy. *J Neurosurg*. (2014) 120:509–21. doi: 10.3171/2013.9.JNS13843

35. Fang C, Zhu T, Zhang P, Xia L, Sun C. Risk factors of neurosurgical site infection after craniotomy: A systematic review and meta-analysis. *Am J Infect Control*. (2017) 45:e123–34. doi: 10.1016/j.ajic.2017.06.009

36. Jimenez-Martinez E, Cuervo G, Hornero A, Ciercoles P, Gabarros A, Cabellos C, et al. Risk factors for surgical site infection after craniotomy: a prospective cohort study. *Antimicrob Resist Infect Control*. (2019) 8:69. doi: 10.1186/s13756-019-0525-3

37. Korinek AM. Risk factors for neurosurgical site infections after craniotomy: a prospective multicenter study of 2944 patients. The French study Group of Neurosurgical Infections, the SEHP, and the C-CLIN Paris-Nord. Service Epidemiologie hygiene et prevention. *Neurosurgery*. (1997) 41:1073–81. doi: 10.1097/00006123-199711000-00010

38. Abode-Iyamah KO, Chiang HY, Winslow N, Park B, Zanaty M, Dlouhy BJ, et al. Risk factors for surgical site infections and assessment of vancomycin powder as a preventive measure in patients undergoing first-time cranioplasty. *J Neurosurg*. (2018) 128:1241–9. doi: 10.3171/2016.12.JNS161967

39. Shi ZH, Xu M, Wang YZ, Luo XY, Chen GQ, Wang X, et al. Post-craniotomy intracranial infection in patients with brain tumors: a retrospective analysis of 5723 consecutive patients. *Br J Neurosurg*. (2017) 31:5–9. doi: 10.1080/02688697.2016.1253827

40. Abu Hamdeh S, Lytsy B, Ronne-Engstrom E. Surgical site infections in standard neurosurgery procedures-a study of incidence, impact and potential risk factors. *Br J Neurosurg*. (2014) 28:270–5. doi: 10.3109/02688697.2013.835376

41. Tenney JH, Vlahov D, Salcman M, Ducker TB. Wide variation in risk of wound infection following clean neurosurgery. Implications for perioperative antibiotic prophylaxis. *J Neurosurg*. (1985) 62:243–7. doi: 10.3171/jns.1985.62.2.0243

42. McClelland S 3rd, Hall WA. Postoperative central nervous system infection: incidence and associated factors in 2111 neurosurgical procedures. *Clin Infect Dis*. (2007) 45:55–9. doi: 10.1086/518580

43. Jensen KK, Henriksen NA, Jorgensen LN. Endoscopic component separation for ventral hernia causes fewer wound complications compared to open components separation: a systematic review and meta-analysis. *Surg Endosc*. (2014) 28:3046–52. doi: 10.1007/s00464-014-3599-2

44. Shabanzadeh DM, Sorensen LT. Laparoscopic surgery compared with open surgery decreases surgical site infection in obese patients: a systematic review and meta-analysis. *Ann Surg*. (2012) 256:934–45. doi: 10.1097/SLA.0b013e318269a46b

frontiers | Frontiers in Neurology

TYPE Original Research
PUBLISHED 09 June 2023
DOI 10.3389/fneur.2023.1171167

OPEN ACCESS

EDITED BY
Zhifeng Shi,
Fudan University, China

REVIEWED BY
Md Shahnur Alam,
University of Pittsburgh, United States
A. N. M. Mamun-Or-Rashid,
Doshisha University, Japan

*CORRESPONDENCE
Xingyu Miao
✉ miaoxyu@163.com

RECEIVED 21 February 2023
ACCEPTED 16 May 2023
PUBLISHED 09 June 2023

CITATION
Cui J, Miao X, Yanghao X and Qin X (2023) Bibliometric research on the developments of artificial intelligence in radiomics toward nervous system diseases.
Front. Neurol. 14:1171167.
doi: 10.3389/fneur.2023.1171167

Bibliometric research on the developments of artificial intelligence in radiomics toward nervous system diseases

Jiangli Cui, Xingyu Miao*, Xiaoyu Yanghao and Xuqiu Qin

Shaanxi Provincial People's Hospital, Xi'an, China

Background: The growing interest suggests that the widespread application of radiomics has facilitated the development of neurological disease diagnosis, prognosis, and classification. The application of artificial intelligence methods in radiomics has increasingly achieved outstanding prediction results in recent years. However, there are few studies that have systematically analyzed this field through bibliometrics. Our destination is to study the visual relationships of publications to identify the trends and hotspots in radiomics research and encourage more researchers to participate in radiomics studies.

Methods: Publications in radiomics in the field of neurological disease research can be retrieved from the Web of Science Core Collection. Analysis of relevant countries, institutions, journals, authors, keywords, and references is conducted using Microsoft Excel 2019, VOSviewer, and CiteSpace V. We analyze the research status and hot trends through burst detection.

Results: On October 23, 2022, 746 records of studies on the application of radiomics in the diagnosis of neurological disorders were retrieved and published from 2011 to 2023. Approximately half of them were written by scholars in the United States, and most were published in Frontiers in Oncology, European Radiology, Cancer, and SCIENTIFIC REPORTS. Although China ranks first in the number of publications, the United States is the driving force in the field and enjoys a good academic reputation. NORBERT GALLDIKS and JIE TIAN published the most relevant articles, while GILLIES RJ was cited the most. RADIOLOGY is a representative and influential journal in the field. "Glioma" is a current attractive research hotspot. Keywords such as "machine learning," "brain metastasis," and "gene mutations" have recently appeared at the research frontier.

Conclusion: Most of the studies focus on clinical trial outcomes, such as the diagnosis, prediction, and prognosis of neurological disorders. The radiomics biomarkers and multi-omics studies of neurological disorders may soon become a hot topic and should be closely monitored, particularly the relationship between tumor-related non-invasive imaging biomarkers and the intrinsic micro-environment of tumors.

KEYWORDS

radiomics, bibliometrics, nervous system diseases, glioblastoma (GBM), deep learning, multi-omics study

1. Introduction

Radiomics was first proposed by PhilippeLambin, a Dutch scholar, in 2012 to measure the shape of tumors and analyze the differences in image texture (1). With the rapid development of medical imaging and artificial intelligence, there has been an increasing number of research in the field of medical image analysis, such as disease prevention, diagnosis, treatment efficacy evaluation, and prognosis prediction (2–7).

In recent years, digital medical imaging has gradually transformed into high-dimensional data suitable for data mining and data science techniques. Aided by powerful computing power and Quantitative Image Analysis (QIA) technologies, radiomics has made rapid development (8). Currently, radiomics and deep learning are the most researched technologies in the field of medical imaging. Radiomics involves high-throughput extraction of a large amount of quantifiable information from regions of interest (ROI) in digital medical images. Deep learning, as a classic artificial intelligence methods, transforms the extractions into hundreds or thousands of quantitative imaging features (9). Then, quantitative extraction and analysis of image features, which roughly include first-order histograms, shape, texture, and wavelets, is performed to establish prediction models for clinical decision support. Unlike traditional computer-aided diagnosis (CAD), radiology focuses on providing information about human diseases from a deep and latent perspective, and the recognition of high-dimensional heterogeneous information in images by radiology is incomparable to traditional CAD.

As the development of Artificial Intelligence (AI) techniques, such as deep learning and convolutional neural networks, it has greatly advanced the performance of computer vision systems (10). These AI methods have enabled vision systems to achieve remarkable results in a wide range of applications, including object detection, video classification, and image segmentation. With the advancement of deep learning algorithms, AI-based methods such as convolutional neural networks (CNNs) (11) and recurrent neural networks (RNNs) (12) have been developed to analyze imaging data and make predictions with high accuracy. Among these applications, AI-based approaches have made preliminary exploration in the field of radiomics. These AI-based radiomics methods have the potential to improve disease diagnosis (13) and treatment decision-making (14), as well as facilitate the development of precision medicine (15).

The workflow of radiomics inspired by AI includes image acquisition and segmentation, radiomics feature extraction, and model building. Once the data is collected and organized, ROI is usually segmented for analysis by qualified professionals such as doctors, either manually or semi-automatically. Some research has shown that the results of automatic image segmentation using deep learning methods are more satisfactory (16, 17). The feature extraction step is noteworthy as different implementations produce different radiomics values, and radiomics models are only applicable to the same feature interpretation. The appearance of the Image Biomarker Standardization Initiative (IBSI) is expected to reduce the impact of this problem (18). Once the image acquisition and radiomics feature extraction are complete, machine learning algorithms can be used to build radiomics models. For example, the software provided by Chen et al. (19) includes the implementation of various modeling algorithms such as decision trees, logistic regression, complex random forests, Bayesian networks, and support vector machines (20–23). These models can also be optimized for specific performance metrics, and the receiver operating characteristic curve (AUC) (6) is widely used for optimization. Another tool to evaluate the models is the calibration plot (24), which describes the relationship between the true sample class and the model prediction probability. Overall, the selection of appropriate modeling algorithms is still an active area of research.

An important reason for the widespread development of radiomics AI methods is that, as the increases of the incidence of neurological diseases and the ratio of disability and death, traditional imaging techniques can only qualitatively describe the lesions, and provide size, shape, and other characteristics which can be similarly recognized by the naked eye. For non-visualized quantitative data such as textures and histograms, direct visualization is not available (25). Radiomics can overcome these shortcomings. Zhang et al. (26) developed an algorithm for fully automatic segmentation of glioblastoma regions in MRI and compared it with a reference established by manual tumor segmentation. The results showed that the algorithm was able to extract most image features with moderate or high accuracy. Meanwhile, Upadhaya et al. (27) attempted to use radiomics for grading and prognostic estimation of glioblastoma multiforme (GBM) and achieved 90% accuracy. Gillies et al. (8) proposed that quantitative features in radiomics include not only imaging features but also clinical and genetic information. This article is currently the most representative review of radiomics research.

In the 2016 World Health Organization Classification of tumors of the central nervous system (WHOC), the key features of the phenotype are combined with genotype, providing new ideas for precise classification, grading, and participation in treatment decision-making of brain tumors (28). The application of machine learning combined with radiomics in the classification, prediction, and prognostic assessment of neurological diseases has increased explosively (29–31). Researchers have gradually shifted their focus to improving the reproducibility of radiomics features, standardizing MRI, and multi-index joint diagnosis, prediction, and prognosis (32–34).

With the continuous progress of radiomics in the study of central nervous system diseases, it is crucial to understand the new trends and key milestones in related knowledge development. However, few systematic analysis have been carried out on these publications. Bibliometrics analysis has been widely used to organize knowledge structures and explore the trends of extensive research fields, including quantitative analysis of patterns in the scientific literature (19). Several studies have shown that CiteSpace focuses on finding the key points in the development of a domain, especially key turning points. Due to its rich functionality, it has become an effective method for analyzing big data at present (35, 36). To the best of our knowledge, there has been no systematic bibliometric analysis of radiomics in neurological disease research. Therefore, we will describe the scientific results of radiomics in the study of central nervous system diseases to identify trends and hotspots, and guide the future work of researchers.

2. Methods

2.1. Search strategy

The data was downloaded from the Science Citation Index Extended database of the Web of Science Core (WoSCC) on October 26, 2022. The following search terms were used: ("radiomics") and ("brain" or "cerebrum" or "encephalon" or "pericranium" or "cerebral*" or "central nervous system") in the Topic field, including title, abstract, author keywords, and KeyWords Plus following continuing of existing search methods (37–39). Original articles and reviews written and published in English between 2011 and 2022 were included. The result of the survey was 764 records, which were obtained from this study.

2.2. Data collection and analysis

All records retrieved from WoSCC were downloaded independently by two authors, including the number of publications published annually; country/region, institution, journal, and author output; citation frequency; and H-index. The H-index represents the number of academic journals or scholars/countries/regions that have published H papers, each of which has been cited at least H times It is used to evaluate the scientific impact of authors or countries. Journal Citation Reports (JCR) 2022 was used to obtain the impact factor (IF) of journal categories. The data were then transformed into Microsoft Excel 2019, VOSviewer, and CiteSpace V for the analysis of basic indicators. Microsoft Excel (v.2019) was used to analyze and organize the data on the basic characteristics of publications and citations by plotting the annual publication output, H-index, total IF, and average IF, citation count per article, and total citation count for each country/region.

VOSviewer (36) was used to create network visualization maps to analyze the collaboration among countries/regions, institutions, and highly cited reference authors. Furthermore, VOSviewer can categorize keywords with high co-occurrence frequency into multiple clusters, and color them simultaneously according to the timeline. Co-occurrence analysis determines the research hotspots and trends. We choose "author keywords" as the unit of analysis.

We use CiteSpace V for a merged analysis of journals, references, and clusters, and further constructed a merged reference timeline view, through which the rise and development periods of some cluster fields can be better understood. In addition, CiteSpace can capture keywords with strong reference outbreaks, and construct a visualization map for all projects. Citation burst is a key indicator for recognizing emerging trends (19). We set the "number of years per slice" and "number of years before each slice" to 1 and 50, respectively. Thus, the network map is extracted from the top 50 references cited in the first year of each article.

3. Results

3.1. Publication output and temporal trend

According to the citation analysis from the Web of Science, a total of 764 publications met the inclusion criteria, consisting

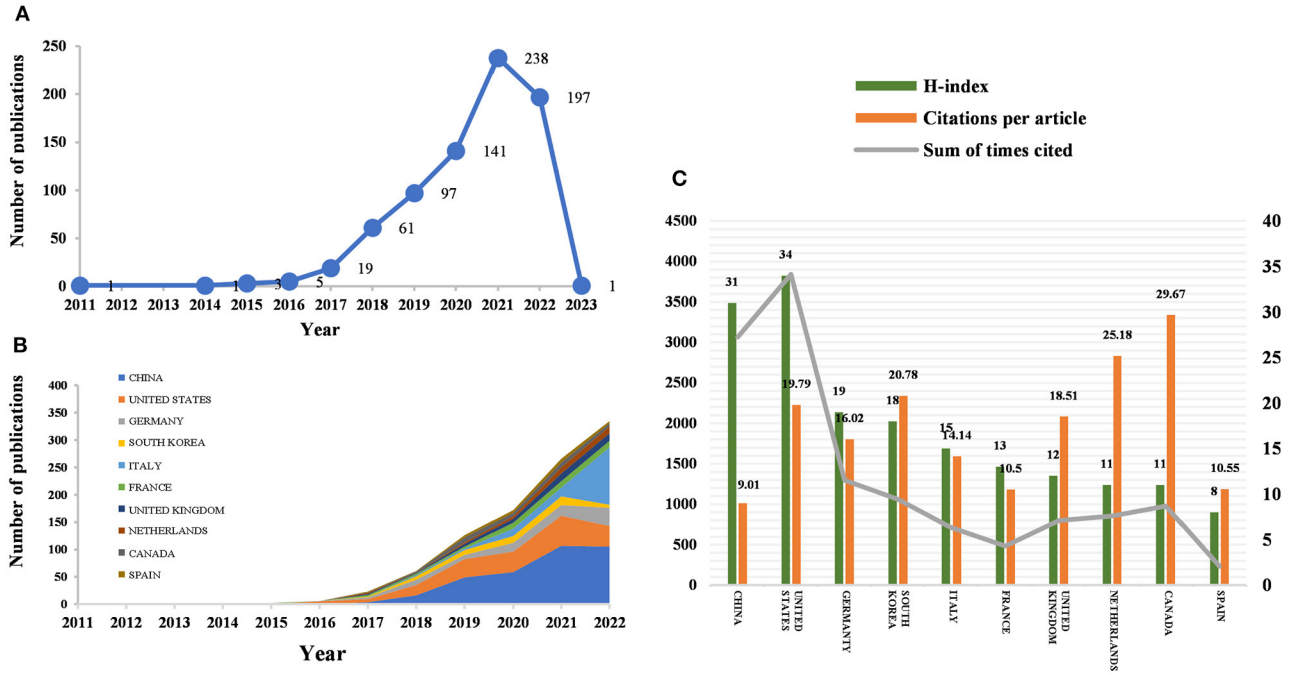

FIGURE 1
Number of publications and analysis trends of radiomics countries/regions in neurological disease research. **(A)** Annual global publication output. **(B)** Trends in publication output growth for the top 10 countries. **(C)** H-index, number of citations per article, and total number of citations in the top 10 countries/regions.

TABLE 1 Top 10 producing countries/regions and institutions related to radiomics in neurological disease research.

Rank	Countries/Regions	Articles (*N*)	Percentage (*N*)	H-index	Citations per article	Times cited	Rank	Institutes	Articles (*N*)	Percentage (*N*)	Location
1	China	340	44.503	31	9.01	3,064	1	Fudan University	45	5.89	China
2	United States	194	25.393	34	19.79	3,839	2	Chinese Academy of Sciences	41	5.366	China
3	Germany	81	10.602	19	16.02	1,298	3	Capital Medical University	38	4.974	China
4	South Korea	51	6.675	18	20.78	1,060	4	General Electric	35	4.581	United States
5	Italy	50	6.545	15	14.14	707	5	Helmholtz Association	34	4.45	Germany
6	France	46	6.021	13	10.5	483	6	Institut National de la Sante et de la Recherche Medicale INSERM	33	4.319	France
7	United Kingdom	45	5.628	12	18.51	833	7	Institute of Automation CAS	27	3.534	China
8	Netherlands	34	4.45	11	25.18	856	8	UDICE French Research Universities	26	3.403	France
9	Canada	33	4.319	11	29.67	979	9	Harvard University	24	3.141	United States
10	Spain	22	2.88	8	10.55	232	10	University of Chinese Academy of Sciences CAS	24	3.141	China

of 647 articles and 117 reviews (Figure 1A). In the early stage of research, the average annual citation frequency of published articles was low due to the lack of research on the application of radiomics in neurological diseases. From 2011 to 2017, the field was in a low-heat period with fewer than 30 articles of related research reports. However, from 2018 to 2022, the number of articles published on radiomics in the field of neurological diseases has been steadily increasing, with 61 articles published in 2018 alone, surpassing the previous total. The situation indicates the increasing attention in this field. Since 2018, the average annual citation frequency of published articles has rapidly increased and stabilized at around 300 per year, further indicating that the study of radiomics in neurological diseases has reached a more mature stage. The reason may be due to an increase in the number of neurological disease patients worldwide, as well as the result of interdisciplinary fusion and continuous innovation. In the past 3 years, the number of papers published in this field has shown a clear upward trend, with more than 90 papers published each year appearing in highly active states. With an average annual increase of 70 papers and an average annual growth rate of 57.43%, this indicates that research in this field has received increasing attention. While 197 articles have been published in 2022 so far, this number does not reflect the total number of publications throughout the year. To date, these articles have been cited 10,187 times, averaging 13.3 citations per article.

3.2. Distribution by country/region and institution

Between 2011 and 2023, all publications were published in 49 countries/regions and 1,291 institutions (Table 1). China has the most publications (194, 44.503%), followed by the United States (81, 25.393%), South Korea (51, 6.675%), Italy (50, 6.545%), and France (46, 6.021%). With the exception of the United States, all other countries have been published after 2017. Since 2018, China has ranked first in annual publication volume. However, among the five most productive countries, China has the lowest average IF. The annual growth rate of publications produced by the United States and Germany also follows a similar trend. Since 2020, although Italy's cumulative publication count from 2011 to 2022 ranked fifth (50), its annual publication output has grown rapidly exceeding China's by 2022. The total trend of the published numbers by these countries each year shows that since 2017, the number of papers has rapidly increased (Figure 1B). China has 3,064 citations and a citation/article ratio of 44.503, ranking first among all selected countries/regions, but its citations per article (9.01) are far lower than that of Canada (29.67). However, Canada's total number of articles (33) and H-index (11) are relatively weak performance. The H-index is a new method for evaluating academic achievements, and a higher H-index indicates that papers are more influential. Combining these paper evaluation indicators, the United States, China, and Canada are the three most influential countries in this research field. From this, we further determined the annual national output of the 10 most productive countries/regions (Figure 1C).

To investigate international cooperation, we constructed a network visualization map of publications in radiomics studies of neurological diseases using VOSviewer. Figure 2A displays

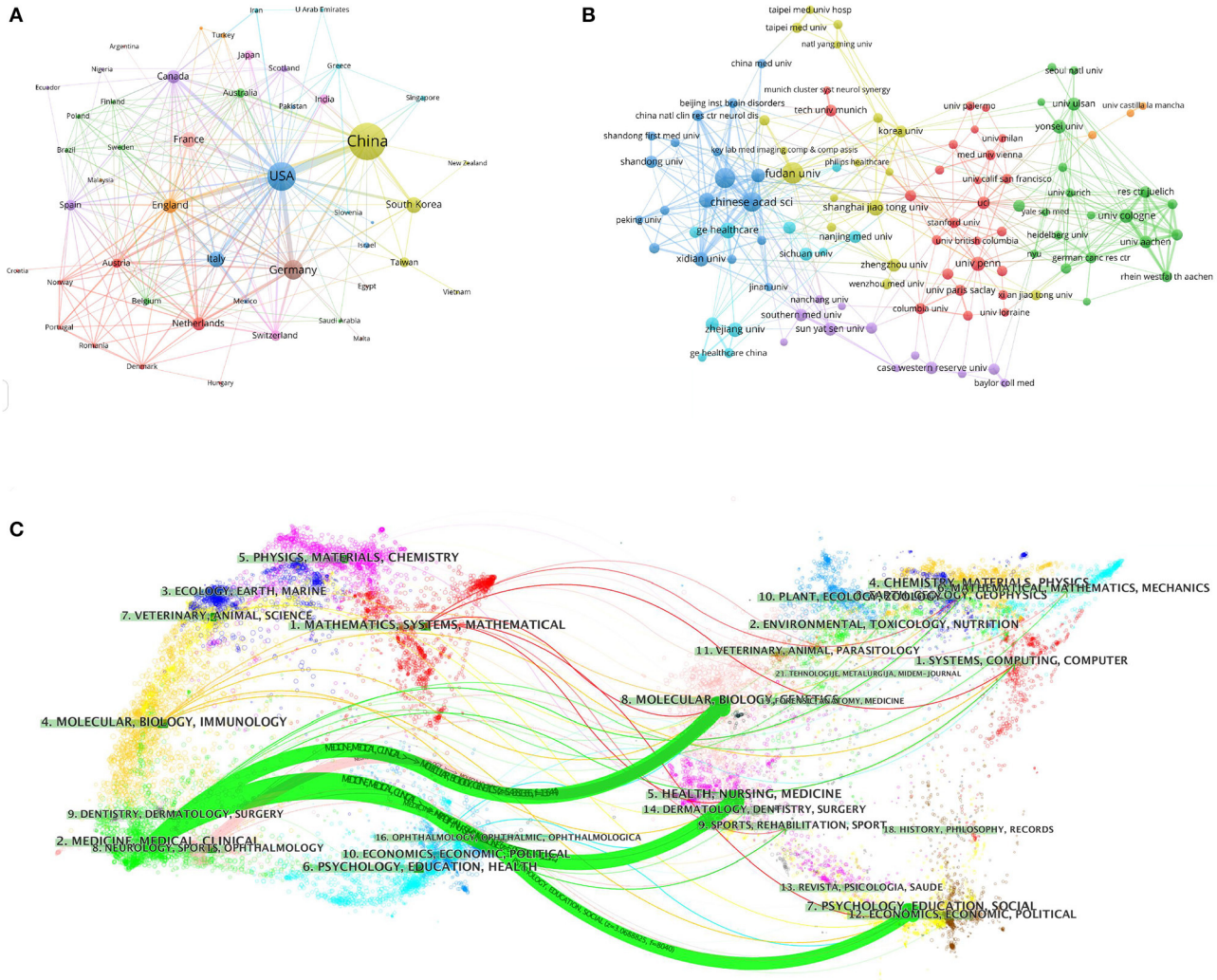

FIGURE 2
Visualization map of the VOSviewer network of countries/regions and institutions involved in radiomics in neurological diseases. **(A)** Collaboration analysis by country/region. **(B)** Collaboration analysis by agency. **(C)** Double graph superposition of citations of articles on the application of radiomics in neurological diseases (the left side is the cited journal, the right side is the cited journal, and the curve path represents the citation relationship).

the collaboration between countries/regions that published more than 10 papers (38 out of 76 papers). Countries/regions with high co-occurrence rates are grouped into the same color. Countries/regions with similar colors are identified as having closer collaboration and forming clusters. The width of the lines represents the scale of cooperation. The United States (220) has the highest total contact strength, indicating its participation in most of the world's collaborations. The countries/regions that cooperate most with the United States are China, Germany, the United Kingdom, Canada, France, and the United States. The yellow cluster is led by China and cooperates most with the United States, Germany, the United Kingdom, and South Korea. As is shown in Figure 2B, there is less cooperation between the most influential countries, and future cooperation should be strengthened to further promote the development of this field. Table 1 shows the 10 most effective institutions in related research. The main institutions are Fudan University (45, 5.89%), the Chinese Academy of Sciences (41, 5.366%), Capital Medical University (38, 4.974%), General Electric (35, 4.581%), and Helmholtz Association (34, 4.45%).

3.3. Distribution by journal

A total of 764 publications on brain disease radiomics research have been published in 257 academic journals. Table 2 lists the 10 most productive and frequently cited journals. FRONTIERS IN ONCOLOGY (62 articles, 7.984%) with an IF of 5.78 has the most publishments, followed by EUROPEAN RADIOLOGY (53 articles, 6.937%), CANCERS (34 articles, 6.97%), SCIENTIFIC REPORTS (33 articles, 4.319%), and FRONTIERS IN NEUROSCIENCE (28, 3.665%). The Journal of MAGNETIC RESONANCE IMAGING has the highest IF (13.029) among the top 10 most influential journals in 2019, while EUROPEAN RADIOLOGY has the highest H-index (19). Among the 10 most productive journals, 4 are

TABLE 2 Top 10 productive and co-cited journals for radiomics research in neu authors and co-cited authors.

Rank	Productive journal	Articles (*N*)	Percentage (*N*)	IF (2022)	H-index	Quartile in category	Rank	Co-cited journal	Articles (*N*)	IF (2022)	H-index	Best quartile
1	FRONTIERS IN ONCOLOGY	61	7.984	5.738	10	Q2	1	RADIOLOGY	552	29.146	4	Q1
2	EUROPEAN RADIOLOGY	53	6.937	7.034	19	Q1	2	EUROPEAN RADIOLOGY	411	7.034	4	Q1
3	CANCERS	34	4.45	6.575	7	Q1	3	SCIENTIFIC REPORTS	396	4.996	15	Q2
4	SCIENTIFIC REPORTS	33	4.319	4.996	15	Q2	4	AMERICAN JOURNAL OF NEURORADIOLOGY	390	4.966	5	Q2
5	FRONTIERS IN NEUROSCIENCE	28	3.665	5.152	7	Q2	5	NEURO ONCOLOGY	379	13.029	9	Q1
6	FRONTIERS IN NEUROLOGY	16	2.094	4.086	4	Q2	6	PLOS ONE	337	3.752	4	Q2
7	MEDICAL PHYSICS	14	1.832	4.506	5	Q2	7	JOURNAL OF MAGNETIC RESONANCE IMAGING	318	5.119	7	Q1
8	NEURO ONCOLOGY	14	1.832	13.029	9	Q1	8	NEUROIMAGE	266	7.4	1	Q1
9	JOURNAL OF MAGNETIC RESONANCE IMAGING	13	1.702	5.119	7	Q1	9	CLINICAL CANCER RESEARCH	251	13.801	4	Q1
10	NEURORADIOLOGY	13	1.702	2.995	6	Q3	10	MAGNETIC RESONANCE IMAGING	240	3.13	3	Q3

10.3389/fneur.2023.1171167

TABLE 3 Top 11 prolific authors and co-cited authors of radiomics studies in neurological diseases.

Rank	Author	Count (*N*)	Rank	Co-cited author	Count (*N*)
1	NORBERT GALLDIKS	166	1	GILLIES RJ	286
2	JIE TIAN	16	2	LAMBIN P	285
3	PHILIPP LOHMANN	13	3	AERTS HJWL	197
4	JI EUN PARK	13	4	LOUIS DN	185
5	HO SUNG KIM	12	5	Van GRIETHUYSEN JJM	174
6	MARTIN KOCHER	12	6	KICKINGEREDER P	153
7	ZHENYU LIU	11	7	OSTROM QT	106
8	PEIPEI PANG	11	8	KUMAR V	104
9	SUNG SOO AHN	10	9	ZWANENBURG A	98
10	DINGGANG SHEN	9	10	HARALICK RM	92
11	KARLJOSEF LANGEN	9	11	STUPP R	86

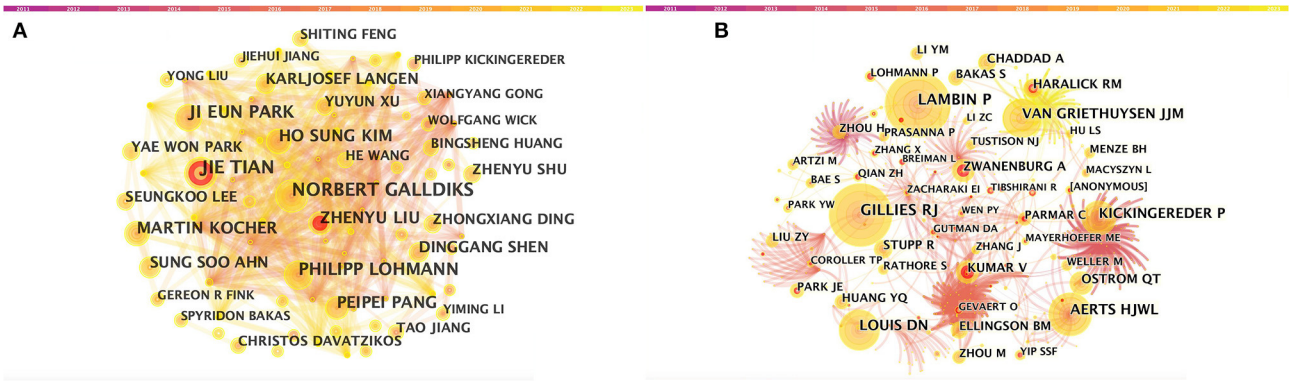

FIGURE 3
CiteSpace visualization of authors. **(A)** Co-occurrence of authors. **(B)** Co-cited authors involved in radiomics neurological disease research. The circle node represents the author of the paper. Links between nodes represent partnerships.

classified in Q1, 5 in Q2, and one in Q3. The most frequently co-cited journal is RADIOLOGY (552 cited, Q1), with the highest IF (29.146) in 2021. The next most frequently cited journals are EUROPEAN RADIOLOGY (411 cited, Q2), SCIENTIFIC REPORTS (396 cited, Q1), the AMERICAN JOURNAL OF NEURORADIOLOGY (390 cited, Q3), and NEURO ONCOLOGY (379 cited, Q1). The dual map shows three main reference paths. The left side shows the research frontier, with articles concentrated in journals in the medical, neurological, and clinical fields, while the right side shows the cited region, with articles primarily published in journals in the molecular, biological, genetic, psychological, health, nursing, and medical fields (Figure 2C).

A total of 5,026 authors participated in the study. Table 3 shows the 11 most productive authors. NORBERT GALLDIKS and JIE TIAN each published 16 articles, ranking first in the number of publications, followed by PHILIPP LOHMANN and JI EUN PARK (13 papers), HO SUNG KIM and MARTIN KOCHER (12 papers), and Zhengyu LIU and ZhengYU LIU (11 papers; Figure 3A and Table 3). It is worth noting that the concentration of authors is relatively low (<0.03), indicating that the authors' impact on neurological disease radiomics research needs to be increased. In this figure, each node represents an author, the larger the node, the more articles are published. The thick lines indicate close cooperation between authors, as can be clearly seen in Figure 3A, there is communication and cooperation between authors in this field. Co-cited authors refer to those commonly cited in publications, which are critical indicators of author contributions. Figure 3B and Table 3 show the top 11 co-cited authors, with only eight authors having more than 100 times citations, where GILLIES RJ (286) ranked first, followed by LAMBIN P (285), AERTS HJWL (197), and LOUIS DN (185). Upadhaya is an early researcher in the field of neurological system radiomics research.

Upadhaya is an early researcher of radiomics research in the nervous system. In 2017, he first proposed a prognostic model of glioblastoma multiforme based on multimodal MRI, marking the beginning of radiomics in the field of the nervous system. Meanwhile, Galldiks et al. (40) has published the most articles. In 2020, he summarized the imaging challenges related to immunotherapy, targeted therapy, and brain metastasis combined with radiotherapy. This paper also reviewed advanced imaging techniques that could overcome some of these imaging challenges. It provides valuable information for the identification

FIGURE 4
Analysis of references related to radiomics in the study of neurological diseases. **(A)** Network of co-cited references. **(B)** Network diagram of co-reference clusters.

of changes and recurrences caused by treatment in brain metastasis lesions, and the evaluation of treatment responses. In the same year, Kim et al. (41) proposed a method using diffusion and perfusion-weighted MRI radiomics models to predict isocitrate dehydrogenase (IDH) mutation and tumor aggressiveness in diffuse low-grade gliomas. In this paper, multiparameter MRI radiomics models are also utilized to predict tumor grades.

In 2021, PHILIPP LOHMANN reviewed the basics, current workflows, and methods of radiomics, and focused on the application of feature-based radiomics in neural tumors with clinical examples. Additionally, he studied the usage of FET-PET radiomics in identifying glioma relapse and progression (42, 43). Park et al. (44) is a senior researcher in the neurological disease radiomics field. By using deep learning to automatically segment diffusion and perfusion MRI radiomics, he provided a reproducible and comparable diagnostic model for glioblastoma. He concluded that the first-level feature extraction based on automatically segmented MRI has high reproducibility and comparable diagnostic efficiency with manual segmentation. This field remains a key focus of radiomics in the research of nervous system diseases.

3.4. Analysis of co-cited references

Among the top 10 co-cited articles, four were critical articles, two were on radiomics, and four were on nervous system diseases. Additionally, these studies are considered reliable references for future relevant research. It's worth noting that among the top five co-cited references, there are no articles about radiomics research in the nervous system, which indicates that the field still requires further research (Figure 4A and Table 4). The network diagram of co-reference clusters is shown in Figure 4B, and the data collection is shown in Table 5. In 2014, Aerts and HJWL extracted 440 features from computer tomography scan data of 1,019 lung or head or neck cancer patients, and conducted radiology analysis on the image intensity, shape, and texture of the tumors. The results concluded that a large number of radiomics features have predictive capabilities in an independent dataset of cancer and head and neck cancer patients. He also proposed the concept of radiomics genomics and showed that radiomics genomics features can capture tumor heterogeneity with underlying gene expression patterns (45). This study is considered a significant milestone and marks the transition of radiomics genomics from basic research to clinical application. Kickingereder et al. (46) demonstrated that compared to established clinical radiomics risk models, radiomics-based magnetic resonance imaging signals can improve the accuracy of predicting survival and stratification of newly diagnosed glioblastoma patients.

In 2017, Bakas et al. (47) collected the segmentation labels and radiological features of preoperative multimodal magnetic resonance imaging (MRI) of gliomas from multiple institutions in the Cancer Genome Atlas (TCGA), and collected stratified gliomas by preoperative scans. The significant value of the study lies in the fact that the data is publicly available. The generated labels and imaging features can be used for repeatable and comparable quantitative studies, providing guidance for addressing reproducibility and feature interpretation problems. Van Griethuysen et al. (48) proposed a theory that the lack of standardized definitions and image processing severely affects the reproducibility and comparability of research results. They developed a flexible open-source platform PyRadiomics and discussed the workflow and architecture of PyRadiomics. This study demonstrates its application in the feature analysis of lung lesions which is expected to address the standardization problem of algorithms and image processing. In 2020, Zwanenburg et al. (18) proposed the Image Bio-Marker Standardization Initiative and standardized 174 radiomics features, providing a foundation for the validation and calibration of different radiomics software. It also provided an effective solution to the current common data island problem. Despite the involvement of a large number of literature in the feature standardization study, it still lacks a better solution.

3.5. Analysis of keyword co-occurrenceclusters

Keywords were condensed and extracted from the content of an article to reflect the topic and content of a representative article. High-frequency keywords are often used to reflect the

TABLE 4 10 commonly cited literatures in imageomics research of nervous system diseases.

Rank	Co-citations (*N*)	Centrality	First author	Year	Title	Journal	DOI	Cluster
1	218	0.01	Gillies, RJ	2016	Radiomics: images are more than pictures, they are data (survey)	Radiology	10.1148/radiol.2015151169	#4
2	176	0	Van Griethuysen, JJM	2017	Computational radiomics system to decode the radiographic phenotype	Cancer Research	10.1158/0008-5472.CAN-17-0339	#4
3	134	0.02	Lambin, P	2017	Radiomics: the bridge between medical imaging and personalized medicine (survey)	Nature Reviews Clinical Oncology	10.1038/nrclinonc.2017.141	#4
4	114	0.01	Louis, DN	2016	The 2016 World Health Organization classification of tumors of the central nervous system: a summary	Acta Neuropathologica	10.1007/s00401-016-1545-1	#4
5	70	0.13	Aerts, HJWL	2014	Decoding tumor phenotype by noninvasive imaging using a quantitative radiomics approach	Nature Communications	10.1038/ncomms5006	#4
6	66	0	Aerts, HJWL	2020	The image biomarker standardization initiative: standardized quantitative Radiomics for high-throughput image-based phenotyping	Radiology	10.1148/radiol.2020191145	#2
7	56	0.1	Kickingereder, P	2016	Radiomic profiling of glioblastoma: identifying an imaging predictor of patient survival with improved Performance over established clinical and radiologic risk models	Radiology	10.1148/radiol.2016160845	#3
8	54	0.01	Bakas, S	2017	Data descriptor: advancing the cancer genome atlas glioma MRI collections with expert segmentation labels and radiomic features	Scientific data	10.1038/sdata.2017.117	#4
9	45	0.04	Yip, SSF	2016	Applications and limitations of radiomics (survey)	Physics in medicine and biology	10.1088/0031-9155/61/13/R150	#4
10	44	0.27	Zhou, H	2017	MRI features predict survival and molecular markers in diffuse lower-grade gliomas	Neuro-oncology	10.1093/neuonc/now256	#3

10.3389/fneur.2023.1171167

TABLE 5 Top 10 co-cited reference clusters for radiomics studies in neurological diseases.

Cluster ID	Size	Silhouette	Mean (Year)	Top terms
0	40	0.896	2016	Glioma imaging
1	40	0.915	2017	Radiotherapy
2	34	0.947	2016	Prognostic biomarker
3	32	0.982	2018	Tumor aggressiveness
4	32	0.992	2014	Stereotactic radiosurgery
5	31	0.921	2016	Multiple pathologic biomarkers
6	29	0.958	2014	Risk stratification
7	29	0.975	2019	Glioblastoma
8	29	0.994	2018	Radiomics classification
9	29	0.959	2018	Machine learning applications

hot topics in the research field. Thus, a keyword co-occurrence network is an analysis method based on text content. The authors collect 383 keywords (Figure 5A) and find the top 25 most frequently cited keywords through keyword burst analysis (Figure 5B). The blue line represents the time interval, and the red line represents the burst period of the keywords. As can be seen from the figure, the burst keywords are mainly concentrated on the research of radiomics and brain-related diseases, including but not limited to disease risk analysis, treatment, and tumor heterogeneity. Feature selection, patterns, magnetic resonance spectroscopy analysis, and image segmentation are the pioneering explorations in the early stage. Since then, positron emission tomography (PET), imaging biomarkers, radiotherapy, support vector machines, feature selection, tumor heterogeneity, image texture features, and disease prognostic evaluation became hot topics. In recent years, computed tomography (CT), nomograms, brain metastasis, machine learning, and gene mutations have become new key keywords for outbreaks.

The results in Figure 5C calculated by the log-likelihood ratio (LLR) show the keyword radiation. The clustering analysis shows outstanding homogeneity through 17 cluster centers with a modularity score of 0.781 and an average silhouette value of 0.8346. They encompass a wide range of radiomics topics in the field of neurological diseases, including artificial intelligence and imaging techniques [# 0 mri (32), # 2 radiomics (32), # 3 nomogram (33), and # 5 deep learning (33)] and indications [# 1 Alzheimer's disease (34), # 4 Meningioma (35), # 6 ruptured aneurysm (36), # 7 brain metastases (37), # 8 treatment (38), # 9 prognosis (38), # 10 high-grade glioma (38), # 11 tumor heterogeneity (38), # 12 intracerebral hemorrhage (39), and # 13 tumor detection (39); Figures 5C, D]. In recent years, the advancement of AI technology has significantly improved the status of radiomics research, making it a hot topic in the field of the combination of medicine and engineering. This has brought new opportunities for clinical diagnosis and treatment. Moreover, radiomics has also been proven to have good performance in the diagnosis, prediction, and prognosis of nervous system diseases. Recent researches are more focused on the relationship between radiomics markers and the internal microenvironment of nervous system diseases, particularly the correlation between tumor heterogeneity, immunity, metabolism, and imaging markers. The reproducibility and reliability of the models have always been a focus of research and are expected to be solved in the future with further development of wireless technology.

4. Discussion

In recent years, increasing numbers of systematic and narrative reviews have focused on the application of radiomics in the study of nervous system diseases (49–52). The use of radiomics techniques is highlighted in image segmentation, prognosis, and non-invasive biomarker applications. An advantage of bibliometrics analysis compared to traditional surveys is that it provides the reader with an intuitive visualization of the research situation on a particular topic. Here, we conducted a novel bibliometric analysis to explore the publications of the past decade and provide a comprehensive view of research trends.

As the concept of radiomics was first proposed in 2012, we searched the data from 2012. The sudden rapid growth is related to the magnetic resonance imaging features proposed by Zhou et al. (53) that it can be used to predict the survival time and molecular distribution of low-grade gliomas (LGGs). Texture analysis of MRI data can accurately predict IDH1 mutation, 1p/19q co-deletion, histological grading, and tumor progression. This highly cited study is considered a leap in radiomics from the macroscopic features of gliomas to the microscopic internal environment, greatly driving the research in this field. A machine learning model based on morphological features derived from Pyradiomics was used to predict aneurysm stability (54), and this marked the beginning of widespread research on radiomics in the field of nervous system diseases. Subsequently, Tupe-Waghmare et al. (55) proposed that compared to traditional risk factors, radiomics models based on deep learning performed better in predicting the survival rate of glioblastoma multiforme. To further this work, they proposed a radiomics nomogram, which proved its good predictive performance and showed that multi-variable models have statistical robustness in survival analysis (56–59). In this section, the narrative logic will unfold from two aspects, traditional explorations and deep learning processing.

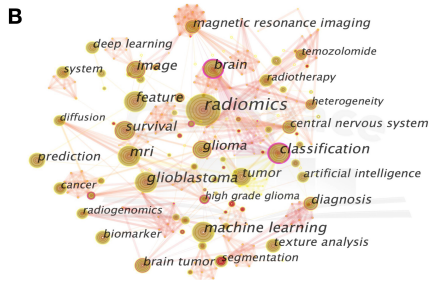

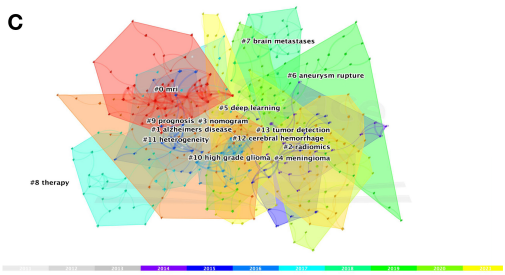

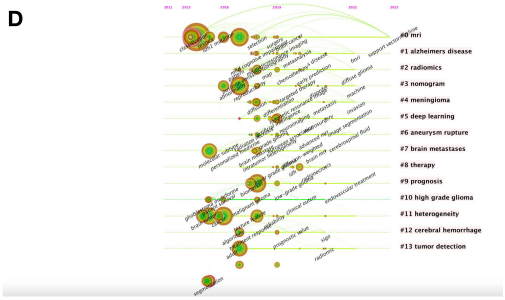

Top 25 Keywords with the Strongest Citation Bursts

A

Keywords	Year	Strength	Begin	End	2011 - 2023
feature selection	2011	2.2	2015	2019	
cancer	2011	2.1	2016	2019	
magnetic resonance spectroscopy	2011	1.87	2016	2018	
resection	2011	2.32	2017	2019	
pattern	2011	2.03	2017	2019	
positron emission tomography	2011	2.95	2018	2019	
imaging biomarker	2011	2.65	2018	2020	
radiation therapy	2011	2.23	2018	2020	
support vector machine	2011	1.96	2018	2019	
selection	2011	1.96	2018	2019	
radiosurgery	2011	1.96	2018	2019	
heterogeneity	2011	1.93	2018	2020	
textural feature	2011	4.71	2019	2020	
segmentation	2011	4.64	2019	2020	
prognosis	2011	2.91	2019	2020	
multiforme	2011	2.06	2019	2021	
meningioma	2011	3.38	2020	2021	
risk	2011	2.39	2020	2021	
therapy	2011	2.27	2020	2021	
mutation	2011	1.94	2020	2023	
machinelearning	2011	3	2021	2023	
nomogram	2011	2.71	2021	2023	
computed tomography	2011	2.29	2021	2023	
brain metastase	2011	1.94	2021	2023	
artificial intelligence	2011	1.94	2021	2023	

FIGURE 5
CiteSpace visualization of keywords in radiomics studies of neurological diseases. **(A)** Key keywords network in radiomics neurological disease research and related research publications. **(B)** Time trend plot of emergent keywords. **(C)** Keyword cluster analysis. **(D)** Timeline view of Keywordclusters.

First we analyze the traditional explorations and traditional imaging techiniques. Since 2018, a large number of radiomics studies in the field of nervous system diseases have emerged, including glioma survival analysis and stratified prediction (60), the differential diagnosis of gliomas (61), and gene mutations (62). Meanwhile, the research on Alzheimer's disease is also growing (63). At the same time, the use of multi-parametric MRI to predict the IDH mutation status in glioblastoma (GBM) by employing multi-region radiomics features was also been discussed (64). The results showed that the multi-region model constructed by the whole-region features performed better than the single-region model, and the best performance was achieved when combined with the age-whole-region. Meanwhile, the research team made another attempt on predicting the O-6-methylguanine-DNA methyltransferase (MGMT) promoter methylation status of GBM based on a multi-region and multi-parametric MRI radiomics model, and the results showed that combining clinical factors with radiomics features does not improve predictive performance (65).

Another exploratory work provided by Bobholz et al. (66) investigated the local relationship between MR-derived radiomics features and histology-derived "tissue" features using a dataset of 16 brain cancer patients. Radiomics features were collected from T1, post-contrast T1, FLAIR, and diffusion-weighted imaging (DWI) acquired before death. Similar tissue features were collected from autopsy samples and registered via magnetic resonance imaging. The results showed that a subset of radiomics features can consistently capture texture information of histological tissue. Su et al. (56) combined eight imaging features and three clinical variables (age, sex, and tumor location) to construct an imaging omic-clinical nomogram. The nomogram presented good discrimination in predicting the isocitrate dehydrogenase 1 (IDH1) mutation status of primary GBMs. On the other hand, Sakai et al. (67) found that the XGBoost model trained on DWI data can achieve an accuracy of 90% in predicting IDH1 mutation status, but the model trained based on combined FLAIR-DWI radiomics features could not improve the accuracy.

Following these ideas, the research became more detailed, including automatic image segmentation (68), multiple sclerosis (31), application of PET radiomics (69), and more advanced non-invasive identification of gene mutations (70). Guo et al. (2) investigated the role of Dsc-PWI dynamic radiomics features in the diagnosis and prognosis prediction of ischemic stroke. Cao et al. (71) used the radiomics features of MRI and 18F-FDG-PET and the joint application of multiple models to identify gliomas.

Alongi et al. (72) used AI-based 18F-FDG-PET to improve the accuracy of AD diagnosis. Yao et al. (73) evaluated the ability of pH and oxygen-sensitive MRI techniques to differentiate glioma genotypes and concluded that pH and oxygen-sensitive MRI is a viable and potentially valuable imaging technology to distinguish glioma subtypes and provide additional prognostic value in clinical practice. Dounavi et al. (74) suggested that FLAIR texture analysis can capture subtle alterations in white matter microstructural.

To analyze the deep learning processing part, one extraordinary method provided by Calabrese et al. (75) combined radiomics features and convolutional neural network (CNN) features, and the collaborative model performed well in predicting IDH1 and TERT promoter hotspot mutations, ATRX and CDKN2A/B pathogenic mutations, and chromosome 7 and 10 combined aneuploidy, but not well in predicting other biomarkers. The hybrid CNN-Transformer encoder based on multimodal MRI proposed by Cheng et al. (76) achieved good performance in both glioma segmentation and IDH gene typing prediction, outperforming single-task learning and other state-of-the-art methods.

Previous studies have found that the use of radiomics features as biomarkers of treatment response and outcome may be correlated with clinical phenotypes, histological features, and genomic features, but robust and reproducible features are needed to address this issue. The low replicability potential of the current study is still the reason why radiomics-based strategies have not yet been translated into routine practice. Tixier et al. (77) found that the robustness of radiomics features varied by category and features calculated based on Gray-level Size-zone Matrix (GLSZM), edge maps, and shape were less robust compared to histograms and co-occurrence matrics. Ma et al. (78) showed that first-order and GLCM features extracted from LoG and wavelet-filtered images were the most crucial factors for glioma recognition. Additionally, some eigenvalues were considered strongly correlated between low-grade glioma (LGG) and high-grade glioma (HGG).

Since plenty of scholars have been involved in studying the robust performance of deep learning feature models, the results are satisfactory compared to traditional machine learning models. However, the results of scientific research are still questionable because the performance of deep learning methods depends on high-level data processing capability and high-quality data requirements. On the other hand, the internal algorithm feature vectors in unsupervised deep learning may not always be transparent (black box) (79). It is worth illustrating that the research of feature reproducibility involves multiple aspects, including support from multi-center data and further research on image segmentation. Moreover, the optimal feature selection methods and the non-uniformity and standardization of features are also urgent problems to be solved.

4.1. Limitations

To the best of our knowledge, this bibliometric analysis is the first exploration of the development and trends of radiomics research in the field of neurological diseases. However, this study has some limitations. Firstly, the data used in this study was extracted only from the WoSCC database, as we believe this database is a reliable software for searching publications and citations, although it may contain fewer documents and journals than other databases such as Google Scholar or Scopus. Secondly, non-English articles were excluded from the database and analysis, which may have led to a source bias. Additionally, we selectively analyzed the characteristics of information, so some key points and details may have been missed.

5. Conclusion

Bibliometrics analysis indicates a good prospect and a significant increase in related publications for radiomics in the field of neurological diseases. The main contributors to this research area have been identified, and the related studies are clustered and mainly focused on the application of radiomics in glioma, brain metastasis, and white matter diseases. Differences between regions and countries still exist, and cooperation between countries needs to be strengthened. In the process of applying deep learning for handling radiomics data, there exists such a problem that the data is in a poorly interpreted form of image features, but this problem will be gradually solved with the advancement of technology. By using these methods, it helps better understand the prospects of radiomics in neurological diseases, and facilitates clinical diagnosis and treatment decisions, simplifies the diagnostic and therapeutic process, and ultimately benefits patients.

Data availability statement

The data was downloaded from the Science Citation Index Extended database of the Web of Science Core (WoSCC) on October 26, 2022. The following search terms were used: ("radiomics") and ("brain" or "cerebrum" or "encephalon" or "pericranium" or "cerebral*" or "central nervous system") in the Topic field, including title, abstract, author keywords, and KeyWords Plus. Original articles and reviews written and published in English between 2011 and 2022 were included. The result of the survey was 764 records, which were obtained from this study.

Author contributions

JC: data analysis and writing. XM: methodology. XY: validation. XQ: formal analysis. All authors contributed to the article and approved the submitted version.

Funding

This work was supported by grants from the ShaanXi Province science and technology plan projects (2022SF-166).

Conflict of interest

The authors declare that the research was conducted in the absence of any commercial or financial relationships that could be construed as a potential conflict of interest.

Publisher's note

References

1. Lambin P, Rios-Velazquez E, Leijenaar R, Carvalho S, Van Stiphout RG, Granton P, et al. Radiomics: extracting more information from medical images using advanced feature analysis. *Eur J Cancer*. (2012) 48:441–6. doi: 10.1016/j.ejca.2011.11.036

2. Guo Y, Yang Y, Cao F, Wang M, Luo Y, Guo J, et al. A focus on the role of DSC-PWI dynamic radiomics features in diagnosis and outcome prediction of ischemic stroke. *J Clin Med*. (2022) 11:5364. doi: 10.3390/jcm11185364

3. Wu G, Chen Y, Wang Y, Yu J, Lv X, Ju X, et al. Sparse representation-based radiomics for the diagnosis of brain tumors. *IEEE Trans Med Imaging*. (2017) 37:893–905. doi: 10.1109/TMI.2017.2776967

4. Liu D, Chen J, Ge H, Hu X, Yang K, Liu Y, et al. Differentiation of malignant brain tumor types using intratumoral and peritumoral radiomic features. *Front Oncol*. (2022) 12:848846. doi: 10.3389/fonc.2022.848846

5. Wu J, Li C, Gensheimer M, Padda S, Kato F, Shirato H, et al. Radiological tumour classification across imaging modality and histology. *Nat Mach Intell*. (2021) 3:787–98. doi: 10.1038/s42256-021-00377-0

6. Xu X, Zhang J, Yang K, Wang Q, Chen X, Xu B. Prognostic prediction of hypertensive intracerebral hemorrhage using CT radiomics and machine learning. *Brain Behav*. (2021) 11:e02085. doi: 10.1002/brb3.2085

7. Verduin M, Primakov S, Compter I, Woodruff HC, van Kuijk SM, Ramaekers BL, et al. Prognostic and predictive value of integrated qualitative and quantitative magnetic resonance imaging analysis in glioblastoma. *Cancers*. (2021) 13:722. doi: 10.3390/cancers13040722

8. Gillies RJ, Kinahan PE, Hricak H. Radiomics: images are more than pictures, they are data. *Radiology*. (2016) 278:563–77. doi: 10.1148/radiol.2015151169

9. Ibrahim A, Primakov S, Beuque M, Woodruff H, Halilaj I, Wu G, et al. Radiomics for precision medicine: Current challenges, future prospects, and the proposal of a new framework. *Methods*. (2021) 188:20–9. doi: 10.1016/j.ymeth.2020.05.022

10. Gu J, Wang Z, Kuen J, Ma L, Shahroudy A, Shuai B, et al. Recent advances in convolutional neural networks. *Pattern Recogn*. (2018) 77:354–77. doi: 10.1016/j.patcog.2017.10.013

11. He KM, Zhang XY, Ren SQ, Sun J. Deep residual learning for image recognition. In: *Proceedings of the IEEE Conference on Computer Vision and Pattern Recognition* (2016). p. 770–8. doi: 10.1109/CVPR.2016.90

12. Sherstinsky A. Fundamentals of recurrent neural network (RNN) and long short-term memory (LSTM) network. *Phys D*. (2020) 404:132306. doi: 10.1016/j.physd.2019.132306

13. Jones DT, Kerber KA. Artificial intelligence and the practice of neurology in 2035: the neurology future forecasting series. *Neurology*. (2022) 98:238–45. doi: 10.1212/WNL.0000000000013200

14. Hillis JM, Bizzo BC. Use of artificial intelligence in clinical neurology. *Semin Neurol*. (2022) 42:39–47. doi: 10.1055/s-0041-1742180

15. Vatansever S, Schlessinger A, Wacker D, Kaniskan HÜ, Jin J, Zhou MM, et al. Artificial intelligence and machine learning-aided drug discovery in central nervous system diseases: state-of-the-arts and future directions. *Med Res Rev*. (2021) 41:1427–73. doi: 10.1002/med.21764

16. Chen LC, Papandreou G, Kokkinos I, Murphy K, Yuille AL. Deeplab: Semantic image segmentation with deep convolutional nets, atrous convolution, and fully connected CRFs. *IEEE Trans Pattern Anal Mach Intell*. (2017) 40:834–48. doi: 10.1109/TPAMI.2017.2699184

17. Chen H, Li S, Zhang Y, Liu L, Lv X, Yi Y, et al. Deep learning-based automatic segmentation of meningioma from multiparametric MRI for preoperative meningioma differentiation using radiomic features: a multicentre study. *Eur Radiol*. (2022) 32:7248–59. doi: 10.1007/s00330-022-08749-9

18. Zwanenburg A, Vallières M, Abdalah MA, Aerts HJ, Andrearczyk V, Apte A, et al. The image biomarker standardization initiative: standardized quantitative radiomics for high-throughput image-based phenotyping. *Radiology*. (2020) 295:328–38. doi: 10.1148/radiol.2020191145

19. Chen C, Dubin R, Kim MC. Emerging trends and new developments in regenerative medicine: a scientometric update (2000-2014). *Expert Opin Biol Ther*. (2014) 14:1295–317. doi: 10.1517/14712598.2014.920813

20. Chen H, Li C, Zheng L, Lu W, Li Y, Wei Q. A machine learning-based survival prediction model of high grade glioma by integration of clinical and dose-volume histogram parameters. *Cancer Med*. (2021) 10:2774–86. doi: 10.1002/cam4.3838

21. Chen C, Ou X, Wang J, Guo W, Ma X. Radiomics-based machine learning in differentiation between glioblastoma and metastatic brain tumors. *Front Oncol*. (2019) 9:806. doi: 10.3389/fonc.2019.00806

22. Wu Y, Jiang JH, Chen L, Lu JY, Ge JJ, Liu FT, et al. Use of radiomic features and support vector machine to distinguish Parkinson's disease cases from normal controls. *Ann Transl Med*. (2019) 7:773. doi: 10.21037/atm.2019.11.26

23. Afshar P, Mohammadi A, Plataniotis KN. Bayescap: a Bayesian approach to brain tumor classification using capsule networks. *IEEE Signal Process Lett*. (2020) 27:2024–8. doi: 10.1109/LSP.2020.3034858

24. Steyerberg EW, Vickers AJ, Cook NR, Gerds T, Gonen M, Obuchowski N, et al. Assessing the performance of prediction models: a framework for some traditional and novel measures. *Epidemiology*. (2010) 21:128. doi: 10.1097/EDE.0b013e3181c30fb2

25. Caruana G, Pessini LM, Cannella R, Salvaggio G, de Barros A, Salerno A, et al. Texture analysis in susceptibility-weighted imaging may be useful to differentiate acute from chronic multiple sclerosis lesions. *Eur Radiol*. (2020) 30:6348–56. doi: 10.1007/s00330-020-06995-3

26. Zhang J, Barboriak DP, Hobbs H, Mazurowski MA. A fully automatic extraction of magnetic resonance image features in glioblastoma patients. *Med Phys*. (2014) 41:042301. doi: 10.1118/1.4866218

27. Upadhaya T, Morvan Y, Stindel E, Le Reste PJ, Hatt M. A framework for multimodal imaging-based prognostic model building: preliminary study on multimodal MRI in glioblastoma multiforme. *IRBM*. (2015) 36:345–50. doi: 10.1016/j.irbm.2015.08.001

28. Colen RR, Hassan I, Elshafeey N, Zinn PO. Shedding light on the 2016 World Health Organization Classification of Tumors of the Central Nervous System in the era of radiomics and radiogenomics. *Magn Reson Imaging Clin N Am*. (2016) 24:741–9. doi: 10.1016/j.mric.2016.07.001

29. Chen C, Zheng A, Ou X, Wang J, Ma X. Comparison of radiomics-based machine-learning classifiers in diagnosis of glioblastoma from primary central nervous system lymphoma. *Front Oncol*. (2020) 10:1151. doi: 10.3389/fonc.2020.01151

30. Hotta M, Minamimoto R, Miwa K. 11C-methionine-PET for differentiating recurrent brain tumor from radiation necrosis: radiomics approach with random forest classifier. *Sci Rep*. (2019) 9:15666. doi: 10.1038/s41598-019-52279-2

31. Eichinger P, Zimmer C, Wiestler B. AI in radiology: where are we today in multiple sclerosis imaging? *Röfo-Fortschritte Auf Dem Geb. Röntgenstrahlen Bildgeb Verfahr*. (2020) 192:847–53. doi: 10.1055/a-1167-8402

32. Song Z, Tang Z, Liu H, Guo D, Cai J, Zhou Z. A clinical-radiomics nomogram may provide a personalized 90-day functional outcome assessment for spontaneous intracerebral hemorrhage. *Eur Radiol*. (2021) 31:4949–59. doi: 10.1007/s00330-021-07828-7

33. Koçak B. Reliability of 2D magnetic resonance imaging texture analysis in cerebral gliomas: influence of slice selection bias on reproducibility of radiomic features. *Istanb Med J*. (2019) 20:413–7. doi: 10.4274/imj.galenos.2019.09582

34. Carré A, Klausner G, Edjlali M, Lerousseau M, Briend-Diop J, Sun R, et al. Standardization of brain MR images across machines and protocols: bridging the gap for MRI-based radiomics. *Sci Rep*. (2020) 10:1–15. doi: 10.1038/s41598-020-69298-z

35. Donnelly JP. A systematic review of concept mapping dissertations. *Eval Program Plann*. (2017) 60:186–93. doi: 10.1016/j.evalprogplan.2016.08.010

36. Van Eck N, Waltman L. Software survey: VOSviewer, a computer program for bibliometric mapping. *Scientometrics*. (2010) 84:523–38. doi: 10.1007/s11192-009-0146-3

37. Han JS, Ho YS. Global trends and performances of acupuncture research. *Neurosci Biobehav Rev*. (2011) 35:680–7. doi: 10.1016/j.neubiorev.2010.08.006

38. Chong Y, Long X, Ho YS. Scientific landscape and trend analysis of keloid research: a 30-year bibliometric review. *Ann Transl Med*. (2021) 9:945. doi: 10.21037/atm-21-508

39. Sweileh WM, Al-Jabi SW, Sawalha AF, AbuTaha AS, Zyoud SH. Bibliometric analysis of publications on campylobacter:(2000-2015). *J Health Popul Nutr*. (2016) 35:1–12. doi: 10.1186/s41043-016-0076-7

40. Galldiks N, Kocher M, Ceccon G, Werner JM, Brunn A, Deckert M, et al. Imaging challenges of immunotherapy and targeted therapy in patients with brain metastases: response, progression, and pseudoprogression. *Neuro-Oncol*. (2020) 22:17–30. doi: 10.1093/neuonc/noz147

41. Kim M, Jung SY, Park JE, Jo Y, Park SY, Nam SJ, et al. Diffusion-and perfusion-weighted MRI radiomics model may predict isocitrate dehydrogenase (IDH) mutation and tumor aggressiveness in diffuse lower grade glioma. *Eur Radiol*. (2020) 30:2142–51. doi: 10.1007/s00330-019-06548-3

42. Lohmann P, Elahmadawy MA, Gutsche R, Werner JM, Bauer EK, Ceccon G, et al. FET PET radiomics for differentiating pseudoprogression from early tumor progression in glioma patients post-chemoradiation. *Cancers*. (2020) 12:3835. doi: 10.3390/cancers12123835

43. Lohmann P, Kocher M, Ceccon G, Bauer EK, Stoffels G, Viswanathan S, et al. Combined FET PET/MRI radiomics differentiates radiation injury from recurrent brain metastasis. *Neuroimage Clin*. (2018) 20:537–42. doi: 10.1016/j.nicl.2018.08.024

44. Park JE, Ham S, Kim HS, Park SY, Yun J, Lee H, et al. Diffusion and perfusion MRI radiomics obtained from deep learning segmentation provides reproducible and comparable diagnostic model to human in post-treatment glioblastoma. *Eur Radiol*. (2021) 31:3127–37. doi: 10.1007/s00330-020-07414-3

45. Aerts HJ, Velazquez ER, Leijenaar RT, Parmar C, Grossmann P, Carvalho S, et al. Decoding tumour phenotype by noninvasive imaging using a quantitative radiomics approach. *Nat Commun*. (2014) 5:4006. doi: 10.1038/ncomms5006

46. Kickingereder P, Burth S, Wick A, Götz M, Eidel O, Schlemmer HP, et al. Radiomic profiling of glioblastoma: identifying an imaging predictor of patient survival with improved performance over established clinical and radiologic risk models. *Radiology*. (2016) 280:880–9. doi: 10.1148/radiol.2016160845

47. Bakas S, Akbari H, Sotiras A, Bilello M, Rozycki M, Kirby JS, et al. Advancing the cancer genome atlas glioma MRI collections with expert segmentation labels and radiomic features. *Sci Data*. (2017) 4:1–13. doi: 10.1038/sdata.2017.117

48. Van Griethuysen JJ, Fedorov A, Parmar C, Hosny A, Aucoin N, Narayan V, et al. Computational radiomics system to decode the radiographic phenotype. *Cancer Res*. (2017) 77:e104–7. doi: 10.1158/0008-5472.CAN-17-0339

49. Park CJ, Park YW, Ahn SS, Kim D, Kim EH, Kang SG, et al. Quality of radiomics research on brain metastasis: a roadmap to promote clinical translation. *Korean J Radiol*. (2022) 23:77. doi: 10.3348/kjr.2021.0421

50. Forghani R. Precision digital oncology: emerging role of radiomics-based biomarkers and artificial intelligence for advanced imaging and characterization of brain tumors. *Radiol-Imaging Cancer*. (2020) 2:e190047. doi: 10.1148/rycan.2020190047

51. Jian A, Jang K, Manuguerra M, Liu S, Magnussen J, Di Ieva A. Machine learning for the prediction of molecular markers in glioma on magnetic resonance imaging: a systematic review and meta-analysis. *Neurosurgery*. (2021) 89:31–44. doi: 10.1093/neuros/nyab103

52. Neromyliotis E, Kalamatianos T, Paschalis A, Komaitis S, Fountas KN, Kapsalaki EZ, et al. Machine learning in meningioma MRI: past to present. A narrative review. *J Magn Reson Imaging*. (2022) 55:48–60. doi: 10.1002/jmri.27378

53. Zhou H, Vallières M, Bai HX, Su C, Tang H, Oldridge D, et al. MRI features predict survival and molecular markers in diffuse lower-grade gliomas. *Neuro-Oncol*. (2017) 19:862–70. doi: 10.1093/neuonc/now256

54. Liu Q, Jiang P, Jiang Y, Ge H, Li S, Jin H, et al. Prediction of aneurysm stability using a machine learning model based on PyRadiomics-derived morphological features. *Stroke*. (2019) 50:2314–21. doi: 10.1161/STROKEAHA.119.025777

55. Tupe-Waghmare P, Malpure P, Kotecha K, Beniwal M, Santosh V, Saini J, et al. Comprehensive genomic subtyping of glioma using semi-supervised multi-task deep learning on multimodal MRI. *IEEE Access*. (2021) 9:167900–10. doi: 10.1109/ACCESS.2021.3136293

56. Su X, Sun H, Chen N, Roberts N, Yang X, Wang W, et al. A radiomics-clinical nomogram for preoperative prediction of IDH1 mutation in primary glioblastoma multiforme. *Clin Radiol*. (2020) 75:963–e7. doi: 10.1016/j.crad.2020.07.036

57. Chougule T, Gupta RK, Saini J, Agrawal S, Gupta M, Vakharia N, et al. Radiomics signature for temporal evolution and recurrence patterns of glioblastoma using multimodal magnetic resonance imaging. *Clin Radiol*. (2022) 35:e4647. doi: 10.1002/nbm.4647

58. Zhang Z, He K, Wang Z, Zhang Y, Wu D, Zeng L, et al. Multiparametric MRI radiomics for the early prediction of response to chemoradiotherapy in patients with postoperative residual gliomas: an initial study. *Front Oncol*. (2021) 11:779202. doi: 10.3389/fonc.2021.779202

59. Li N, Mo Y, Huang C, Han K, He M, Wang X, et al. A clinical semantic and radiomics nomogram for predicting brain invasion in WHO grade II meningioma based on tumor and tumor-to-brain interface features. *Front Oncol*. (2021) 11:752158. doi: 10.3389/fonc.2021.752158

60. Tian Q, Yan LF, Zhang X, Zhang X, Hu YC, Han Y, et al. Radiomics strategy for glioma grading using texture features from multiparametric MRI. *J Magn Reson Imaging*. (2018) 48:1518–28. doi: 10.1002/jmri.26010

61. Artzi M, Liberman G, Blumenthal DT, Aizenstein O, Bokstein F, Ben Bashat D. Differentiation between vasogenic edema and infiltrative tumor in patients with high-grade gliomas using texture patch-based analysis. *J Magn Reson Imaging*. (2018) 48:729–36. doi: 10.1002/jmri.25939

62. Arita H, Kinoshita M, Kawaguchi A, Takahashi M, Narita Y, Terakawa Y, et al. Lesion location implemented magnetic resonance imaging radiomics for predicting IDH and TERT promoter mutations in grade II/III gliomas. *Sci Rep*. (2018) 8:11773. doi: 10.1038/s41598-018-30273-4

63. Chaddad A, Desrosiers C, Niazi T. Deep radiomic analysis of MRI related to Alzheimer's disease. *IEEE Access*. (2018) 6:58213–21. doi: 10.1109/ACCESS.2018.2871977

64. Li ZC, Bai H, Sun Q, Zhao Y, Lv Y, Zhou J, et al. Multiregional radiomics profiling from multiparametric MRI: identifying an imaging predictor of IDH1 mutation status in glioblastoma. *Cancer Med*. (2018) 7:5999–6009. doi: 10.1002/cam4.1863

65. Li ZC, Bai H, Sun Q, Li Q, Liu L, Zou Y, et al. Multiregional radiomics features from multiparametric MRI for prediction of MGMT methylation status in glioblastoma multiforme: a multicentre study. *Eur Radiol*. (2018) 28:3640–50. doi: 10.1007/s00330-017-5302-1

66. Bobholz SA, Lowman AK, Barrington A, Brehler M, McGarry S, Cochran EJ, et al. Radiomic features of multiparametric MRI present stable associations with analogous histological features in patients with brain cancer. *Tomography*. (2020) 6:160–9. doi: 10.18383/j.tom.2019.00029

67. Sakai Y, Yang C, Kihira S, Tsankova N, Khan F, Hormigo A, et al. MRI radiomic features to predict IDH1 mutation status in gliomas: a machine learning approach using gradient tree boosting. *Int J Mol Sci*. (2020) 21:8004. doi: 10.3390/ijms21218004

68. Bhandari A, Koppen J, Agzarian M. Convolutional neural networks for brain tumour segmentation. *Insights Imaging*. (2020) 11:1–9. doi: 10.1186/s13244-020-00869-4

69. Muzi M, Wolsztynski E, Fink JR, O'sullivan JN, O'sullivan F, Krohn KA, et al. Assessment of the prognostic value of radiomic features in 18F-FMISO PET imaging of hypoxia in postsurgery brain cancer patients: secondary analysis of imaging data from a single-center study and the multicenter ACRIN 6684 trial. *Tomography*. (2020) 6:14–22. doi: 10.18383/j.tom.2019.00023

70. Calabrese E, Villanueva-Meyer JE, Cha S. A fully automated artificial intelligence method for non-invasive, imaging-based identification of genetic alterations in glioblastomas. *Sci Rep*. (2020) 10:11852. doi: 10.1038/s41598-020-68857-8

71. Cao X, Tan D, Liu Z, Liao M, Kan Y, Yao R, et al. Differentiating solitary brain metastases from glioblastoma by radiomics features derived from MRI and 18F-FDG-PET and the combined application of multiple models. *Sci Rep*. (2022) 12:5722. doi: 10.1038/s41598-022-09803-8

72. Alongi P, Laudicella R, Panasiti F, Stefano A, Comelli A, Giaccone P, et al. Radiomics analysis of brain [18F] FDG PET/CT to predict Alzheimer's disease in patients with amyloid PET positivity: a preliminary report on the application of SPM cortical segmentation, pyradiomics and machine-learning analysis. *Diagnostics*. (2022) 12:933. doi: 10.3390/diagnostics12040933

73. Yao J, Hagiwara A, Oughourlian TC, Wang C, Raymond C, Pope WB, et al. Diagnostic and prognostic value of pH-and oxygen-sensitive magnetic resonance imaging in glioma: a retrospective study. *Cancers*. (2022) 14:2520. doi: 10.3390/cancers14102520

74. Dounavi ME, Low A, Muniz-Terrera G, Ritchie K, Ritchie CW, Su L, et al. Fluid-attenuated inversion recovery magnetic resonance imaging textural features as sensitive markers of white matter damage in midlife adults. *Brain Commun*. (2022) 4:fcac116. doi: 10.1093/braincomms/fcac116

75. Calabrese E, Rudie JD, Rauschecker AM, Villanueva-Meyer JE, Clarke JL, Solomon DA, et al. Combining radiomics and deep convolutional neural network features from preoperative MRI for predicting clinically relevant genetic biomarkers in glioblastoma. *Neuro-Oncol Adv*. (2022) 4:vdac060. doi: 10.1093/noajnl/vdac060

76. Cheng J, Liu J, Kuang H, Wang J. A fully automated multimodal MRI-based multi-task learning for glioma segmentation and IDH genotyping. *IEEE Trans Med Imaging*. (2022) 41:1520–32. doi: 10.1109/TMI.2022.3142321

77. Tixier F, Um H, Young RJ, Veeraraghavan H. Reliability of tumor segmentation in glioblastoma: impact on the robustness of MRI-radiomic features. *Med Phys*. (2019) 46:3582–91. doi: 10.1002/mp.13624

78. Ma L, Xiao Z, Li K, Li S, Li J, Yi X. Game theoretic interpretability for learning based preoperative gliomas grading. *Future Gener Comput Syst Int J Escience*. (2020) 112:1–10. doi: 10.1016/j.future.2020.04.038

79. Mitchell-Hay RN, Ahearn TS, Murray AD, Waiter GD. Investigation of the inter- and intrascanner reproducibility and repeatability of radiomics features in T1-weighted brain MRI. *J Magn Reson Imaging*. (2022) 56:1559–68. doi: 10.1002/jmri.28191

Frontiers in Oncology

Advances knowledge of carcinogenesis and tumor progression for better treatment and management

The third most-cited oncology journal, which highlights research in carcinogenesis and tumor progression, bridging the gap between basic research and applications to imrpove diagnosis, therapeutics and management strategies.

Discover the latest Research Topics

See more →

Frontiers

Avenue du Tribunal-Fédéral 34
1005 Lausanne, Switzerland
frontiersin.org

Contact us

+41 (0)21 510 17 00
frontiersin.org/about/contact